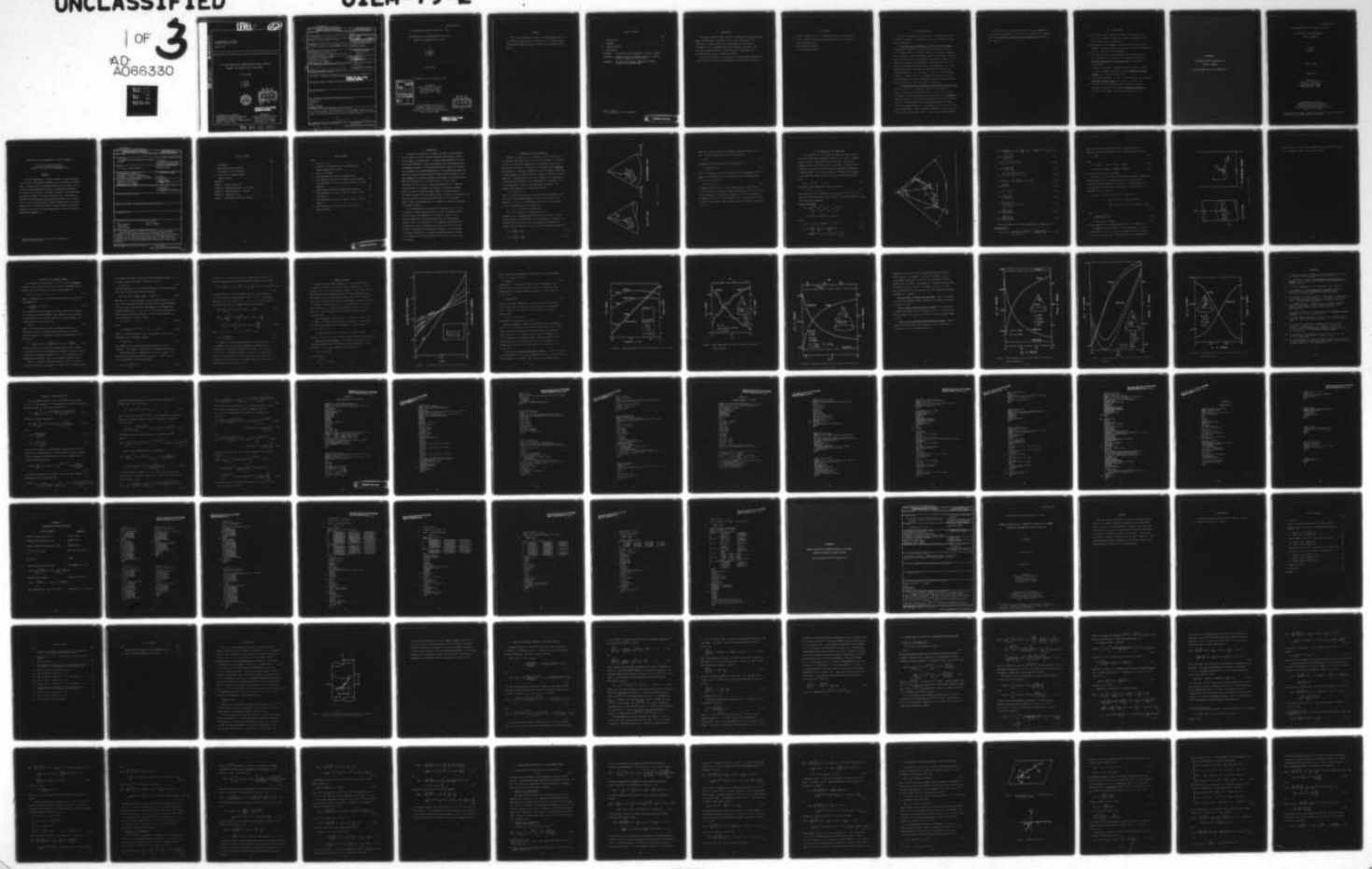


AD-A066 330

ILLINOIS UNIV AT URBANA-CHAMPAIGN ELECTROMAGNETICS LAB F/G 9/5  
AN INVESTIGATION ON CHARACTERIZING MUTUAL COUPLING BETWEEN TWO --ETC(U)  
JAN 79 S W LEE, R MITTRA, J BOERSMA, E YUNG N00019-78-C-0064  
UIEM-79-2 NL

UNCLASSIFIED

OF 3  
AD A066330



**LEVEL II**

**12**  
B.S.

DDC FILE COPY AD A0 66330

ELECTROMAGNETICS LABORATORY  
TECHNICAL REPORT NO. 79-2

JANUARY 1979

AN INVESTIGATION ON CHARACTERIZING MUTUAL COUPLING  
BETWEEN TWO ANTENNA SLOTS ON A CONE

FINAL REPORT

S. W. Lee  
R. Mittra  
J. Boersma  
E. Yung



**APPROVED FOR PUBLIC RELEASE:  
DISTRIBUTION UNLIMITED**

ELECTROMAGNETICS LABORATORY  
DEPARTMENT OF ELECTRICAL ENGINEERING  
ENGINEERING EXPERIMENT STATION  
UNIVERSITY OF ILLINOIS AT URBANA-CHAMPAIGN  
URBANA, ILLINOIS 61801

Supported by  
Contract No. N00019-78-C-0064  
Department of the Navy  
Naval Air Systems Command  
Washington, D.C. 20361

79 03 22 032

UNCLASSIFIED

SECURITY CLASSIFICATION OF THIS PAGE (When Data Entered)

REPORT DOCUMENTATION PAGE		READ INSTRUCTIONS BEFORE COMPLETING FORM
1. REPORT NUMBER	2. GOVT ACCESSION NO.	3. RECIPIENT'S CATALOG NUMBER
4. TITLE (and Subtitle)		5. TYPE OF REPORT & PERIOD COVERED
6. An Investigation on Characterizing Mutual Coupling Between Two Antenna Slots on a Cone		Final Report 16 Nov 1977 - 15 Jan 1979
7. AUTHOR(s)		8. CONTRACT OR GRANT NUMBER(s)
9. S. W./Lee, R./Mitra, J./Boersma, and E./Yung		15. N00019-78-C-0064
9. PERFORMING ORGANIZATION NAME AND ADDRESS		10. PROGRAM ELEMENT, PROJECT, TASK AREA & WORK UNIT NUMBERS
Electromagnetics Laboratory Department of Electrical Engineering, University of Illinois, Urbana, IL 61801		12. 196p.
11. CONTROLLING OFFICE NAME AND ADDRESS		12. REPORT DATE
Department of the Navy Naval Air Systems Command Washington, D.C. 20361		11. January 1979
14. MONITORING AGENCY NAME & ADDRESS (if different from Controlling Office)		13. NUMBER OF PAGES
14. UIEM-79-2 UILU-ENG-79-2541		197
15. SECURITY CLASS. (of this report)		15. SECURITY CLASS. (of this report)
		Unclassified
15a. DECLASSIFICATION/DOWNGRADING SCHEDULE		
16. DISTRIBUTION STATEMENT (of this Report)		
Distribution unlimited. (Reproduction in whole or in part is permitted for any purpose of the United States Government.)		
<b>APPROVED FOR PUBLIC RELEASE: DISTRIBUTION UNLIMITED</b>		
17. DISTRIBUTION STATEMENT (of the abstract entered in Block 20, if different from Report)		
18. SUPPLEMENTARY NOTES		
19. KEY WORDS (Continue on reverse side if necessary and identify by block number)		
Creeping Wave Surface ray GTD Mutual Coupling Conformal Arrays		
20. ABSTRACT (Continue on reverse side if necessary and identify by block number)		
This is the final report for Naval Air Systems Command Contract on the mutual coupling effect in a conformal array. It contains a brief administrative summary plus three attachments which give the technical details.		

79 03 22 032

408 102

JOB

Electromagnetics Laboratory Report No. 79-2

AN INVESTIGATION ON CHARACTERIZING MUTUAL COUPLING  
BETWEEN TWO ANTENNA SLOTS ON A CONE

by

S. W. Lee  
R. Mittra  
J. Boersma  
E. Yung

Final Report

November 16, 1977 to January 15, 1979

ACCESSION for	
DTIC	White Section <input checked="" type="checkbox"/>
DDC	Diff Section <input type="checkbox"/>
UNANNOUNCED	<input type="checkbox"/>
JUSTIFICATION.....	
BY.....	
DISTRIBUTION/AVAILABILITY CODES	
Dist.	AVAIL. and/or SPECIAL
A	

Supported by  
Contract No. N00019-78-C-0064  
Department of the Navy  
Naval Air Systems Command  
Washington, D.C. 20361

Electromagnetics Laboratory  
Department of Electrical Engineering  
Engineering Experiment Station  
University of Illinois at Urbana-Champaign  
Urbana, Illinois 61801

DDC  
RECEIVED  
MAR 26 1979  
D

APPROVED FOR PUBLIC RELEASE:  
DISTRIBUTION UNLIMITED

ABSTRACT

This is the final report for Naval Air Systems Command Contract on the mutual coupling effect in a conformal array. It contains a brief administrative summary plus three attachments which give the technical details.

TABLE OF CONTENTS

	Page
I. INTRODUCTION. . . . .	1
II. PERSONNEL . . . . .	2
III. TECHNICAL RESULTS . . . . .	3
IV. PUBLICATIONS. . . . .	5
ATTACHMENT A: GTD SOLUTION OF SLOT ADMITTANCE ON A CONE OR CYLINDER *	
ATTACHMENT B: SURFACE FIELD DUE TO A MAGNETIC DIPOLE ON A CYLINDER: ASYMPTOTIC EXPANSION OF EXACT SOLUTION	
ATTACHMENT C: GTD CALCULATION OF MUTUAL ADMITTANCE AND ELEMENT PATTERN OF SLOT CONFORMAL ARRAY	

---

\* Each attachment has its own pagination.

PRECEDING PAGE BLANK

## I. INTRODUCTION

The contract N00019-78-C-0064 entitled "An Investigation on Characterizing Mutual Coupling Between Two Antenna Slots on a Cone" was awarded to the University of Illinois by Naval Air Systems Command for the period of 16 November 1977 to 15 November 1978 and with funding of \$53,000.00. The contract was later extended to 15 January 1979 with no additional cost. The contract monitor is Mr. J. Willis of AIR-310B.

This is the final report of the contract, covering personnel (Section II), technical results (Section III and attachments) and publications (Section IV).

## II. PERSONNEL

S. W. Lee, Professor of Electrical Engineering, Principal investigator.

R. Mitra, Professor of Electrical Engineering, Principal investigator.

E. Yung, Research Associate

L. Grun, Research Assistant

C. L. Law, Research Assistant

### III. TECHNICAL RESULTS

Our study of the mutual coupling effect in a conformal array has been successfully concluded. In the present contract, the following two tasks have been carried out:

(i) GTD solution of self-admittance of slot on a cone or cylinder.

In applying GTD formulas to calculate the self-admittance of a slot on a cone (cylinder), there is a difficulty which was not previously presented in the calculation of mutual admittance, namely, the GTD Greens' function  $G$  for the surface field has a  $r^{-3}$ -singularity at the source point  $r = 0$ . We removed this difficulty by subtracting  $G_0$  from  $G$ , where  $G_0$  is the Green's function for a planar conducting surface. The contribution of  $G_0$  to the self-admittance can be calculated by a Fourier transform method. The remaining function  $(G - G_0)$  is of order  $r^{-1.5}$  as  $r \rightarrow 0$ , and is therefore integrable. When the slot is on a cylinder, our GTD results of the slot self-admittance are in excellent agreement with those calculated from the known exact solution. Details are given in Attachment A.

(ii) Justification of the transverse curvature term in the GTD solution.

In our GTD solution for the magnetic field on a convex conducting surface, there exists a rather peculiar term. Contrary to all previous GTD theories, this term depends on the surface curvature in the transverse direction of the ray. For many practical situations, the inclusion of this term is of critical importance in getting accurate numerical solutions. This term was first introduced by us in November 1976 as a conjecture. Now, we have shown through a rigorous asymptotic expansion of an exact solution that our conjecture is indeed correct. Details are given in Attachment B.

Our work on the GTD calculation of mutual coupling is summarized in a review article (Attachment C), which will be included in the forthcoming book entitled Principles and Applications of Antenna Design sponsored by IEE (London).

#### IV. PUBLICATIONS

- S. W. Lee, E. Yung, and R. Mittra, "GTD solution of slot admittance on a cone or cylinder," University of Illinois, Electromagnetics Lab. Tech. Report No. 78-12, December 1978.
- J. Boersma and S. W. Lee, "Asymptotic solution of a surface field due to a magnetic dipole on a cylinder," University of Illinois, Electromagnetics Lab. Tech. Report No. 78-17, December 1978.
- S. W. Lee, "GTD calculation of mutual admittance and element pattern of slot conformal array," to appear in the forthcoming book entitled Principles and Applications of Antenna Design, to be published by IEE (London).
- S. W. Lee and S. Safavi-Naini, "Approximate asymptotic solution of surface field due to a magnetic dipole on a cylinder," IEEE Trans. Antennas Propagat., vol. AP-26, pp. 593-598, 1978.
- S. W. Lee, "Mutual admittance of slots on a cone: solutions by ray technique," IEEE Trans. Antennas Propagat., vol. AP-26, pp. 768-773, 1978.
- S. W. Lee and R. Mittra, "Accurate computation of mutual coupling in conformal arrays using ray techniques," Antennas and Propagation, pp. 302-306, IEE (London) Conference Publication No. 169, 1978.

ATTACHMENT A

GTD SOLUTION OF SLOT ADMITTANCE ON A  
CONE OR CYLINDER

(Each attachment has its own pagination.)

UILU-ENG 78-2554

Electromagnetics Laboratory Report No. 78-12

GTD SOLUTION OF SLOT ADMITTANCE ON A  
CONE OR CYLINDER

by

S. W. Lee  
E. Yung  
R. Mittra

Technical Report

December 1978

Supported by  
Contract No. N00019-78-C-0064  
Department of the Navy  
Naval Air Systems Command  
Washington, D.C. 20361

Electromagnetics Laboratory  
Department of Electrical Engineering  
Engineering Experiment Station  
University of Illinois at Urbana-Champaign  
Urbana, Illinois 61801

Distribution is unlimited. (Reproduction in whole or in part is permitted  
for any purpose of the United States Government.)

GTD SOLUTION OF SLOT ADMITTANCE ON A CONE OR CYLINDER\*

S. W. Lee, E. Yung, and R. Mittra  
Department of Electrical Engineering  
University of Illinois at Urbana-Champaign, 1978

ABSTRACT

The input admittance of an elemental radiator on a curved surface, e.g., a slot on a cone, plays an important role in the design of conformal arrays. A search through the literature reveals that at present, there is no reliable theoretical method available for computing this admittance. The objective of this paper is to provide a solution to this problem using a surface ray approach — within the framework of GTD. The solution is verified for the limiting case where the cone degenerates into a cylinder and it is shown that the GTD results compare extremely well with the exact modal solution to the cylinder problem. Extensive numerical results are presented in the paper for the input admittance of a cone as a function of various design parameters.

\*This work was supported by Naval Air Systems Command under Contract N00019-78-C-0064.

Unclassified

SECURITY CLASSIFICATION OF THIS PAGE (When Data Entered)

REPORT DOCUMENTATION PAGE		READ INSTRUCTIONS BEFORE COMPLETING FORM
1. REPORT NUMBER	2. GOVT ACCESSION NO.	3. RECIPIENT'S CATALOG NUMBER
4. TITLE (and Subtitle) GTD SOLUTION OF SLOT ADMITTANCE ON A CONE OR CYLINDER		5. TYPE OF REPORT & PERIOD COVERED Technical
7. AUTHOR(s) S. W. Lee, E. Yung, R. Mittra		6. PERFORMING ORG. REPORT NUMBER EM 78-12; UILU-ENG-78-2554
9. PERFORMING ORGANIZATION NAME AND ADDRESS Electromagnetics Laboratory Department of Electrical Engineering University of Illinois, Urbana, IL 61801		8. CONTRACT OR GRANT NUMBER(s) N00019-78-C-0064
11. CONTROLLING OFFICE NAME AND ADDRESS Department of the Navy Naval Air Systems Command Washington, D. C. 20361		10. PROGRAM ELEMENT, PROJECT, TASK AREA & WORK UNIT NUMBERS PR-RJ001
14. MONITORING AGENCY NAME & ADDRESS (if different from Controlling Office)		12. REPORT DATE December 1978
		13. NUMBER OF PAGES 53
		15. SECURITY CLASS. (of this report) UNCLASSIFIED
		15a. DECLASSIFICATION/DOWNGRADING SCHEDULE
16. DISTRIBUTION STATEMENT (of this Report)		
17. DISTRIBUTION STATEMENT (of the abstract entered in Block 20, if different from Report)		
18. SUPPLEMENTARY NOTES		
19. KEY WORDS (Continue on reverse side if necessary and identify by block number) GTD slot on cone slot admittance slot on cylinder surface rays conformal array		
20. ABSTRACT (Continue on reverse side if necessary and identify by block number) The input admittance of a slot on a cone is an important parameter in the design of some conformal arrays, but no theoretical result is yet available. In this paper, the surface rays of GTD are used for the admittance determination. For the special case in which the cone degenerates into a cylinder, the GTD solution yields excellent numerical results (within 0.5% in magnitude and 1° in phase) when compared with the known exact modal series solution.		

TABLE OF CONTENTS

	Page
1. INTRODUCTION. . . . .	1
2. FORMULATION OF INPUT ADMITTANCE . . . . .	2
3. GTD SOLUTION OF INPUT ADMITTANCE. . . . .	5
4. FINITE PART OF DIVERGENT INTEGRAL . . . . .	11
5. NUMERICAL RESULTS . . . . .	15
REFERENCES. . . . .	25
APPENDIX A SIMPLIFICATION OF $Y_0^d$ . . . . .	26
APPENDIX B1 COMPUTER PROGRAM OF Y FOR CYLINDER . . . . .	29
APPENDIX B2 COMPUTER PROGRAM OF Y FOR CONE . . . . .	33
APPENDIX B3 SUBROUTINES OF $Y_0^d$ . . . . .	38
APPENDIX C SUBROUTINES FOR SPECIAL FUNCTIONS . . . . .	40

LIST OF FIGURES

Figure	Page
1. A slot on a cone . . . . .	3
2. Geometry of a developed cone for calculating Green's function between points 1 and 2. . . . .	6
3. A slot on a cylinder . . . . .	9
4. Input admittance of a slot on an infinite plane. . . . .	16
5. Input admittance of a slot on an infinitely long cylinder. .	18
6. Input admittance of a slot on a cone as a function of radial distance $c$ . . . . .	19
7. Same as Figure 6 except with larger radial distance $c$ . . . .	20
8. Input admittance of a slot on a cone as a function of half- cone angle $\theta_0$ . . . . .	22
9. Input admittance of a slot on a cone as a function of slot length $a$ . . . . .	23
10. Input admittance of a slot on a cone as a function of orientation angle $\omega$ . . . . .	24

## 1. INTRODUCTION

Because of its simplicity of geometry and ease of flush-mounting, the slot radiator is one of the most frequently used elemental radiators in the design of conformal arrays. A crucial design parameter of a slot is its input admittance  $Y$ , whose value depends on the slot dimensions and the geometrical property of the conducting surface on which it is mounted. In the simplest case, the mounting surface is an infinite ground plane, in which  $Y$  of a thin slot can be related through the duality relation to the input impedance of a thin-wire antenna in free space. The latter quantity was first calculated by P. S. Carter in 1932 [1] - [3]. Direct calculations of  $Y$  of a slot on a plane were reported in [4]. When the mounting surface is a cylinder, the solution of  $Y$  has been expressed exactly in terms of cylindrical modes, namely, an infinite series in the azimuthal direction and a spectral integral in the axial direction [5], [6]. This modal solution is suitable when the radius  $R$  of the cylinder is small in terms of wavelength ( $kR < 10$ ); otherwise, its numerical evaluation is extremely laborious.

In the present paper, we consider the calculation of  $Y$  of a slot on a cone (or cylinder) using surface rays in GTD. The general concept of surface rays was introduced by J. B. Keller in 1956 [7]. The explicit formulas for surface rays adopted here are those reported recently in [8]. Our solution of  $Y$  is an asymptotic solution which is valid when the radii of curvature at all points on the cone are large in terms of wavelength (or high frequency solution). Its calculation is relatively simple, and its accuracy is surprisingly good as verified by the comparison with the exact modal solution for the case of a slot on a cylinder.

## 2. FORMULATION OF INPUT ADMITTANCE

Referring to Figure 1a, let us consider a slot on the surface of an infinitely large conducting cone with a half-cone-angle  $\theta_0$ . The slot is relatively small when compared with its surrounding cone surface, and the shape of the slot is assumed to be rectangular on the developed cone (Figure 1b). Note that, depending on the exact manner in which the feeding waveguide is fitted into the cone surface, the shape of the slot mapped onto a developed cone can be quite irregular. The assumption of rectangular shapes represents a good approximation for practical cases; at the same time, it simplifies the subsequent calculations. The location and dimensions of the slot are described by

$$(c, \omega), \text{ and } (a \times b) \quad ,$$

where  $c$  is the radial distance of the center of the slot from the cone tip, and  $\omega$  is the angular deviation of the slot axis from the cone generator ( $\omega = \pi/2$  for a circumferential slot and  $\omega = 0$  for a radial slot). Throughout this work, we assume that

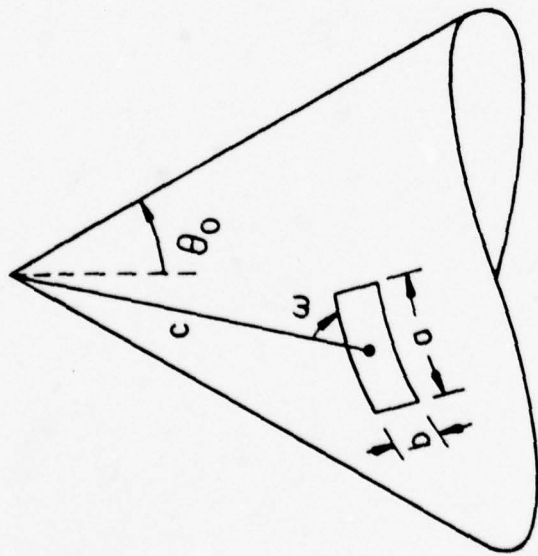
$$(i) \quad kc \gg 1 \quad (\text{slot away from cone tip}) \quad ,$$

$$(ii) \quad ka \approx \pi \text{ and } kb \ll 1 \quad (\text{resonant thin slot}) \quad .$$

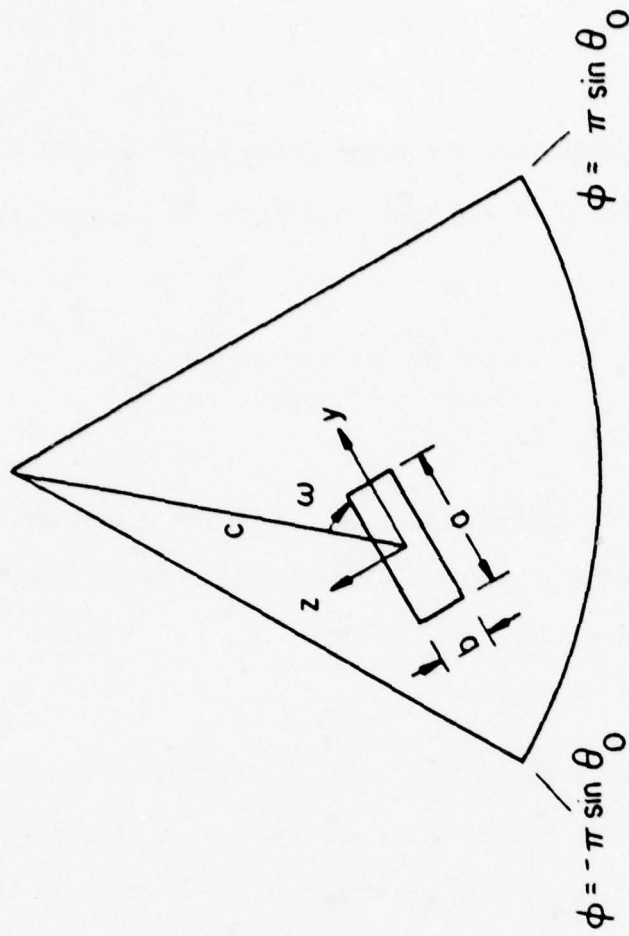
Assumption (i) is necessary because near the tip the cone is highly curved and GTD is not valid there. As a consequence of assumption (ii), the aperture field of the slot can be adequately approximated by a simple cosine distribution, i.e., the so-called "one-mode approximation":

$$\vec{E} = \hat{z}V\sqrt{\frac{2}{ab}} \cos\left(\frac{\pi y}{a}\right) \quad , \quad (2-1a)$$

$$\vec{H} = -\hat{y}I\sqrt{\frac{2}{ab}} \cos\left(\frac{\pi y}{a}\right) \quad , \quad (2-1b)$$



(a) 3-D view



(b) developed cone

Figure 1. A slot on a cone.

where  $V$  and  $I$  are, respectively, the modal voltage and current of the slot. The input admittance of the slot is defined by

$$Y = \frac{I}{V} \quad (2.2)$$

Alternatively, it can be calculated by the expression

$$Y = \frac{-1}{V^2} \iint_A \vec{H} \cdot \vec{K} \, ds \quad (2.3)$$

Here  $A$  is the aperture ( $a \times b$ ) of the slot.  $\vec{K}$  is the equivalent surface magnetic current density due to the application of a field  $\vec{E}$  described in (2.1a), and is given by

$$\vec{K} = \vec{E} \times \hat{n} = \vec{E} \times \hat{x} \quad (2.4)$$

The magnetic field  $\vec{H}$  in (2.3) is the field produced by  $\vec{K}$  when the slot is short-circuited. Under the one-mode approximation, this  $\vec{H}$  is identified with the radiation of  $\vec{K}$  located on a completely filled cone (without slot). We emphasize that (2.3) is an approximation of (2.2) because of the manner in which  $\vec{H}$  is calculated, and is valid only under the one-mode approximation in (2.1).

### 3. GTD SOLUTION OF INPUT ADMITTANCE

To calculate  $\vec{H}$  in (2.3), we first determine the Green's function  $\vec{h}(1,2)$  which represents the magnetic field at point 2 due to a magnetic dipole at point 1. Both points 1 and 2 are on the surface of the completely filled cone (after the slot is removed), as shown in Figure 2. According to GTD,  $\vec{h}(1,2)$  has the following two dominant contributions at high-frequency:  $\vec{h}^d$  due to the direct ray  $\widehat{12}$  going from the source to the observation point, and  $\vec{h}^t$  due to the tip-diffracted ray  $\widehat{102}$ . Thus,

$$\vec{h}(1,2) \sim \vec{h}^d + \vec{h}^t \quad ; \quad k \rightarrow \infty \quad . \quad (3.1)$$

Accordingly, input admittance  $Y$  also has two parts

$$Y \sim Y^d + Y^t \quad ; \quad k \rightarrow \infty \quad . \quad (3.2)$$

The calculation of  $\vec{h}^d$  is detailed in [8], and that of  $\vec{h}^t$  in [5], [8].

Applying the above results in (2.3),  $Y^d$  and  $Y^t$  on a cone are found as follows (for  $\exp j\omega t$  time convention):

Direct contribution:

$$Y^d = -\frac{2}{ab} \int_{-a/2}^{a/2} dy_1 \int_{-b/2}^{b/2} dz_1 \int_{-a/2}^{a/2} dy_2 \int_{-b/2}^{b/2} dz_2 \times \cos\left(\frac{\pi y_1}{a}\right) \cos\left(\frac{\pi y_2}{a}\right) g(y_1, z_1; y_2, z_2) \quad , \quad (3.3)$$

where

$$g(y_1, z_1; y_2, z_2) = H_b \sin^2 \theta + H_t \cos^2 \theta \quad , \quad (3.4)$$

$$H_b = G(s) \left\{ \left( 1 - \frac{j}{ks} \right) \tau v(\xi) - \left( \frac{1}{ks} \right)^2 \tau^3 u(\xi) + j(\sqrt{2kR_t})^{-2/3} [\tau v'(\xi) + (\bar{R}_t/\bar{R}_b) \tau^3 u'(\xi)] \right\} \quad , \quad (3.5)$$

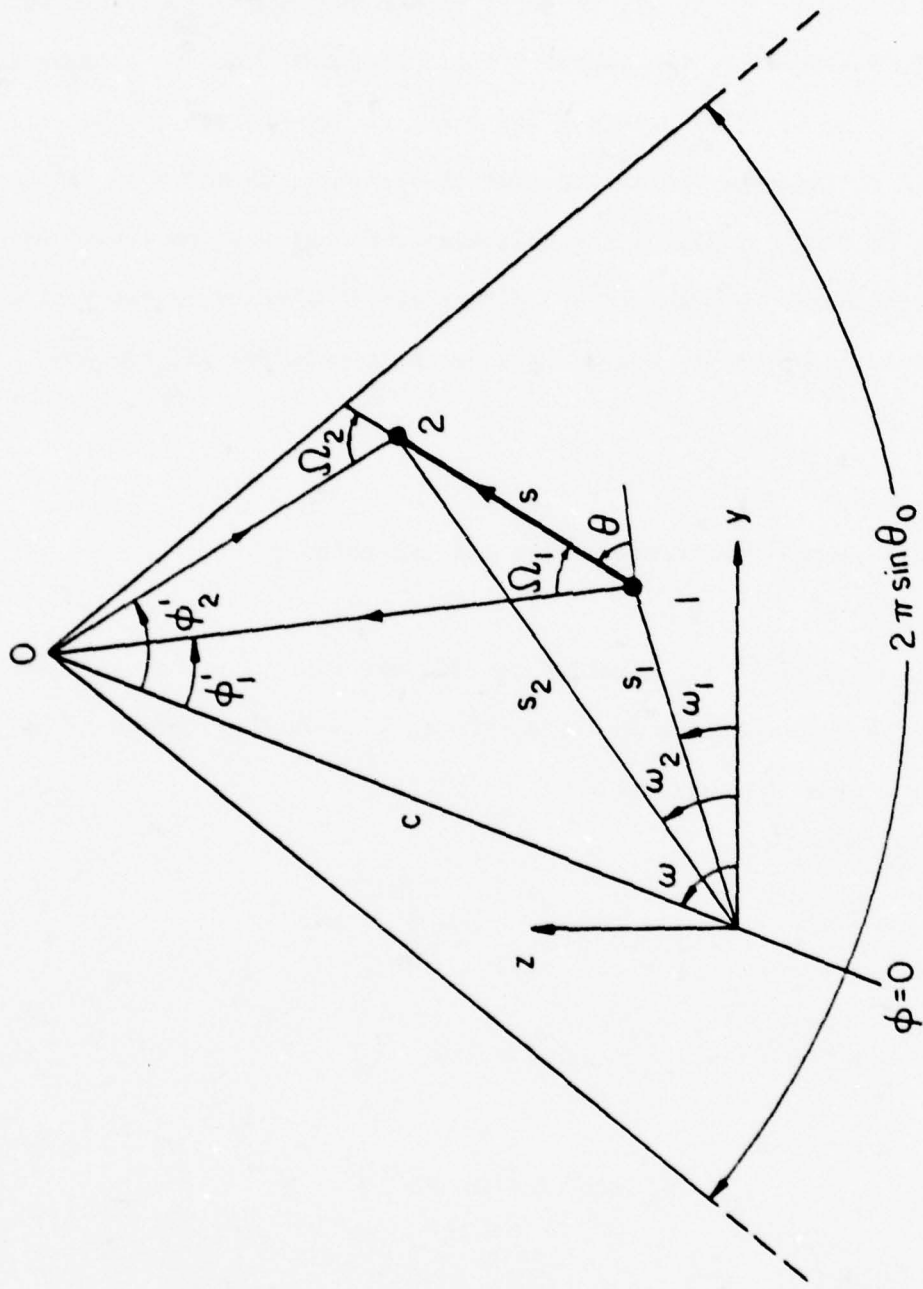


Figure 2. Geometry of a developed cone for calculating Green's function between points 1 and 2.

$$H_t = G(s) \left( \frac{j}{ks} \right) \left[ \tau v(\xi) + \left( 1 - \frac{2j}{ks} \right) \tau^3 u(\xi) + j(\sqrt{2kR_t})^{-2/3} \tau^3 u'(\xi) \right], \quad (3.6)$$

$$G(s) = \frac{k^2}{j240\pi^2} \frac{e^{-jks}}{ks}, \quad (3.7)$$

$$s = \sqrt{(y_2 - y_1)^2 + (z_2 - z_1)^2}, \quad (3.8)$$

$$\theta = \tan^{-1} \left( \frac{z_2 - z_1}{y_2 - y_1} \right), \quad (3.9)$$

$$\Omega_n = \sqrt{c^2 + s_n^2 - 2cs_n \cos(\omega - \omega_n)}, \quad (3.10)$$

$$\phi'_n = \phi_n \sin \theta_0 = \sin^{-1} \left\{ \frac{s_n}{\Omega_n} \sin(\omega - \omega_n) \right\}, \quad (3.11)$$

$$s_n = \sqrt{y_n^2 + z_n^2}, \quad (3.12)$$

$$\omega_n = \tan^{-1} (z_n/y_n), \quad (3.13)$$

$$\tau = \frac{\sin |\phi'_2 - \phi'_1|}{|\phi'_2 - \phi'_1|}, \quad (3.14)$$

$$\xi = \left( \frac{kr_1 \sin \Omega_1}{2 \tan^2 \theta_0} \right)^{1/3} |\phi'_2 - \phi'_1|, \quad (3.15)$$

$$\bar{R}_t = \frac{\sqrt{r_1 r_2} \tan \theta_0}{\sin \Omega_1 \sin \Omega_2}, \quad (3.16)$$

$$\bar{R}_b = \frac{\sqrt{r_1 r_2} \tan \theta_0}{\cos \Omega_1 \cos \Omega_2}. \quad (3.17)$$

Fock's functions (u,v) and their derivatives are described in [9].

Tip contribution:

$$Y^T = \sigma_0 \sin^2 \omega \frac{(1+j)ab}{60\pi^4 c^2 \sin \theta_0} \left( \frac{\tan \theta_0}{\pi} \right)^{1/2} \left[ \frac{\sin(kb/2)}{kb/2} \right]^2 e^{-j2kc}. \quad (3.18)$$

Here  $\sigma_0$  is the zeroth-order tip-diffraction coefficient and is a function of the half-cone-angle  $\theta_0$ . It is approximately given by [8]

$$\sigma_0 = Ae^{jB} \quad , \quad (3.19)$$

where

$$A = 1.3057\theta_0^{-1} - 1.755 + 2.772\theta_0 - 1.459\theta_0^2 \quad , \quad (3.20)$$

$$B = 2.7195 + 1.4608\theta_0 - 1.1295\theta_0^2 + 0.6566\theta_0^3 \quad , \quad (3.21)$$

in which both  $\theta_0$  and B are in radians.

If the slot is on a cylinder and is oriented along the circumferential direction (Figure 3), the same expression in (3.3) can be used to calculate the input admittance Y (there is no tip contribution for the cylinder case). The GTD solution of the Green's function, which is determined in [9], is given by

$$\begin{aligned} g(y_1, z_1; y_2, z_2) = G(s) \{ & v(\xi) [\sin^2 \theta + \frac{j}{ks} \cos 2\theta] \\ & + \frac{j}{ks} u(\xi) [\cos^2 \theta (1 - \frac{2j}{ks}) + \frac{j}{ks} \sin^2 \theta] \\ & + \frac{j}{ks} \xi [v'(\xi) \sin^2 \theta + u'(\xi) \cos^2 \theta (\tan^4 \theta + \frac{j}{ks})] \} \quad , \end{aligned} \quad (3.22)$$

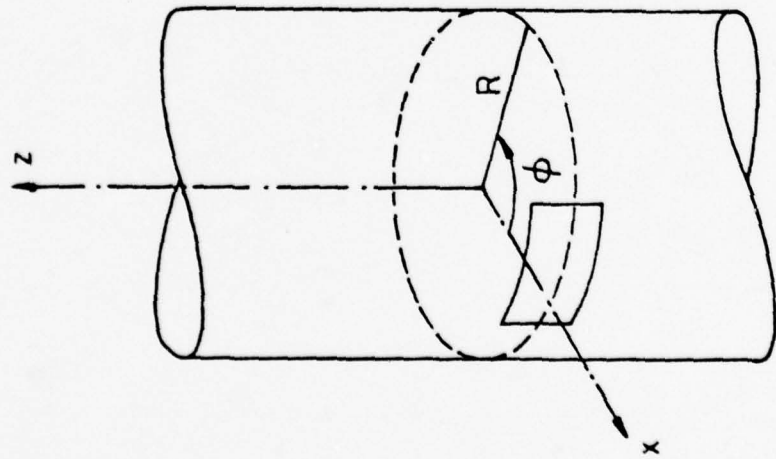
where

$$\xi = \left( \frac{kR \cos^4 \theta}{2} \right)^{1/3} \frac{s}{R} \quad , \quad (3.23)$$

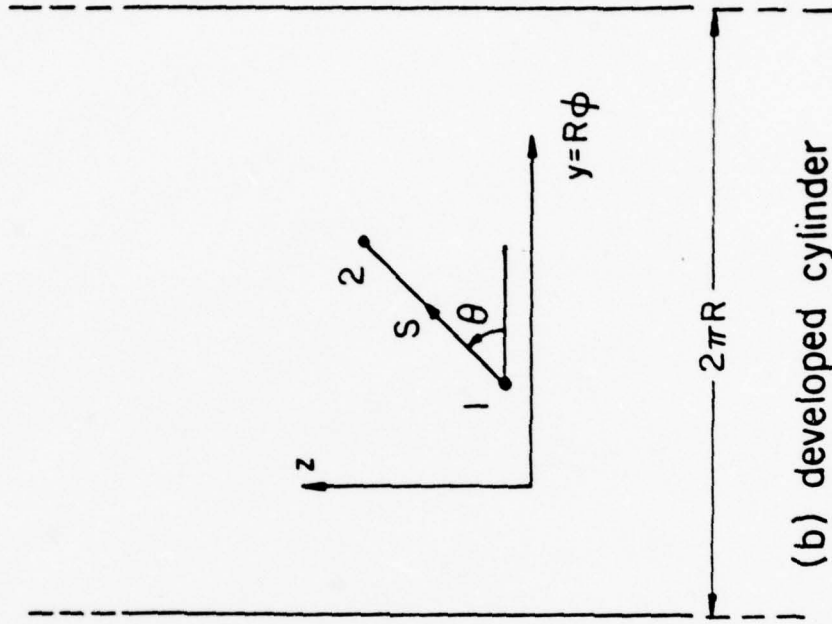
$$R = \text{radius of the cylinder.} \quad (3.24)$$

The functions G(s), s,  $\theta$  are defined earlier in (3.7) through (3.9).

In summary, the GTD solution of the input admittance of a slot on a cone is given in (3.2), (3.3), and (3.18); while that of a cylinder is given in (3.3) and (3.22). These solutions are approximately valid



(a) 3-D view



(b) developed cylinder

Figure 3. A slot on a cylinder.

when the radii of curvature in the neighborhood of the slot on the cone or the cylinder are large in terms of wavelength.

#### 4. FINITE PART OF DIVERGENT INTEGRAL

The integral for calculating  $Y^d$  in (3.3) is in fact a divergent integral. This is due to the fact that, as point 1 approaches point 2, (Figure 2) the Green's function in (3.4) becomes infinite as

$$g(y_1, z_1; y_2, z_2) \sim Cs^{-3}, \quad s \rightarrow 0, \quad (4.1a)$$

where  $s$ , defined in (3.8), is the distance between the two points, and the parameter  $C$  is

$$C = \frac{1}{j240\pi^2 k} (2 - 3 \sin^2 \theta). \quad (4.1b)$$

It is well-known that the singularity of cubic power is non-integrable with respect to a surface integral. This difficulty can be traced back to the derivation of the Green's function  $g$ . Strictly speaking,  $g$  is a distribution and can be written as

$$g = D\bar{g}, \quad (4.2)$$

where  $D$  is a second-order differential operator with respect to coordinates of point 2, and  $\bar{g}$  is the Green's function of a vector potential component. A "legitimate" expression corresponding to (3.3) should read

$$Y^d = -\frac{2}{ab} \iint dy_2 dz_2 \cos\left(\frac{\pi y_2}{a}\right) \{D[\iint dy_1 dz_1 \cos\left(\frac{\pi y_1}{a}\right)\bar{g}]\}, \quad (4.3)$$

which is convergent, and  $Y^d$  has a well-defined finite value. However, in writing (3.3), we have interchanged the differential operator  $D$  and the second surface integration operator in (4.3). This interchange is not permissible and, therefore, leads to the divergent integral in (3.3).

Since (4.3) contains a differential operator and is not suitable for numerical evaluation, we prefer to work with (3.3), provided of course

we can extract the correct finite part from the divergent integral. To this end, we rewrite the Green's function in (3.4) as

$$g = g_0 + g_1 \quad (4.4)$$

The first term  $g_0$  in (4.4) is the Green's function of an infinite ground plane, and is given by the well-known expression

$$g_0 = G(s) \left[ \sin^2 \theta + \frac{j}{ks} \left( 1 - \frac{j}{ks} \right) (2 - 3 \sin^2 \theta) \right] \quad (4.5)$$

Note that, as  $s \rightarrow 0$ ,  $g_0$  has exactly the same singular behavior in (4.1) as  $g$ . This is expected, because in the sufficiently small neighborhood of a point source, the cone can be approximated by its tangent plane.

The second term  $g_1$  ( $g_1 = g - g_0$ ) in (4.4) is the difference between the Green's function of a cone and that of a plane. Near the source, it can be shown from (3.4) and (4.5) that

$$g_1 \sim C_1 s^{-3/2}, \quad s \rightarrow 0, \quad (4.6a)$$

where

$$C_1 = (1920R_t)^{-1} k^{-1/2} \pi^{-3/2} (1 - j)(2 - 3 \cos^2 \theta) \quad (4.6b)$$

When (4.4) is substituted into (3.3), the admittance  $Y^d$  on a cone is decomposed into two components, namely,

$$Y^d = Y_0^d + Y_1^d \quad (4.7)$$

The singularity of  $g_1$  at the source point specified in (4.6) is integrable. Thus, there is no difficulty in evaluating  $Y_1^d$  numerically.

The first term  $Y_0^d$  is the admittance of a slot on a plane. It is defined by (3.3) after replacing  $g$  by  $g_0$  in (4.5). From (3.7) and (4.5), we recognize the following identity:

$$g_0 = \left( 1 + \frac{1}{k^2} \frac{\partial^2}{\partial y_2^2} \right) G(s) \quad (4.8)$$

Note that (4.8) is in the form of (4.2). Substituting (4.8) into (3.3) and interchanging integration and differentiation operators, we obtain

$$Y_0^d = -\frac{2}{ab} \iint dy_2 dz_2 \cos\left(\frac{\pi y_2}{a}\right) \left\{ \left(1 + \frac{1}{k^2} \frac{\partial^2}{\partial y_2^2}\right) \left[ \iint dy_1 dz_1 \cos\left(\frac{\pi y_1}{a}\right) G(s) \right] \right\}. \quad (4.9)$$

The integral in (4.9) is now convergent, and (4.9) can be considered as the "finite part" of the divergent integral in (3.3). For numerical evaluation, (4.9) is converted to that in the Fourier transform domain. Following Rhodes [10], it is simplified to become (Appendix A)

$$\operatorname{Re} Y_0^d = \frac{a}{15\pi^4 k} \int_0^k d\alpha C(\alpha) \beta \left\{ \int_0^{\beta b} J_0(t) dt - J_1(\beta b) \right\}, \quad (4.10a)$$

$$\begin{aligned} \operatorname{Im} Y_0^d = \frac{-a}{15\pi^4 k} \left\{ \int_0^k d\alpha C(\alpha) \beta \left[ \int_0^{\beta b} Y_0(t) dt - Y_1(\beta b) - \frac{2}{\pi \beta b} \right] \right. \\ \left. + \frac{2}{\pi} \int_k^\infty d\alpha C(\alpha) \gamma \left[ \int_0^{\gamma b} K_0(t) dt + K_1(\gamma b) - \frac{1}{\gamma b} \right] \right\}, \quad (4.10b) \end{aligned}$$

where  $\beta = (k^2 - \alpha^2)^{1/2}$ ,  $\gamma = (\alpha^2 - k^2)^{1/2}$ , and

$$C(\alpha) = \frac{\cos^2(\alpha a/2)}{1 - (\alpha a/\pi)^2}. \quad (4.11)$$

In summary, the direct contribution  $Y^d$  on a cone as given in (3.3) is divergent, due to an "illegal" interchange of integration and differentiation operators in the derivation process. The (correct) finite part of the divergent integral is given in (4.7), where  $Y_0^d$  is given in (4.10), and  $Y_1^d$  in (3.3) after replacing  $g$  by  $g_1$ . The same difficulty arises in the case of a cylinder, and it is treated by the same procedure as in the case of a cone.

## 5. NUMERICAL RESULTS

We have derived the input admittance  $Y$  of a slot on three types of surfaces: (i) For an infinite plane, the final solution  $Y = Y^d$  is given in (4.10). (ii) For an infinite cylinder,  $Y = Y^d$  is given in (4.7), where  $Y_1^d$  is calculated numerically from (3.3) after replacing  $g$  by  $g_1$ . The explicit form of  $g_1$  can be gathered from (4.4), (3.22), and (4.5). (iii) For an infinite cone,  $Y$  has two contributions as described in (3.2).  $Y^t$  is given in (3.18) and  $Y^d$  in (4.7). To calculate  $Y_1^d$ , we use (3.3) after replacing  $g$  by  $g_1$ , where  $g_1$  can be gathered from (4.4), (3.4), and (4.5). Numerical results of  $Y$  on the above three surfaces are presented below.

Slot on a plane. As a function of slot length  $a$ , we plot  $(a/2b)Y$  in Figure 4 for three different values of slot width  $b$ . Those curves are practically linear, and can be described to a good accuracy by, for  $0.4 \leq (a/\lambda) \leq 0.6$ ,

$$Y \approx \frac{2b}{a} \{ [1.029 + j0.596] + (3.75 + jB) \left( \frac{a}{\lambda} - 0.5 \right) \} \text{ millimho} \quad (5.1)$$

where  $B = 44, 33,$  and  $21$  for  $b = 0.0001\lambda, 0.001\lambda,$  and  $0.01\lambda,$  respectively.

Relation to dipole impedance. As discussed in [11], there is an alternative definition for the (input or mutual) admittance of a slot. Instead of (2.1), a modal voltage  $\bar{V}$  can be defined by

$$\vec{E} = \hat{z} \bar{V} \frac{1}{b} \cos \left( \frac{\pi}{a} y \right) \quad , \quad (5.2)$$

or equivalently,

$$\bar{V} = \int_{-b/2}^{b/2} (\vec{E} \cdot \hat{z})_{y=0} dz \quad (5.3)$$

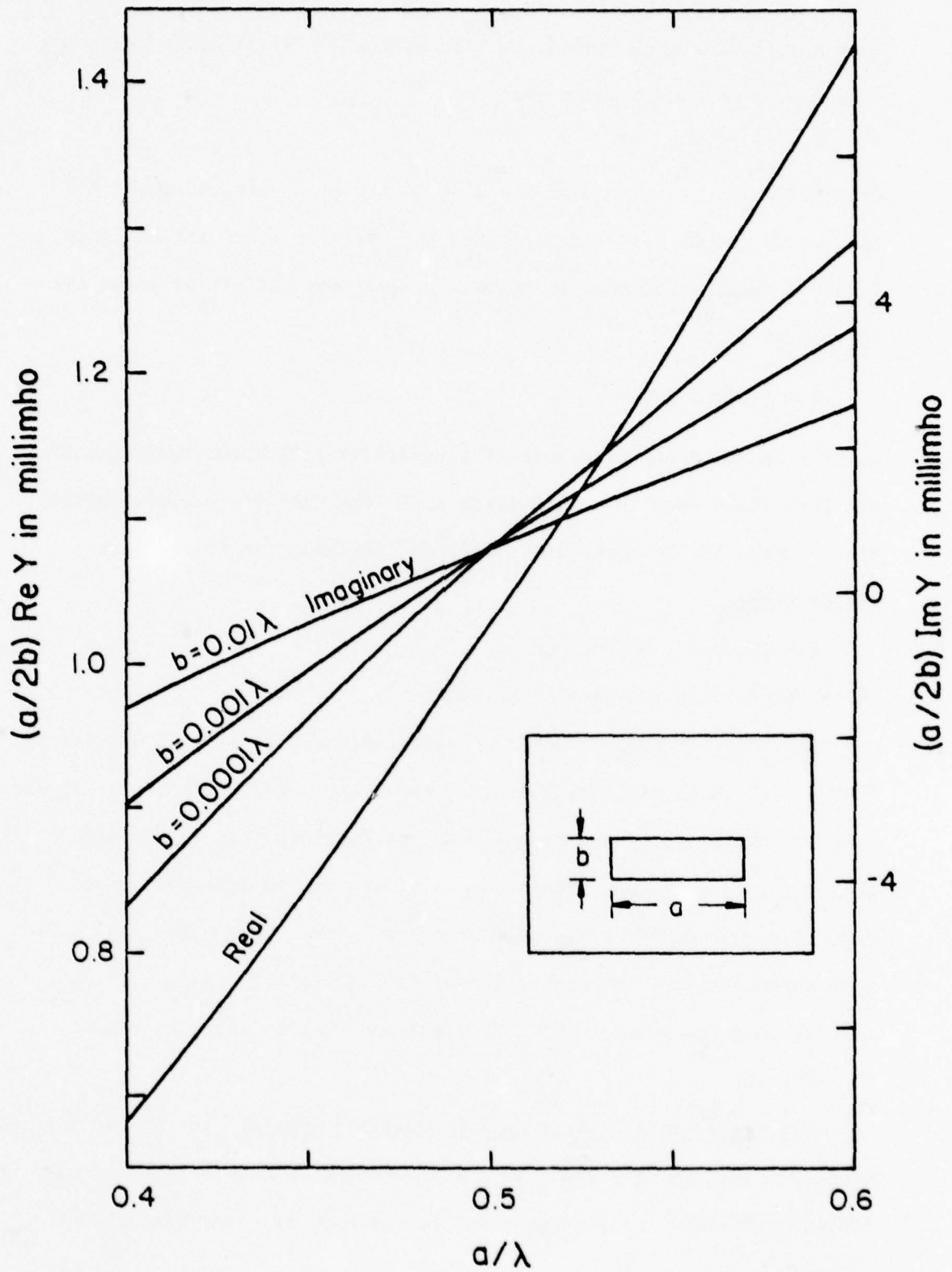


Figure 4. Input admittance of a slot on an infinite plane.

Then a different input impedance  $\bar{Y}$  is defined by (2.3) after replacing  $V$  by  $\bar{V}$ . It is easily shown that

$$\bar{Y} = (a/2b)Y \quad . \quad (5.4)$$

Conventionally,  $Y$  is used if the slot is fed by a waveguide, while  $\bar{Y}$  is used if the slot is centrally fed by a pair of transmission lines. From the duality relation in Maxwell's equations, it can be shown that (p. 519 of [2])

$$\bar{Z} = \frac{1}{4}(120\pi)^2(2\bar{Y}) \quad , \quad (5.5)$$

where  $\bar{Z}$  is the input impedance of a centrally fed dipole radiating in the free space (not in a half-space as in the case of a waveguide-fed slot). From (5.1), (5.4) and (5.5), we find that for a half-wave length dipole,

$$\bar{Z} = 73.12 + j 42.36 \quad \text{ohm} \quad , \quad (5.6)$$

which agrees with the results in [2], [10].

Slot on a cylinder. Consider a circumferential slot of dimensions 0.9" x 0.4" on an infinitely long cylinder whose radius is 3.8". Figure 5 shows  $Y$  calculated by the present GTD solution and that by the modal series solution in [5]. These two solutions are in agreement within 0.5% in magnitude and one degree in phase. Note that, under the "one-mode approximation," the modal series solution [5] is exact. It is amazing that the present GTD solution gives such an accurate result for  $kR \sim 18$ .

Slot on a cone: variation with radial distance. In all the following cone calculations, the slot has the dimensions of  $0.5\lambda \times 0.05\lambda$ , except where stated otherwise. In Figures 6 and 7, the slot is circumferentially

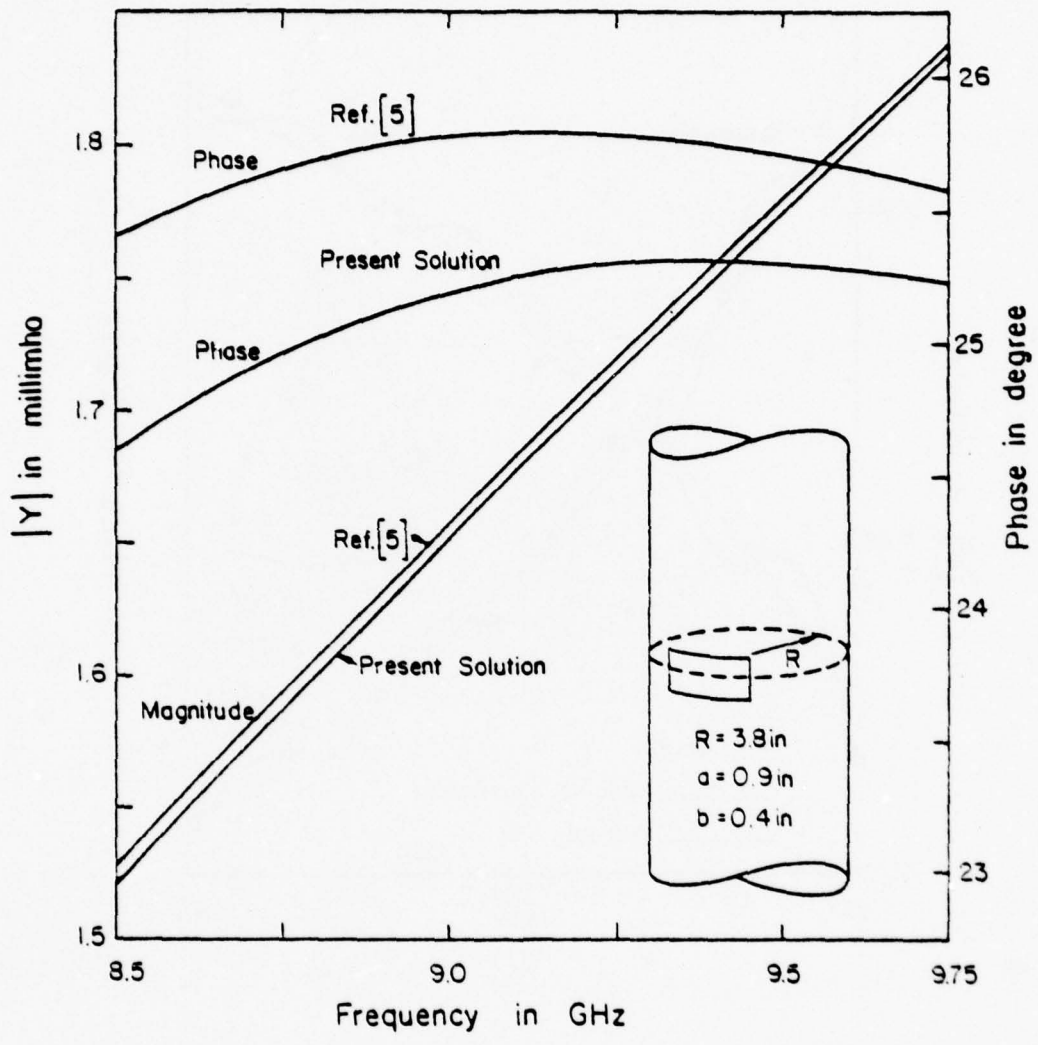


Figure 5. Input admittance of a slot on an infinitely long cylinder.

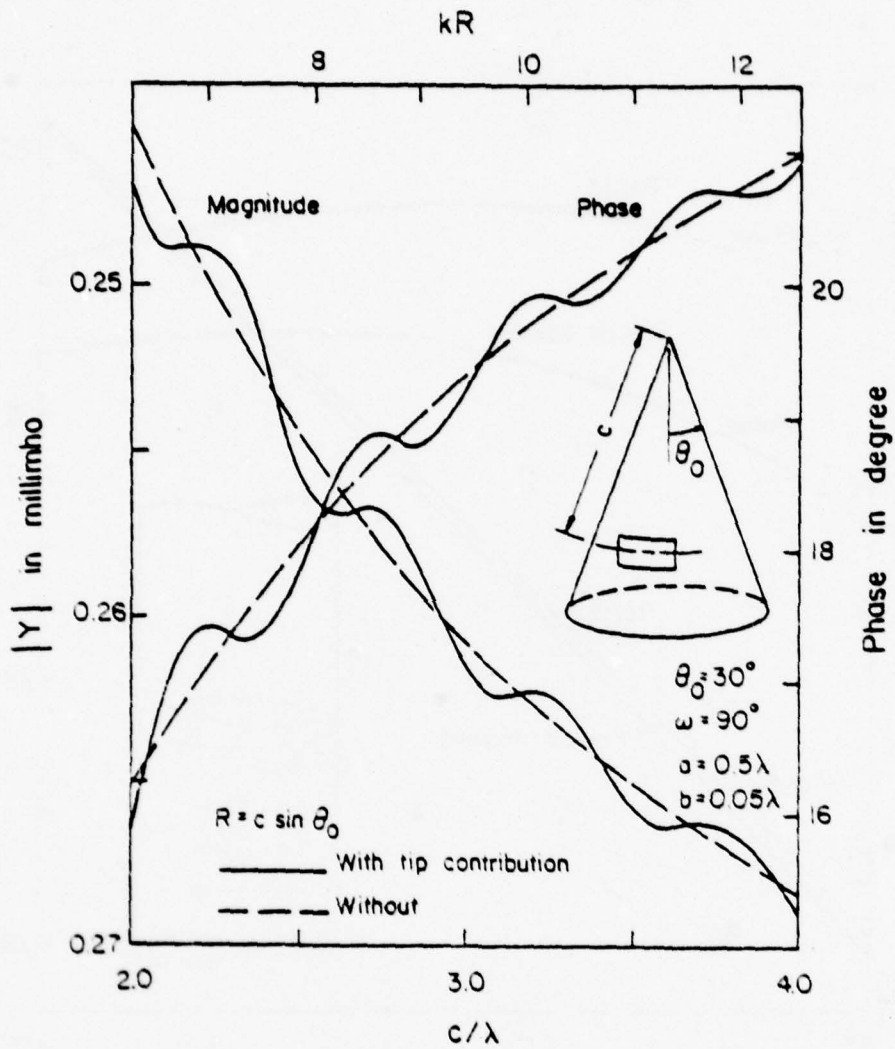


Figure 6. Input admittance of a slot on a cone as a function of radial distance  $c$ .

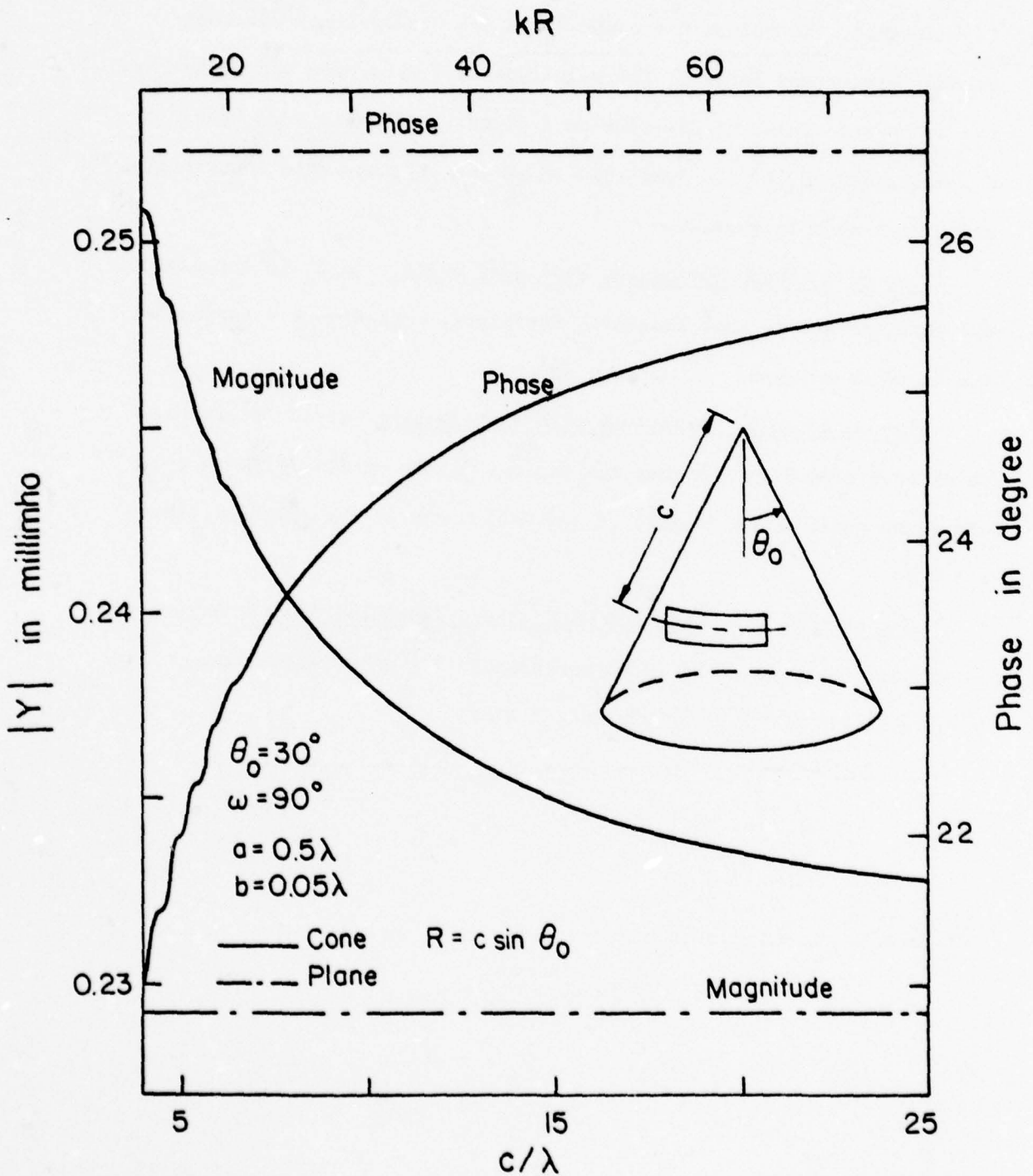


Figure 7. Same as Figure 6 except with larger radial distance  $c$ .

oriented on a cone with  $\theta_0 = 30^\circ$ , and the variation of  $Y$  with the radial distance  $c$  is presented. We observe two effects: (i) As  $c$  is increased, the radius  $R = c \sin \theta_0$  of the "equivalent" cylinder becomes larger and larger. The magnitude of  $Y$  decreases and approaches the asymptotic value of the slot on a plane. (ii) At  $c = 2\lambda$ , the tip contribution  $|Y^t|$  is less than 1% of the  $|Y|$ , and this contribution diminishes as  $c$  increases.

Slot on a cone: variations with cone angle. As  $\theta_0$  is increased, the cone surface becomes flatter. Therefore,  $Y$  in Figure 8 approaches its value on a plane.

Slot on a cone: variations with slot length. It is interesting to observe from Figure 9 that the minimum values of  $|Y|$  for both cone and plane cases occur roughly at  $a = 0.45\lambda$ , not at the resonant length  $a = 0.5\lambda$ .

Slot on a cone: variation with slot orientation angle. Figure 10 shows that there is about a 10% increase in  $|Y|$  as  $\omega$  varies from 0 (radial slot) to  $\pi/2$  (circumferential slot).

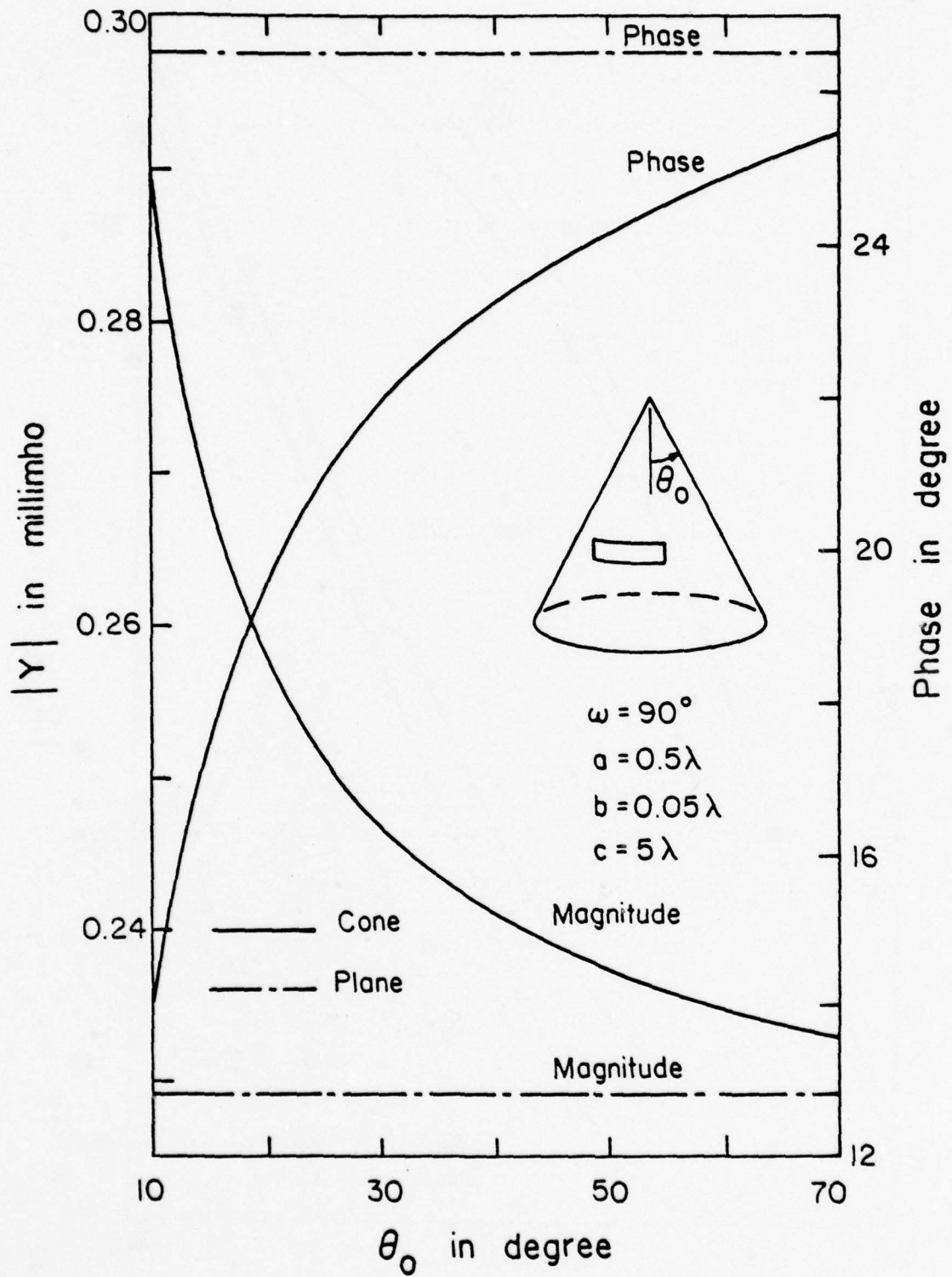


Figure 8. Input admittance of a slot on a cone as a function of half-cone angle  $\theta_0$ .

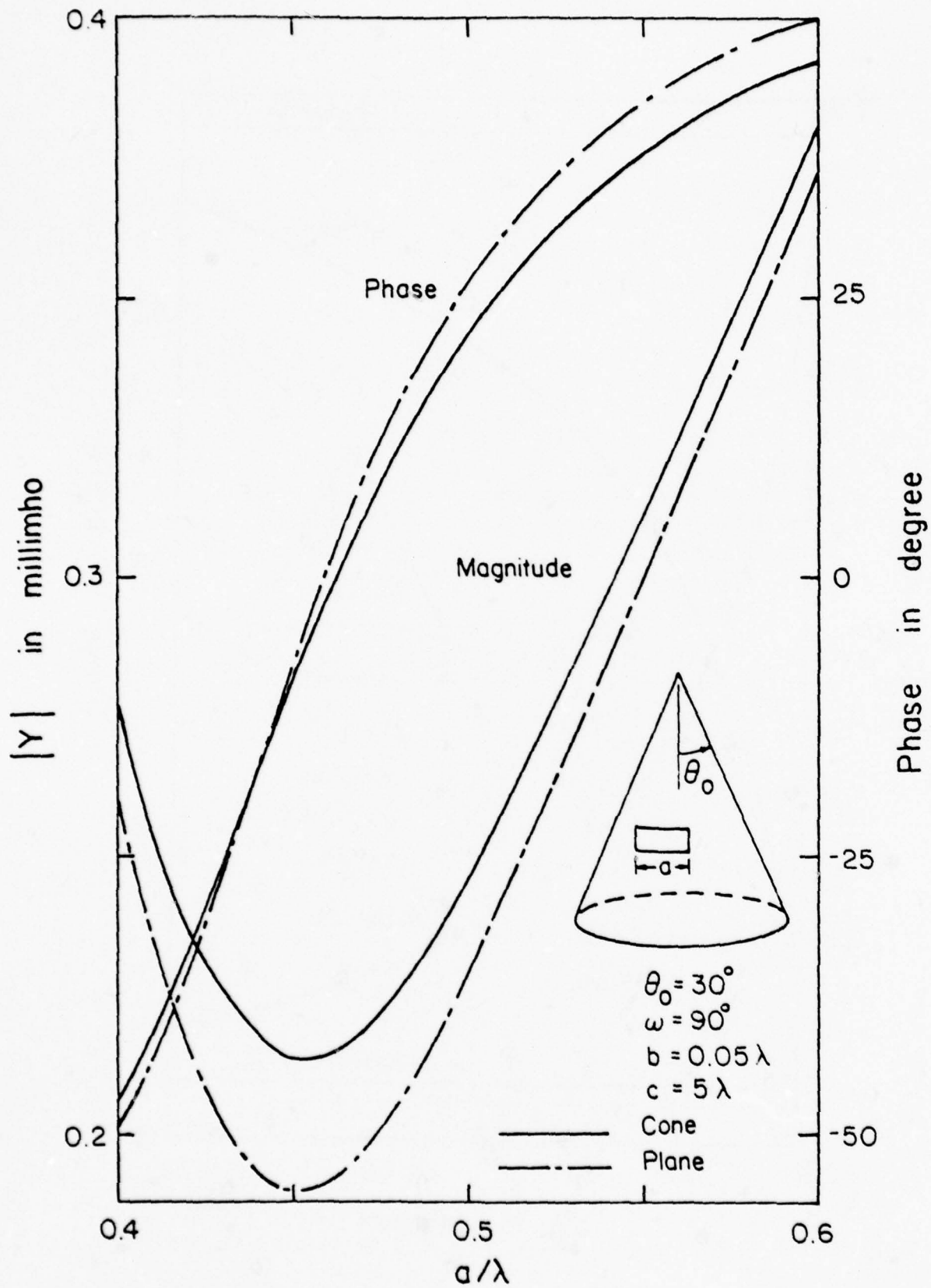


Figure 9. Input admittance of a slot on a cone as a function of slot length  $a$ .

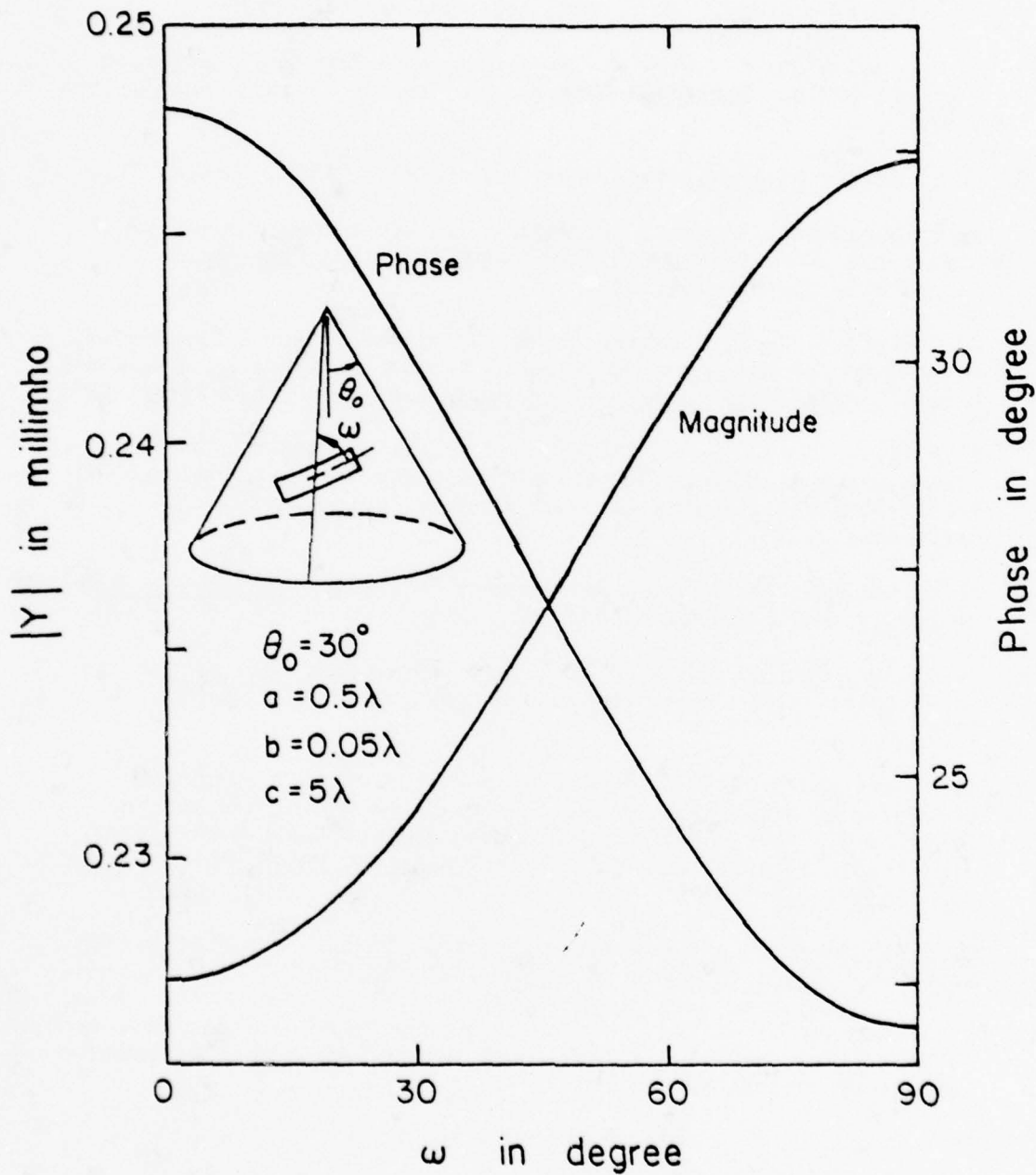


Figure 10. Input admittance of a slot on a cone as a function of orientation angle  $\omega$ .

#### REFERENCES

- [1] P. S. Carter, "Circuit relations in radiating systems and application to antenna problems," Proc. IRE, vol. 20, p. 1004, 1932.
- [2] E. C. Jordan and K. Balmain, Electromagnetic Waves and Radiating Systems, 2nd Ed. Englewood Cliffs, New Jersey: Prentice-Hall, 1968, Chapters 13 and 14.
- [3] J. D. Kraus, Antennas, New York: McGraw-Hill, 1950, Chapter 10.
- [4] G. V. Borgiotti, "A novel expression for the mutual admittance of planar radiating elements," IEEE Trans. Antennas Propagat., Vol. AP-16, pp. 329-334, 1968.
- [5] K. E. Golden, G. E. Stewart, and D. C. Pridmore-Brown, "Approximation techniques for the mutual admittance of slot antennas on metallic cones," IEEE Trans. Antennas Propagat., vol. AP-22, pp. 43-48, 1974.
- [6] P. C. Bargeliotis, A. T. Villeneuve, and W. H. Kummer, "Conformal phased array breadboard," Quarterly Progress Reports, Contract N00019-76-C-0495, Hughes Aircraft Company, Culver City, California, 1976.
- [7] J. B. Keller, "Diffraction by a convex cylinder," IEEE Trans. Antennas Propagat., vol. AP-14, pp. 312-321, 1956.
- [8] S. W. Lee, "Mutual admittance of slots on a cone: solution by ray techniques," IEEE Trans. Antennas Propagat., vol. AP-26, pp. 768-773, 1978.
- [9] S. W. Lee and S. Safavi-Naini, "Asymptotic solution of surface field due to a magnetic dipole on a cylinder," University of Illinois at Urbana-Champaign, Electromagnetics Laboratory Report No. 76-11, 1976; see also IEEE Trans. Antennas Propagat., vol. AP-26, pp. 593-598, 1978.
- [10] D. R. Rhodes, "On a fundamental principle in the theory of planar antennas," Proc. IEEE., vol. 52, pp. 1013-1021, 1964.
- [11] S. W. Lee and R. Mittra, "Mutual admittance between slots on a cylinder or cone," University of Illinois at Urbana-Champaign, Electromagnetics Laboratory, Report No. 77-24, December 1977.

APPENDIX A SIMPLIFICATION OF  $Y_0^d$

The input admittance  $Y_0^d$  of a slot on an infinite plane is given in (4.9). In this appendix, it is transformed into a form more suitable for numerical evaluation. Making use of the identity

$$G(s) = \frac{-k}{480\pi^3} \iint_{-\infty}^{\infty} dk_y dk_z \frac{\exp \{-j[k_y(y_2-y_1) + k_z(z_2-z_1)]\}}{(k^2 - k_y^2 - k_z^2)^{1/2}} \quad (A-1)$$

Equation (4.9) may be rewritten as

$$Y_0^d = \frac{ab}{60\pi^5 k} \iint_{-\infty}^{\infty} dk_y dk_z C(k_y) S(k_z) \frac{k^2 - k_y^2}{(k^2 - k_y^2 - k_z^2)^{1/2}} \quad (A-2)$$

where

$$S(k_z) = \frac{\sin^2(k_z b/2)}{(k_z b/2)^2} \quad (A-3)$$

$$C(k_y) = \frac{\cos^2(k_y a/2)}{1 - (k_y a/\pi)^2} \quad (A-4)$$

This result is identical to that obtained by Borgiotte [4], which is derived from a different method. Following Rhodes [10] who has studied a similar integral, we separate (A-2) into real and imaginary parts.

Consider first the real part

$$\text{Re}Y_0^d = \frac{ab}{15\pi^5 k} \int_0^k dk_y C(k_y) (k^2 - k_y^2) \int_0^{(k^2 - k_y^2)^{1/2}} dk_z \frac{S(k_z)}{(k^2 - k_y^2 - k_z^2)^{1/2}} \quad (A-5)$$

By a change of variable  $k_z = (k^2 - k_y^2)^{1/2} \cos \eta$ , the inner integral of the preceding equation is transformed into

$$\int_0^{(k^2 - k_y^2)^{1/2}} dk_z \frac{S(k_z)}{(k^2 - k_y^2 - k_z^2)^{1/2}} = \frac{4}{b^2 (k^2 - k_y^2)} \int_0^{\pi/2} d\eta \frac{\sin^2(\cos \eta (k^2 - k_y^2)^{1/2} b/2)}{\cos^2 \eta} \quad (A-6)$$

Differentiating the integral on the right twice with respect to the parameter  $b(k^2 - k_y^2)^{1/2}$ , we obtain

$$\frac{1}{2} \int_0^{\pi/2} d\eta \cos(b(k^2 - k_y^2)^{1/2} \cos \eta) \quad , \quad (A-7)$$

which is equal to  $\pi/4 J_0(b(k^2 - k_y^2)^{1/2})$ . Then, integrating  $J_0$  twice and applying the recurrence formulas of Bessel's functions, the integral in (A-6) becomes

$$\frac{\pi}{b(k^2 - k_y^2)^{1/2}} \left\{ \int_0^{b(k^2 - k_y^2)^{1/2}} dt J_0(t) - J_1(b(k^2 - k_y^2)^{1/2}) \right\} \quad . \quad (A-8)$$

Substituting this result into Equation A-5, the real part of  $Y_0^d$  is reduced to

$$\text{Re}\{Y_0^d\} = \frac{a}{15\pi^4 k} \int_0^k dk_y C(k_y) (k^2 - k_y^2)^{1/2} \left\{ \int_0^{b(k^2 - k_y^2)^{1/2}} dt J_0(t) - J_1(b(k^2 - k_y^2)^{1/2}) \right\} \quad . \quad (A-9)$$

Next, we study the imaginary part of  $Y_0^d$ , which is

$$\begin{aligned} I_m Y_0^d = \frac{ab}{15\pi^5 k} \left\{ \int_0^k dk_y C(k_y) (k^2 - k_y^2)^{1/2} \int_{(k^2 - k_y^2)^{1/2}}^{\infty} dk_z \frac{S(k_z)}{(k_z^2 - (k^2 - k_y^2))^{1/2}} \right. \\ \left. - \int_k^{\infty} dk_y C(k_y) (k_y^2 - k^2)^{1/2} \int_0^{\infty} dk_z \frac{S(k_z)}{(k_z^2 + (k_y^2 - k^2))^{1/2}} \right\} \quad . \quad (A-10) \end{aligned}$$

By another change of variables,  $k_z = (k^2 - k_y^2)^{1/2} \cosh \eta$  in the first inner integral of the above equation and  $k_z = (k_y^2 - k^2)^{1/2} \sinh \eta$  in the second integral, we have

$$\int_{(k^2 - k_y^2)^{1/2}}^{\infty} dk_z \frac{S(k_z)}{k_z^2 - (k^2 - k_y^2)} = \frac{4}{b^2(k^2 - k_y^2)} \int_0^{\infty} d\eta \frac{\sin^2(\cosh \eta (k^2 - k_y^2)^{1/2} b/2)}{\cosh^2 \eta} \quad , \quad (A-11)$$

$$\int_0^{\infty} dk_z \frac{S(k_z)}{(k_z^2 + (k_y^2 - k^2))^{1/2}} = \frac{4}{b^2(k_y^2 - k^2)} \int_0^{\infty} d\eta \frac{\sin^2(\sinh \eta (k_y^2 - k^2)^{1/2} b/2)}{\sinh^2 \eta} \quad (A-12)$$

It can be shown that the integrals on the right-hand sides of (A-11)

and (A-12) are, respectively, related to Neumann's functions

$(Y_0, Y_1)$  and the modified Bessel's functions of the second kind

$(K_0, K_1)$  by

$$\int_0^{\infty} d\eta \frac{\sin^2(\cosh \eta (k^2 - k_y^2)^{1/2} b/2)}{\cosh^2 \eta} = -\frac{\pi}{4} b(k^2 - k_y^2)^{1/2} \left\{ \int_0^{b(k^2 - k_y^2)^{1/2}} dt Y_0(t) - Y_1(b(k^2 - k_y^2)^{1/2}) - \frac{2}{\pi b(k^2 - k_y^2)^{1/2}} \right\} \quad (A-13)$$

and

$$\int_0^{\infty} d\eta \frac{\sin^2(\sinh \eta (k_y^2 - k^2)^{1/2} b/2)}{\sinh^2 \eta} = b(k_y^2 - k^2)^{1/2} \left\{ \int_0^{b(k_y^2 - k^2)^{1/2}} dt K_0(t) + K_1(b(k_y^2 - k^2)^{1/2}) - \frac{1}{b(k_y^2 - k^2)^{1/2}} \right\} \quad (A-14)$$

Substituting these results into (A-10), the imaginary part of  $Y_0^d$  is

reduced to

$$\begin{aligned} I_m Y_0^d = & -\frac{a}{15\pi^4 k} \left\{ \int_0^k dk_y C(k_y) (k^2 - k_y^2)^{1/2} \left[ \int_0^{b(k^2 - k_y^2)^{1/2}} dt Y_0(t) \right. \right. \\ & \left. \left. - Y_1(b(k^2 - k_y^2)^{1/2}) - \frac{2}{\pi b(k^2 - k_y^2)^{1/2}} \right] + \frac{2}{\pi} \int_k^{\infty} dk_y C(k_y) (k_y^2 - k^2)^{1/2} \right. \\ & \left. \cdot \left[ \int_0^{b(k_y^2 - k^2)^{1/2}} dt K_0(t) + K_1(b(k_y^2 - k^2)^{1/2}) - \frac{1}{b(k_y^2 - k^2)^{1/2}} \right] \right\} \quad (A-15) \end{aligned}$$

The final results in (A-9) and (A-15) are duplicated in (4.10) after an obvious change of notations.

THIS PAGE IS BEST QUALITY PRACTICABLE  
FROM COPY FURNISHED TO DDC

APPENDIX B1

COMPUTER PROGRAM OF Y FOR CYLINDER

```
PROGRAM MAIN ( INPUT,OUTPUT,TAPE3=OUTPUT )
COMPLEX Y11,YPL,YDIF,PY11,PYPL,PYDIF,CJ,CONA
COMMON A,B,R,AK,AKA,AKB,AKR,SB,SC,SE,THIRD,PI,CONST,CJ,CONA
CJ=(0.,1.)
PI=3.1415926536
THIRD=1./3.
READ*,AIN,BIN,RIN,FREQ
AK=20.*PI*FREQ/3.
A=AIN*0.0254
B=BIN*0.0254
R=RIN*0.0254
AKA=AK*A
AKB=AK*B
AKR=AK*R
CALL PLANE ( YPL,AK,A,B )
CALL DIFF ( YDIF,5 )
Y11=YPL+YDIF
PYPL=YPL
PYDIF=YDIF
PY11=Y11
CALL XTOP ( PYPL )
CALL XTOP ( PY11 )
CALL XTOP ( PYDIF )
WRITE(3,1) FREQ,A,AIN,B,BIN,R,RIN,YPL,PYPL,YDIF,PYDIF,Y11,PY11
1  FORMAT(/T10,"INPUT :",/T10,"FREQ =",F8.3," GHZ",
$/T10,"A    =",F8.3," METER =",F8.3," INCH",
$/T10,"B    =",F8.3," METER =",F8.3," INCH",
$/T10,"R    =",F8.3," METER =",F8.3," INCH",
$///T10,"OUTPUT :",/T10,"Y11",
$/T23,"REAL",T38,"IMAGINARY",T53,"MAGNITUDE",T68,"PHASE",
$/T10,"PLANE",T20,3E15.7,E12.4,
$/T10,"DIFFERENCE",T20,3E15.7,E12.4,
$/T10,"CYLINDER",T20,3E15.7,E12.4)
STOP
END
```

```
SUBROUTINE SELF ( RESULT )
COMPLEX FTH,FY,RESA,RESD,RES1,RES2,RES3,RESY,RESULT,CJ,CONA
EXTERNAL FTH,FA,FY
COMMON A,B,R,AK,AKA,AKB,AKR,SB,SC,SE,THIRD,PI,CONST,CJ,CONA
COMMON /DATA2/ Y1,Z1,Y2,ZL,ZU
Y1=0.
Z1=0.
SB=0.7*SC
SD=0.7*SC
THL=PI/2.
CALL RGG ( FA,0.,THL,B,RES )
RESA=CONA*SQRT(2.*A)*RES
CALL CGR ( FTH,0.,THL,B,RESD )
CALL CGR ( FY,0.,SD,SD,RES1 )
CALL CGR ( FY,SD,SC,SD,RES2 )
CALL CGR ( FY,SC,SE,SD,RES3 )
RESY=RES1-RES2+RES3
RESULT=4.* RESA+RESD+RESY )
RETURN
END
```

PRECEDING PAGE BLANK

THIS PAGE IS BEST QUALITY PRACTICABLE  
FROM COPY FURNISHED TO DDG

```
SUBROUTINE DIFF ( YDIF,NY )
COMPLEX FY2,CJ,CONA,SPLINE,YDIF
COMPLEX TOTAL,RESULT,RES1,RES2,RES3,RES4
REAL SP(12)
EXTERNAL FY2
COMMON A,B,R,AK,AKA,AKB,AKR,SB,SC,SE,THIRD,PI,CONST,CJ,CONA
COMMON /DATA2/ Y1,Z1,Y2,ZL,ZU
DATA SP/7.,16.,14.,16.,14.,16.,14.,15.,14.,15.,14.,16./
CONA=(1.-CJ)/( 1920.*R*PI*SQRT(AK*PI) )
AN4=4*NY
N2=2*NY-1
DY=A/AN4
DZ=B/10.
SC=AMIN1(DY/3.,DZ,.1E-1)
SE=3.*SC
CALL SELF ( RESULT )
YDIF=(0.,0.)
DO 200 IZ=1,5,2
IF(IZ.EQ.1) EZ=1.
IF(IZ.NE.1) EZ=2.
Z1=DZ*(IZ-1)
SPLINE=(0.,0.)
DO 100 IY=1,N2,2
ISP=(IY+1)/2
Y1=DY*(IY-1)
RES1=RES2=RES3=RES4=(0.,0.)
ZL=-B/2.
ZU= B/2.
YL=-A/2.
YU=Y1-SE
IF(YU.GT.YL) CALL CGQ ( FY2,YL,YU,B,RES1 )
YL=Y1+SE
YU=A/2.
IF(YU.GT.YL) CALL CGQ ( FY2,YL,YU,B,RES2 )
YL=Y1-SE
YU=Y1
ZL=-B/2.
ZU=Z1-SC
IF(ZU.GT.ZL) CALL CGQ ( FY2,YL,YU,B,RES3 )
ZL=Z1+SC
ZU=B/2.
IF(ZU.GT.ZL) CALL CGQ ( FY2,YL,YU,B,RES4 )
TOTAL=RESULT+RES1+RES2+RES3+RES4+RES3+RES4
TOTAL=TOTAL*COS(PI*Y1/A)
SPLINE=SPLINE+SP( ISP )*TOTAL
100 CONTINUE
SPLINE=2.*DY*SPLINE/15.
YDIF=YDIF+EZ*SPLINE
200 CONTINUE
YDIF=DZ*YDIF
YDIF=-B.*YDIF/A/B
RETURN
END
```

THIS PAGE IS BEST QUALITY PRACTICABLE  
 FROM COPY FURNISHED TO DDQ

```

FUNCTION FATH)
COMPLEX CJ,CONA
COMMON A,B,R,AK,AKA,AKB,AKR,SB,SC,SE,THIRD,PI,CONST,CJ,CONA
COSX=COS(TH)
COSX=ABS(COSX)
X=PI*COSX*SB/A
CALL FRESNEL ( C,S,X )
FA=C*COSX*(2.-3.*COSX*COSX)*SQRT(COSX)
RETURN
END
  
```

```

COMPLEX FUNCTION FTH(TH)
COMPLEX FS,CJ,CONA,CONV
EXTERNAL FS
COMMON /DATA/ SIN2,COS2,SIN4,COS4,COS2X,XCON,YCON,CONV
COMMON A,B,R,AK,AKA,AKB,AKR,SB,SC,SE,THIRD,PI,CONST,CJ,CONA
COSX=COS(TH)
COS2=COSX*COSX
SIN2=1.-COS2
SIN4=SIN2*SIN2
COS4=COS2*COS2
COS2X=1.-2.*SIN2
XCON=AKR*COS4/2.
YCON=XCON**THIRD/R
CONST=COS4/(2.*AKR*AKR)
CONV=CJ*CONST**THIRD
CALL CGQ2 ( FS,0.,SB,32,FTH )
RETURN
END
  
```

```

COMPLEX FUNCTION FS(S)
COMPLEX UX,UX,UPX,UPX,GS
COMPLEX GCYL,GPL,GDIF,APP,CJ,JONS,CONA,CONV
COMMON /DATA/ SIN2,COS2,SIN4,COS4,COS2X,XCON,YCON,CONV
COMMON A,B,R,AK,AKA,AKB,AKR,SB,SC,SE,THIRD,PI,CONST,CJ,CONA
FS=(0.,0.)
IF(S.LT.1.E-50) RETURN
AKS=AK*S
JONS=CJ/AKS
K=XCON*S
CALL FOCK ( X,UX,UX,UPX,UPX )
GS=CMPLX( COS(AKS),-SIN(AKS) )/AKS
GCYL=UX*(SIN2+JONS*COS2X)
$   +UPX*CONV*SIN2
$   +UPX*CONV*JONS*COS2
IF(COS2.GE.1.E-50) GCYL=GCYL+UPX*CONV*SIN4/COS2
IF(COS2.LT.1.E-50) GCYL=GCYL+0.375*(1.-CJ)*SQRT(PI*AKS)/AKR
GPL=SIN2+JONS*(2.-3.*SIN2)*(1.-JONS)
GDIF=GS*(GCYL-GPL)
IF(S.GT.1.E-9) GOTO 10
RE=REAL(GDIF)
GDIF=CMPLX(RE,-RE)
GDIF=RS*GDIF
APP=CONA*COS2*(2.-3.*COS2)/SQRT(S)
FS=GDIF-APP
FS=FS*COS(YCON)
RETURN
END
  
```

10

THIS PAGE IS BEST QUALITY PRACTICABLE  
FROM COPY FURNISHED TO DDC

```
COMPLEX FUNCTION FY(Y2)
COMPLEX FZ,CJ,CONA
EXTERNAL FZ
COMMON A,B,R,AK,AKA,AKB,AKR,SB,SC,SE,THIRD,PI,CONST,CJ,CONA
COMMON /DATA2/ Y1,Z1,TY,ZL,ZU
TY=Y2
IF(SB.GE.Y2) ZL=SQRT(SB*SB-Y2*Y2)
IF(SB.LT.Y2) ZL=0.
CALL CGQ2 ( FZ,ZL,SC,9,FY )
FY=FY*COS(PI*Y2/A)
RETURN
END
```

```
COMPLEX FUNCTION FZ(Z2)
COMPLEX UX,UX,UPX,UPX,GS
COMPLEX BCYL,GPL,CJ,JONS,CONA,CONV
COMMON A,B,R,AK,AKA,AKB,AKR,SB,SC,SE,THIRD,PI,CONST,CJ,CONA
COMMON /DATA2/ Y1,Z1,Y2,ZL,ZU
OY=Y2-Y1
OZ=Z2-Z1
S=SQRT(OY*OY+OZ*OZ)
IF(S.LT.1.E-50) RETURN
COSX=OY/S
COS2=COSX*COSX
SIN2=1.-COS2
SIN4=SIN2*SIN2
COS4=COS2*COS2
COS2X=1.-2.*SIN2
AKB=AK*S
JONS=CJ/AKS
K=AKR*COS4/2.
L=X**THIRD*S/R
CALL FOCK ( X,UX,UX,UPX,UPX )
GS=CMPLX( COS(AKS),-SIN(AKS) )/AKS
CONST=COS4/(2.*AKR*AKR)
CONV=CJ*CONST**THIRD
BCYL=UX*(SIN2+JONS*COS2X)
      +UX*JONS*(COS2*(1.-2.*JONS)+JONS*SIN2)
      +UPX*CONV*SIN2
      +UPX*CONV*JONS*COS2
IF(COS2.GE.1.E-50) BCYL=BCYL+UPX*CONV*SIN4/COS2
IF(COS2.LT.1.E-50) BCYL=BCYL+0.375*(1.-CJ)*SQRT(PI*AKS)/AKR
GPL=SIN2+JONS*(2.-3.*SIN2)*(1.-JONS)
FZ=GS*(BCYL-GPL)
RETURN
END
```

```
COMPLEX FUNCTION FY2(Y2)
COMPLEX FZ,CJ,CONA
EXTERNAL FZ
COMMON A,B,R,AK,AKA,AKB,AKR,SB,SC,SE,THIRD,PI,CONST,CJ,CONA
COMMON /DATA2/ Y1,Z1,TY,ZL,ZU
TY=Y2
OY=ABS(Y2-Y1)
NI=8
IF(OY.LT..5E-1) NI=16
IF(OY.LT..1E-1) NI=32
CALL CGQ2 ( FZ,ZL,ZU,NI,FY2 )
FY2=FY2*COS(PI*Y2/A)
RETURN
END
```

THIS PAGE IS BEST QUALITY PRACTICABLE  
FROM COPY FURNISHED TO DDO

APPENDIX B2

COMPUTER PROGRAM OF Y FOR CONE

```
PROGRAM MAIN ( INPUT,OUTPUT,TAPE3=OUTPUT )
COMPLEX YPL,YDIF,YTIP,YDIR,Y11,PYPL,PYDIF,PYDIR,PY11
COMMON PI,AK,A,B,B2,B3,B6,C,OMEQ,SINO,COSO,TANO,BEL
PI=3.1415926536
READ *,FREQ,A,B,C,OME,THETA
AK=20.*PI*FREQ/3.
THETAQ=THETA*PI/180.
OMEQ=OME*PI/180.
SINO=SIN(OMEQ)
COSO=COS(OMEQ)
TANO=TAN(THETAQ)
B2=B/2.
B3=B/3.
B6=B/6.
CALL PLANE ( YPL,AK,A,B )
CALL DIFFER ( YDIF,3 )
TANO=THETAQ
CALL TIP ( YTIP )
AIN=A/0.0254
BIN=B/0.0254
CIN=C/0.0254
YDIR=YPL+YDIF
Y11=YDIR+YTIP
PYPL=YPL
PYDIF=YDIF
PYDIR=YDIR
PYTIP=YTIP
PY11=Y11
CALL XTOP ( PYPL )
CALL XTOP ( PYDIF )
CALL XTOP ( PYDIR )
CALL XTOP ( PYTIP )
CALL XTOP ( PY11 )
WRITE(3,1) FREQ,THETA,OME,A,AIN,B,BIN,C,CIN,
YPL,PYPL,YDIF,PYDIF,YDIR,PYDIR,YTIP,PYTIP,Y11,PY11
STOP
```

```
1  FORMAT(/T10,'INPUT :',/T10,'FREQ =',F12.7,' GHZ',
$ T10,'THETA =',F12.7,' DEGREE',
$/T10,'OMEGA =',F12.7,' DEGREE',
$/T10,'A =',F12.7,' METER =',F12.7,' INCH',
$/T10,'B =',F12.7,' METER =',F12.7,' INCH',
$/T10,'C =',F12.7,' METER =',F12.7,' INCH',
$/T10,'OUTPUT :',/T10,'Y11',
$/T3,'REAL',T38,'IMAGINARY',T53,'MAGNITUDE',T58,'PHASE',
$/T10,'PLANE',T20,3E15.7,E12.4,
$/T10,'DIFFERENCE',T20,3E15.7,E12.4,
$/T10,'DIRECT',T20,3E15.7,E12.4,
$/T10,'TIP',T20,3E15.7,E12.4,
$/T10,'CONE',T20,3E15.7,E12.4)
END
```

THIS PAGE IS BEST QUALITY PRACTICABLE  
FROM COPY FURNISHED TO DDC

```
SUBROUTINE DIFFER ( YDIF,NY )
COMPLEX YDIF,CJ,SUMY,RESULT
COMMON PI,AK,A,B,B2,B3,B6,C,OME0,SINO,COSO,TANO,DEL
DATA CJ/(0.,1.)/
N2=2*NY-1
DY=A/FLDAT(2*NY)
YDIF=(0.,0.)
DO 100 IZ=1,3
Z1=B3*(IZ-2)
SUMY=(0.,0.)
DO 200 IY=1,N2
Y1=DY*(IY-NY)
CALL HY2 ( RESULT,Y1,Z1 )
RESULT=RESULT*COS(PI*Y1/A)
IS=((IY+1)/2)-(IY/2)
SUMY=SUMY+RESULT*(1+IS*2)
200 CONTINUE
YDIF=YDIF+SUMY*DY/15.
100 CONTINUE
YDIF=CJ*AK*AK*B3*YDIF/(120.*PI*PI*AK*B)
RETURN
END
```

```
SUBROUTINE TIP ( YTIP )
COMPLEX CJ,YTIP,T,SIGMA
COMMON PI,AK,A,B,B2,B3,B6,C,OME0,SINO,COSO,THETA,DEL
CJ=(0.,1.)
SA=1.3057/THETA-1.755+2.772*THETA-1.459*THETA*THETA
SB=2.7195+1.4608*THETA-1.1295*THETA*THETA+0.6566*THETA**3
SIGMA=SA*( COS(SB)+CJ*SIN(SB) )
AKB2=AK*B/2.
SINX=SIN(AKB2)/AKB2
AKC2=2.*AK*C
T=COS(AKC2)-CJ*SIN(AKC2)
T=SIGMA*AK*B*SINX*SINX*(1.+CJ)*T/(30.*PI*AK*C)
T=T/SQRT(SIN(THETA)*COS(THETA)*4.*PI)
YTIP=T*SINO*SINO
RETURN
END
```

```
COMPLEX FUNCTION FA(TH)
COMPLEX CJ
COMMON PI,AK,A,B,B2,B3,B6,C,OME0,SINO,COSO,TANO,DEL
COMMON /DATA/ Y1,Z1,R1,PH1,Y2,PTH
DATA CJ/(0.,1.)/
COST=ABS(COS(TH))
ARG=PI*DEL*COST/A
CALL FRESNEL ( CF,SF,ARG )
CON=SQRT(2.*A/COST)
FA=SQRT(DEL)*SIN(ARG)-CON/C.*SF
FA=-CJ*AK*DEL/ARG*FA+CON*CF
SINA=SIN(OME0+PH1-TH)
FA=FA*(2.-3.*COST*COST)*SINA*SINA
RETURN
END
```

THIS PAGE IS BEST QUALITY PRACTICABLE  
FROM COPY FURNISHED TO DDO

```
SUBROUTINE HY2 ( RESULT,Y1,Z1 )
COMPLEX CJ,FY2,FTH,FA,RES1,RES2,RESULT
EXTERNAL FY2,FTH,FA
COMMON PI,AK,A,B,B2,B3,B6,C,OME0,SINO,COSO,TANO,DEL
COMMON /DATA/ Y1,TZ1,R1,PH1,Y2,TH
DATA ZERO,CJ/.1E-50,(0.,1.)/
TY1=Y1
TZ1=Z1

DEL=0.95*AMIN1((B2-Z1),(Z1+B2))
S1SQ=Z1*Z1+Y1*Y1
IF(S1SQ.LT.ZERO) GOTO 100
S1=SQRT(S1SQ)
SINI=Z1/S1
COS1=Y1/S1
SIND=SINO*COS1-COSO*SINI
COSD=COSO*COS1+SINO*SINI
R1SQ=C*C+S1SQ-2.*C*S1*COSD
R1=SQRT(R1SQ)
PHI=ASIN(S1*SIND/R1)
GOTO 200
100 R1=C
PHI=0.
200 CONTINUE

THL=OME0+PHI
THU=THL+PI/2.
CALL CGQ ( FA,THL,THU,8,RES1 )
THL=THU
THU=THL+PI/2.
CALL CGQ ( FA,THL,THU,8,RES2 )
RESULT=(1.+CJ)*SQRT(PI/AK)/(4.*KAN*AK*R1*TANO)*(RES1+RES2)
THL=OME0+PHI
THU=THL+PI
CALL CGQ ( FTH,THL,THU,8,RES1 )
THL=THU
THU=THL+PI
CALL CGQ ( FTH,THL,THU,8,RES2 )
RESULT=RESULT+RES1+RES2
RES1=(0.,0.)
YL=-A/2.
YU=Y1-DEL
NI=16.*(YU-YL)/A
IF(YU.GT.YL) CALL CGQ ( FY2,YL,YU,NI,RES1 )
RESULT=RESULT+RES1
NI=12.*DEL/B2
YL=YU
YU=Y1
CALL CGQ ( FY2,YL,YU,NI,RES1 )
YL=YU
YU=Y1+DEL
CALL CGQ ( FY2,YL,YU,NI,RES2 )
RESULT=RESULT+RES1+RES2
RES2=(0.,0.)
YL=YU
YU=A/2.
NI=16.*(YU-YL)/A
IF(YU.GT.YL) CALL CGQ ( FY2,YL,YU,NI,RES2 )
RESULT=RESULT+RES2
RETURN
END
```

THIS PAGE IS BEST QUALITY PRACTICABLE  
FROM COPY FURNISHED TO DDC

```
COMPLEX FUNCTION FTH(TH)
COMPLEX FS
EXTERNAL FS
COMMON PI,AK,A,B,B2,B3,B6,C,OME0,SINO,COSO,TANO,DEL
COMMON /DATA/ Y1,Z1,R1,PH1,Y2,PTH
PTH=TH
CALL CGQ2 ( FS,0.,DEL,16,FTH )
RETURN
END
```

```
COMPLEX FUNCTION FS(S)
COMPLEX FZ2
COMMON PI,AK,A,B,B2,B3,B6,C,OME0,SINO,COSO,TANO,DEL
COMMON /DATA/ Y1,Z1,R1,PH1,Y2,TH
Y2=S*COS(TH)
Z2=S*SIN(TH)
FS=FZ2(Z2)
FS=S*FS*COS(PI*Y2/A)
RETURN
END
```

```
COMPLEX FUNCTION FY2(Y2)
COMPLEX FZ2,RES1,RES2,RES3
EXTERNAL FZ2
COMMON PI,AK,A,B,B2,B3,B6,C,OME0,SINO,COSO,TANO,DEL
COMMON /DATA/ Y1,Z1,R1,PH1,Y2,TH
TY2=Y2
RES1=RES2=RES3=(0.,0.)
DY=ABS(Y2-Y1)
N1=N2=3
IF(Z1.GT. DEL) N2=16
IF(Z1.LT.-DEL) N1=16
IF(DY.GT.DEL) GOTO 1000
ZC=SQRT(DEL*DEL-DY*DY)
ZU=B2
ZL=Z1+ZC
IF(ZU.GT.ZL) CALL CGQ2 ( FZ2,ZL,ZU,N1,RES1 )
ZU=Z1-ZC
ZL=-B2
IF(ZU.GT.ZL) CALL CGQ2 ( FZ2,ZL,ZU,N2,RES2 )
FY2=RES1+RES2
GOTO 3000
1000 IF(DY.GE.B3) GOTO 2000
ZU=B2
ZL=Z1-DEL/2.
CALL CGQ2 ( FZ2,ZL,ZU,N1,RES1 )
ZU=ZL
ZL=Z1-DEL/2.
CALL CGQ2 ( FZ2,ZL,ZU,15,RES2 )
ZU=ZL
ZL=-B2
CALL CGQ2 ( FZ2,ZL,ZU,N2,RES3 )
FY2=RES1+RES2+RES3
GOTO 3000
2000 ZU=B2
ZL=-B2
CALL CGQ2 ( FZ2,ZL,ZU,4,FY2 )
3000 FY2=FY2*COS(PI*Y2/A)
RETURN
END
```

THIS PAGE IS BEST QUALITY PRACTICABLE  
FROM COPY FURNISHED TO DDG

```
COMPLEX FUNCTION FZ2(Z2)
COMPLEX U,U,VP,UP,GS
COMPLEX CJ,JOKS,HB,HT,GC,GP,GA
COMMON PI,AK,A,B,B2,B3,B4,C,OME0,SINO,COSO,TANO,DEL
COMMON /DATA/ Y1,Z1,R1,PH1,Y2,TH
DATA ZERO,THIRD,CJ/.1E-50,.3333333333333333,(0.,1.)
S2SQ=Z2*Z2+Y2*Y2
IF(S2SQ.LT.ZERO) GOTO 1000
S2=SQRT(S2SQ)
SIN2=Z2/S2
COS2=Y2/S2
SIND=SINO*COS2-COSO*SIN2
COSD=COSO*COS2+SINO*SIN2
R2SQ=C*C+S2SQ-2.*C*S2*COSD
R2=SQRT(R2SQ)
PH2=ASIN(S2*SIND/R2)
GOTO 2000
1000 R2=C
PH2=0.

2000 ANG=ABS(PH2-PH1)
DZ=Z2-Z1
DY=Y2-Y1
SSQ=DZ*DZ+DY*DY
IF(SSQ.LT.ZERO) GOTO 3000
S=SQRT(SSQ)
IF(ANG.LT.ZERO) GOTO 100
SINA=SIN(ANG)
SINO1=R2*SINA/S
SINO2=R1*SINA/S
RT=SQRT(R1*R2)*TANO/SINO1/SINO2
RTORB=SQRT((1.-SINO1*SINO1)*(1.-SINO2*SINO2))/SINO1/SINO2
CONP=(2.*AK*AK*RT*RT)*(-THIRD)
TAUSQ=SINA/ANG
TAU=SQRT(TAUSQ)
TAU3=TAU*TAU3
ZETA3=AK*R1*SINO1*ANG**3/(2.*TANO*TANO)
ZETA=ZETA3**THIRD
GOTO 200
100 SINO1=SINO2=ZETA=CONP=0.
TAU=TAU3=1.
RB=TANO*SQRT(R1*R2)
200 CONTINUE
CALL FOCK ( ZETA,U,U,VP,UP )
AKS=AK*S
JOKS=CJ/AKS
HB=(1.-JOKS)*TAU*V+JOKS*JOKS*TAU3*U+CJ*CONP*TAU*VP
IF(ANG.GE.ZERO) HB=HB+CJ*CONP*RTORB*TAU3*UP
IF(ANG.LT.ZERO) HB=HB+.375*(1.-CJ)*SQRT(PI*KB)/RB
HT=TAU*V+(1.-2.*JOKS)*TAU3*U+CJ*CONP*TAU3*UP
HT=JOKS*HT
SINTSQ=DZ*DZ/SSQ
COSTSQ=1.-SINTSQ
GC=HB*SINTSQ+HT*COSTSQ
GP=SINTSQ+JOKS*(1.-JOKS)*(2.-3.*SINTSQ)
GS=COS(AKS)-CJ*SIN(AKS)
GS=GS/AKS
FZ2=GS*(GC-GP)
IF(S.GT.DEL) RETURN
GA=(0.,0.)
IF(ANG.GE.ZERO)
$ GA=(1.-CJ*AKS)*(1.+CJ)*(3.*SINTSQ-1.)*SQRT(PI/AKS)
$ *SINO1*SINO1/(8.*AKS*AK*R1*TANO)
FZ2=FZ2-GA
RETURN
3000 FZ2=GA=(0.,0.)
RETURN
END
```

THIS PAGE IS BEST QUALITY PRACTICABLE  
FROM COPY FURNISHED TO DDG

APPENDIX B3

SUBROUTINES OF  $Y_0^d$

```
SUBROUTINE PLANE ( YPL,TAK,TA,TB )
COMPLEX YPL,CF1,RES1,RES2
EXTERNAL CF1,RF1
COMMON /PLANAR/ PI,AK,A,B,AKA,AKB,CON2
DATA PI/3.1415926536/
AK=TAK
A=TA
B=TB
AKA=AK*A
AKB=AK*B
CON2=PI**5*B**0.5/A**4
PERIOD=2.*PI/A
RES1=XL=0.
XU=PERIOD/2.
IF(XU.GE.AK) GOTO 200
CALL CGQ2 ( CF1,XL,XU,B,RES1 )
210 XL=XU
XU=XL+PERIOD
IF(XU.GE.AK) GOTO 200
CALL CGQ2 ( CF1,XL,XU,B,RES2 )
RES1=RES1+RES2
GOTO 210
200 CALL CGQ2 ( CF1,XL,AK,32,RES2 )
RES1=RES1+RES2

CALL BICI ( SI,CI,AKA )
RES3=COS(AKA/2.)
RES3=2.*RES3*RES3-AKA*SIN(AKA)+AKA*AKA*CI
RES3=RES3*CON2/(4.*AK*AK)
NU=2.*AK/PERIOD
XU=(NU+2)*PERIOD/2.
IF(XU.LE.AK) XU=XU+PERIOD/2.
CALL RGQ2 ( RF1,AK,XU,B,RES4 )
RES3=RES3+RES4
100 XL=XU
XU=XL+PERIOD
CALL RGQ2 ( RF1,XL,XU,B,RES4 )
RES3=RES3+RES4
RATIO=ABS(RES4/RES3)
IF(RATIO.GT.1.E-5) GOTO 100

YPL=RES1+CMPLX(0.,-2.*RES3/PI)
YPL=YPL/A/(15.*AKB*PI**4)
RETURN
END
```

THIS PAGE IS BEST QUALITY PRACTICABLE  
FROM COPY FURNISHED TO DDC

```
COMPLEX FUNCTION CF1(AKY)
COMPLEX CF2
COMMON /PLANAR/ PI,AK,A,B,AKA,AKB,CON2
X=B*SQRT(AK*AK-AKY*AKY)
CF1=CX(AKY)*CF2(X)
RETURN
END
```

```
FUNCTION RF1(AKY)
COMMON /PLANAR/ PI,AK,A,B,AKA,AKB,CON2
X=B*SQRT(AKY*AKY-AK*AK)
P1=CX(AKY)*RF2(X)
P2=COS(AKY*A/2.)
P3=CON2*P2*P2/AKY**3
RF1=P1-P2
RETURN
END
```

```
FUNCTION CY(AKY)
COMMON /PLANAR/ PI,AK,A,B,AKA,AKB,CON2
CY=COS(AKY*A/2.)/(1.-(AKY*A/PI)**2)
CY=CX*CY
RETURN
END
```

```
COMPLEX FUNCTION CF2(X)
CALL ZHOI ( ZJOI,ZYOI,X )
REAL=X*( ZJOI-ZJ1(X) )
AIMAG=X*( ZYOI-ZY1(X) )-2./3.1415926536
CF2=CMPLX( REAL,-AIMAG )
RETURN
END
```

```
FUNCTION RF2(X)
RF2=X*( ZNOI(X)+ZN1(X) )-1.
RETURN
END
```

APPENDIX C

SUBROUTINES FOR SPECIAL FUNCTIONS

SPECIAL FUNCTION	SUBPROGRAM
Bessel's Functions $J_0(x)$ , $J_1(x)$	ZJ0(X), ZJ1(X)
Neumann's Functions $Y_0(x)$ , $Y_1(x)$	ZYO(X), ZY1(X)
Modified Bessel's Functions $K_0(x)$ , $K_1(x)$	ZK0(X), ZK1(X)
$\int_0^x J_0(t)dt$ , $\int_0^x Y_0(t)dt$	CALL ZHOI (ZJOI, ZYOI, X)
$\int_0^x K_0(t)dt$	ZK0I(X)
Fresnel Sine and Cosine Integrals	CALL FRESNEL (C, S, X)
$S(x) = \frac{1}{\sqrt{2\pi}} \int_0^x \frac{\sin t}{\sqrt{t}} dt$ , $C(x) = \frac{1}{\sqrt{2\pi}} \int_0^x \frac{\cos t}{\sqrt{t}} dt$	
Sine and Cosine Integrals	CALL SICI (SI, CI, X)
$Si(x) = \int_0^x \frac{\sin t}{t} dt$ , $Ci(x) = - \int_x^\infty \frac{\cos t}{t} dt$	
Fock's Functions $V(x)$ , $U(x)$ , $V'(x)$ , $U'(x)$	CALL FOCK (X, V, U, VP, UP)

THIS PAGE IS BEST QUALITY PRACTICABLE  
FROM COPY FURNISHED TO DDC

```
FUNCTION ZJ0(X)
IF(X.GT.3.) GOTO 1000
X3=X/3.
ZJ0=1.-2.2499997*X3**2
1 +1.2656208*X3**4
2 -0.3163866*X3**6
3 +0.0444479*X3**8
4 -0.0039444*X3**10
5 +0.0002100*X3**12
RETURN
1000 X3=3./X
F0= 0.79788456
1-0.00000077*X3
2-0.00552740*X3**2
3-0.00009512*X3**3
4+0.00137237*X3**4
5-0.00072805*X3**5
6+0.00014476*X3**6
THETA=X-0.78539816
1-0.04166397*X3
2-0.00003954*X3**2
3+0.00262573*X3**3
4-0.00054125*X3**4
5-0.00029333*X3**5
6+0.00013558*X3**6
ZJ0=F0*COS(THETA)/SQRT(X)
RETURN
END
```

```
FUNCTION ZJ1(X)
IF(X.GT.3.) GOTO 1000
X3=X/3.
ZJ1=0.5-0.56249985*X3**2
1+0.21093573*X3**4
2-0.03954289*X3**6
3+0.00443519*X3**8
4-0.00031751*X3**10
5+0.00001109*X3**12
ZJ1=ZJ1**X
RETURN
1000 X3=3./X
F1=0.79788456+0.00000156*X3
1+0.01559567*X3**2
2+0.00017105*X3**3
3-0.00249511*X3**4
4+0.00113653*X3**5
5-0.00020033*X3**6
THETA=X-2.35619449
1+0.12499612*X3
2+0.00005650*X3**2
3-0.00637879*X3**3
4+0.00074348*X3**4
5+0.00079824*X3**5
6-0.00029156*X3**6
ZJ1=F1*COS(THETA)/SQRT(X)
RETURN
END
```

```
FUNCTION ZK0(X)
IF(X.LT.1.E-50) GOTO 2000
IF(X.GT.2.) GOTO 1000
T=X/2.
ZK0=-ALOG(0.5*X)*ZI0(X)-0.57721566
1+0.42278420*T**2
2+0.23069756*T**4
3+0.03488590*T**6
4+0.00262698*T**8
5+0.00010750*T**10
6+0.00000740*T**12
RETURN
1000 T=2./X
ZK0=1.25331414-0.07832358*T
1+0.02189568*T**2
2-0.01062446*T**3
3+0.00587872*T**4
4-0.00251540*T**5
5+0.00053208*T**6
ZK0=ZK0*EXP(-X)/SQRT(X)
RETURN
2000 ZK0=1.E50
RETURN
END
```

```
FUNCTION ZK1(X)
IF(X.LT.1.E-50) GOTO 2000
IF(X.GT.2.) GOTO 1000
T=X/2.
ZK1=X*ALOG(0.5*X)*ZI1(X)+1.
1+0.15443144*T**2
2-0.67278579*T**4
3-0.18156897*T**6
4-0.01919402*T**8
5-0.00110404*T**10
6-0.00004686*T**12
ZK1=ZK1/X
RETURN
1000 T=2./X
ZK1=1.25331414+0.23498619*T
1-0.03655620*T**2
2+0.01504268*T**3
3-0.00780353*T**4
4+0.00325614*T**5
5-0.00068245*T**6
ZK1=ZK1*EXP(-X)/SQRT(X)
RETURN
2000 ZK1=1.E50
RETURN
END
```

THIS PAGE IS BEST QUALITY PRACTICABLE  
FROM COPY FURNISHED TO DDC

```
FUNCTION ZY0(X)
IF(X.LT.1.E-50) GOTO 2000
IF(X.GT.3.) GOTO 1000
X3=X/3.
ZY0=2./3.141592654**ALOG(0.5*X)*ZJ0(X)
1+0.36746691
2+0.60559366*X3**2
3-0.74350384*X3**4
4+0.25300117*X3**6
5-0.04261214*X3**8
6+0.00427916*X3**10
7-0.00024846*X3**12
RETURN
1000 X3=3./X
F0= 0.79788456
1-0.00000077*X3
2-0.00552740*X3**2
3-0.00009512*X3**3
4+0.00137237*X3**4
5-0.00072905*X3**5
6+0.00014476*X3**6
THETA=X-0.79539816
1-0.04166397*X3
2-0.00003954*X3**2
3+0.00262573*X3**3
4-0.00054125*X3**4
5-0.00029333*X3**5
6+0.00013558*X3**6
ZY0=F0*SIN(THETA)/SQRT(X)
RETURN
2000 ZY0=-1.E50
RETURN
END
```

```
FUNCTION ZY1(X)
IF(X.LT.1.E-50) GOTO 2000
IF(X.GT.3.) GOTO 1000
X3=X/3.
ZY1=2./3.141592654*X**ALOG(0.5*X)*ZJ1(X)-0.6366198
1+0.2212091*X3**2
2+2.1682709*X3**4
3-1.3164827*X3**6
4+0.3123751*X3**8
5-0.0400976*X3**10
6+0.0027873*X3**12
ZY1=ZY1/X
RETURN
1000 X3=3./X
F1=0.79788456+0.00000156*X3
1+0.01659667*X3**2
2+0.00017105*X3**3
3-0.00249511*X3**4
4+0.00113653*X3**5
5-0.00020033*X3**6
THETA=X-2.35617449
1+0.12499612*X3
2+0.00005650*X3**2
3-0.00637979*X3**3
4+0.00074348*X3**4
5+0.00079824*X3**5
6-0.00029166*X3**6
ZY1=F1*SIN(THETA)/SQRT(X)
RETURN
2000 ZY1=-1.E50
RETURN
END
```





THIS PAGE IS BEST QUALITY PRACTICABLE  
FROM COPY FURNISHED TO DDC

SUBROUTINE FRESNEL ( C,S,XX )

FRESNEL SINE AND COSINE INTEGRALS FOR A GIVEN XX

EDWARD K. YUNG  
JULY, 1978

C  
C  
C  
C  
C

REAL CV(7),SV(7),AV(9),BV(9)

DATA	CV,SV,AV,BV/	.79788455E+00,	-.79788405E-01,
#	.36938596E-02,	-.85224622E-04,	.11605294E-05,
#	-.10140729E-07,	.50998348E-10,	.26395149E+00,
#	-.19997110E-01,	.60435371E-03,	-.10525853E-04,
#	.11225331E-06,	-.66777447E-09,	0.
#	.19947115E+00,	-.12079994E-05,	-.93149105E-02,
#	-.40271450E-03,	.74282459E-02,	-.72716901E-02,
#	.34014090E-02,	-.66339256E-03,	0.
#	-.44440909E-08,	-.24933215E-01,	-.16064281E-04,
#	.59721508E-02,	-.30953412E-03,	-.67928011E-02,
#	.79709430E-02,	-.41692894E-02,	.87582580E-03/

X=ABS(XX)

2

IF(X,GT.4.) GOTO 4

XSQ=SQRT(X)

X2=XX

TEMP=1.

C=S=0.

DO 100 I=1,7

C=C+CV(I)\*TEMP

S=S+SV(I)\*TEMP

100

TEMP=TEMP\*X2

C=C\*XSQ

S=S\*XSQ

GOTO 1

4

X=4./X

TEMP=1.

P=Q=0.

DO 200 I=1,9

P=P+AV(I)\*TEMP

Q=Q+BV(I)\*TEMP

200

TEMP=TEMP\*X4

Y4SQ=SQRT(X4)

C=0.5+Y4SQ\*( SIN(X)\*P-COS(X)\*Q )

S=0.5+Y4SQ\*( -COS(X)\*P+SIN(X)\*Q )

1

C=SIGN(C,XX)

S=SIGN(S,XX)

RETURN

END

THIS PAGE IS BEST QUALITY PRACTICABLE  
 FROM COPY FURNISHED TO DDC

```

SUBROUTINE SICI ( SI,CI,X )
C
C SINE AND COSINE INTEGRALS
C
C EDWARD K. YUNG
C JULY, 1978
C
REAL AF(4),BF(4),AG(4),BG(4)
DATA AF,BF,AG,BG/
$ 38.027264, 265.187033, 335.677320, 38.102495,
$ 40.021433, 322.624911, 570.236290, 157.105423,
$ 42.242855, 302.757865, 352.018498, 21.821899,
$ 48.196927, 482.485984, 1114.978885, 449.590326/
SI=0.
CI=-1.E99
IF(X.EQ.0.) RETURN
X2=X**2
IF(X.LE.1.) GOTO 2000
XT=X**8
FD=FN=GD=GN=XT
DO 1000 I=1,4
  XT=XT/X2
  FD=FD+BF(I)*XT
  FN=FN+AF(I)*XT
  GD=GD+BG(I)*XT
  GN=GN+AG(I)*XT
1000 CONTINUE
F=FN/FD/X
G=GN/GD/X2
COSX=COS(X)
SINX=SIN(X)
FI=1.57079632678-F*COSX-G*SINX
CI=FI*SINX-G*COSX
RETURN
2000 XT=DEN=FTL=1.
SI=CI=0.
DO 3000 I=1,6
  SI=SI+XT/DEN/FTL
  XT=-XT**2
  DEN=DEN+1.
  FTL=FTL*DEN
  CI=CI+XT/DEN/FTL
  DEN=DEN+1.
  FTL=FTL*DEN
3000 CONTINUE
SI=X**SI
CI=0.5772156649+ALOG(X)+CI
RETURN
END

```

THIS PAGE IS BEST QUALITY PRACTICABLE  
FROM COPY FURNISHED TO DDO

C  
C  
C  
C  
C  
C

SUBROUTINE FOCK ( Z,U,V,UP,UP )  
FOCK'S FUNCTIONS : U,V,U',AND U' FOR A GIVEN REAL Z

EDWARD K. YUNG  
JULY, 1978

```

COMPLEX CONU,CONV,CONVP,CONUP,CONZ
COMPLEX U,V,UP,UP,CZ,ECZTN,ECZTNP
REAL TN(10),TNP(10)
COMPLEX US(4),US(4),UPS(4),UPS(4)
DATA US/      (-.31332953433,      -.31332953433),
$              (.0,              .11666666667),
$              (.01713515422,     -.01713515422),
$              (-.004141,         .0)/
DATA US/      (-.62665706866,     -.62665706866),
$              (.0,              .41666666667),
$              (.09791516698,     -.09791516698),
$              (-.03701,         .0)/
DATA UPS/     (-.46999280149,     -.46999280149),
$              (.0,              .35),
$              (.077108194,       -.077108194),
$              (-.02485,         .0)/
DATA UPS/     (-.93998560299,     -.93998560299),
$              (.0,              1.25),
$              (.44061825140,     -.44061825140),
$              (-.2221,         .0)/
DATA TN/      2.33811,  4.08795,  5.52056,
$              5.78671,  7.99417,  9.02265, 10.04017,
$              11.00852, 11.93602, 12.82878/
DATA TNP/     1.01379,  3.24820,  4.82010,
$              5.15331,  7.37213,  8.48849, 9.53545,
$              10.52766, 11.47506, 12.38479/
DATA CONU,CONV,CONVP,CONUP,CONZ/
$              ( 1.7120589505,      0.4587448132),
$              ( 2.5066282746,      2.5066282746),
$              (-1.2533141373,     -1.2533141373),
$              ( 3.7599424120,      3.7599424120),
$              (-0.3660254038,     -0.5)/
X=SQRT(Z)
X3=X**3
IF(Z.LE..7) GOTO 1000
CZ=CONZ*X
U=U+UP=UP*(0..0.)
DO 100 N=1,10
ECZTN= CEXP( CZ*TN(N) )
ECZTNP=CEXP( CZ*TNP(N) )
V=U+ECZTN/TNP(N)
U=U+ECZTN
VP=UP+ECZTNP
UP=UP+ECZTN*TNP(N)
100 CONTINUE
VP=CONV*V/2./X + X*CONVP*VP
UP=X*CONUP*( U+2.*CZ/3.*UP )
V=X*CONU*V
U=X3*CONU*U
RETURN
1000 Y6=X3*X3
X9=X3*X6
X12=X3*X9
X4=X3*X
X7=X3*X4
X10=X3*X7
V=1.+US(1)*X3+US(2)*X6+US(3)*X9+US(4)*X12
U=1.+US(1)*X3+US(2)*X6+US(3)*X9+US(4)*X12
UP=UPS(1)*X+UPS(2)*X4+UPS(3)*X7+UPS(4)*X10
UP=UPS(1)*X+UPS(2)*X4+UPS(3)*X7+UPS(4)*X10
RETURN
END

```

ATTACHMENT B

SURFACE FIELD DUE TO A MAGNETIC DIPOLE ON A CYLINDER:

ASYMPTOTIC EXPANSION OF EXACT SOLUTION

(Each attachment has its own pagination.)

REPORT DOCUMENTATION PAGE		READ INSTRUCTIONS BEFORE COMPLETING FORM
1. REPORT NUMBER	2. GOVT ACCESSION NO.	3. RECIPIENT'S CATALOG NUMBER
4. TITLE (and Subtitle) Surface Field Due to a Magnetic Dipole on a Cylinder: Asymptotic Expansion of Exact Solution		5. TYPE OF REPORT & PERIOD COVERED Technical
7. AUTHOR(s) J. Boersma and S. W. Lee		6. PERFORMING ORG. REPORT NUMBER EM 78-17; UILU-ENG-78-2560
9. PERFORMING ORGANIZATION NAME AND ADDRESS Electromagnetics Laboratory Department of Electrical Engineering University of Illinois, Urbana, Illinois 61801		8. CONTRACT OR GRANT NUMBER(s) N00019-78-C-0064
11. CONTROLLING OFFICE NAME AND ADDRESS Department of the Navy Naval Air Systems Command Washington, D. C. 20361		10. PROGRAM ELEMENT, PROJECT, TASK AREA & WORK UNIT NUMBERS
14. MONITORING AGENCY NAME & ADDRESS (if different from Controlling Office)		12. REPORT DATE December 1978
		13. NUMBER OF PAGES 62
		15. SECURITY CLASS. (of this report) Unclassified
		15a. DECLASSIFICATION DOWNGRADING SCHEDULE
16. DISTRIBUTION STATEMENT (of this Report) Distribution unlimited. (Reproduction in whole or in part is permitted for any purpose of the United States Government.)		
17. DISTRIBUTION STATEMENT (of the abstract entered in Block 20, if different from Report)		
18. SUPPLEMENTARY NOTES		
19. KEY WORDS (Continue on reverse side if necessary and identify by block number) Green's function for cylinder GTD Surface ray Creeping wave		
20. ABSTRACT (Continue on reverse side if necessary and identify by block number) The paper studies the asymptotic solution of the surface magnetic field due to a magnetic dipole on an infinitely long cylinder whose radius is large in terms of wavelength. Starting from the exact modal series solution, we extract a dyadic Green's function for the magnetic field which is valid for all points on the cylinder. In particular, our solution justifies for the first time the $(ks)^{-1/2}$ behavior of the field propagating along the generator of the cylinder, where $s$ is the distance between the dipole and the observation point.		

UILU-ENG-78-2560

Electromagnetics Laboratory Report No. 78-17

SURFACE FIELD DUE TO A MAGNETIC DIPOLE ON A CYLINDER:  
ASYMPTOTIC EXPANSION OF EXACT SOLUTION

by

J. Boersma\*  
S. W. Lee

Technical Report

December 1978

Supported by  
Contract No. N00019-78-C-0064  
Department of the Navy  
Naval Air Systems Command  
Washington, D.C. 20361

Electromagnetics Laboratory  
Department of Electrical Engineering  
Engineering Experiment Station  
University of Illinois at Urbana-Champaign  
Urbana, Illinois 61801

\* J. Boersma is with the Department of Mathematics, Technological University, Eindhoven, the Netherlands, and was a visiting professor at the University of Illinois.

## ABSTRACT

The paper studies the asymptotic solution of the surface magnetic field due to a magnetic dipole on an infinitely long cylinder whose radius is large in terms of wavelength. Starting from the exact modal series solution, we extract a dyadic Green's function for the magnetic field which is valid for all points on the cylinder. In particular, our solution justifies for the first time the  $(ks)^{-1/2}$  behavior of the field propagating along the generator of the cylinder, where  $s$  is the distance between the dipole and the observation point.

ACKNOWLEDGMENT

The authors appreciate useful discussions with R. C. Hansen,  
W. H. Kummer, R. Mittra, and J. Willis.

TABLE OF CONTENTS

	Page
1. INTRODUCTION . . . . .	1
2. DEBYE-TYPE ASYMPTOTIC EXPANSION OF THE HANKEL FUNCTION . . .	4
3. SURFACE MAGNETIC FIELD DUE TO A CIRCUMFERENTIAL MAGNETIC DIPOLE . . . . .	8
3.1 Magnetic field component $H_{\phi}^c$ . . . . .	8
3.2 Magnetic field component $H_z^c$ . . . . .	14
4. SURFACE MAGNETIC FIELD DUE TO AN AXIAL MAGNETIC DIPOLE . . .	18
4.1 Magnetic field component $H_{\phi}^a$ . . . . .	18
4.2 Magnetic field component $H_z^a$ . . . . .	18
5. REPRESENTATION OF THE SURFACE MAGNETIC FIELD IN DYADIC FORM.	22
6. MATCHING TO AN EXPANSION IN TERMS OF FOCK FUNCTIONS. . . . .	27
6.1 Magnetic field component $H_{\phi}^c$ . . . . .	29
6.2 Magnetic field component $H_z^c = H_{\phi}^a$ . . . . .	35
6.3 Magnetic field component $H_z^a$ . . . . .	36
6.4 Representation in a dyadic form . . . . .	37
7. NUMERICAL RESULTS. . . . .	39
8. CONCLUSIONS. . . . .	53
REFERENCES . . . . .	54

LIST OF FIGURES

Figure		Page
1.	A surface ray (geodesic) from source point P to observation point Q on an infinitely long circular cylinder. . . . .	2
2.	Unit vectors ( $\hat{t}'$ , $\hat{b}'$ , $\hat{t}$ , $\hat{b}$ ) and surface ray PQ on developed cylinder . . . . .	23
3.	Integration contour $\Gamma$ . . . . .	23
4a.	Surface magnetic field $H_{\phi}^c$ due to a circumferential dipole on a cylinder for a ray propagating in the direction $\theta = 0^\circ$ . . . . .	40
4b.	Same as Figure 4a except for larger ks . . . . .	41
5a.	Same as Figure 4a except for $\theta = 45^\circ$ . . . . .	42
5b.	Same as Figure 4a except for $\theta = 45^\circ$ and larger ks . . . . .	43
6a.	Same as Figure 4a except for $\theta = 90^\circ$ . . . . .	44
6b.	Same as Figure 4a except for $\theta = 90^\circ$ and larger ks . . . . .	45
7.	Surface magnetic field $H_z^a$ due to an axial dipole on a cylinder for a ray propagating in the direction $\theta = 0^\circ$ . . . . .	46
8.	Same as Figure 7 except for $\theta = 45^\circ$ . . . . .	47
9.	Same as Figure 7 except for $\theta = 90^\circ$ . . . . .	48
10.	Two identical slots on a cylinder. . . . .	49

LIST OF TABLES

Table	Page
1. MUTUAL ADMITTANCE BETWEEN TWO CIRCUMFERENTIAL SLOTS . . . .	51
2. MUTUAL ADMITTANCE BETWEEN TWO AXIAL SLOTS . . . . .	52

## 1. INTRODUCTION

Let  $(r, \phi, z)$  be cylindrical coordinates. An infinitely long, perfectly conducting circular cylinder is described by  $r = a$ . A tangential magnetic dipole with magnetic point source current density  $\vec{M}$  is located at  $P(r = a, \phi = 0, z = 0)$  on the surface of the cylinder. A time dependence  $\exp(j\omega t)$  is assumed throughout and suppressed. The problem is to determine the surface magnetic field  $\vec{H}$  at an observation point  $Q = (a, \phi, z)$  on the surface of the cylinder under the assumption that  $ka$  is large ( $k = 2\pi/\lambda$  is the wave number).  $P$  and  $Q$  are connected through a surface ray (geodesic) which makes an angle  $\theta$  with the  $\phi$ -direction; the distance from  $P$  to  $Q$  is denoted by  $s$ ; see Fig. 1. The present high-frequency diffraction problem was studied by Chang, Felsen and Hessel [1] and by Lee and Safavi-Naini [2], however, their results differ in various ways. In particular, Lee et al. [2, Eq. (2.18)] predict a rather peculiar term in the approximation of the component  $H_\phi(Q)$  when  $\theta = \pi/2$ , i.e., when  $P$  and  $Q$  lie on the same generator of the cylinder. This term behaves like

$$\frac{1}{ka\sqrt{ks}} \exp(-jks)$$

for large  $ks$  and is introduced in a rather arbitrary manner. It is the aim of this report to clarify the appearance of this peculiar term and other points in which the asymptotic solutions [1] and [2] differ.

We shall start from the exact modal solution for the surface magnetic field as presented in [1]. Then the quotients of the Hankel function and its derivative are replaced by a Debye-type approximation. As a result, we find a two-term approximation for the surface magnetic field. The leading term is equal to the so-called planar solution, that is, the

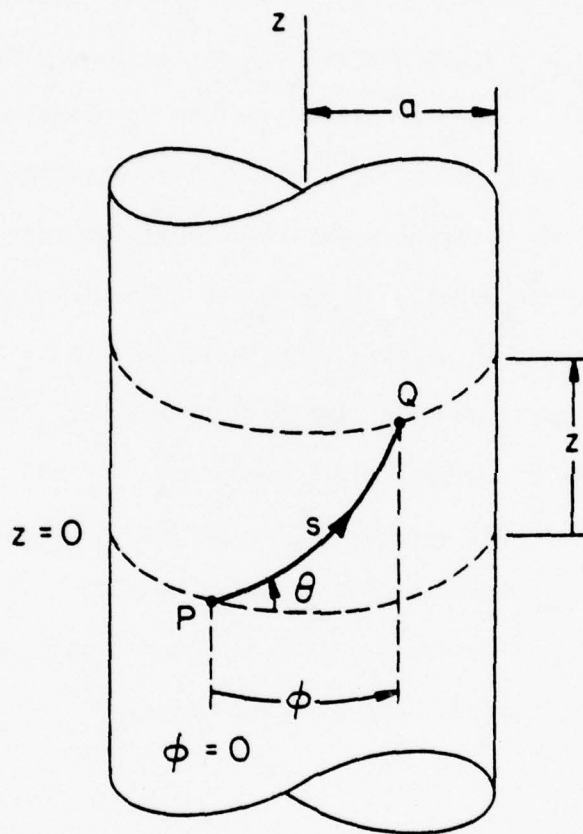


Figure 1. A surface ray (geodesic) from source point P to observation point Q on an infinitely long circular cylinder.

solution for the surface field due to a tangential magnetic dipole on a flat ground plane. The present approach differs from that of [1] where the Hankel functions are replaced by their uniform asymptotic expansions in terms of Airy functions. Then the resulting approximation for the surface magnetic field is expressed in terms of Fock functions. The Debye-type approximation of the Hankel function is discussed in the next section.

## 2. DEBYE-TYPE ASYMPTOTIC EXPANSION OF THE HANKEL FUNCTION

Consider the Hankel function  $H_\nu^{(2)}(z)$  with both  $\nu$  and  $z$  being large and positive. From Watson [3, Secs. 8.4 and 8.41] we quote the Debye-type asymptotic expansions, taking into account two terms:

$$\begin{aligned} H_\nu^{(2)}(\nu \operatorname{sech} \alpha) &\approx -jY_\nu(\nu \operatorname{sech} \alpha) \\ &\approx 2j \frac{e^{\nu(\alpha - \tanh \alpha)}}{\sqrt{2\pi\nu \tanh \alpha}} \left[ 1 - \frac{3 \coth \alpha - 5 \coth^3 \alpha}{24\nu} + O\left(\frac{1}{\nu^2}\right) \right], \\ \alpha &> 0, \end{aligned} \quad (2.1)$$

and

$$\begin{aligned} H_\nu^{(2)}(\nu \sec \beta) &\approx \frac{2e^{-j\nu(\tan \beta - \beta) + j\pi/4}}{\sqrt{2\pi\nu \tan \beta}} \left[ 1 + j \frac{3 \cot \beta + 5 \cot^3 \beta}{24\nu} + O\left(\frac{1}{\nu^2}\right) \right], \\ \beta &> 0; \end{aligned} \quad (2.2)$$

the former approximation applies when the argument is less than the order, while the second approximation applies when the argument is greater than the order. Replacing  $\nu \operatorname{sech} \alpha$  and  $\nu \sec \beta$  by  $z$ , we find

$$\begin{aligned} H_\nu^{(2)}(z) &\approx j \sqrt{\frac{2}{\pi}} \frac{\exp \left[ \nu \cosh^{-1} \left( \frac{\nu}{z} \right) - \sqrt{\nu^2 - z^2} \right]}{(\nu^2 - z^2)^{1/4}} \left[ 1 + \frac{2\nu^2 + 3z^2}{24(\nu^2 - z^2)^{3/2}} + O\left(\frac{1}{\nu^2}\right) \right], \\ z &< \nu, \end{aligned} \quad (2.3)$$

and

$$\begin{aligned} H_\nu^{(2)}(z) &\approx \sqrt{\frac{2}{\pi}} \frac{\exp \left[ -j\sqrt{z^2 - \nu^2} + j\nu \cos^{-1} \left( \frac{\nu}{z} \right) + \frac{j\pi}{4} \right]}{(z^2 - \nu^2)^{1/4}} \left[ 1 + j \frac{2\nu^2 + 3z^2}{24(z^2 - \nu^2)^{3/2}} + O\left(\frac{1}{\nu^2}\right) \right], \\ z &> \nu. \end{aligned} \quad (2.4)$$

It can be shown that the asymptotic expansions of  $H_\nu^{(2)'}(z)$  are obtainable from (2.3) and (2.4) by a term-by-term differentiation; see Abramowitz-Stegun

[4, pp. 366-367]. Through division we obtain the asymptotic expansions of the quotient  $H_\nu^{(2)}(z)/H_\nu^{(2)'}(z)$ , viz.,

$$\frac{H_\nu^{(2)}(z)}{H_\nu^{(2)'}(z)} \approx -\frac{z}{\sqrt{z^2 - \nu^2}} - \frac{z^3}{2(\nu^2 - z^2)^2} + O\left(\frac{1}{\nu^2}\right), \quad z < \nu, \quad (2.5)$$

and

$$\frac{H_\nu^{(2)}(z)}{H_\nu^{(2)'}(z)} \approx \frac{jz}{\sqrt{z^2 - \nu^2}} - \frac{z^3}{2(z^2 - \nu^2)^2} + O\left(\frac{1}{\nu^2}\right), \quad z > \nu. \quad (2.6)$$

These asymptotic approximations are essentially the same. Notice that for fixed  $z > 0$ , the quotient  $H_\nu^{(2)}(z)/H_\nu^{(2)'}(z)$  is an analytic function of  $\nu$  in the whole complex  $\nu$ -plane except for poles at the zeros of  $H_\nu^{(2)'}(z)$ . These zeros lie in the second and fourth quadrants of the  $\nu$ -plane and are approximately given by

$$\nu_p = \pm[z + e^{-j\pi/3} q_p (z/2)^{1/3} + O(z^{-1/3})], \quad p = 1, 2, 3, \dots \quad (2.7)$$

where  $-q_p$  are the negative zeros of the Airy function  $\text{Ai}(x)$ , i.e.,  $\text{Ai}(-q_p) = 0$ ; see Keller, Rubinow and Goldstein [5]. In order to uniquely define the square root  $\sqrt{z^2 - \nu^2}$ , we introduce branch cuts from  $\nu = z$  downwards and from  $\nu = -z$  upwards in the complex  $\nu$ -plane. Then it is easily seen that  $\sqrt{z^2 - \nu^2}$  in (2.6) passes into  $-j\sqrt{z^2 - \nu^2}$  in (2.5), when  $\nu$  passes above the branch point  $z$  or below the branch point  $-z$ . This shows the equivalence of (2.5) and (2.6). In the sequel we shall use the approximation (2.6), whereby it is understood that  $\sqrt{z^2 - \nu^2} \rightarrow -j\sqrt{z^2 - \nu^2}$  when  $|\nu| > z$ .

The approximations (2.5) and (2.6) apply when either  $|\nu|$ , or  $z$ , or both  $|\nu|$  and  $z$  are large, the error being of order  $\nu^{-2}$  or  $z^{-2}$ , whichever is smallest. The approximations are not valid in the transition region

$|\nu \pm z| \leq O(z^{1/3})$  and  $z$  large. Further difficulties appear when both  $\nu$  and  $z$  are small. For example, from the power-series expansion of  $H_0^{(2)}(z)$ , one may find

$$\frac{H_0^{(2)}(z)}{H_0^{(2)'}(z)} = z \log\left(\frac{1}{2}z\right) + \left(\gamma + \frac{j\pi}{2}\right)z + O(z^3 \log^2 z), \quad z \rightarrow 0 \quad (2.8)$$

where  $\gamma$  denotes Euler's constant. The latter result does not agree with (2.6) when  $\nu = 0$ . On the other hand, when  $\nu = 0$  and  $z$  is large, we find from the asymptotic expansion of  $H_0^{(2)}(z)$ :

$$\frac{H_0^{(2)}(z)}{H_0^{(2)'}(z)} = j - \frac{1}{2z} + O\left(\frac{1}{z^2}\right), \quad z \rightarrow \infty \quad (2.9)$$

which is in perfect agreement with (2.6) when  $\nu = 0$ . Similarly, when  $z$  is small and  $|\nu|$  is large, we may find from the power-series expansion of  $H_\nu^{(2)}(z)$ :

$$\frac{H_\nu^{(2)}(z)}{H_\nu^{(2)'}(z)} = -\frac{z}{\nu} - \frac{z^3}{2\nu^3} + O\left(\frac{z^3}{\nu^4}\right), \quad (2.10)$$

in agreement with (2.5).

In subsequent sections the approximation (2.6) is going to be used in integrals of the form

$$\int_{-\infty}^{\infty} e^{-j\nu\phi} \frac{H_\nu^{(2)}(k_t a)}{H_\nu^{(2)'}(k_t a)} d\nu, \quad (2.11)$$

where  $\phi > 0$ ,  $k_t = \sqrt{k_z^2 - k^2}$ ,  $k_t$  is real when  $k_z^2 < k^2$ , and  $k_t$  negative imaginary when  $k_z^2 > k^2$ . In order to justify the replacement of

$H_\nu^{(2)}(k_t a)/H_\nu^{(2)'}(k_t a)$  by the approximation in (2.6), we distinguish three cases: (1) If  $k_t a$  is real and large, the integration contour in (2.11) is

deformed by introducing semicircular indentations above  $k_{\epsilon}a$  and below  $-k_{\epsilon}a$ , both of radius  $O((k_{\epsilon}a)^{1/3})$ . Along the deformed contour the approximation (2.6) is certainly valid. After making the replacement of the integrand by (2.6), the contour is deformed back to the real axis. Notice that in both deformations no poles or branch points of the integrand are crossed.

(ii) If  $k_{\epsilon}a$  is negative imaginary and large, the approximation (2.6) is valid along the real  $v$ -axis and no deformation of contours is needed.

(iii) If  $k_{\epsilon}a$  is small due to  $k_z \approx k$ , then the approximation (2.6) is not valid when  $|v|$  is also small; it is valid though when  $|v|$  is large. It is not clear what effect this will have on the error in the resulting approximation to the integral (2.11). This case certainly needs further consideration. For later use we also establish an approximation for the quotient  $H_{\nu}^{(2)'}(z)/H_{\nu}^{(2)}(z)$ :

$$\frac{H_{\nu}^{(2)'}(z)}{H_{\nu}^{(2)}(z)} \approx -\frac{j\sqrt{z^2 - \nu^2}}{z} - \frac{z}{2(z^2 - \nu^2)}, \quad (2.12)$$

where it is understood that  $\sqrt{z^2 - \nu^2} \rightarrow -j\sqrt{\nu^2 - z^2}$  when  $|v| > z$ .

### 3. SURFACE MAGNETIC FIELD DUE TO A CIRCUMFERENTIAL MAGNETIC DIPOLE

#### 3.1 Magnetic field component $H_\phi^c$ .

In the case of a circumferential dipole

$$\vec{M} = \hat{\phi} \quad , \quad (3.1)$$

the resulting surface magnetic field components are denoted by  $H_\phi^c(Q)$  and  $H_z^c(Q)$ . Neglecting the contribution of creeping waves which have travelled around the cylinder, it is found in [1, Eqs. (18) and (19)] that

$$H_\phi^c(Q) = \frac{j}{4\pi^2 \omega \mu_0 a^3} \int_{-\infty}^{\infty} dk_z e^{-jk_z z} \frac{k_z^2}{k_t^3} \int_{-\infty}^{\infty} dv e^{-jv\phi} v^2 \frac{H_v^{(2)}(k_t a)}{H_v^{(2)'}(k_t a)} \\ - \frac{jk^2}{4\pi^2 \omega \mu_0 a} \int_{-\infty}^{\infty} dk_z e^{-jk_z z} \frac{1}{k_t} \int_{-\infty}^{\infty} dv e^{-jv\phi} \frac{H_v^{(2)'}(k_t a)}{H_v^{(2)}(k_t a)} \quad , \quad (3.2)$$

where  $k_t = \sqrt{k^2 - k_z^2}$ ,  $k_t$  is real when  $k_z^2 < k^2$ , and  $k_t$  negative imaginary when  $k_z^2 > k^2$ . If necessary, one may think of  $k$  having a small negative imaginary part. Then  $k_t = \sqrt{k^2 - k_z^2}$  has branch cuts from  $k_z = k$  downwards and from  $k_z = -k$  upwards in the complex  $k_z$ -plane.

In (3.2) we replace the quotient of the Hankel function and its derivative by the approximations in (2.6) and (2.12). Furthermore, we set  $v = k_y a$  in the inner integrals in (3.2). Then we are led to the following approximation for  $H_\phi^c(Q)$ :

$$\begin{aligned}
H_{\phi}^c(Q) &= \frac{j}{4\pi^2 \omega \mu_0} \int_{-\infty}^{\infty} \int_{-\infty}^{\infty} \exp[-jk_z z - jk_y a\phi] \left[ \frac{k_z^2 k_y^2}{k_t^3} \left\{ \frac{jk_t}{\sqrt{k_t^2 - k_y^2}} - \frac{1}{a} \frac{k_t^3}{2(k_t^2 - k_y^2)^2} \right\} \right. \\
&\quad \left. + \frac{k_t^2}{k_t} \left\{ \frac{j\sqrt{k_t^2 - k_y^2}}{k_t} + \frac{1}{a} \frac{k_t}{2(k_t^2 - k_y^2)} \right\} \right] dk_y dk_z = - \frac{Y}{4\pi^2 k} \int_{-\infty}^{\infty} \int_{-\infty}^{\infty} \exp[-jk_z z - jk_y a\phi] \\
&\quad \cdot \left[ \frac{k^2 - k_y^2}{\sqrt{k^2 - k_y^2 - k_z^2}} - \frac{j}{2a} \frac{k^4 - k^2 k_y^2 - k^2 k_z^2 - k_y^2 k_z^2}{(k^2 - k_y^2 - k_z^2)^2} \right] dk_y dk_z \quad (3.3)
\end{aligned}$$

where  $Y = \sqrt{\epsilon_0 / \mu_0}$ ; the square root  $\sqrt{k^2 - k_y^2 - k_z^2}$  is positive when  $k_y^2 + k_z^2 < k^2$  and negative imaginary when  $k_y^2 + k_z^2 > k^2$ . Notice that  $(a\phi, z)$  are just the rectangular coordinates of  $Q$  on the developed cylinder.

The result in (3.3) can be expressed in terms of the derivatives of the following two key integrals

$$I_1(a\phi, z) = \int_{-\infty}^{\infty} \int_{-\infty}^{\infty} \exp[-jk_z z - jk_y a\phi] \frac{dk_y dk_z}{\sqrt{k^2 - k_y^2 - k_z^2}} \quad (3.4)$$

and

$$I_2(a\phi, z) = \int_{-\infty}^{\infty} \int_{-\infty}^{\infty} \exp[-jk_z z - jk_y a\phi] \frac{dk_y dk_z}{(k^2 - k_y^2 - k_z^2)^2}, \quad (3.5)$$

both of which can be evaluated in closed form. To that purpose we introduce polar-coordinate variables  $k_y = t \cos \alpha$ ,  $k_z = t \sin \alpha$ ,  $a\phi = s \cos \theta$ ,  $z = s \sin \theta$ . Then by use of Watson [3, Eqs. 2.3(1) and 13.47(4)],  $I_1$  reduces to

$$\begin{aligned}
I_1(a\phi, z) &= \int_0^{\infty} t dt \int_0^{2\pi} d\alpha \frac{\exp[-jst \cos(\alpha - \theta)]}{\sqrt{k^2 - t^2}} = 2\pi j \int_0^{\infty} J_0(st) \frac{t}{\sqrt{t^2 - k^2}} dt \\
&= 2\pi j \frac{e^{-jks}}{s} \quad (3.6)
\end{aligned}$$

Notice that we made the replacement  $\sqrt{k^2 - t^2} \rightarrow -j\sqrt{t^2 - k^2}$ , and that in the latter integral the path of integration passes above  $t = k$ .

In a similar manner  $I_2$  reduces to

$$I_2(a\phi, z) = \int_0^\infty t dt \int_0^{2\pi} d\alpha \frac{\exp[-jst \cos(\alpha - \theta)]}{(k^2 - t^2)^2} = 2\pi \int_0^\infty J_0(st) \frac{t}{(t^2 - k^2)^2} dt. \quad (3.7)$$

According to [3, Eq. 13.6(2)] and [4, Eq. 11.4.44], we have

$$\int_0^\infty \frac{t J_0(at)}{(t^2 + z^2)^2} dt = \frac{a}{2z} K_{-1}(az) = \frac{a}{2z} K_1(az) \quad (3.8)$$

valid for  $a > 0$ ,  $\text{Re } z > 0$ . Remember that  $k$  has a small negative imaginary part, if needed, hence  $\text{Re}(jk) > 0$ . Setting  $a = s$ ,  $z = jk$  in (3.8), we obtain for  $I_2$ :

$$I_2(a\phi, z) = \frac{\pi s}{jk} K_1(jks) = -\frac{\pi^2 s}{2jk} H_1^{(2)}(ks) \quad (3.9)$$

by use of [4, Eq. 9.6.4].

Returning to the result (3.3) for  $H_\phi^c(Q)$ , we have

$$\begin{aligned} H_\phi^c(Q) \approx & -\frac{Y}{4\pi^2 k} \left[ \left\{ k^2 + \frac{\partial^2}{\partial(a\phi)^2} \right\} I_1(a\phi, z) - \frac{j}{2a} \left\{ k^4 + k^2 \frac{\partial^2}{\partial(a\phi)^2} + k^2 \frac{\partial^2}{\partial z^2} \right. \right. \\ & \left. \left. - \frac{\partial^4}{\partial z^2 \partial(a\phi)^2} \right\} I_2(a\phi, z) \right] = \frac{Y}{2\pi jk} \left[ \left\{ k^2 + \cos^2 \theta \frac{\partial^2}{\partial s^2} + \sin^2 \theta \frac{1}{s} \frac{\partial}{\partial s} \right\} \left( \frac{e^{-jks}}{s} \right) \right. \\ & \left. - \frac{j\pi}{8ka} \left\{ k^4 + k^2 \left( \frac{\partial^2}{\partial s^2} + \frac{1}{s} \frac{\partial}{\partial s} \right) - \cos^2 \theta \sin^2 \theta \frac{\partial^4}{\partial s^4} - (1 - 6\cos^2 \theta \sin^2 \theta) \frac{1}{s} \frac{\partial^3}{\partial s^3} \right. \right. \\ & \left. \left. + (2 - 15 \cos^2 \theta \sin^2 \theta) \frac{1}{s^2} \frac{\partial^2}{\partial s^2} - (2 - 15 \cos^2 \theta \sin^2 \theta) \frac{1}{s^3} \frac{\partial}{\partial s} \right\} (\text{sh}_1^{(2)}(ks)) \right] \quad (3.10) \end{aligned}$$

The derivatives of the Hankel function  $H_1^{(2)}(ks)$  can be evaluated and simplified by means of the well-known recurrence relations for Bessel functions\*; see e.g., [3, Sec. 3.2] and [4, Eqs. 9.1.27 and 9.1.30]. Thus we obtain as our final result for  $H_\phi^c(Q)$ :

$$H_\phi^c(Q) \approx \frac{k^2 Y}{2\pi j} \frac{e^{-jks}}{ks} [\sin^2 \theta + \frac{j}{ks} (2 - 3\sin^2 \theta) + \frac{1}{k^2 s^2} (2 - 3\sin^2 \theta)] - \frac{k^2 Y}{16ka} [3H_0^{(2)}(ks) - \frac{1}{ks} H_1^{(2)}(ks) + ksH_3^{(2)}(ks) \cos^2 \theta \sin^2 \theta]. \quad (3.11)$$

Notice that except for the Debye-type approximation to the Hankel function quotients, no further approximations were involved in the derivation of (3.11). The Hankel function  $H_3^{(2)}(ks)$  in (3.11) can be expressed in terms of  $H_0^{(2)}$  and  $H_1^{(2)}$  through

$$ksH_3^{(2)}(ks) = -4H_0^{(1)}(ks) - ksH_1^{(1)}(ks) + \frac{8}{ks} H_1^{(1)}(ks) \quad (3.12)$$

The first term in (3.11) is exactly equal to the planar solution, that is, the solution for  $H_\phi$  due to a magnetic dipole  $\vec{M} = \hat{\phi}$  on a flat ground plane; see [1, Appendix D] and [2, Eq. (2.18a)]. The second term in (3.11) represents the effect of the finite, but large, radius of curvature of the cylinder. For large  $ks$  the Hankel functions in (3.11) can be replaced by their large-argument asymptotic expansions, thus leading to

---

\* In (3.10) the differential operator in front of  $sH_1^{(2)}(ks)$  can be rewritten as

$$k^4 + k^2 s^2 D^2 + 2k^2 D - s^2 D^3 - D^2 - s^4 D^4 \cos^2 \theta \sin^2 \theta$$

where  $D = \frac{1}{s} \frac{\partial}{\partial s}$ .

$$H_{\phi}^c(Q) = \frac{k^2 Y}{2\pi j} \frac{e^{-jks}}{ks} \left[ \sin^2 \theta + \frac{j}{ks} (2 - 3\sin^2 \theta) + \frac{1}{k^2 s^2} (2 - 3\sin^2 \theta) \right. \\ \left. + \frac{1}{4ka} \left(\frac{\pi}{2}\right)^{1/2} e^{-j\pi/4} (ks)^{1/2} \left\{ 3 - \cos^2 \theta \sin^2 \theta (jks + \frac{35}{8}) + O\left(\frac{1}{ks}\right) \right\} \right]^* \quad (3.13)$$

Let the term of order  $\frac{1}{ka}$  in (3.13) be denoted by  $W$ , then for  $\theta = \pi/2$  one has

$$W = \frac{3}{4ka} \left(\frac{\pi}{2}\right)^{1/2} e^{-j\pi/4} (ks)^{1/2} \quad , \quad (3.14)$$

which is in exact agreement with the peculiar term in Lee et al. [2, Eq. (2.18c)].

We shall now compare our approximate results in (3.11) and (3.13) to the solutions presented in [1] and [2]. Chang et al. [1] have two different formulas for  $H_{\phi}^c$ , namely, the asymptotic formula [1, Eq. (124)]

$$H_{\phi}^c(Q) \approx \frac{k^2 Y}{2\pi j} \frac{e^{-jks}}{ks} \left[ \sin^2 \theta v_0(\xi) + \frac{j}{ks} (\cos^2 \theta - \frac{61}{24} \sin^2 \theta - \frac{1}{9} \frac{\sin^2 \theta}{\cos^2 \theta}) v_0(\xi) \right. \\ \left. + \frac{j}{ks} \frac{1}{\cos^2 \theta} u_0(\xi) \right] \quad (3.15)$$

not valid when  $\theta$  gets close to  $\pi/2$ , and the "full formula" [1, Eq. (130)]

$$H_{\phi}^c(Q) \approx \frac{k^2 Y}{2\pi j} \frac{e^{-jks}}{ks} \left[ \sin^2 \theta v_0(\xi) + \frac{j}{ks} (2 \cos^2 \theta - \sin^2 \theta - 1) v_0(\xi) \right. \\ \left. - \frac{j}{ks} \frac{\sin^2 \theta v_1(\xi) - u_0(\xi)}{\cos^2 \theta} \right] \quad (3.16)$$

which remains finite on  $\theta = \pi/2$ . Lee et al. [2] present the formula [2, Eq. (2.16b)]

\* On extending the result in (3.13), it is found that the term of order  $O\left(\frac{1}{ks}\right)$  is equal to

$$\frac{j}{ks} \left( -\frac{5}{8} + \frac{945}{128} \cos^2 \theta \sin^2 \theta \right) + O\left(\frac{1}{k^2 s^2}\right) \quad (3.13a)$$

$$\begin{aligned}
H_{\phi}^c(Q) \approx & \frac{k^2 Y}{2\pi j} \frac{e^{-jks}}{ks} \left[ \sin^2 \theta v(\xi) + \frac{j}{ks} (\cos^2 \theta - \sin^2 \theta) v(\xi) + \frac{j}{ks} \cos^2 \theta u(\xi) \right. \\
& + \frac{1}{k^2 s^2} (2 \cos^2 \theta - \sin^2 \theta) u(\xi) + \frac{2^{-1/3} j}{(ka)^{2/3}} \cos^{4/3} \theta \{ \sin^2 \theta v'(\xi) \\
& \left. + \frac{\sin^4 \theta}{\cos^2 \theta} u'(\xi) + \frac{j}{ks} \cos^2 \theta u'(\xi) \} \right] . \quad (3.17)
\end{aligned}$$

In (3.15) - (3.17),

$$\xi = 2^{-1/3} \frac{ks}{(ka)^{2/3}} \cos^{4/3} \theta ,$$

and  $v_0 = v$ ,  $u_0 = u$  stand for certain Fock functions as defined in [1] and [2].

We shall now re-expand the solutions (3.15) - (3.17) in the case of large  $ka$ , up to and including order  $\frac{1}{ka}$ . For large  $ka$ ,  $\xi$  is small and we replace the Fock functions by the leading terms of their small-argument expansions quoted from [1] and [2], viz.,

$$\left\{ \begin{array}{l} v_0(\xi) = v(\xi) \approx 1 - \frac{\sqrt{\pi}}{4} e^{j\pi/4} \xi^{3/2} , \\ u_0(\xi) = u(\xi) \approx 1 - \frac{\sqrt{\pi}}{2} e^{j\pi/4} \xi^{3/2} , \\ v_1(\xi) \approx 1 + \frac{\sqrt{\pi}}{2} e^{j\pi/4} \xi^{3/2} , \\ v'(\xi) \approx -\frac{3\sqrt{\pi}}{8} e^{j\pi/4} \xi^{1/2} , \quad u'(\xi) \approx -\frac{3\sqrt{\pi}}{4} e^{j\pi/4} \xi^{1/2} . \end{array} \right. \quad (3.18)$$

Then the results (3.15) and (3.16) of Chang et al. [1] become

$$\begin{aligned}
H_{\phi}^c(Q) \approx & \frac{k^2 Y}{2\pi j} \frac{e^{-jks}}{ks} \left[ \sin^2 \theta + \frac{j}{ks} \left( 2 - \frac{85}{24} \sin^2 \theta + \frac{8}{9} \frac{\sin^2 \theta}{\cos^2 \theta} \right) \right. \\
& \left. + \frac{1}{4ka} \left( \frac{\pi}{2} \right)^{1/2} e^{-j\pi/4} (ks)^{1/2} \left\{ 3 - \frac{10}{9} \sin^2 \theta - \cos^2 \theta \sin^2 \theta \left( jks + \frac{85}{24} \right) \right\} \right] , \quad (3.19)
\end{aligned}$$

and

$$H_{\phi}^c(Q) \approx \frac{k^2 Y}{2\pi j} \frac{e^{-jks}}{ks} \left[ \sin^2 \theta + \frac{1}{ks} (2 - 3\sin^2 \theta) + \frac{1}{4ka} \left(\frac{\pi}{2}\right)^{1/2} e^{-j\pi/4} (ks)^{1/2} \{3 + \sin^2 \theta - \cos^2 \theta \sin^2 \theta (jks + 3)\} \right], \quad (3.20)$$

and the result (3.17) of Lee et al. [2] becomes

$$H_{\phi}^c(Q) \approx \frac{k^2 Y}{2\pi j} \frac{e^{-jks}}{ks} \left[ \sin^2 \theta + \frac{1}{ks} (2 - 3\sin^2 \theta) + \frac{1}{k^2 s^2} (2 - 3\sin^2 \theta) + \frac{1}{4ka} \left(\frac{\pi}{2}\right)^{1/2} e^{-j\pi/4} (ks)^{1/2} \left\{3 - \cos^2 \theta \sin^2 \theta (jks + \frac{11}{2}) - \frac{1}{ks} \cos^2 \theta (1 - 3\sin^2 \theta)\right\} \right]. \quad (3.21)$$

The asymptotic formula (3.19) due to Chang et al. [1] agrees with (3.13) only at  $\theta = 0$ . Even the leading term in (3.19) agrees with the planar solution only at  $\theta = 0$ . The "full formula" (3.20) of Chang et al. and the solution (3.21) of Lee et al. do have the planar solution as their leading term. The next term of order  $\frac{1}{ka}$  in (3.20) is in agreement with (3.13) only on  $\theta = 0$  and certainly not on  $\theta = \pi/2$ . The corresponding term in (3.21) agrees with (3.13) both at  $\theta = 0$  and at  $\theta = \pi/2$ , however, in between, the agreement is only partial.

### 3.2 Magnetic field component $H_z^c$ .

In this section we consider the z-component  $H_z^c$  of the surface magnetic field due to a circumferential magnetic dipole  $\vec{M} = \hat{\phi}$ . The contribution of creeping waves that have travelled around the cylinder is again neglected. Then according to [1, Eq. (20)],  $H_z^c$  is given by

$$H_z^c(Q) = \text{sgn}(\phi) \text{sgn}(z) \frac{-j}{4\pi^2 \omega \mu_0 a^2} \int_{-\infty}^{\infty} dk_z e^{-jk_z |z|} \frac{k_z}{k_t} \int_{-\infty}^{\infty} dv e^{-jv|\phi|} \sqrt{\frac{H_v^{(2)}(k_t a)}{H_v^{(2)'}(k_t a)}} \quad (3.22)$$

where  $k_t = \sqrt{k^2 - k_z^2}$  as before. In (3.22), the quotient of the Hankel function and its derivative is replaced by the approximation (2.6), and we set  $v = k_y a$ . Thus we obtain

$$H_z^c(Q) \approx \frac{Y}{4\pi^2 k} \int_{-\infty}^{\infty} \int_{-\infty}^{\infty} \exp[-jk_z z - jk_y a\phi] \left\{ \frac{k_y k_z}{\sqrt{k^2 - k_y^2 - k_z^2}} + \frac{j}{2a} \frac{k_y k_z (k^2 - k_z^2)}{(k^2 - k_y^2 - k_z^2)^2} \right\} dk_y dk_z. \quad (3.23)$$

The latter integral can again be expressed in terms of the derivatives of  $I_1(a\phi, z)$  and  $I_2(a\phi, z)$ , as defined by (3.4) and (3.5), viz.,

$$H_z^c(Q) \approx -\frac{Y}{4\pi^2 k} \left[ \frac{\partial^2}{\partial z \partial (a\phi)} I_1(a\phi, z) + \frac{j}{2a} \frac{\partial^2}{\partial z \partial (a\phi)} \left( k^2 + \frac{\partial^2}{\partial z^2} \right) I_2(a\phi, z) \right]. \quad (3.24)$$

On substituting the explicit values of  $I_1$  and  $I_2$  from (3.6) and (3.9), we find

$$H_z^c(Q) \approx \frac{Y}{2\pi j k} \cos \theta \sin \theta \left[ \left\{ \frac{\partial^2}{\partial s^2} - \frac{1}{s} \frac{\partial}{\partial s} \right\} \left\{ \frac{e^{-jks}}{s} \right\} + \frac{j\pi}{8ka} \{ k^2 s^2 D^2 + \sin^2 \theta s^4 D^4 + 3s^2 D^3 \} (sH_1^{(2)}(ks)) \right] \quad (3.25)$$

where  $D = \frac{1}{s} \frac{\partial}{\partial s}$ . By use of the well-known recurrence relations for Bessel functions, we ultimately obtain

$$H_z^c(Q) \approx -\frac{k^2 Y}{2\pi j ks} e^{-jks} \cos \theta \sin \theta \left[ 1 - \frac{3j}{ks} - \frac{3}{k^2 s^2} \right] - \frac{k^2 Y}{16ka} \cos \theta \sin \theta \left[ H_2^{(2)}(ks) - ksH_3^{(2)}(ks) \cos^2 \theta \right]. \quad (3.26)$$

In deriving (3.26) only the Debye-type approximation to the Hankel function quotient is involved. The first term in (3.26) is again the planar solution for  $H_z^c(Q)$  as given in [1, Appendix D]. For large  $ks$  the Hankel functions in (3.26) can be replaced by their large-argument asymptotic expansions, yielding

$$H_z^c(Q) \approx -\frac{k^2 Y}{2\pi j} \frac{e^{-jks}}{ks} \cos \theta \sin \theta \left[ 1 - \frac{3j}{ks} - \frac{3}{k^2 s^2} + \frac{1}{4ka} \left(\frac{\pi}{2}\right)^{1/2} e^{-j\pi/4} (ks)^{1/2} \{1 - \cos^2 \theta (jks + \frac{35}{8}) + o(\frac{1}{ks})\} \right]. \quad (3.27)$$

On extending the result in (3.27), it is found that the term of order  $o(\frac{1}{ks})$  is equal to

$$\frac{j}{ks} \left(-\frac{15}{8} + \frac{945}{128} \cos^2 \theta\right) + o\left(\frac{1}{k^2 s^2}\right). \quad (3.28)$$

Notice that the approximate result (3.26) for  $H_z^c(Q)$  vanishes when  $\theta = 0$  or  $\theta = \pi/2$ . The same holds true for the exact value of  $H_z^c(Q)$  in (3.22).

The present approximate results in (3.26) and (3.27) are now compared to the solutions derived in [1] and [2]. Chang et al. [1] present the asymptotic formula [1, Eq. (125)]

$$H_z^c(Q) \approx -\frac{k^2 Y}{2\pi j} \frac{e^{-jks}}{ks} \cos \theta \sin \theta \left[ v_0(\xi) + \frac{j}{ks} \left(-\frac{23}{8} + \frac{5}{9} \frac{\sin^2 \theta}{\cos^2 \theta}\right) v_0(\xi) \right] \quad (3.29)$$

and the "full formula" [1, Eq. (105)]

$$H_z^c(Q) \approx -\frac{k^2 Y}{2\pi j} \frac{e^{-jks}}{ks} \cos \theta \sin \theta \left[ v_0(\xi) - \frac{3j}{ks} v_0(\xi) \right]. \quad (3.30)$$

From Lee et al. [2, Eq. (2.6)] we quote the solution

$$\begin{aligned} H_z^c(Q) &= -\cos \theta \sin \theta [H_b(Q) - H_t(Q)] \\ &= -\frac{k^2 Y}{2\pi j} \frac{e^{-jks}}{ks} \cos \theta \sin \theta \left[ \left(1 - \frac{2j}{ks}\right) v(\xi) - \left(\frac{j}{ks} + \frac{3}{k^2 s^2}\right) u(\xi) \right. \\ &\quad \left. + \frac{2^{-1/3} j}{(ka)^{2/3}} \cos^{4/3} \theta \left\{ v'(\xi) + \frac{\sin^2 \theta}{\cos^2 \theta} u'(\xi) - \frac{j}{ks} u'(\xi) \right\} \right]. \quad (3.31) \end{aligned}$$

The solutions (3.29) - (3.31) are re-expanded for large  $ka$  by means of (3.18).

Then the results (3.29) and (3.30) of Chang et al. [1] become

$$H_z^c(Q) \approx -\frac{k^2 Y}{2\pi j} \frac{e^{-jks}}{ks} \cos \theta \sin \theta \left[ 1 + \frac{j}{ks} \left( -\frac{23}{8} + \frac{5}{9} \frac{\sin^2 \theta}{\cos^2 \theta} \right) + \frac{1}{4ka} \left( \frac{\pi}{2} \right)^{1/2} e^{-j\pi/4} (ks)^{1/2} \left\{ \frac{5}{9} - \cos^2 \theta (jks + \frac{247}{72}) \right\} \right], \quad (3.32)$$

and

$$H_z^c(Q) \approx -\frac{k^2 Y}{2\pi j} \frac{e^{-jks}}{ks} \cos \theta \sin \theta \left[ 1 - \frac{3j}{ks} + \frac{1}{4ka} \left( \frac{\pi}{2} \right)^{1/2} e^{-j\pi/4} (ks)^{1/2} \cdot \{-\cos^2 \theta (jks + 3)\} \right], \quad (3.33)$$

whereas the result (3.31) of Lee et al.[2] becomes

$$H_z^c(Q) \approx -\frac{k^2 Y}{2\pi j} \frac{e^{-jks}}{ks} \cos \theta \sin \theta \left[ 1 - \frac{3j}{ks} - \frac{3}{k^2 s^2} + \frac{1}{4ka} \left( \frac{\pi}{2} \right)^{1/2} e^{-j\pi/4} (ks)^{1/2} \left\{ 3 - \cos^2 \theta (jks + \frac{11}{2}) + \frac{3j}{ks} \cos^2 \theta \right\} \right]. \quad (3.34)$$

The asymptotic formula (3.32) agrees with (3.27) only at  $\theta = 0$ . Both the "full formula" (3.33) of Chang et al. and the solution (3.34) of Lee et al. have the planar solution as their leading term. As for the next terms of order  $\frac{1}{ka}$  in (3.33) and 3.34), there is only partial agreement with (3.27).

#### 4. SURFACE MAGNETIC FIELD DUE TO AN AXIAL MAGNETIC DIPOLE

In this section we consider the case of an axial dipole

$$\vec{M} = \hat{z} \quad (4.1)$$

The resulting surface magnetic field components are denoted by  $H_{\phi}^a(Q)$  and  $H_z^a(Q)$ . Exact results for  $H_{\phi}^a(Q)$  and  $H_z^a(Q)$  are presented in [1, Eqs. (26) and (27)], subject to a neglect of the contribution due to creeping waves which have travelled around the cylinder.

##### 4.1. Magnetic field component $H_{\phi}^a$ .

The result for  $H_{\phi}^a$  in [1, Eq. (27)] is identical to that for the component  $H_z^c$ , as given in (3.22). Thus when applying the Debye-type approximation to the Hankel function quotient, we are led to the results (3.26) and (3.27) for  $H_{\phi}^a$ . Also the asymptotic formula [1, Eq. (127)]\* and the "full formula" [1, Eq. (112)]\* of Chang et al. for  $H_{\phi}^a$  are the same as those for  $H_z^c$ . Hence Eqs. (3.29), (3.30), (3.32) and (3.33) also hold for  $H_{\phi}^a(Q)$ . Also the solutions (3.31) and (3.34) of Lee et al. for  $H_z^c(Q)$  hold true for  $H_{\phi}^a(Q)$  as well.

##### 4.2. Magnetic field component $H_z^a$ .

According to [1, Eq. (26)],  $H_z^a$  is given by\*\*

$$H_z^a(Q) = \frac{j}{4\pi^2 \omega \mu_0 a} \int_{-\infty}^{\infty} dk_z e^{-jk_z z} k_t \int_{-\infty}^{\infty} dv e^{-jv\phi} \frac{H_{\nu}^{(2)}(k_t a)}{H_{\nu}^{(2)'}(k_t a)} \quad (4.2)$$

\* Minor printing errors: in Eq. (127), replace  $\frac{23}{4}$  by  $\frac{23}{8}$ ; in Eq. (112), replace  $H_z^a$  by  $H_{\phi}^a$ .

\*\* Notice that there is a misprint in [1, Eq. (26)]:  $-j$  in front of the integral should be  $+j$ .

In (4.2), the quotient of the Hankel function and its derivative is replaced by the approximation (2.6) and we set  $v = k_y a$ . Thus we obtain

$$H_z^a(Q) \approx -\frac{Y}{4\pi^2 k} \int_{-\infty}^{\infty} \int_{-\infty}^{\infty} \exp[-jk_z z - jk_y a\phi] \left\{ \frac{k^2 - k_z^2}{\sqrt{k^2 - k_y^2 - k_z^2}} + \frac{j}{2a} \frac{(k^2 - k_z^2)^2}{(k^2 - k_y^2 - k_z^2)^2} \right\} dk_y dk_z. \quad (4.3)$$

The latter integral can be expressed in terms of the derivatives of  $I_1(a\phi, z)$  and  $I_2(a\phi, z)$ , as defined by (3.4) and (3.5), viz.,

$$H_z^a(Q) \approx -\frac{Y}{4\pi^2 k} \left[ \left\{ k^2 + \frac{\partial^2}{\partial z^2} \right\} I_1(a\phi, z) + \frac{j}{2a} \left\{ k^2 + \frac{\partial^2}{\partial z^2} \right\}^2 I_2(a\phi, z) \right]. \quad (4.4)$$

On substituting the explicit values of  $I_1$  and  $I_2$  from (3.6) and (3.9), we find

$$H_z^a(Q) \approx \frac{Y}{2\pi j k} \left[ \left\{ k^2 + \sin^2 \theta \frac{\partial^2}{\partial s^2} + \cos^2 \theta \frac{1}{s} \frac{\partial}{\partial s} \right\} \left( \frac{e^{-jks}}{s} \right) + \frac{j\pi}{8ka} \left\{ k^4 + 2k^2 \sin^2 \theta s^2 D^2 + 2k^2 D + \sin^4 \theta s^4 D^4 + 6 \sin^2 \theta s^2 D^3 + 3D^2 \right\} (\text{sh}_1^{(2)}(ks)) \right] \quad (4.5)$$

where  $D = \frac{1}{s} \frac{\partial}{\partial s}$ . Using the well-known recurrence relations for Bessel functions, we ultimately obtain

$$H_z^a(Q) \approx \frac{k^2 Y}{2\pi j} \frac{e^{-jks}}{ks} \left[ \cos^2 \theta + \frac{j}{ks} (2 - 3 \cos^2 \theta) + \frac{1}{k^2 s^2} (2 - 3 \cos^2 \theta) \right] - \frac{k^2 Y}{16ka} \left[ -2 \cos^2 \theta H_2^{(2)}(ks) - \frac{1}{ks} H_1^{(2)}(ks) + ks H_3^{(2)}(ks) \cos^4 \theta \right]. \quad (4.6)$$

Notice that except for the Debye-type approximation to the Hankel function quotient in (4.2), no further approximations were involved in the derivation of (4.6). The first term in (4.6) equals the planar solution, that is, the solution for  $H_z$  due to an axial magnetic dipole  $\vec{M} = \hat{z}$  on a flat ground

plane; see [1, Appendix D] and [2, Eq. (2.17)]. For large  $ks$  the Hankel functions in (4.6) can be replaced by their large-argument asymptotic expansions, yielding

$$H_z^a(Q) \approx \frac{k^2 Y}{2\pi j} \frac{e^{-jks}}{ks} \left[ \cos^2 \theta + \frac{j}{ks} (2 - 3 \cos^2 \theta) + \frac{1}{k^2 s^2} (2 - 3 \cos^2 \theta) \right. \\ \left. + \frac{1}{4ka} \left(\frac{\pi}{2}\right)^{1/2} e^{-j\pi/4} (ks)^{1/2} \{2 \cos^2 \theta - \cos^4 \theta (jks + \frac{35}{8}) + O(\frac{1}{ks})\} \right] . \quad (4.7)$$

Let the term of order  $\frac{1}{ka}$  in (4.7) be denoted by  $\tilde{W}$ , then for  $\theta = \pi/2$  one has  $\tilde{W} = 0$ . Hence, there is no term of the form (3.14) in the approximate result for  $H_z^a$ . This agrees with Lee et al. [2, Eq. (2.17)] where there is no such term either. On extending the result in (4.7), it is found that the term of order  $O(\frac{1}{ks})$  is equal to

$$\frac{j}{ks} \left( -1 - \frac{15}{4} \cos^2 \theta + \frac{945}{128} \cos^4 \theta \right) + O\left(\frac{1}{k^2 s^2}\right) . \quad (4.8)$$

The present approximate results in (4.6) and (4.7) are now compared to the solutions obtained by Chang et al. [1] and Lee et al. [2]. In [1] two different formulas for  $H_z^a$  are presented, namely, the asymptotic formula [1, Eq. (126)]

$$H_z^a(Q) \approx \frac{k^2 Y}{2\pi j} \frac{e^{-jks}}{ks} \left[ \cos^2 \theta v_0(\xi) + \frac{j}{ks} \left( \frac{20}{9} \sin^2 \theta - \frac{29}{24} \cos^2 \theta \right) v_0(\xi) \right] , \quad (4.9)$$

and the "full formula" [1, Eq. (111)]

$$H_z^a(Q) \approx \frac{k^2 Y}{2\pi j} \frac{e^{-jks}}{ks} \left[ \cos^2 \theta v_0(\xi) + \frac{j}{ks} (2 \sin^2 \theta - \cos^2 \theta) v_0(\xi) \right] . \quad (4.10)$$

From Lee et al. [2, Eq. (2.15b)] we quote the solution

$$\begin{aligned}
H_z^a(Q) \approx & \frac{k^2 Y}{2\pi j} \frac{e^{-jks}}{ks} \left[ \cos^2 \theta v(\xi) - \frac{j}{ks} (\cos^2 \theta - \sin^2 \theta) v(\xi) + \frac{j}{ks} \sin^2 \theta u(\xi) \right. \\
& + \frac{1}{k^2 s^2} (2 \sin^2 \theta - \cos^2 \theta) u(\xi) + \frac{2^{-1/3} j}{(ka)^{2/3}} \cos^{4/3} \theta \{ \cos^2 \theta v'(\xi) \\
& \left. + \sin^2 \theta u'(\xi) + \frac{j}{ks} \sin^2 \theta u'(\xi) \} \right] . \quad (4.11)
\end{aligned}$$

The solutions (4.9) - (4.11) are re-expanded for large  $ka$ , that is, for small  $\xi$ , by means of (3.18). Then the solutions (4.9) and (4.10) of Chang et al. [1] become

$$\begin{aligned}
H_z^a(Q) \approx & \frac{k^2 Y}{2\pi j} \frac{e^{-jks}}{ks} \left[ \cos^2 \theta + \frac{j}{ks} \left( \frac{20}{9} - \frac{247}{72} \cos^2 \theta \right) \right. \\
& \left. + \frac{1}{4ka} \left( \frac{\pi}{2} \right)^{1/2} e^{-j\pi/4} (ks)^{1/2} \left\{ \frac{20}{9} \cos^2 \theta - \cos^4 \theta \left( jks + \frac{247}{72} \right) \right\} \right] , \quad (4.12)
\end{aligned}$$

and

$$\begin{aligned}
H_z^a(Q) \approx & \frac{k^2 Y}{2\pi j} \frac{e^{-jks}}{ks} \left[ \cos^2 \theta + \frac{j}{ks} (2 - 3 \cos^2 \theta) \right. \\
& \left. + \frac{1}{4ka} \left( \frac{\pi}{2} \right)^{1/2} e^{-j\pi/4} (ks)^{1/2} \left\{ 2 \cos^2 \theta - \cos^4 \theta (jks + 3) \right\} \right] , \quad (4.13)
\end{aligned}$$

whereas the solution (4.11) due to Lee et al. [2] becomes

$$\begin{aligned}
H_z^a(Q) \approx & \frac{k^2 Y}{2\pi j} \frac{e^{-jks}}{ks} \left[ \cos^2 \theta + \frac{j}{ks} (2 - 3 \cos^2 \theta) + \frac{1}{k^2 s^2} (2 - 3 \cos^2 \theta) \right. \\
& \left. + \frac{1}{4ka} \left( \frac{\pi}{2} \right)^{1/2} e^{-j\pi/4} (ks)^{1/2} \left\{ 6 \cos^2 \theta - \cos^4 \theta \left( jks + \frac{11}{2} \right) + \frac{j}{ks} \cos^2 \theta (2 - 3 \sin^2 \theta) \right\} \right] . \quad (4.14)
\end{aligned}$$

The asymptotic formula (4.12) due to Chang et al. [1] does not agree with (4.7), even its leading term does not agree with the planar solution.

The "full formula" (4.13) of Chang et al. and the solution (4.14) of Lee et al. do have the planar solution as their leading term. The next terms of order  $\frac{1}{ka}$  in (4.13) and (4.14) agree only partially with the corresponding term in (4.7).

## 5. REPRESENTATION OF THE SURFACE MAGNETIC FIELD IN DYADIC FORM

According to Lee et al. [2, Eq. (2.6a)], the asymptotic solution for the surface magnetic field at Q due to a magnetic dipole  $\vec{M}$  at P can be expressed in the following dyadic form:

$$\vec{H}(Q) \approx \vec{M} \cdot [\hat{b}'\hat{b}H_b(Q) + \hat{t}'\hat{t}H_t(Q)] \quad (5.1)$$

Here,  $\hat{t}'$  and  $\hat{b}'$  are the unit tangent and unit binormal of the surface ray at the source point P, and similarly,  $\hat{t}$  and  $\hat{b}$  are the unit tangent and unit binormal of the surface ray at the observation point Q; see Fig. 2 for a picture of these vectors on the developed cylinder.

In Chang et al. [1, Eq. (128)], the surface magnetic field is represented by a different dyadic form, namely,

$$\vec{H}(Q) \approx \vec{M} \cdot [\hat{b}'\hat{b}A + \hat{t}'\hat{t}B + \hat{\phi}'\hat{\phi}C] \quad (5.2)$$

where  $\hat{\phi}'$  and  $\hat{\phi}$  are unit vectors at P and Q in the direction of increasing  $\phi$ . The result in (5.2) is based on the "full formula" for the magnetic field components. The main difference between (5.1) and (5.2) is that the result of Chang et al. [1] contains a cross term C, whereas no such term is present in the result of Lee et al. [2].

We now examine the possibility of expressing our results for the surface magnetic field in a dyadic form similar to either (5.1) or (5.2). Starting from (5.1) in the case of a circumferential dipole  $\vec{M} = \hat{\phi}$ , the surface magnetic field has components  $H_b^C(Q)$  and  $H_t^C(Q)$  given by

$$H_b^C(Q) = H_b \sin^2 \theta + H_t \cos^2 \theta \quad (5.3)$$

and

$$H_t^C(Q) = - (H_b - H_t) \sin \theta \cos \theta \quad (5.4)$$

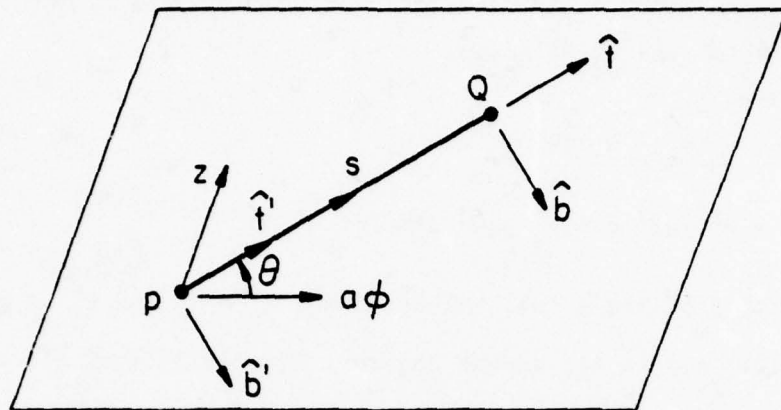


Figure 2. Unit vectors ( $\hat{t}'$ ,  $\hat{b}'$ ,  $\hat{t}$ ,  $\hat{b}$ ) and surface ray PQ on developed cylinder.

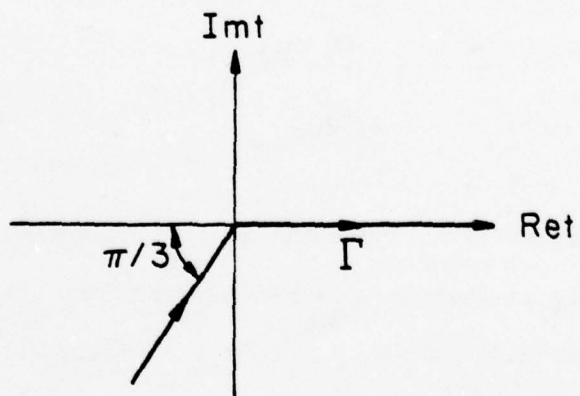


Figure 3. Integration contour  $\Gamma$ .

Similarly, for an axial magnetic dipole  $\vec{M} = \hat{z}$  the surface magnetic field components  $H_\phi^a(Q)$  and  $H_z^a(Q)$  become

$$H_\phi^a(Q) = - (H_b - H_t) \sin \theta \cos \theta, \quad (5.5)$$

$$H_z^a(Q) = H_b \cos^2 \theta + H_t \sin^2 \theta \quad . \quad (5.6)$$

On substitution of the actual values of  $H_\phi^c$ ,  $H_z^c = H_\phi^a$  and  $H_z^a$  as given by (3.11), (3.26) and (4.6), we can consider Eqs. (5.3) - (5.6), as a system of four equations for the two components  $H_b$  and  $H_t$ . It is easily seen that this system is incompatible and does not have a solution for  $H_b$  and  $H_t$ . Indeed, when taking the difference of (5.6) and (5.3), we find

$$H_b - H_t = \frac{H_z^a(Q) - H_\phi^c(Q)}{\cos^2 \theta - \sin^2 \theta} \quad , \quad (5.7)$$

whereas according to (5.4), we have

$$H_b - H_t = - \frac{H_z^c(Q)}{\sin \theta \cos \theta} \quad . \quad (5.8)$$

Now it can easily be verified that

$$\frac{H_z^a(Q) - H_\phi^c(Q)}{\cos^2 \theta - \sin^2 \theta} \neq - \frac{H_z^c(Q)}{\sin \theta \cos \theta} \quad . \quad (5.9)$$

In conclusion, it is not possible to express our results for the surface magnetic field in the two-component dyadic form (5.1), as found by Lee et al. [2].

Next, we try to express our results for the surface magnetic field in a four-component dyadic form, viz.,

$$\vec{H}(Q) \approx \vec{M} \cdot [\hat{b}'\hat{b}H_{bb} + \hat{t}'\hat{t}H_{tt} + \hat{b}'\hat{t}H_{bt} + \hat{t}'\hat{b}H_{tb}] \quad (5.10)$$

which is similar to (5.2). Then the magnetic field components for the cases of a circumferential or an axial dipole become

$$\begin{cases} H_{\phi}^c(Q) = H_{bb} \sin^2 \theta + H_{tt} \cos^2 \theta + (H_{bt} + H_{tb}) \sin \theta \cos \theta , \\ H_z^c(Q) = - (H_{bb} - H_{tt}) \sin \theta \cos \theta + H_{bt} \sin^2 \theta - H_{tb} \cos^2 \theta , \\ H_{\phi}^a(Q) = - (H_{bb} - H_{tt}) \sin \theta \cos \theta - H_{bt} \cos^2 \theta + H_{tb} \sin^2 \theta , \\ H_z^a(Q) = H_{bb} \cos^2 \theta + H_{tt} \sin^2 \theta - (H_{bt} + H_{tb}) \sin \theta \cos \theta . \end{cases} \quad (5.11)$$

Since  $H_{\phi}^a(Q) = H_z^c(Q)$ , as found in Sec. 4.1, we have  $H_{bt} = H_{tb}$ . Then the system of equations (5.11) can be readily solved, yielding

$$\begin{cases} H_{bb}(Q) = H_{\phi}^c(Q) \sin^2 \theta + H_z^a(Q) \cos^2 \theta - 2H_z^c(Q) \sin \theta \cos \theta , \\ H_{tt}(Q) = H_{\phi}^c(Q) \cos^2 \theta + H_z^a(Q) \sin^2 \theta + 2H_z^c(Q) \sin \theta \cos \theta , \\ H_{bt}(Q) = H_{tb}(Q) = [H_{\phi}^c(Q) - H_z^a(Q)] \sin \theta \cos \theta - H_z^c(Q)(\cos^2 \theta - \sin^2 \theta) . \end{cases} \quad (5.12)$$

We now substitute the actual values of  $H_{\phi}^c(Q)$ ,  $H_z^c(Q)$  and  $H_z^a(Q)$ , taken from (3.11), (3.26) and (4.6). Then we obtain

$$\begin{aligned} H_{bb}(Q) \approx \frac{k^2 \gamma}{2\pi j} \frac{e^{-jks}}{ks} \left[ 1 - \frac{j}{ks} - \frac{1}{k^2 s^2} \right] - \frac{k^2 \gamma}{16ka} [3H_0^{(2)}(ks) \sin^2 \theta - \frac{1}{ks} H_1^{(2)}(ks) \\ - 2H_2^{(2)}(ks) \cos^2 \theta + ksH_3^{(2)}(ks) \cos^2 \theta] , \end{aligned} \quad (5.13)$$

and

$$H_{tt}(Q) \approx \frac{k^2 \gamma}{2\pi j} \frac{e^{-jks}}{ks} \left[ \frac{2j}{ks} + \frac{2}{k^2 s^2} \right] - \frac{k^2 \gamma}{16ka} [3H_0^{(2)}(ks) \cos^2 \theta - \frac{1}{ks} H_1^{(2)}(ks)] , \quad (5.14)$$

and

$$H_{bt}(Q) = H_{tb}(Q) \approx - \frac{k^2 \gamma}{16ka} \sin \theta \cos \theta [3H_0^{(2)}(ks) + H_2^{(2)}(ks)] . \quad (5.15)$$

Notice that the leading terms of (5.13) and (5.14) agree with the planar solution for  $H_b$  and  $H_t$ , as given in [1, Appendix D] and [2, Eqs. 2.8a,b)]. For large  $ks$  the Hankel functions in (5.13) - (5.15) can be replaced by their large-argument asymptotic expansions, thus leading to

$$H_{bb}(Q) \approx \frac{k^2 Y}{2\pi j} \frac{e^{-jks}}{ks} \left[ 1 - \frac{j}{ks} - \frac{1}{k^2 s^2} + \frac{1}{4ka} \left(\frac{\pi}{2}\right)^{1/2} e^{-j\pi/4} (ks)^{1/2} \left\{ 3 - \cos^2 \theta \left( jks + \frac{43}{8} \right) + \frac{j}{ks} \left( -\frac{5}{8} + \frac{417}{128} \cos^2 \theta \right) + o\left(\frac{1}{k^2 s^2}\right) \right\} \right], \quad (5.16)$$

and

$$H_{tt}(Q) \approx \frac{k^2 Y}{2\pi j} \frac{e^{-jks}}{ks} \left[ \frac{2j}{ks} + \frac{2}{k^2 s^2} + \frac{1}{4ka} \left(\frac{\pi}{2}\right)^{1/2} e^{-j\pi/4} (ks)^{1/2} \left\{ 3 \cos^2 \theta + \frac{j}{ks} \left( -1 + \frac{3}{8} \cos^2 \theta \right) + o\left(\frac{1}{k^2 s^2}\right) \right\} \right], \quad (5.17)$$

and

$$H_{bt}(Q) = H_{tb}(Q) \approx \frac{k^2 Y}{2\pi j} \frac{e^{-jks}}{ks} \cdot \frac{1}{4ka} \left(\frac{\pi}{2}\right)^{1/2} e^{-j\pi/4} (ks)^{1/2} \cos \theta \sin \theta \cdot \left\{ 2 + \frac{9j}{4ks} + o\left(\frac{1}{k^2 s^2}\right) \right\}. \quad (5.18)$$

Alternatively, the surface magnetic field  $\vec{H}(Q)$  can also be represented by the form (5.2). From a comparison of (5.2) and (5.10), we find that A, B, and C are given by

$$A = H_{bb} - H_{bt} \frac{\sin \theta}{\cos \theta}, \quad B = H_{tt} - H_{bt} \frac{\cos \theta}{\sin \theta}, \quad C = \frac{H_{bt}}{\sin \theta \cos \theta}. \quad (5.19)$$

AD-A066 330

ILLINOIS UNIV AT URBANA-CHAMPAIGN ELECTROMAGNETICS LAB

F/G 9/5

AN INVESTIGATION ON CHARACTERIZING MUTUAL COUPLING BETWEEN TWO --ETC(U)

JAN 79 S W LEE, R MITTRA, J BOERSMA, E YUNG

N00019-78-C-0064

UNCLASSIFIED

UIEM-79-2

NL

2 OF 3  
AD  
A066330



## 6. MATCHING TO AN EXPANSION IN TERMS OF FOCK FUNCTIONS

In Sections 3 and 4 we derived approximations to the surface field components  $H_\phi^c$ ,  $H_z^c$  and  $H_\phi^a$ ,  $H_z^a$  due to a circumferential or an axial magnetic dipole on the surface of a cylinder; see (3.11), (3.13), (3.26), (3.27), (4.6) and (4.7) for the final results. These approximations were obtained by starting from the exact solution in [1] and replacing the quotient of the Hankel function and its derivative by the Debye approximation as given in (2.6) and (2.12). Although the use of the Debye approximation has not been fully justified, it is believed that our approximate results for the surface field components are valid for large ka and small  $\xi$  where

$$\xi = 2^{-1/3} \frac{ks}{(ka)^{2/3}} \cos^{4/3} \theta.$$

For large  $\xi$ , i.e., in the deep shadow, the surface field decays exponentially as a function of  $\xi$ ; see [1] and [2]. This  $\xi$ -dependence of the surface field is properly described in terms of Fock functions  $u(\xi)$  and  $v(\xi)$ . Following [2, Appendix], the Fock functions  $u(\xi)$  and  $v(\xi)$  are defined by

$$v(\xi) = \frac{e^{j\pi/4}}{2\sqrt{\pi}} \xi^{1/2} \int_{\Gamma} \frac{w_2(t)}{w_2'(t)} e^{-j\xi t} dt, \quad (6.1)$$

and

$$u(\xi) = \frac{e^{3j\pi/4}}{\sqrt{\pi}} \xi^{3/2} \int_{\Gamma} \frac{w_2'(t)}{w_2(t)} e^{-j\xi t} dt, \quad (6.2)$$

where  $w_2(t)$  is an Airy function, viz.,

$$w_2(t) = \sqrt{\pi} [\text{Bi}(t) - j\text{Ai}(t)] = 2\sqrt{\pi} e^{-j\pi/6} \text{Ai}(te^{-2j\pi/3}) \quad (6.3)$$

and the contour  $\Gamma$  is sketched in Fig. 3 (see Page 23).

The "hard" Fock function  $v(\xi)$  arises when approximating integrals with an integrand containing  $H_\nu^{(2)}(k_t a) / H_\nu^{(2)'}(k_t a)$ ; similarly, the "soft" Fock

function  $u(\xi)$  arises when the integrand contains  $H_V^{(2)'}(k_t a)/H_V^{(2)}(k_t a)$ . In [1, Appendix B] the notations  $v_0(\xi)$  and  $u_0(\xi)$  are used for  $v(\xi)$  and  $u(\xi)$ , respectively. By closing the contour  $\Gamma$  at infinity in (6.1) and (6.2), we arrive at the following residue-series representations for  $v(\xi)$  and  $u(\xi)$ :

$$v(\xi) = e^{-j\pi/4} \sqrt{\pi} \xi^{1/2} \sum_{n=1}^{\infty} \frac{\exp[-j\xi t'_n]}{t'_n}$$

$$u(\xi) = 2e^{j\pi/4} \sqrt{\pi} \xi^{3/2} \sum_{n=1}^{\infty} \exp[-j\xi t_n] \quad ; \quad (6.4)$$

see [1, Eqs. (B20) and (B37)] and [2, Eqs. (A-7) and (A-8)]. Here  $t_n = |t_n| e^{-j\pi/3}$  and  $t'_n = |t'_n| e^{-j\pi/3}$ , with  $\text{Ai}(-|t_n|) = 0$  and  $\text{Ai}'(-|t'_n|) = 0$ ; see [2, p. 34] for a table of the zeros  $|t_n|$  and  $|t'_n|$ . It is clear from (6.4), that the Fock functions  $v(\xi)$  and  $u(\xi)$  decay exponentially as  $\xi \rightarrow \infty$ . Notice that  $u(\xi)$  decays faster than  $v(\xi)$ , since  $|t'_n| < |t_n|$ . For small  $\xi$ , the Fock functions can be represented by the power-series expansions

$$v(\xi) = 1 - \frac{\sqrt{\pi}}{4} e^{j\pi/4} \xi^{3/2} + \frac{7j}{60} \xi^3 + \frac{7\sqrt{\pi}}{512} e^{-j\pi/4} \xi^{9/2} + o(\xi^6) \quad ,$$

$$u(\xi) = 1 - \frac{\sqrt{\pi}}{2} e^{j\pi/4} \xi^{3/2} + \frac{5j}{12} \xi^3 + \frac{5\sqrt{\pi}}{64} e^{-j\pi/4} \xi^{9/2} + o(\xi^6) \quad , \quad (6.5)$$

quoted from [1, Eqs. (B19) and (B36)], and [2, Eqs. (A-12) and (A-13)].

We shall now match the previous approximations for the surface field components  $H_D^c$ ,  $H_z^c = H_D^a$  and  $H_z^a$ , to a new set of approximations in terms of Fock functions  $v(\xi)$  and  $u(\xi)$ . More specifically, we construct new approximations involving Fock functions in such a manner that for small  $\xi$  the new approximations reduce to those obtained in Sections 3 and 4, whereby the Fock functions are replaced by their power-series expansions in (6.5). It is hoped that these new approximations are valid uniformly in  $\xi$ .

### 6.1 Magnetic field component $H_\phi^c$ .

The exact solution for  $H_\phi^c$  is given by (3.2) and consists of two terms. Following [1, Eqs. (18) and (19)], we denote these terms by  $H_\phi^{\prime\prime c}$  and  $H_\phi^{\prime c}$ . Both terms are double integrals; the integrand of the term  $H_\phi^{\prime\prime c}$  contains the quotient  $H_V^{(2)}(k_t a)/H_V^{(2)\prime}(k_t a)$ , whereas the term  $H_\phi^{\prime c}$  has an integrand which contains the quotient  $H_V^{(2)\prime}(k_t a)/H_V^{(2)}(k_t a)$ . Thus,  $H_\phi^{\prime\prime c}$  should be matched to an approximation involving the hard Fock function  $v(\xi)$ , whereas  $H_\phi^{\prime c}$  is matched to an approximation which involves the soft Fock function  $u(\xi)$ . In the exact solutions for  $H_\phi^{\prime\prime c}$  and  $H_\phi^{\prime c}$ , we replace the Hankel function quotients by the Debye approximations in (2.6) and (2.12), respectively. Furthermore we set  $v = k_y a$  in the inner integral. Then we are led to the following approximations for  $H_\phi^{\prime\prime c}(Q)$  and  $H_\phi^{\prime c}(Q)$ :

$$\begin{aligned}
 H_\phi^{\prime\prime c}(Q) &\approx \frac{1}{4\pi^2 \omega \mu_0} \int_{-\infty}^{\infty} \int_{-\infty}^{\infty} \exp[-jk_z z - jk_y a \phi] \left\{ \frac{k_z^2 k_y^2}{k_t^3} \left\{ \frac{jk_t}{\sqrt{k_t^2 - k_y^2}} - \frac{1}{2a} \frac{k_t^3}{(k_t^2 - k_y^2)^2} \right\} \right\} dk_y dk_z \\
 &= -\frac{Y}{4\pi^2 k} \int_{-\infty}^{\infty} \int_{-\infty}^{\infty} \exp[-jk_z z - jk_y a \phi] \left\{ \frac{k^2 - k_v^2}{\sqrt{k^2 - k_y^2 - k_z^2}} - \frac{k^2}{k^2 - k_z^2} \sqrt{k^2 - k_y^2 - k_z^2} \right. \\
 &\quad \left. + \frac{1}{2a} \frac{k_v^2 k_z^2}{(k^2 - k_y^2 - k_z^2)^2} \right\} dk_y dk_z, \quad (6.6)
 \end{aligned}$$

and

$$\begin{aligned}
 H_\phi^{\prime c}(Q) &\approx \frac{-jk^2}{4\pi^2 \omega \mu_0} \int_{-\infty}^{\infty} \int_{-\infty}^{\infty} \exp[-jk_z z - jk_y a \phi] \left\{ -\frac{j\sqrt{k_t^2 - k_y^2}}{k_t^2} - \frac{1}{2a} \frac{1}{k_t^2 - k_y^2} \right\} dk_y dk_z \\
 &= -\frac{Yk^2}{4\pi^2 k} \int_{-\infty}^{\infty} \int_{-\infty}^{\infty} \exp[-jk_z z - jk_y a \phi] \left\{ \frac{\sqrt{k^2 - k_y^2 - k_z^2}}{k^2 - k_z^2} - \frac{1}{2a} \frac{1}{k^2 - k_y^2 - k_z^2} \right\} dk_y dk_z. \quad (6.7)
 \end{aligned}$$

Notice that the sum of (6.6) and (6.7) is equal to (3.3).

The double integrals in (6.6) and (6.7) can be expressed in terms of  $I_1(a\phi, z)$  and  $I_2(a\phi, z)$ , as defined by (3.4) and (3.5), and another key integral  $I_3(a\phi, z)$  defined by

$$I_3(a\phi, z) = \int_{-\infty}^{\infty} \int_{-\infty}^{\infty} \exp[-jk_z z - jk_y a\phi] \frac{\sqrt{k^2 - k_y^2 - k_z^2}}{k^2 - k_z^2} dk_y dk_z \quad (6.8)$$

The latter integral can be evaluated in closed form by use of the relation

$$\begin{aligned} \left(\frac{\partial^2}{\partial z^2} + k^2\right) I_3(a\phi, z) &= \int_{-\infty}^{\infty} \int_{-\infty}^{\infty} \exp[-jk_z z - jk_y a\phi] \sqrt{k^2 - k_y^2 - k_z^2} dk_y dk_z \\ &= \left[ \frac{\partial^2}{\partial (a\phi)^2} + \frac{\partial^2}{\partial z^2} + k^2 \right] I_1(a\phi, z) \quad (6.9) \end{aligned}$$

On substitution of the value of  $I_1(a\phi, z)$  from (3.6), we are led to the following differential equation for  $I_3(a\phi, z)$ :

$$\begin{aligned} \left(\frac{\partial^2}{\partial z^2} + k^2\right) I_3(a\phi, z) &= \left(\frac{d^2}{ds^2} + \frac{1}{s} \frac{d}{ds} + k^2\right) 2\pi j \frac{e^{-jks}}{s} = 2\pi j e^{-jks} \left(\frac{jk}{s^2} + \frac{1}{s}\right) \\ &= \pi\sqrt{2\pi} k^{3/2} s^{-3/2} H_{3/2}^{(2)}(ks) \quad (6.10) \end{aligned}$$

where  $s = \sqrt{(a\phi)^2 + z^2}$  is the distance from the source point P to the observation point Q along the surface ray; see Fig. 1.

The differential equation (6.10) can be solved by Fourier transformation. On defining the Fourier transform of  $I_3$  by

$$F_z\{I_3(a\phi, z)\} = \int_{-\infty}^{\infty} I_3(a\phi, z) e^{jzt} dz = 2 \int_0^{\infty} I_3(a\phi, z) \cos(zt) dz \quad (6.11)$$

we readily find from (6.10)

$$\begin{aligned}
F_z\{I_3(a\phi, z)\} &= -\frac{\pi\sqrt{2\pi}k^{3/2}}{t^2 - k^2} F_z\{[(a\phi)^2 + z^2]^{-3/4} H_{3/2}^{(2)}(k\sqrt{(a\phi)^2 + z^2})\} \\
&= -4\pi j (a\phi)^{-1} \frac{K_1(a\phi\sqrt{t^2 - k^2})}{\sqrt{t^2 - k^2}} \quad (6.12)
\end{aligned}$$

where the Fourier transform of the Hankel function was quoted from [6, Eq. 1.13(42)].\* In (6.12) it is understood that  $\sqrt{t^2 - k^2} \rightarrow \sqrt{k^2 - t^2}$  when  $t < k$ , in accordance with  $k$  having a small negative imaginary part.

By inverse Fourier transformation we have from (6.12),

$$\begin{aligned}
I_3(a\phi, z) &= -\frac{4\pi j}{2\pi} (a\phi)^{-1} 2 \int_0^\infty \frac{K_1(a\phi\sqrt{t^2 - k^2})}{\sqrt{t^2 - k^2}} \cos(zt) dt = -2\pi k^{-1} (a\phi)^{-2} e^{-jks} \\
&= -\frac{2\pi}{ks^2 \cos^2 \theta} e^{-jks} \quad , \quad (6.13)
\end{aligned}$$

where the Fourier cosine transform of  $K_1$  was obtained from [6, Eq. 1.13(44)]. The present result for  $I_3(a\phi, z)$  was checked by back-substitution into (6.10). In fact, the general solution of the differential equation (6.10) is given by

$$I_3(a\phi, z) = -2\pi k^{-1} (a\phi)^{-2} e^{-jks} + A \cos kz + B \sin kz \quad , \quad (6.14)$$

where  $A$  and  $B$  are arbitrary constants which may depend on  $a\phi$ .

Now since  $I_3(a\phi, z)$  is an even function of  $z$ , one has  $B = 0$ . By a direct calculation of  $I_3(a\phi, z = 0)$  it is found that  $A = 0$  as well. Thus the result in (6.13) is correct.

We now return to the magnetic field components  $H_\phi^{i,c}$  and  $H_\phi^{i,c}$ , as given by (6.6) and (6.7). As mentioned before, the double integrals can

\* There are some obvious misprints in this formula: in the first part of the transform result  $H_V^{(2)}$  should be  $H_V^{(2)}$ ; the range of validity of the second part should be  $b < y < \infty$  instead of  $0 < y < b$ . All results have been checked in an independent manner by means of [3, Sec. 13.47].

be expressed in terms of derivatives of the key integrals  $I_1$ ,  $I_2$  and  $I_3$ .

Thus we find for  $H_\phi'^c$ ,

$$H_\phi'^c(Q) = -\frac{Y}{4\pi^2 k} \left[ \left\{ k^2 + \frac{\partial^2}{\partial (a\phi)^2} \right\} I_1(a\phi, z) - k^2 I_3(a\phi, z) + \frac{j}{2a} \frac{\partial^4}{\partial (a\phi)^2 \partial z^2} I_2(a\phi, z) \right], \quad (6.15)$$

and for  $H_\phi^c$ ,

$$H_\phi^c(Q) = -\frac{Yk^2}{4\pi^2 k} \left[ I_3(a\phi, z) - \frac{j}{2a} \left\{ k^2 + \frac{\partial^2}{\partial (a\phi)^2} + \frac{\partial^2}{\partial z^2} \right\} I_2(a\phi, z) \right]. \quad (6.16)$$

We now insert the actual values of  $I_1$ ,  $I_2$  and  $I_3$  as given by (3.6), (3.9) and (6.13). The derivatives of the Hankel function  $H_1^{(2)}(ks)$  are evaluated and simplified by means of the well-known recurrence relations for Bessel functions; see e.g., [3, Sec. 3.2] and [4, Eqs. 9.1.27 and 9.1.30]. Thus we obtain as our final result for the constituents  $H_\phi'^c$  and  $H_\phi^c$ :

$$H_\phi'^c(Q) = \frac{k^2 Y}{2\pi j} \frac{e^{-jks}}{ks} \left[ \sin^2 \theta + \frac{j}{ks} (2 - 3 \sin^2 \theta - \frac{1}{\cos^2 \theta}) + \frac{1}{k^2 s^2} (2 - 3 \sin^2 \theta) \right] \\ - \frac{k^2 Y}{16ka} \left[ H_0^{(2)}(ks) - \frac{1}{ks} H_1^{(2)}(ks) + ks H_3^{(2)}(ks) \cos^2 \theta \sin^2 \theta \right], \quad (6.17)$$

and

$$H_\phi^c(Q) = \frac{k^2 Y}{2\pi j} \frac{e^{-jks}}{ks} \left[ \frac{j}{ks} \frac{1}{\cos^2 \theta} \right] - \frac{k^2 Y}{16ka} \left[ 2H_0^{(2)}(ks) \right]. \quad (6.18)$$

As before, we observe that except for the Debye-type approximation to the Hankel function quotients, no further approximations were involved in the derivation of (6.17) and (6.18). The sum of (6.17) and (6.18) is equal to the field component  $H_\phi^c(Q)$  as given by (3.11).

For large  $ks$  the Hankel functions in (6.17) and (6.18) can be replaced by their large-argument asymptotic expansions, thus leading to

$$\begin{aligned}
H_{\phi}^{\prime\prime c}(Q) &= \frac{k^2 Y}{2\pi j} \frac{e^{-jks}}{ks} \left[ \sin^2 \theta + \frac{j}{ks} (2 - 3 \sin^2 \theta - \frac{1}{\cos^2 \theta}) + \frac{1}{k^2 s^2} (2 - 3 \sin^2 \theta) \right. \\
&\quad + \frac{1}{4ka} \left(\frac{\pi}{2}\right)^{1/2} e^{-j\pi/4} (ks)^{1/2} \left\{ 1 - \cos^2 \theta \sin^2 \theta (jks + \frac{35}{8}) \right. \\
&\quad \left. \left. + \frac{j}{ks} \left(-\frac{7}{8} + \frac{945}{128} \cos^2 \theta \sin^2 \theta\right) + o\left(\frac{1}{k^2 s^2}\right) \right\} \right] , \quad (6.19)
\end{aligned}$$

and

$$H_{\phi}^{\prime c}(Q) = \frac{k^2 Y}{2\pi j} \frac{e^{-jks}}{ks} \left[ \frac{j}{ks} \frac{1}{\cos^2 \theta} + \frac{1}{4ka} \left(\frac{\pi}{2}\right)^{1/2} e^{-j\pi/4} (ks)^{1/2} \left\{ 2 + \frac{j}{4ks} + o\left(\frac{1}{k^2 s^2}\right) \right\} \right] . \quad (6.20)$$

We now match these approximations to a new set of approximations of a form similar to that of Lee et al. [2] (see (3.17)), involving Fock functions. The new approximation for  $H_{\phi}^{\prime\prime c}$  involves the hard Fock function  $v(\xi)$  and its derivative  $v'(\xi)$ , whereas the approximation for  $H_{\phi}^{\prime c}$  contains the soft Fock functions  $u(\xi)$  and  $u'(\xi)$ . Therefore, guided by (3.17), we set

$$H_{\phi}^{\prime\prime c}(Q) = \frac{k^2 Y}{2\pi j} \frac{e^{-jks}}{ks} \left[ Av(\xi) + \frac{2^{-1/3} j}{(ka)^{2/3}} \cos^{4/3} \theta Bv'(\xi) \right] , \quad (6.21)$$

and

$$H_{\phi}^{\prime c}(Q) = \frac{k^2 Y}{2\pi j} \frac{e^{-jks}}{ks} \left[ Cu(\xi) + \frac{2^{-1/3} j}{(ka)^{2/3}} \cos^{4/3} \theta Du'(\xi) \right] , \quad (6.22)$$

where the constants A, B, C and D are determined by matching to (6.19) and (6.20) for small  $\xi$ .

For small  $\xi$  we replace  $v(\xi)$  and  $u(\xi)$  and their derivatives by the approximations

$$\begin{aligned}
v(\xi) &\approx 1 - \frac{\sqrt{\pi}}{4} e^{j\pi/4} \xi^{3/2} , \\
u(\xi) &\approx 1 - \frac{\sqrt{\pi}}{2} e^{j\pi/4} \xi^{3/2} ,
\end{aligned}$$

$$v'(\xi) \approx -\frac{3\sqrt{\pi}}{8} e^{j\pi/4} \xi^{-1/2}, \quad u'(\xi) \approx -\frac{3\sqrt{\pi}}{4} e^{j\pi/4} \xi^{-1/2}, \quad (6.23)$$

taken from (6.5). Then, the results (6.21) and (6.22) become

$$H_{\phi}^{c,c}(Q) \approx \frac{k^2 Y}{2\pi j} \frac{e^{-jks}}{ks} \left[ A + \frac{1}{4ka} \left(\frac{\pi}{2}\right)^{1/2} e^{-j\pi/4} (ks)^{1/2} \{-jksA \cos^2 \theta + \frac{3}{2}B \cos^2 \theta\} \right], \quad (6.24)$$

and

$$H_{\phi}^{c,c}(Q) \approx \frac{k^2 Y}{2\pi j} \frac{e^{-jks}}{ks} \left[ C + \frac{1}{4ka} \left(\frac{\pi}{2}\right)^{1/2} e^{-j\pi/4} (ks)^{1/2} \{-2jksC \cos^2 \theta + 3D \cos^2 \theta\} \right]. \quad (6.25)$$

By identifying (6.24) and (6.25) with (6.19) and (6.20), respectively,

we can readily determine the constants A, B, C and D, viz.,

$$\begin{cases} A = \sin^2 \theta + \frac{j}{ks} \left(2 - 3\sin^2 \theta - \frac{1}{\cos^2 \theta}\right) + \frac{1}{k^2 s^2} (2 - 3 \sin^2 \theta) \\ B = \frac{4}{3} \frac{\sin^2 \theta}{\cos^2 \theta} - \frac{11}{12} \sin^2 \theta + \frac{j}{ks} \left(\frac{3}{4} - \frac{7}{12} \frac{\sin^2 \theta}{\cos^2 \theta} + \frac{187}{64} \sin^2 \theta\right) \end{cases}, \quad (6.26)$$

and

$$C = \frac{j}{ks} \frac{1}{\cos^2 \theta}, \quad D = \frac{j}{12ks} \frac{1}{\cos^2 \theta}. \quad (6.27)$$

The values of A, B, C and D, thus obtained are to be inserted into (6.21) and (6.22). Then by addition of (6.21) and (6.22), we obtain the following approximation in terms of Fock functions for the surface field component

$H_{\phi}^c(Q)$ :

$$\begin{aligned} H_{\phi}^c(Q) \approx \frac{k^2 Y}{2\pi j} \frac{e^{-jks}}{ks} & \left[ \sin^2 \theta v(\xi) + \frac{j}{ks} \left(2 - 3 \sin^2 \theta - \frac{1}{\cos^2 \theta}\right) v(\xi) + \frac{j}{ks} \frac{1}{\cos^2 \theta} u(\xi) \right. \\ & + \frac{1}{k^2 s^2} (2 - 3 \sin^2 \theta) v(\xi) + \frac{2^{-1/3} j}{(ka)^{2/3}} \cos^{4/3} \theta \left( \frac{4}{3} \frac{\sin^2 \theta}{\cos^2 \theta} - \frac{11}{12} \sin^2 \theta \right) v'(\xi) \\ & \left. + \frac{j}{ks} \left(\frac{3}{4} - \frac{7}{12} \frac{\sin^2 \theta}{\cos^2 \theta} + \frac{187}{64} \sin^2 \theta\right) v'(\xi) + \frac{j}{12ks} \frac{1}{\cos^2 \theta} u'(\xi) \right]. \quad (6.28) \end{aligned}$$

The present approximation is of a similar form as that of Lee et al. [2], as given in (3.17). Notice, however, that the coefficients of  $v(\xi)$ ,  $u(\xi)$ ,  $v'(\xi)$  and  $u'(\xi)$  are somewhat different.

### 6.2 Magnetic field component $H_z^c = H_\phi^a$ .

As pointed out in Section 4.1, the exact solution for the field component  $H_z^c$  due to a circumferential dipole is identical to that for the field component  $H_\phi^a$  due to an axial dipole. Then the approximate solutions for  $H_z^c$  and  $H_\phi^a$  are also the same.

The exact solution for  $H_z^c$  is given in (3.22), as quoted from [1]. The integrand of the double integral in (3.22) contains the quotient  $H_V^{(2)}(k_t a) / H_V^{(2)'}(k_t a)$ . Therefore, we match our previous approximation to a new approximation which involves the hard Fock function  $v(\xi)$  and its derivative  $v'(\xi)$ . Thus we start from an approximation for  $H_z^c(Q)$  of the form (6.21) with constants A and B yet to be determined. For small  $\xi$ , when replacing  $v(\xi)$  and  $v'(\xi)$  by (6.23), this approximation passes into the form (6.24). Then by identifying this form with our previous approximation (3.27) and (3.28), we find for the constants A and B:

$$A = -\cos \theta \sin \theta \left[ 1 - \frac{3j}{ks} - \frac{3}{k^2 s^2} \right] ,$$

$$B = -\cos \theta \sin \theta \left[ \frac{2}{3} \frac{\sin^2 \theta}{\cos^2 \theta} - \frac{1}{4} + \frac{j}{ks} \left( \frac{187}{64} - \frac{5}{4 \cos^2 \theta} \right) \right] . \quad (6.29)$$

When inserting these values into the form (6.21), we obtain the following approximation in terms of Fock functions for the surface field components

$$H_z^c(Q) = H_\phi^a(Q):$$

$$\begin{aligned}
H_z^c(Q) = H_p^a(Q) \approx & -\frac{k^2 Y}{2\pi j} \frac{e^{-jks}}{ks} \cos \theta \sin \theta \left[ \left(1 - \frac{3j}{ks} - \frac{3}{k^2 s^2}\right) v(\xi) \right. \\
& \left. + \frac{2^{-1/3} j}{(ka)^{2/3}} \cos^{4/3} \theta \left\{ \left(\frac{2}{3} \frac{\sin^2 \theta}{\cos^2 \theta} - \frac{1}{4}\right) v'(\xi) + \frac{j}{ks} \left(\frac{187}{64} - \frac{5}{4 \cos^2 \theta}\right) v'(\xi) \right\} \right].
\end{aligned} \tag{6.30}$$

The present approximation should be compared to the result of Lee et al. [2], as given in (3.31). The main difference is that the result in (3.31) involves both the hard and soft Fock functions, whereas our approximation in (6.30) is in terms of the hard Fock function only.

### 6.3 Magnetic field component $H_z^a$ .

The exact solution for the field component  $H_z^a$  due to an axial dipole is given by (4.2), as quoted from [1]. Since the integrand of the double integral in (4.2) contains the quotient  $H_v^{(2)}(k_t a)/H_v^{(2)'}(k_t a)$ , we construct an approximation for  $H_z^a(Q)$  in terms of the hard Fock function  $v(\xi)$  only. We start again from an approximation of the form (6.21) with constants A and B to be determined. For small  $\xi$  we replace  $v(\xi)$  and  $v'(\xi)$  by (6.23), then the approximation for  $H_z^a(Q)$  reduces to the form (6.24). Then by matching this form to our previous approximation (4.7) and (4.8), we can readily determine the constants A and B, viz.,

$$\begin{aligned}
A &= \cos^2 \theta + \frac{j}{ks} (2 - 3 \cos^2 \theta) + \frac{1}{k^2 s^2} (2 - 3 \cos^2 \theta) \quad , \\
B &= -\frac{11}{12} \cos^2 \theta + \frac{j}{ks} \left(-\frac{7}{6} - \frac{2}{3 \cos^2 \theta}\right) + \frac{187}{64} \cos^2 \theta.
\end{aligned} \tag{6.31}$$

On inserting these values into the form (6.21), we obtain the following approximation in terms of Fock functions for the surface field component  $H_z^a(Q)$ :

$$\begin{aligned}
H_z^a(Q) = & \frac{k^2 Y}{2\pi j} \frac{e^{-jks}}{ks} \left[ \cos^2 \theta v(\xi) + \frac{j}{ks} (2 - 3 \cos^2 \theta) v(\xi) + \frac{1}{k^2 s^2} (2 - 3 \cos^2 \theta) v(\xi) \right. \\
& + \frac{2^{-1/3} j}{(ka)^{2/3}} \cos^{4/3} \theta \left\{ -\frac{11}{12} \cos^2 \theta v'(\xi) + \frac{j}{ks} \left( -\frac{11}{6} - \frac{2}{3} \frac{\sin^2 \theta}{\cos^2 \theta} \right. \right. \\
& \left. \left. + \frac{187}{64} \cos^2 \theta \right) v'(\xi) \right\} \left. \right]. \quad (6.32)
\end{aligned}$$

The present approximation should be compared to the result of Lee et al. [2], as given in (4.11). Again the main difference is that the result in (4.11) involves both the hard and soft Fock functions, whereas our approximation in (6.32) contains only the hard Fock function  $v(\xi)$  and its derivative.

#### 6.4 Representation in a dyadic form.

As in Section 5, we now represent the surface magnetic field at Q due to a magnetic dipole  $\vec{M}$  at P in the dyadic form (5.10), viz.,

$$\vec{H}(Q) = \vec{M} \cdot [\hat{b}'\hat{b}H_{bb} + \hat{t}'\hat{t}H_{tt} + \hat{b}'\hat{t}H_{bt} + \hat{t}'\hat{b}H_{tb}] \quad , \quad (6.33)$$

where the unit vectors  $\hat{b}'$ ,  $\hat{b}$ ,  $\hat{t}'$  and  $\hat{t}$  are shown in Fig. 2. Then the dyadic components  $H_{bb}$ ,  $H_{tt}$ ,  $H_{bt}$  and  $H_{tb}$  are related to the surface field components  $H_\phi^c$ ,  $H_z^c = H_\phi^a$  and  $H_z^a$  through (5.12). In (5.12), replace the field components by their approximations (6.28), (6.30) and (6.32) in terms of Fock functions. Then we obtain the following approximations in terms of Fock functions for the dyadic components  $H_{bb}$ ,  $H_{tt}$  and  $H_{bt} = H_{tb}$ :

$$\begin{aligned}
H_{bb}(Q) = & \frac{k^2 Y}{2\pi j} \frac{e^{-jks}}{ks} \left[ v(\xi) - \frac{j}{ks} \frac{1}{\cos^2 \theta} v(\xi) + \frac{j}{ks} \frac{\sin^2 \theta}{\cos^2 \theta} u(\xi) - \frac{1}{k^2 s^2} v(\xi) \right. \\
& + \frac{2^{-1/3} j}{(ka)^{2/3}} \cos^{4/3} \theta \left\{ \left( \frac{4}{3} \frac{\sin^2 \theta}{\cos^2 \theta} - \frac{11}{12} \right) v'(\xi) + \frac{j}{12ks} \frac{\sin^2 \theta}{\cos^2 \theta} u'(\xi) \right. \\
& \left. \left. + \frac{j}{ks} \left( \frac{209}{192} - \frac{7}{12} \frac{\sin^2 \theta}{\cos^2 \theta} \right) v'(\xi) \right\} \right] \quad , \quad (6.34)
\end{aligned}$$

and

$$\begin{aligned}
 H_{tt}(Q) &= \frac{k^2 Y}{2\pi j} \frac{e^{-jks}}{ks} \left[ \frac{j}{ks} v(\xi) + \frac{j}{ks} u(\xi) + \frac{2}{k^2 s^2} v(\xi) \right. \\
 &\quad \left. + \frac{2^{-1/3} j}{(ka)^{2/3}} \cos^{4/3} \theta \left\{ \frac{j}{ks} \left( \frac{3}{4} - \frac{2}{3} \frac{\sin^2 \theta}{\cos^2 \theta} \right) v'(\xi) + \frac{j}{12ks} u'(\xi) \right\} \right], \quad (6.35)
 \end{aligned}$$

and

$$\begin{aligned}
 H_{bt}(Q) = H_{tb}(Q) &= \frac{k^2 Y}{2\pi j} \frac{e^{-jks}}{ks} \cos \theta \sin \theta \left[ -\frac{j}{ks} \frac{1}{\cos^2 \theta} v(\xi) + \frac{j}{ks} \frac{1}{\cos^2 \theta} u(\xi) \right. \\
 &\quad \left. + \frac{2^{-1/3} j}{(ka)^{2/3}} \cos^{4/3} \theta \left\{ \frac{2}{3 \cos^2 \theta} v'(\xi) + \frac{j}{ks} \frac{4}{3 \cos^2 \theta} v'(\xi) \right. \right. \\
 &\quad \left. \left. + \frac{j}{12ks} \frac{1}{\cos^2 \theta} u'(\xi) \right\} \right]. \quad (6.36)
 \end{aligned}$$

The present results have been checked by re-expansion for small  $\xi$ . When replacing the Fock functions by (6.23), it is found that (6.34) - (6.36) reduce precisely to (5.17) - (5.19).

## 7. NUMERICAL RESULTS

For the numerical calculations, we concentrate on  $H_\phi^c$  (the  $\phi$ -component of  $\vec{H}$  due to a circumferential dipole) and  $H_z^a$  (the  $z$ -component of  $\vec{H}$  due to an axial dipole). Three sets of approximate solutions are used in the calculations, namely,

- (i) the "full formulas" of Chang et al. [1], which are given in (3.16) and (4.10) of the present report;
- (ii) the formulas of Lee et al. [2], which are given in (3.17) and (4.11); and
- (iii) the present formulas in (6.28) and (6.32).

The radius of the cylinder is  $ka = 9.5325$ . The ray directions are  $\theta = 0^\circ, 45^\circ$  and  $90^\circ$ . As a function of  $ks$ , numerical values of  $H_\phi^c$  are presented in Figures 4 to 6, and those of  $H_z^a$  in Figures 7 to 9. In these figures, we use the following notations:

Mag = absolute value of  $(H_\phi^c/k^2)$  or  $(H_z^a/k^2)$

Normalized phase = phase of  $(H_\phi^c e^{+jks})$  or  $(H_z^a e^{+jks})$

The db value of Mag is calculated by  $20 \log_{10}(\text{Mag in ampere-meter})$ .

As another accuracy test, we calculate the mutual admittance  $Y_{12}$  between two identical slots on a cylinder by using the three formulas described in (i) to (iii) above. The geometry is sketched in Figure 10 with the parameters

Frequency = 9 GHz ,  $\lambda = 1.3123''$  ,  $a = 1.991''$

Slot dimension =  $0.9'' \times 0.4''$

Slot separation described by  $(\phi_0, z_0)$

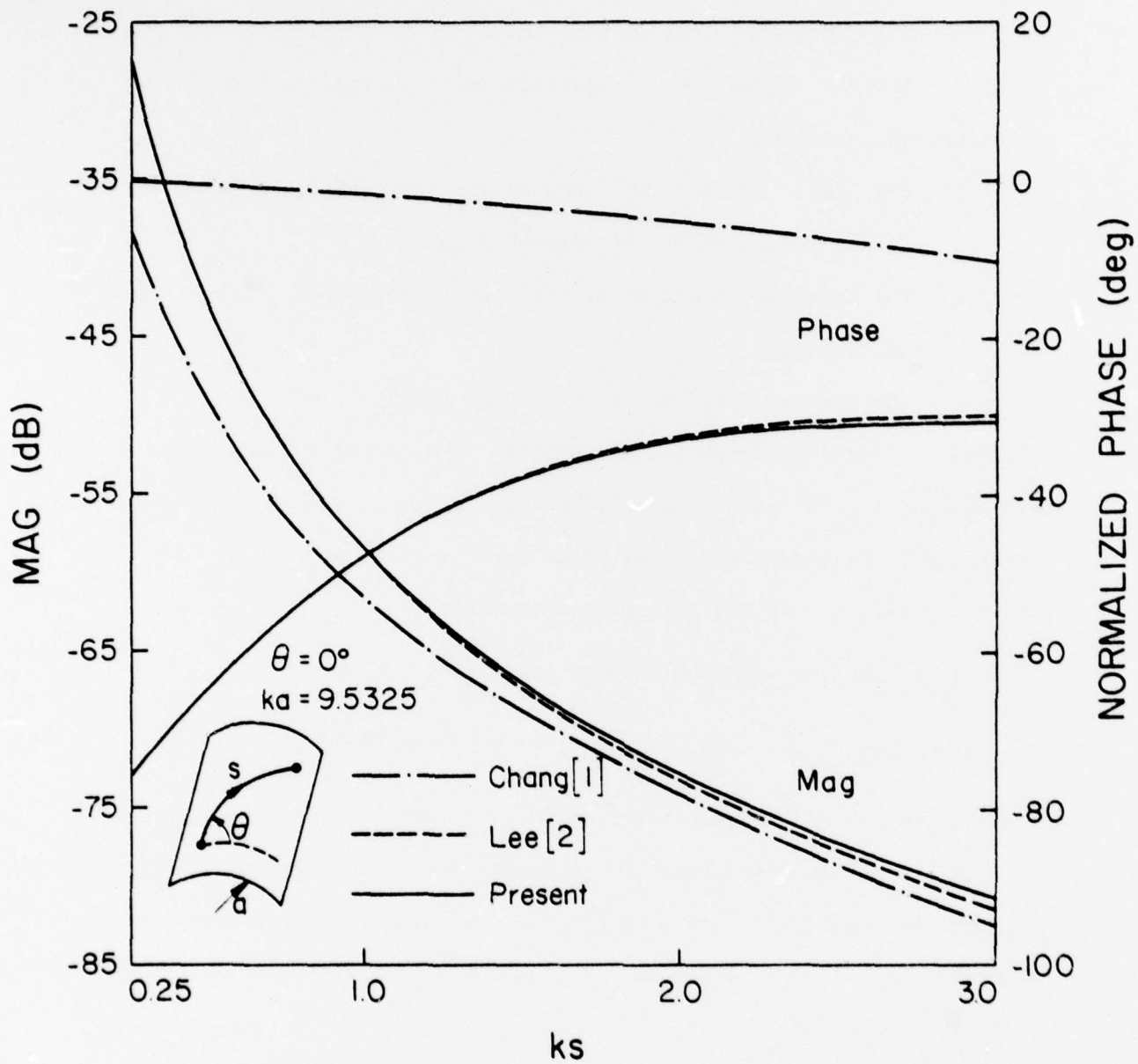


Figure 4a. Surface magnetic field  $H_b^c$  due to a circumferential dipole on a cylinder for a ray propagating in the direction  $\theta = 0^\circ$ .

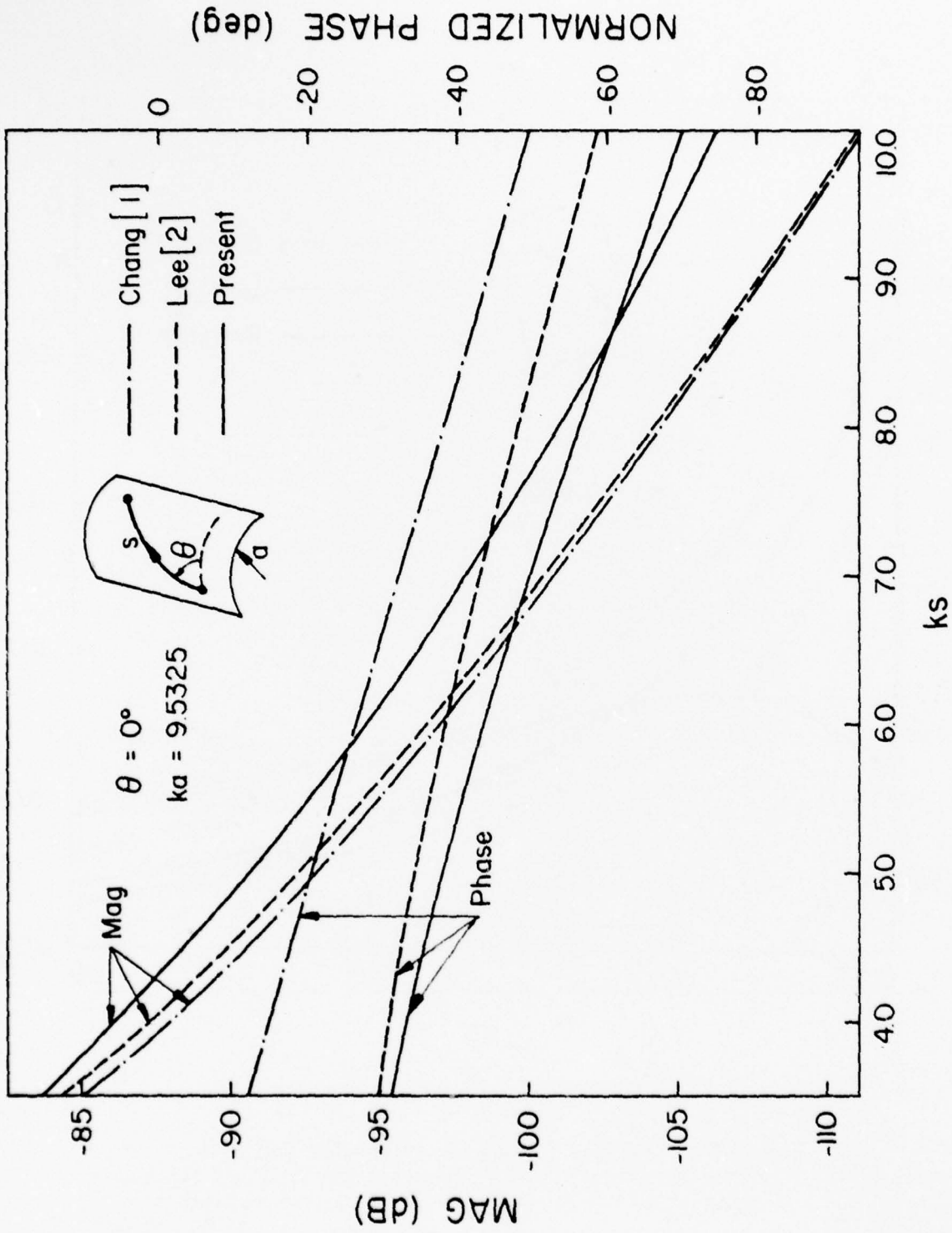


Figure 4b. Same as Figure 4a except for larger  $ks$ .

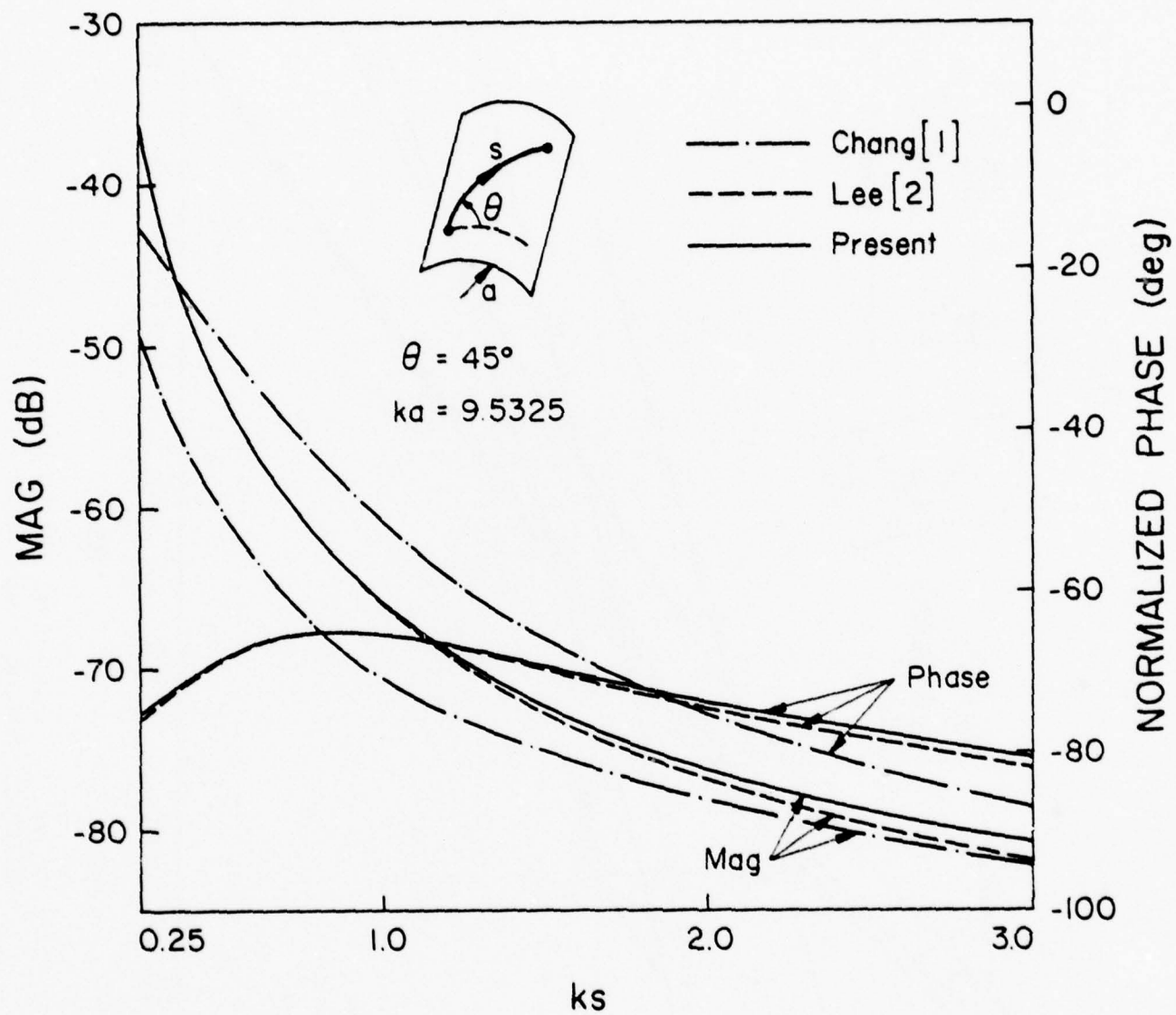


Figure 5a. Same as Figure 4a except for  $\theta = 45^\circ$ .

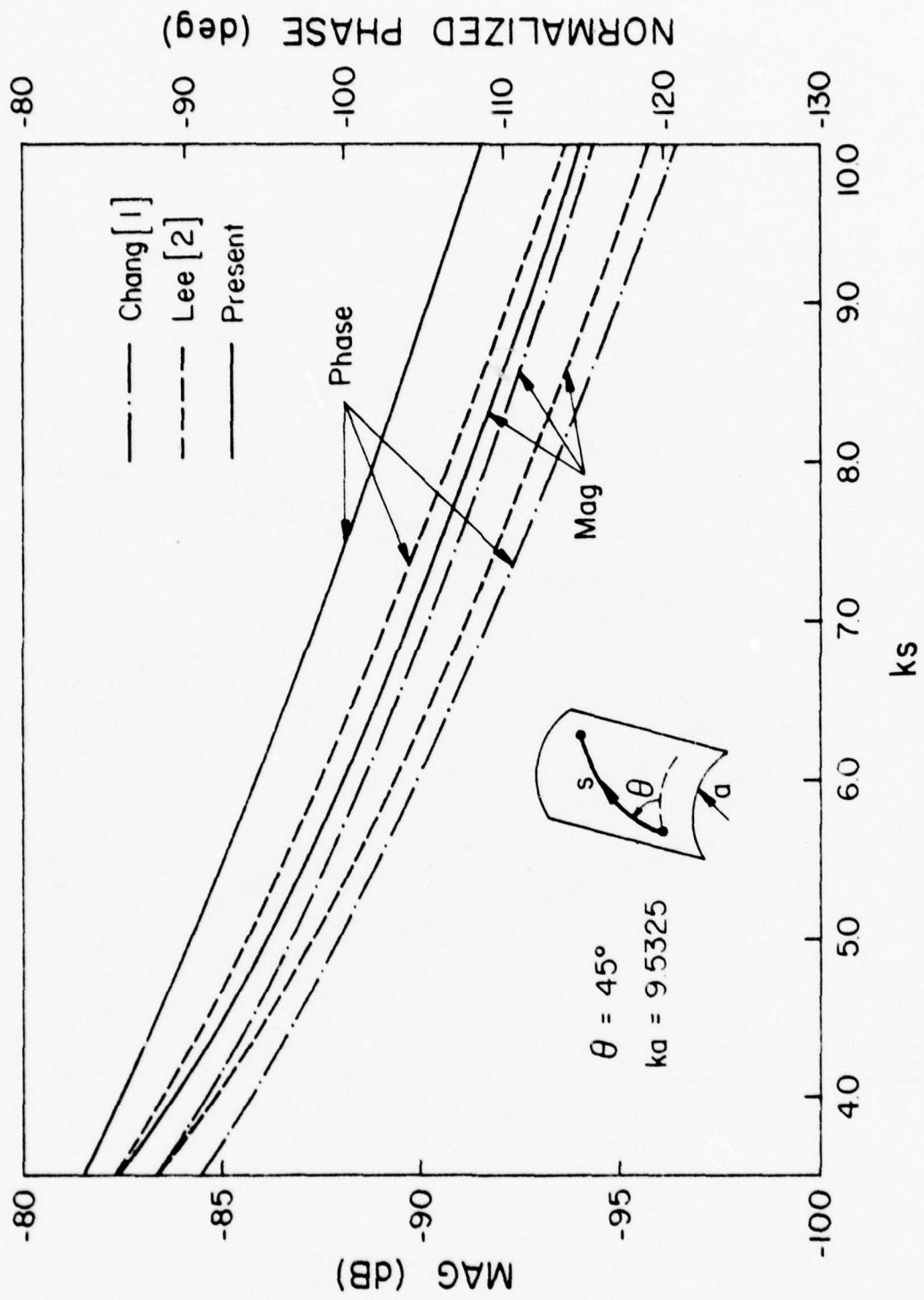


Figure 5b. Same as Figure 4a except for  $\theta = 45^\circ$  and larger ks.

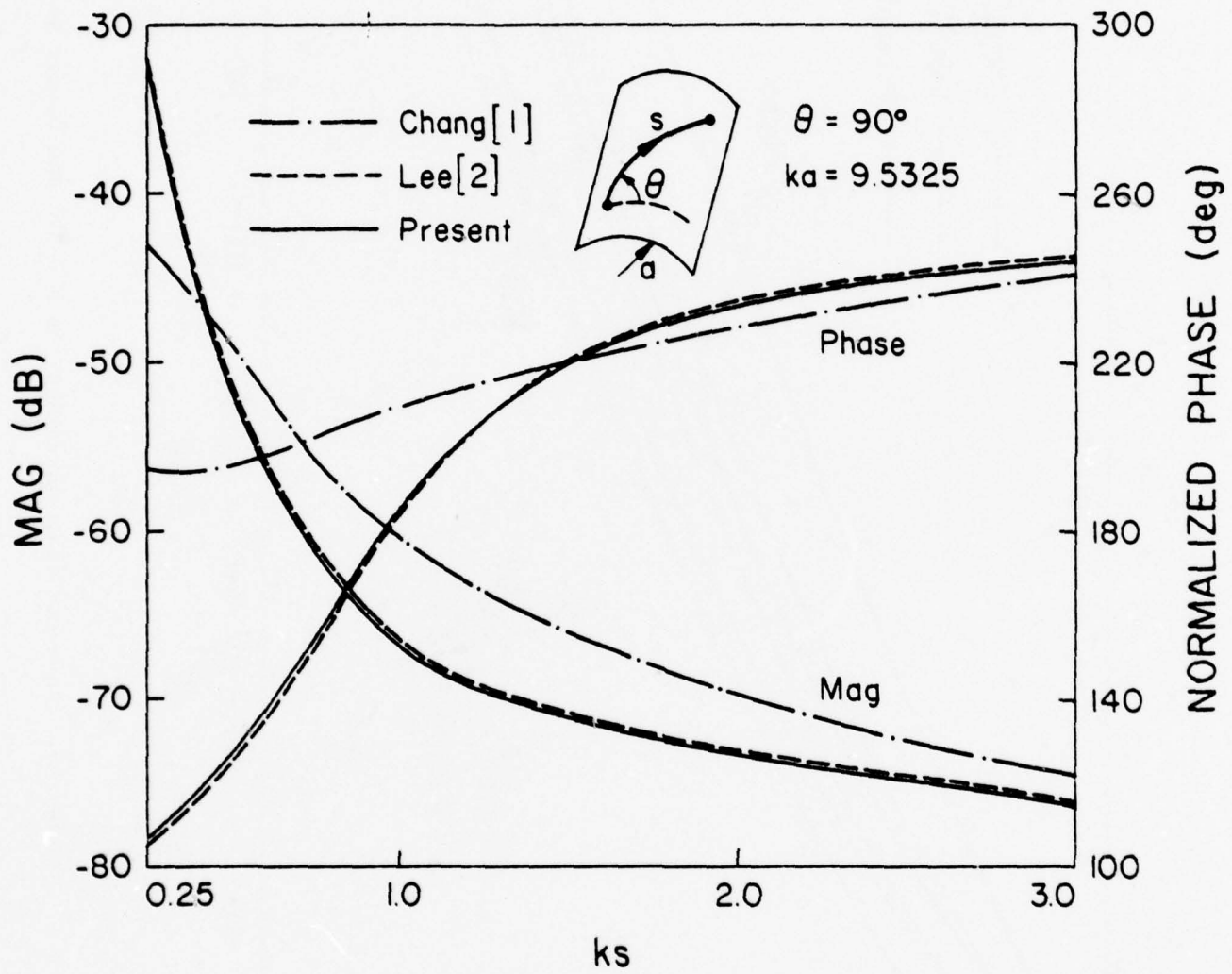


Figure 6a. Same as Figure 4a except for  $\theta = 90^\circ$ .

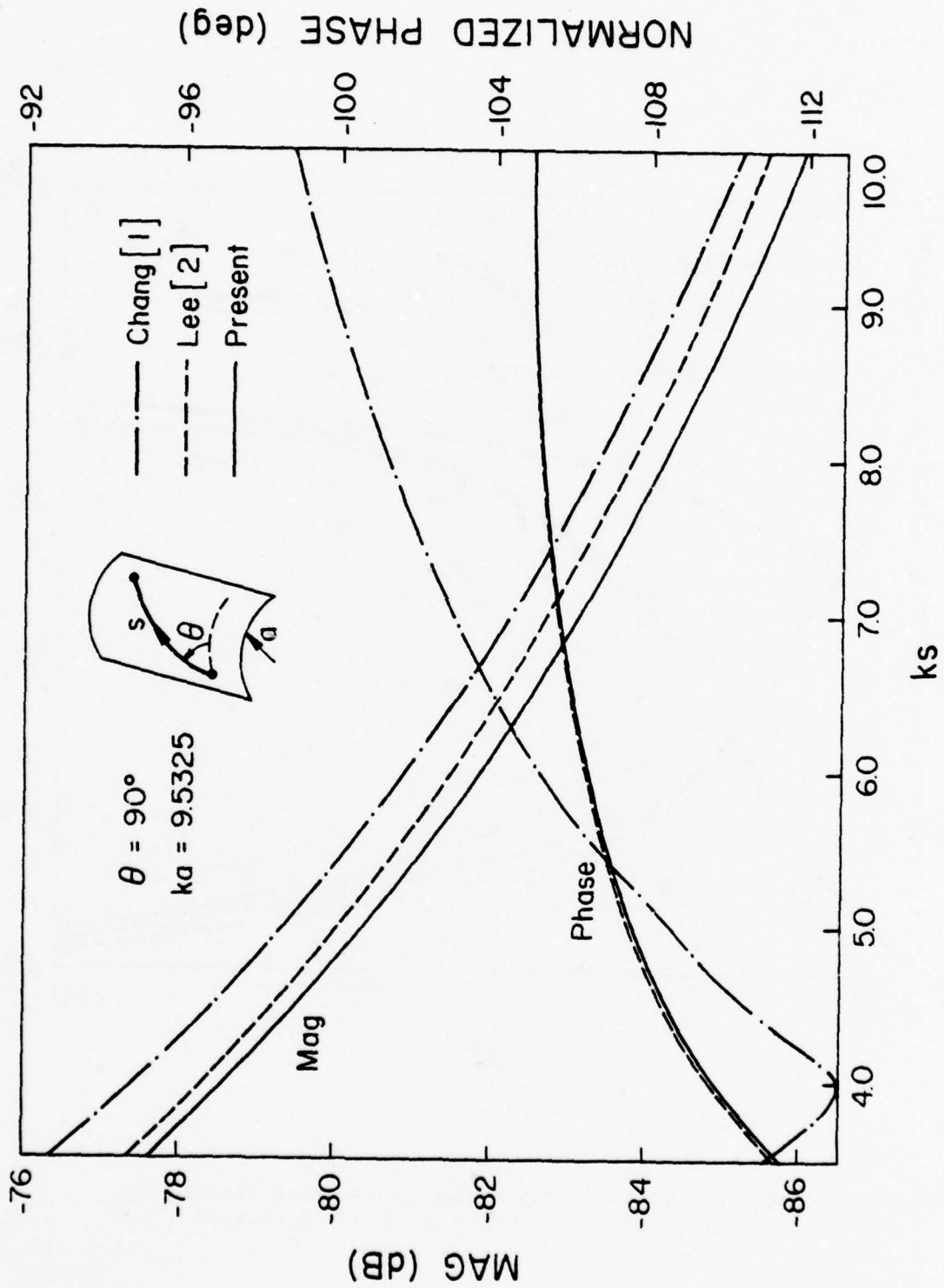


Figure 6b. Same as Figure 4a except for  $\theta = 90^\circ$  and larger  $ks$ .

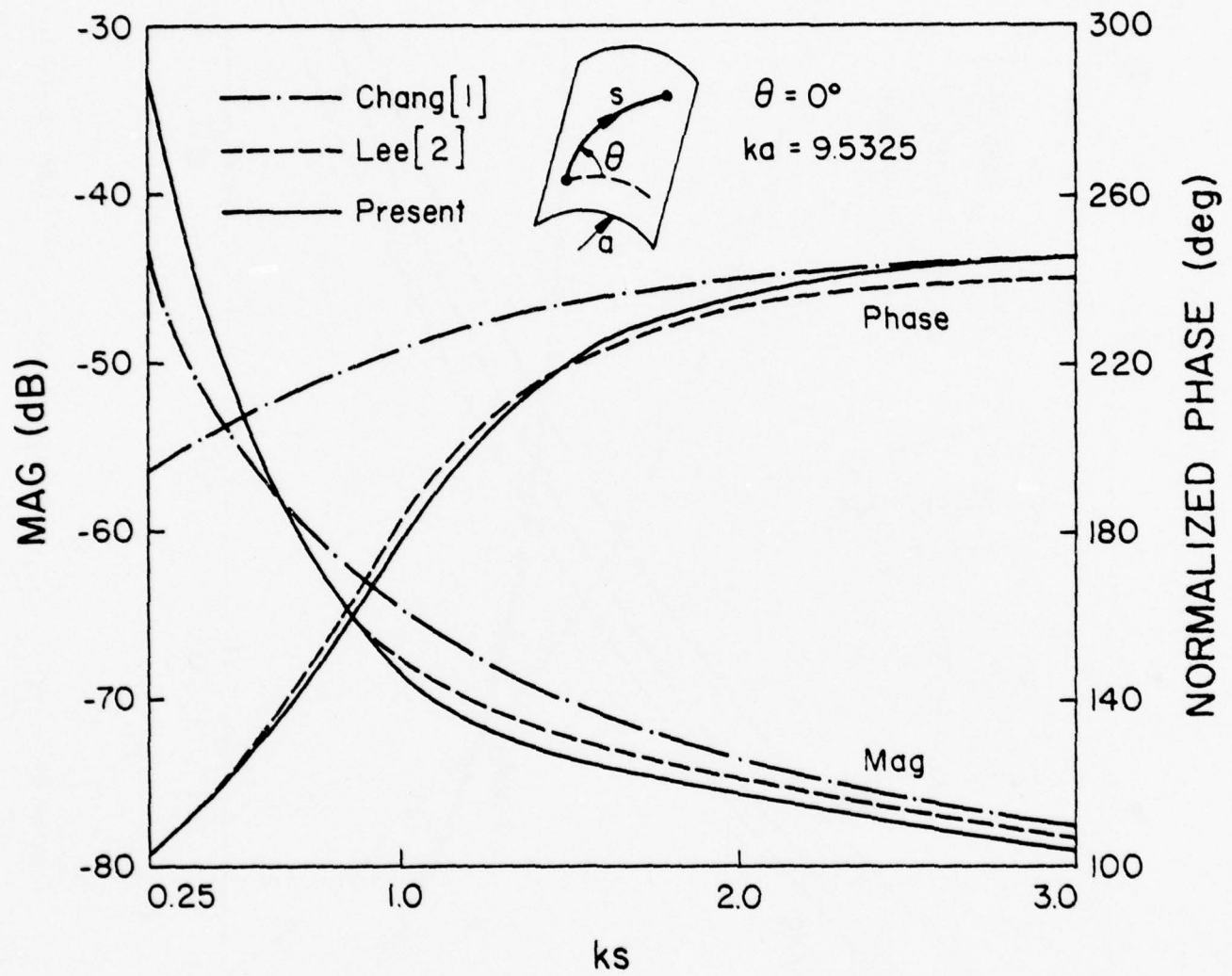


Figure 7. Surface magnetic field  $H_z^a$  due to an axial dipole on a cylinder for a ray propagating in the direction  $\theta = 0^\circ$ .

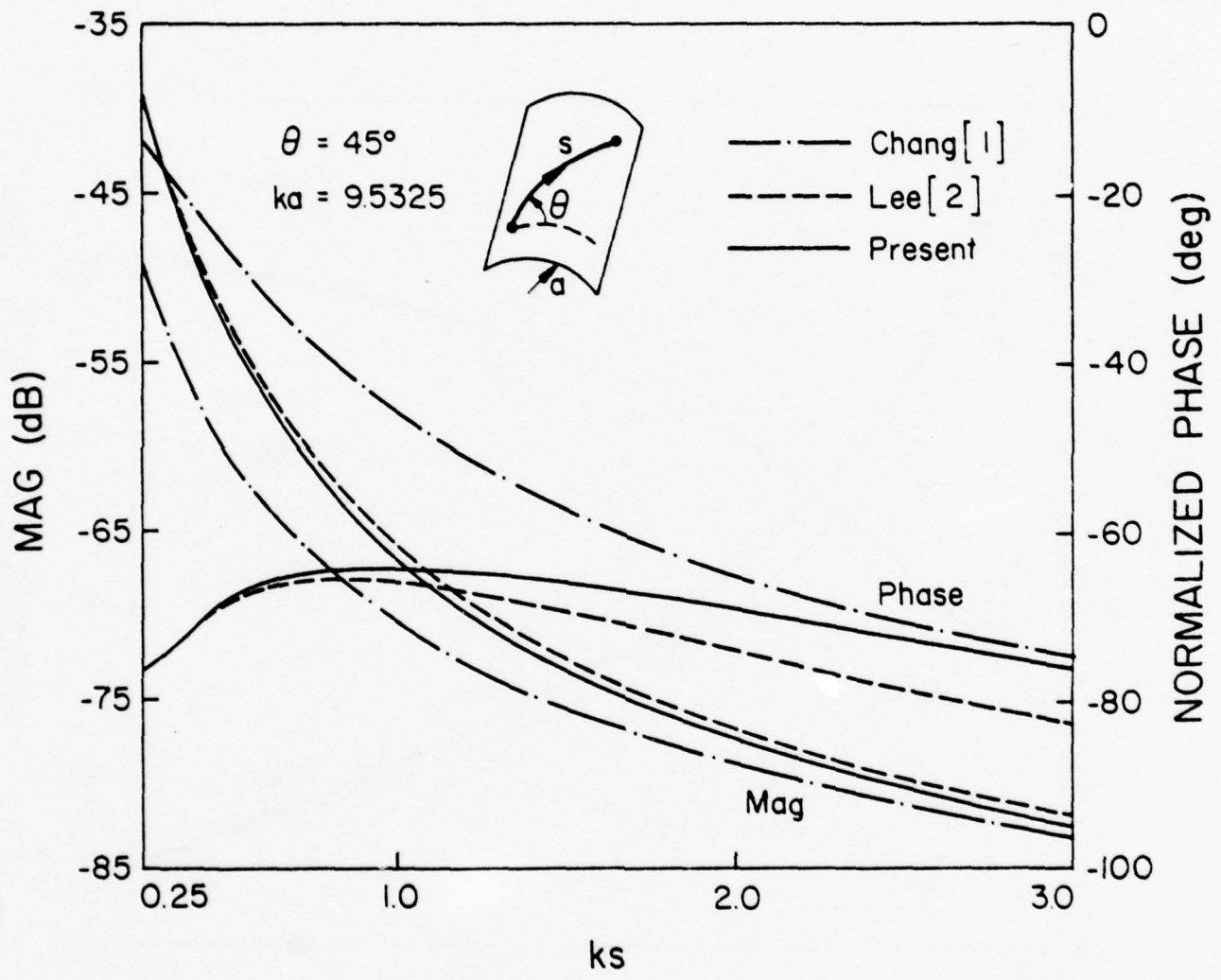


Figure 8. Same as Figure 7 except for  $\theta = 45^\circ$ .

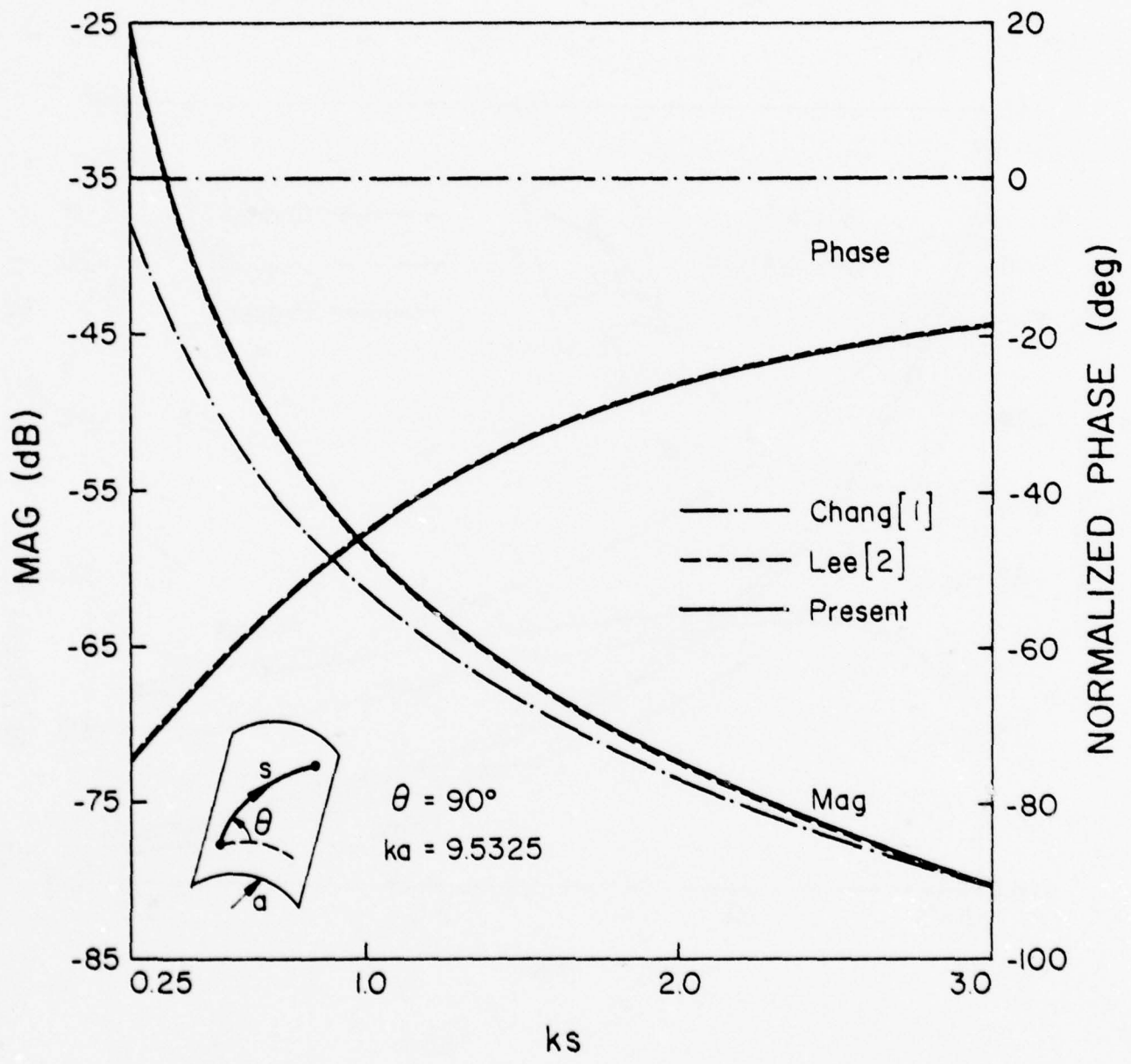
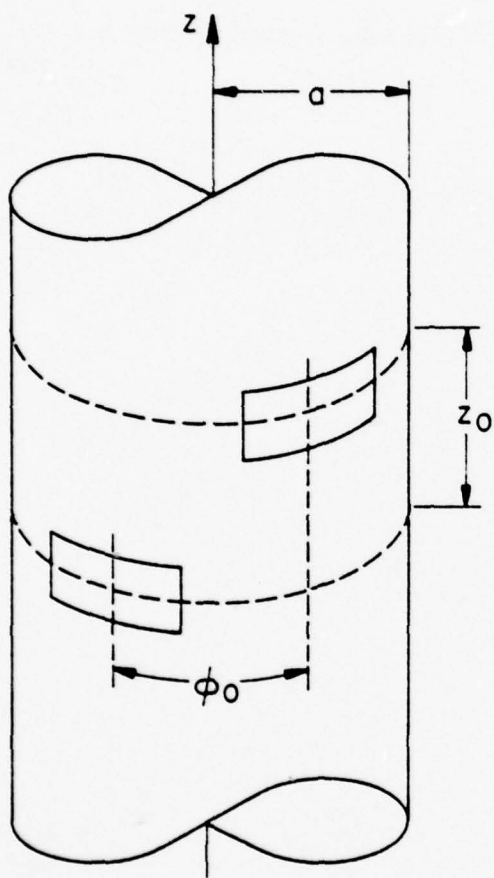
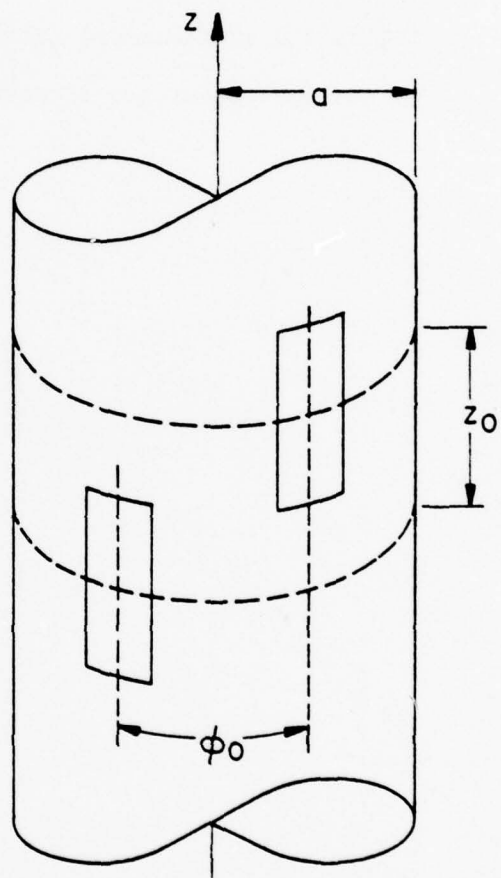


Figure 9. Same as Figure 7 except for  $\theta = 90^\circ$ .



CIRCUMFERENTIAL SLOTS



AXIAL SLOTS

Figure 10. Two identical slots on a cylinder.

The steps for calculating  $Y_{12}$  can be found in [1], [2] and [7]. The results for two (identical) circumferential slots are given in Table 1, and those for the two axial slots in Table 2. Values of  $Y_{12}$  are listed in (db =  $20 \log_{10} |Y_{12}|$ , phase in degree) format. In addition to three asymptotic solutions based on (i) to (iii), an exact solution of  $Y_{12}$  calculated by the modal series [7] and [8] is also listed in the two tables for comparison purpose.

TABLE 1. MUTUAL ADMITTANCE BETWEEN TWO CIRCUMFERENTIAL SLOTS

$\theta_0 = 0^\circ$	Exact	Asymptotic solutions		
$\alpha_0$		Chang [1]	Lee [2]	Present
0.5"	-62.62 db	-61.7	-62.54	-62.41
	-72°	-68°	-72°	-73°
4"	-71.78	-70.96	-71.66	-71.84
	-117°	-118°	-116°	-119°
8"	-81.84	-80.80	-81.83	-82.18
	34°	34°	37°	30°
16"	-86.48	-85.26	-86.60	-86.96
	-4°	-4°	-1°	-9°
40"	-91.95	-90.83	-92.46	-92.77
	-115°	-112°	-110°	-120°

TABLE 2. MUTUAL ADMITTANCE BETWEEN TWO AXIAL SLOTS

$z_0 = 0$	Exact	Asymptotic Solutions		
$\phi_0$		Chang [1]	Lee [2]	Present
30°	-81.33 db	-83.14	-81.34	-80.83
	-77°	-60°	-75°	-81°
40°	-89.87	-91.11	-90.02	-88.69
	168°	180°	170°	159°
50°	-96.37	-97.43	-96.72	-94.35
	53°	69°	61°	45°
60°	-101.97	-102.93	-102.48	-98.96
	-49°	-39°	-47°	-66°

## 8. CONCLUSIONS

The surface magnetic field due to a magnetic dipole on a cylinder can be found exactly in terms of cylindrical modal functions and Fourier integrals. This solution, however, is not suitable for computations at high frequencies ( $ka \gg 1$ ) because of its slow convergence rate. The present paper is devoted to extracting an asymptotic solution ( $ka \rightarrow \infty$ ) from the exact one. Explicit results have been obtained for the following cases:

- (i) In the penumbra region on the cylinder where  $\xi$  is small, the asymptotic dyadic Green's function is given in (5.10) and (5.13) - (5.15).
- (ii) In order to obtain a solution uniformly valid for all points on the cylinder (from the penumbra to the deep shadow), the asymptotic solution in (i) is matched to the well-known creeping wave representation via Fock's functions. The final dyadic Green's function is given in (6.34) - (6.36).

The present solution has been compared with two previous ones: Chang et al. [1] and Lee et al. [2]. Of particular interest is that, through rigorous asymptotic expansions, we have confirmed the peculiar  $(ks)^{-1/2}$  field behavior along the generator of the cylinder (sometimes known as the "transverse curvature term" in the field solution). This term plays a most important role for rays parallel or almost parallel to a generator of the cylinder. Until the present confirmation, its existence was predicted only through speculation.

#### REFERENCES

- [1] Z. W. Chang, L. B. Felsen and A. Hessel, "Surface ray methods for mutual coupling in conformal arrays on cylindrical and conical surfaces," Final Report, Contract N00123-76-C-0236, POLY-EE EP-76-016, July 1976.
- [2] S. W. Lee and S. Safavi-Naini, "Asymptotic solution of surface field due to a magnetic dipole on a cylinder," University of Illinois, Electromagnetics Laboratory Technical Report No. 76-11, November 1976 (A shortened version appeared in IEEE Trans. Antennas Propagat., vol. AP-26, pp. 593-598, 1978).
- [3] G. N. Watson, A treatise on the theory of Bessel functions, Cambridge University Press, Cambridge, 1941.
- [4] M. Abramowitz and I. A. Stegun (eds.), Handbook of Mathematical Functions with formulas, graphs, and mathematical tables, Dover Publ., New York, 1965.
- [5] J. B. Keller, S. I. Rubinow and M. Goldstein, "Zeros of Hankel functions and poles of scattering amplitudes", J. Math. Phys., vol. 4, pp. 829-832, 1963.
- [6] A. Erdélyi, W. Magnus, F. Oberhettinger and F. G. Tricomi, Tables of Integral Transforms, vol. I, McGraw-Hill, New York, 1954.
- [7] S. W. Lee, S. Safavi-Naini and R. Mittra, "Mutual admittance between slots on a cylinder," University of Illinois, Electromagnetics Laboratory Technical Report No. 77-8, March 1977.
- [8] K. E. Golden, G. E. Stewart and D. C. Pridmore-Brown, "Approximation techniques for the mutual admittance of slot antennas on metallic cones," IEEE Trans. Antennas Propagat., vol. AP-22, pp. 43-48, 1974.

ATTACHMENT C

GTD CALCULATION OF MUTUAL ADMITTANCE AND ELEMENT  
PATTERN OF SLOT CONFORMAL ARRAY

(Each attachment has its own pagination.)

GTD CALCULATION OF MUTUAL ADMITTANCE  
AND ELEMENT PATTERN OF SLOT  
CONFORMAL ARRAY\*

(PREPARED FOR THE BOOK "PRINCIPLES AND APPLICATIONS OF ANTENNA DESIGN")

S. W. Lee

Department of Electrical Engineering  
Electromagnetics Laboratory  
University of Illinois  
Champaign-Urbana, Illinois 61801

---

\* This work was supported by Naval Air Systems Command under contract  
N000 19-78-C-0064.

## 1. INTRODUCTION

In the design of a conformal array, the two most important electromagnetic parameters are the mutual admittance between elements and the active element pattern. These two parameters have been calculated by the following two techniques:

(i) Modal analysis [1] - [3] applied to problems with separable geometry. The solution is usually rigorous, and is in the form of infinite series/integrals. Because of the convergence rate, it is suitable for numerical calculations only when the radii of curvature of the array surface are small in terms of wavelength. In other words, modal analysis is a low-frequency technique.

(ii) Ray technique [4] - [10] is based on surface rays, first introduced by Keller in his Geometrical Theory of Diffraction (GTD). It normally yields an asymptotic solution valid for high frequencies. Because of the wide range of its applicability and simplicity of its final solution, the ray technique is a most attractive tool in solving conformal array problems.

This part of the book will describe the ray technique for calculating the mutual admittance and active element pattern. We will concentrate on conformal arrays which have rectangular slots as their elements.

## 2. CIRCUIT DESCRIPTION OF SLOT ARRAY

Consider an array of  $N$  slots over a curved conducting surface  $\Sigma$  (Figure 1). Each slot is fed by a rectangular waveguide (Figure 2), where only the dominant  $TE_{10}$  mode propagates and all other modes attenuate. The electromagnetic properties of the array can be conveniently described by circuit parameters detailed below.

Let us concentrate on a typical element  $n$  in the array. At a sufficiently large distance  $\ell$  from the aperture, only the dominant  $TE_{10}$  mode is present. Then the transverse field vectors in the  $n^{\text{th}}$  guide can be represented by

$$\vec{E}(x,y,z=-\ell) = V_n \vec{e}(x,y) \quad (2.1a)$$

$$\vec{H}(x,y,z=-\ell) = I_n (\hat{z} \times \vec{e}) \quad (2.1b)$$

where

$$\vec{e}(x,y) = \hat{y} \left(\frac{2}{ab}\right)^{1/2} \cos\left(\frac{\pi}{a} x\right) \quad (2.2a)$$

$$V_n = \text{modal voltage in } n^{\text{th}} \text{ element} \quad (2.2b)$$

$$I_n = \text{modal current in } n^{\text{th}} \text{ element} \quad (2.2c)$$

Note that the field in (2.1) is the total field consisting of waves travelling in both  $+z$  and  $-z$  directions. Because of the linearity of the Maxwell's equations, the current in the  $m^{\text{th}}$  element is linearly proportional to the voltages in all elements in the array, i.e.,

$$I_m = \sum_{n=1}^N Y_{mn} V_n, \quad m = 1, 2, \dots, N \quad (2.3)$$

In matrix notation, (2.3) may be rewritten as

$$\bar{I} = \bar{Y}\bar{V} \quad (2.4)$$

where  $\bar{I}$  and  $\bar{V}$  are column matrices with elements  $\{I_n\}$  and  $\{V_n\}$ , and  $\bar{Y}$  is a square matrix with elements  $\{Y_{mn}\}$ .

The proportional constant  $Y_{12}$  in (2.3), for example, is called the mutual admittance between slots 1 and 2. By reciprocity,  $Y_{12} = Y_{21}$ . We may calculate (measure)  $Y_{12}$  from the following setup (Figure 3):

- (i) Element 1 is excited so that the (total) voltage at the reference plane ( $z = -\ell$ ) is  $V_1$ .
- (ii) Conducting planes are placed at the reference planes of all other elements so that  $V_n = 0$  for  $n \neq 1$ .

Then it follows from (2.3) that

$$Y_{12} = \frac{I_2}{V_1} \Big|_{\text{short all except 1}} \quad (2.5)$$

which may be considered as the definition of  $Y_{12}$ .

As a transmitting antenna, the  $n^{\text{th}}$  element in the slot array in Figure 1 is excited by an incident  $TE_{10}$  mode with voltage  $V_n^+$ , where the superscript "+" signifies that the wave propagates toward the aperture in the +z direction. The discontinuity at the aperture causes a reflected  $TE_{10}$  mode with voltage  $V_n^-$ , which travels in the -z direction. Then the (total) voltage at the reference plane ( $z = -\ell$ ) is

$$V_n = V_n^+ + V_n^- \quad (2.6a)$$

while its corresponding current is

$$I_n = Y_c (V_n^+ - V_n^-) \quad (2.6b)$$

where  $Y_c$  is the characteristic admittance of  $TE_{10}$  mode

$$Y_c = \frac{1}{120\pi} [1 - (\frac{\pi}{ka})^2]^{1/2} \quad (2.7)$$

For a given set of incident voltages  $\{V_n^+\}$ , we can determine the reflected voltages  $\{V_n^-\}$  and the (total) voltages  $\{V_n\}$  from (2.6) and (2.4). The results are

$$\bar{V}^- = (\bar{I} + \bar{Y}_c^{-1} \bar{Y})^{-1} (\bar{I} - \bar{Y}_c^{-1} \bar{Y}) \bar{V}^+ \quad (2.8)$$

$$\bar{V} = 2(\bar{I} + \bar{Y}_c^{-1} \bar{Y})^{-1} \bar{V}^+ \quad (2.9)$$

where  $\bar{I}$  is an identity matrix, and  $\bar{Y}_c = Y_c \bar{I}$ .

In addition to admittance  $\{Y_{mn}\}$ , another set of important parameters is the short-circuited active element patterns  $\{P_n(\theta, \phi)\}$ . For example,  $P_1(\theta, \phi)$  is defined as the radiation pattern (of  $E_\theta$  or  $E_\phi$  component) when  $V_1 = 1$ , and  $V_n = 0$  if  $n \neq 1$  (Figure 3). The term "active" means that the radiating element is situated in an array environment (not in an isolated environment). When an array is excited by an incident voltage vector  $\bar{V}^+$ , the radiation pattern of the whole array is then given by

$$P_{\text{array}}(\theta, \phi) = \sum_{n=1}^N V_n P_n(\theta, \phi) = \bar{V}^T \bar{P} \quad (2.10)$$

where  $\{V_n\}$  can be calculated from (2.9), and T is a transpose operator.

### 3. SCATTERING DESCRIPTION OF SLOT ARRAY

For the same slot array in Figure 1, a different and equivalent description may be given in terms of scattering parameters, instead of circuit parameters.

Parallel to (2.3), the basic relation in the second description is

$$V_m^- = \sum_{n=1}^N S_{mn} V_n^+ \quad , \quad m = 1, 2, \dots, N \quad , \quad (3.1a)$$

or in matrix notation,

$$\bar{V}^- = \bar{S} \bar{V}^+ \quad . \quad (3.1b)$$

Here  $\bar{S} = [S_{mn}]$  is a scattering matrix.  $S_{12} = S_{21}$ , for example, is the induced voltage at element 2 when

- (i) element 1 is excited with  $V_1^+ = 1$  (not  $V_1 = 1$ ), and
- (ii) all other elements are terminated with a matched load,

in the manner sketched in Figure 4. Sometimes,  $S_{12}$  is also known as the coupling coefficient between elements 1 and 2. The comparison of (3.1b) with (2.8) leads immediately to

$$\bar{S} = (\bar{I} + \bar{Y}_c^{-1} \bar{Y})^{-1} (\bar{I} - \bar{Y}_c^{-1} \bar{Y}) \quad (3.2)$$

which relates  $\bar{S}$  to the admittance matrix  $\bar{Y}$ . For the special case  $N = 2$ , we have

$$S_{12} = \frac{-2Y_c Y_{12}}{(Y_c + Y_{11})^2 - Y_{12}^2} \quad (3.3)$$

For a given incident voltage vector  $\bar{V}^+$ , the (voltage) reflection coefficient in element  $m$  is defined by

$$R_m = \frac{V_m^-}{V_m^+}, \quad m = 1, 2, \dots, N \quad (3.4a)$$

and is found from (3.1a) to be

$$R_m = \sum_{n=1}^N S_{mn} (V_n^+ / V_m^+) \quad (3.4b)$$

The input admittance of the TE<sub>10</sub> mode in element  $m$  is given by

$$Y_m^{(in)} = \frac{V_m}{I_m} = Y_c \frac{1 + R_m}{1 - R_m} \quad (3.5)$$

Unlike  $Y_{mn}$ , we note that  $R_m$  and  $Y_m^{(in)}$  are functions of the array excitations.

Under the condition sketched in Figure 4, the radiation pattern is called the match-loaded active element pattern  $Q_1(\theta, \phi)$ . For a given incident voltage vector  $\bar{V}^+$ , the pattern of the whole array is given by

$$P_{array}(\theta, \phi) = \sum_{n=1}^N V_n^+ Q_n(\theta, \phi) = (\bar{V}^+)^T \bar{Q} \quad (3.6)$$

With the help of (2.9), the comparison of (3.6) and (2.10) leads to

$$\bar{Q} = 2[(\bar{I} + \bar{Y}_c^{-1} \bar{Y})^{-1}]^T \bar{P} \quad (3.7)$$

which relates two types of active element patterns. Note that  $Q_1(\theta, \phi)$ , for example, depends on  $P_1(\theta, \phi)$ ,  $P_2(\theta, \phi)$ , ...,  $P_N(\theta, \phi)$  through the matrix relation in (3.7).

#### 4. ONE-MODE APPROXIMATION

In the discussion of Sections 2 and 3, the reference plane for the voltage and current is taken to be a distance  $\ell$  from the aperture (Figure 1). Specifically,  $\ell$  should be chosen sufficiently large so that all reflected modes other than  $TE_{10}$  attenuate to negligible values within  $\ell$ . As an example, with parameters (Figure 2)

$$a = 0.9", b = 0.4", f = 9 \text{ GHz} \quad ,$$

$\ell$  should be at least 0.45" in order that the next higher-order mode  $TE_{20}$  attenuate to one-tenth of its magnitude within  $\ell$ .

For a finite  $\ell$ , the calculation of  $\{Y_{mn}\}$  and other scattering parameters is quite difficult. Hence, in practice, we often set

$$\ell = 0 \quad . \quad (4.1)$$

When (4.1) is used, all of the analysis in Sections 2 and 3 becomes approximate. This approximation is valid if, despite the discontinuity of the guide and the coupling in the array, the aperture field of the slot essentially contains no other modes than  $TE_{10}$ . For this reason, the approximation in (4.1) is known as the "one-mode approximation." It has been verified experimentally and theoretically that one-mode approximation is a good one if (i) the slots are thin, and (ii) their length is roughly a half-wavelength.

Under the one-mode approximation, the expression of the mutual admittance in (2.5) can be replaced by

$$Y_{12} = \frac{1}{V_1 V_2} \int_{A_2} \vec{E}_2 \times \vec{H}_1 \cdot d\vec{s}_2 \quad (4.2)$$

where

$A_2$  = aperture of slot 2

$\vec{H}_1$  = magnetic field when slot 1 is excited with voltage  $V_1$ , and all other slots are covered by perfect conductors at their openings ( $l = 0$  in Fig. 2)

$\vec{E}_2$  = electric field when slot 2 is excited with voltage  $V_2$ , and all other slots are covered by perfect conductors at their openings.

Because  $\vec{H}_1 = I_2 \vec{h}_2$  and  $\vec{E}_2 = V_2 \vec{e}_2$ , it is a simple matter to verify that (4.2) and (2.5) are equivalent under the one-mode approximation.

There is an alternative definition of mutual admittance. Instead of (2.1), a modal voltage  $\bar{V}_1$  (with a bar) may be defined through the expression for the aperture field of slot 1 as follows:

$$\vec{E} = \hat{y} \frac{1}{b} \bar{V}_1 \cos\left(\frac{\pi}{a} x\right) \quad (4.3a)$$

or equivalently

$$\bar{V}_1 = \int_0^b (\hat{y} \cdot \vec{E})_{x=0} dy \quad (4.3b)$$

Then a different mutual admittance  $\bar{Y}_{12}$  is defined by (4.2) after replacing  $(V_1, V_2)$  by  $(\bar{V}_1, \bar{V}_2)$ . It can be shown that

$$\bar{Y}_{12} = \frac{a}{2b} Y_{12} \quad (4.4)$$

Two remarks are in order: (i) In the limiting case that  $b \rightarrow 0$ ,  $Y_{12}$  goes to zero in proportion to  $b$ , whereas  $\bar{Y}_{12}$  approaches a constant independent of  $b$ . (ii) For the special case when  $a = \lambda/2$  and the slots are arranged on a plane (planar array), it is  $\bar{Y}_{12}$ , not  $Y_{12}$ , that is related, by the

Babinet principle, to the mutual impedance  $Z_{12}$  between two corresponding dipoles calculated by the classical Carter's formula [11], [12]. (iii) When the slots are excited by waveguides (transmission lines), one often uses  $Y_{12}$  ( $\bar{Y}_{12}$ ). From here on, we will concentrate on  $Y_{12}$  instead of  $\bar{Y}_{12}$ .

Under the one-mode approximation, the short-circuited active pattern  $P_1(\theta, \phi)$  of slot 1 (Figure 3) becomes the pattern of a single slot when all other slots are covered by conductors at their openings ( $\ell = 0$  in Figure 3). Its calculation is thus greatly simplified.

## 5. GTD GREEN'S FUNCTION FOR SURFACE FIELD ON A CYLINDER

Under the one-mode approximation, the mutual admittance between two slots in an array can be calculated from (4.2). We will now apply it to a slot array on an infinitely long conducting cylinder. The key step lies in the calculation of  $\vec{H}_1$ , the magnetic field at the aperture of slot 2 due to a voltage excitation in slot 1. To this end, we consider the following Green's function problem.

At point  $Q'$  on the surface of the cylinder of radius  $R$  (Fig. 5a), there is a tangential magnetic dipole source described by a magnetic current density (for  $\exp +j\omega t$  time convention)

$$\vec{K}(\vec{r}) = \vec{M} \frac{1}{R} \delta(r - R) \delta(\phi) \delta(z) \quad (5.1)$$

where  $\vec{M}$  is the magnetic dipole moment, and  $(r = R, \phi = 0, z = 0)$  are the cylindrical coordinates of  $Q'$ . The problem is to determine  $\vec{H}$  at another point  $Q = (R, \phi, z)$  on the same surface. The ray technique described below applies when  $kR$  is large (say 10 or more).

According to GTD [13], [14], the dominant contribution of  $\vec{H}$  at  $Q$  is the field on the surface ray from  $Q'$  to  $Q$ . The surface ray is a geodesic on the conducting surface, and in the present case is a helical path (Figure 5). The arclength of the surface ray is

$$s = \sqrt{(R\phi)^2 + z^2} \quad (5.2)$$

The tangent, normal, and binormal of the surface ray are  $(\hat{t}', -\hat{n}', -\hat{b}')$  at  $Q'$ , and  $(\hat{t}, -\hat{n}, -\hat{b})$  at  $Q$ . Thus,  $(\hat{t}, \hat{n}, \hat{b})$  form a moving trihedron along a surface ray, pointing toward the longitudinal and two transverse directions. At any point on the surface ray, the curvature of the conducting surface is described by two parameters:

$R_t$  = the radius of curvature in the direction of  $\hat{t}$  (or that in the longitudinal direction of the surface ray), and

$R_b$  = the radius of curvature in the direction of  $\hat{b}$  (or that in the transverse direction of the surface ray).

On a convex surface, both  $R_t$  and  $R_b$  are nonnegative. For the present case of a conducting cylinder, one has

$$R_t = \frac{R}{\cos^2 \theta} \quad , \quad R_b = \frac{R}{\sin^2 \theta} \quad (5.3)$$

where  $\theta$  is measured from the  $R\phi$ -axis in Fig. 5b, and takes a value between 0 and  $2\pi$ . The large parameter for our asymptotic expansion is

$$m = \left(\frac{1}{2} kR_t\right)^{1/3} \quad . \quad (5.4)$$

Thus, the solution to be presented is an approximate asymptotic solution valid for  $m \rightarrow \infty$ . Furthermore, let us introduce a distance parameter

$$\xi = \frac{ms}{R_t} = (k/2R_t^2)^{1/3} s = \frac{ks}{2m^2} \quad (5.5)$$

which is the arclength normalized by  $k$  and  $R_t$ . Note that  $\xi = 0$  defines the lit region ( $\theta = \pi/2$ ),  $\xi \sim 1$  defines the penumbra region, and  $\xi \gg 1$  defines the deep shadow region. Our solution is uniformly valid for all  $\xi \geq 0$ .

Due to the point source in (5.1), the final asymptotic solution for the magnetic field on the surface derived in [9] is given by

$$\vec{H}(Q) \approx \vec{M} \cdot (\hat{b}'\hat{b}H_b + \hat{t}'\hat{t}H_t) \quad (5.6a)$$

where the transverse component is

$$H_b(Q) \sim \left[ \left(1 - \frac{j}{ks}\right)v(\xi) - \left(\frac{1}{ks}\right)^2 u(\xi) + j(\sqrt{2} kR_t)^{-2/3} v'(\xi) + j(\sqrt{2} kR_t)^{-2/3} (R_t/R_b)u'(\xi) \right] G(s) \quad , \quad (5.6b)$$

the longitudinal component is

$$H_t(Q) \sim \left(\frac{j}{ks}\right) [v(\xi) + (1 - \frac{2j}{ks}) u(\xi) + j(\sqrt{2} kR_t)^{-2/3} u'(\xi)] G(s) \quad (5.6c)$$

and the function  $G(s)$  is

$$G(s) = \frac{k^2 Y_0}{2\pi j} \frac{e^{-jks}}{ks} \quad (5.6d)$$

$Y_0 = (\epsilon_0/\mu_0)^{1/2} = (120\pi)^{-1}$ ,  $v$  and  $u$  are defined in the Appendix, and  $v'$  is the derivative of  $v$ . The solution in (5.6) is largely based on the classical work of Fock [17].

Let us consider several limiting cases of the solution given in (5.6). If the radius of the cylinder becomes infinite

$$kR \rightarrow \infty \quad (5.7)$$

the use of (A-11) through (A-15) in the Appendix in (5.6) leads to

$$H_b(Q) \sim [1 - \frac{j}{ks} - (\frac{1}{ks})^2] G(s) \quad , \quad kR \rightarrow \infty \quad (5.8a)$$

$$H_t(Q) \sim (\frac{2j}{ks})(1 - \frac{j}{ks})G(s) \quad , \quad kR \rightarrow \infty \quad (5.8b)$$

When (5.8) is substituted into (5.6a), we find that  $\vec{H}$  in (5.6a) is identical to the exact solution of the surface field due to a magnetic dipole on a flat ground plane [15].

The second limiting case occurs when

$$\theta \rightarrow \pi/2 \quad (5.9)$$

We find from (5.6) that  $H_t$  is again given by (5.8b), but  $H_b$  becomes

$$H_b(Q) \sim [1 - \frac{j}{ks} - (\frac{1}{ks})^2 + \frac{3}{4}(\frac{\pi}{2})^{1/2} e^{-j\pi/4} \frac{(ks)^{1/2}}{kR}] G(s) \quad , \quad \theta = \frac{\pi}{2} \quad (5.10a)$$

In terms of the planar solution in (5.8a), we may rewrite (5.10a) as

$$H_b(Q) \sim [H_b(Q)]_{\text{planar}} + \frac{3}{8} \sqrt{\frac{1}{2\pi}} k^2 Y_0 e^{-j3\pi/4} \frac{1}{kR} \frac{e^{-jks}}{\sqrt{ks}}, \quad \theta = \frac{\pi}{2} \quad (5.10b)$$

The result in (5.10) is most interesting and, in fact, somewhat surprising. The surface ray traveling in direction  $\theta = \pi/2$  (Fig. 5) is a *straight* line ( $kR_t \rightarrow \infty$ ). However, due to the finite curvature in the binormal direction ( $R_b = R$ ),  $H_b$  on the cylindrical surface differs from its counterpart on a planar surface by the additional term in (5.10b). At a large distance away from the source ( $ks \rightarrow \infty$ ) in the direction  $\theta = \pi/2$ , and for a fixed  $kR$ , we find that  $H_b$  on a planar surface and that on a cylindrical surface are given by, respectively,

$$[H_b(Q)]_{\text{planar}} \sim A \frac{e^{-jks}}{ks} \quad (5.11)$$

$$H_b(Q) \sim B \frac{1}{kR} \frac{e^{-jks}}{\sqrt{ks}} + A \frac{e^{-jks}}{ks}, \quad (5.12)$$

where A and B are constants independent of s and R. Thus, for large ks,  $H_b$  on a cylinder is *stronger* than that on a plane.

As a third limiting case, let

$$\xi \rightarrow \infty \quad (5.13)$$

which occurs when observation point Q is in the deep shadow. Making use of (A-6) through (A-10), we can derive from (5.6):

$$H_b(Q) \sim \frac{k^2 \cos^{2/3} \theta}{1528(kR)^{1/3} (ks)^{1/2}} \exp[-0.88\xi - j(\frac{5\pi}{12} + 0.51\xi + ks)] \quad \xi \rightarrow \infty \quad (5.14a)$$

$$H_t(Q) \sim \frac{1}{ks} H_b(Q) \quad \xi \rightarrow \infty \quad (5.14b)$$

Therefore, in the deep shadow, the field is a slow wave and decays exponentially along the surface ray.

## 6. MUTUAL ADMITTANCE BETWEEN SLOTS ON A CYLINDER

Return to the calculation of  $Y_{12}$  from (4.2) for two identical circumferential slots on a cylinder (Figure 6a). To calculate  $H_1$ , the voltage excitation  $V_1$  in slot 1 can be replaced by an equivalent magnetic surface current density (Figure 7).

$$\vec{K}_1 = \vec{E}_1 \hat{x} = \hat{z} V_1 \cos\left(\frac{\pi}{a} y\right), \text{ for } (y, z) \text{ in slot 1,} \quad (6.1)$$

which radiates in a completely filled cylinder [16]. In (6.1),  $y = R\phi$ . Making use of the Green's function in (5.6a),  $\vec{H}_1$  is calculated from the superposition integral

$$\vec{H}_1 = \int_{A_1} dy_1 dz_1 [V_1 \sqrt{\frac{2}{ab}} \cos\left(\frac{\pi}{a} y_1\right)] [\hat{b} H_b \sin \theta + \hat{t} H_t \cos \theta] \quad (6.2)$$

where we have written the source point  $(y, z)$  as  $(y_1, z_1)$ . Making use of (6.2) and the electric field distribution of slot 2 in (4.2), we obtain the final expression for  $Y_{12}$  between two identical circumferential slots on a cylinder, namely,

$$Y_{12} = \frac{-2}{ab} \int_{A_1} dy_1 dz_1 \int_{A_2} dy_2 dz_2 [\cos\left(\frac{\pi}{a} y_1\right)] [\cos\left(\frac{\pi}{a} (y_2 - R\phi_0)\right)] g_\phi(1,2). \quad (6.3)$$

Here  $(y_1, z_1)$ , and  $(y_2, z_2)$  are two typical points in slots 1 and 2, respectively. The Green's function  $g_\phi$  is

$$g_\phi(1,2) = H_b \sin^2 \theta + H_t \cos^2 \theta \quad (6.4)$$

where  $(H_b, H_t)$  are given in (5.6) with

$$s = \sqrt{(y_2 - y_1)^2 + (z_2 - z_1)^2} \quad (6.5a)$$

$$\theta = \tan^{-1} \{(z_2 - z_1)/(y_2 - y_1)\} \quad (6.5b)$$

In a very similar manner, the mutual admittance between two identical axial slots (Figure 6b) can be derived. The final result reads

$$Y_{12} = \frac{-2}{ab} \int_{A_1} dy_1 dz_1 \int_{A_2} dy_2 dz_2 \left\{ \cos \frac{\pi}{b} z_1 \right\} \left\{ \cos \frac{\pi}{b} (z_2 - z_0) \right\} g_z(1,2) \quad (6.6)$$

where the Green's function  $g_z$  is

$$g_z(1,2) = H_b \cos^2 \theta + H_t \sin^2 \theta \quad (6.7)$$

The two surface integrals in (6.3) or (6.6) must be evaluated numerically. Extensive numerical results are given in [8], while some representative examples are quoted below. All values of  $Y_{12}$  are presented in (db, phase in degrees) format, where db =  $20 \log_{10}(|Y_{12}| \text{ in mho})$ .

(i) Agreement between GTD and exact modal solutions. Under the one-modal approximation, an exact solution of  $Y_{12}$  on a cylinder can be found in terms of cylindrical functions (the so-called "exact modal solution") [1] - [3], [8]. Consider two identical circumferential slots with parameters

$$a = 0.9'' \quad , \quad b = 0.4'' \quad , \quad R = 1.991'' \quad (6.8a)$$

$$f = 9 \text{ GHz} \quad , \quad \lambda = 1.3123'' \quad (6.8b)$$

For various slot separations, values of  $Y_{12}$  calculated by GTD solutions in (6.3) and by the exact modal solution are presented in Table A. We note that they are in excellent agreement.

(ii) Effect of transverse curvature term. As explained in the discussion of (5.9) through (5.12), the ray travelling along the generator of the cylinder is straight. However, the field  $H_b$  on it is stronger than that on a ray travelling on a planar conducting

TABLE A.  $Y_{12}$  OF CIRCUMFERENTIAL SLOTS ON A CYLINDER

$\phi_0$ (deg.)	$z_0$ (inch)	Modal Solution	GTD Solution
0	0.5"	-62.62 db -72°	-62.54 -72°
	2.0"	-71.78 -117°	-71.66 -116°
	8.0"	-81.84 34°	-81.83 37°
	40.0"	-91.95 -115°	-92.46 -110°
30°	2"	-77.42 175°	-77.69 177°
60°		-90.00 -3°	-90.17 -1°
90°		-102.52 120°	-103.10 116°
30°	0	-81.33 -77°	-81.34 -75°
40°		-89.87 168°	-90.02 170°
60°		-101.97 -49°	-102.48 -47°

Parameters of slots are given in (68).

surface. Such a dependence on the surface curvature in the transverse direction of the ray is most interesting, and can be seen in Figure 8, where we plot the ratio

$$\left| \frac{Y_{12} \text{ on a cylinder with radius } R}{Y_{12} \text{ on a plane}} \right|$$

as a function of  $R$  for  $z_0 = 8''$  and  $\phi_0 = 0$ . We note that the convergence rate of the cylindrical  $Y_{12}$  to the planar  $Y_{12}$  is not as rapid as one would normally expect. For example, at  $kR = 50$ , the cylindrical  $Y_{12}$  is still about 10 percent higher than the planar one. The exact modal solution in this figure is truncated at  $kR = 50$ , because beyond this radius, it becomes extremely slowly convergent.

(iii) Additional numerical results of  $Y_{12}$  between two identical slots on a cylinder are given in Figures 9 to 12. The normalized phase is defined by the phase of  $Y_{12} \exp(+jks_0)$ , where  $s_0$  is the center-to-center distance of the slots and is equal to  $(z_0^2 + R^2 \phi_0^2)^{1/2}$ .

## 7. GTD GREEN'S FUNCTION FOR A SURFACE FIELD ON A GENERAL CONVEX SURFACE

To calculate the mutual admittance between slots on a general convex surface, we have to generalize the GTD Green's function for the cylinder in (5.6). Referring to Figure 13, let us consider a perfectly conducting convex surface  $\Sigma$ , whose radii of curvature at any point are large in terms of wavelength. At a point  $Q_1$ , described by position vector  $\vec{r}_1$  on  $\Sigma$ , there is a tangential magnetic dipole source described by a magnetic current density

$$\vec{K}(\vec{r}) = \vec{M}\delta(\vec{r} - \vec{r}_1) \quad (7.1)$$

where  $\vec{M}$  is the magnetic dipole moment and lies in the tangent plane of  $\Sigma$ . The problem is to determine a high-frequency asymptotic solution of  $\vec{H}$  at a general point  $Q_2$  described by position vector  $\vec{r}_2$  on  $\Sigma$ . In other words, the GTD Green's function for the surface magnetic field for points  $\vec{r}_1$  and  $\vec{r}_2$  is to be found.

Before presenting the solution, let us introduce several definitions and parameters. According to GTD [13], [14], the dominant high-frequency contribution to  $\vec{H}(\vec{r}_2)$  is the field on the surface ray from  $\vec{r}_1$  to  $\vec{r}_2$ . The surface ray is a geodesic of  $\Sigma$ . Some of the geometrical properties are described by (Figure 13) (i) the arc length  $\bar{s}$  which is chosen such that  $\bar{s} = 0$  at the source point  $\vec{r}_1$  and  $\bar{s} = s$  at the observation point  $\vec{r}_2$ ; (ii) the tangent, normal, and binormal, denoted by  $(\hat{t}_n, -\hat{n}_n, -\hat{b}_n)$  at  $\vec{r}_n$  where  $n = 1, 2$ ; and (iii) its two radii of curvature  $R_t(\bar{s})$ , and  $R_b(\bar{s})$  of  $\Sigma$  at point  $\bar{s}$  in the directions of tangent and binormal, respectively. (On a general convex surface, both radii are nonnegative.)

From the above parameters, we may calculate the following quantities that are needed for the solution of the Green's function:

(i) The large parameter in our asymptotic expansion of the Green's function is

$$m(\bar{s}) = \left[ \frac{1}{2} k R_t(\bar{s}) \right]^{1/3}, \quad (7.2)$$

which is a function of position along the ray from  $\vec{r}_1$  to  $\vec{r}_2$ .

(ii) A distance parameter from  $\vec{r}_1$  to  $\vec{r}_2$  is defined by

$$\xi = \int_{\vec{r}_1}^{\vec{r}_2} \frac{k}{2m^2(\bar{s})} d\bar{s}. \quad (7.3)$$

For the special case when  $R_t$  is not a function of  $\bar{s}$  (constant ray curvature),  $\xi$  is reduced to  $(ks/2m^2)$ , a well-known parameter introduced first by Fock [17].

(iii) The ray curvatures at the source and observation points enter in a parameter defined by

$$\tau = \left[ \frac{ks}{2m(0) m(s) \xi} \right]^{1/2}, \quad (7.4)$$

which is positive real for a convex surface, and is reduced to unity for the special case of a constant ray curvature.

(iv) Consider a small pencil of surface rays originating from  $\vec{r}_1$  and propagating toward  $\vec{r}_2$  (Figure 13). The angle extended by the pencil at  $\vec{r}_1$  is  $d\psi_1$ , and that at  $\vec{r}_2$  is  $d\psi_2$ . The divergence factor DF of the pencil is defined by

$$DF = \left[ \frac{sd\psi_1}{\rho d\psi_2} \right]^{1/2} \quad (7.5)$$

where  $\rho$  is the caustic distance of the wavefront at  $\vec{r}_2$  and is always

positive. For example, if  $\Sigma$  is a sphere and  $\vec{r}_1$  is the north pole, DF at point  $\vec{r}_2 = (r, \theta, \phi)$  is

$$DF = \left[ \frac{\theta}{\sin \theta} \right]^{1/2}$$

which varies from one at the north pole ( $\theta = 0$ ) to infinity at the south pole ( $\theta = \pi$ ) as  $\vec{r}_2$  moves along a great circle.

(v) The "mean" radii of curvature between  $\vec{r}_1$  and  $\vec{r}_2$  are defined by

$$\bar{R}_t = [R_t(0) R_t(s)]^{1/2} \quad (7.6a)$$

$$\bar{R}_b = [R_b(0) R_b(s)]^{1/2} \quad (7.6b)$$

Throughout this work, we always assume that  $\Sigma$  is a smooth surface with a slowly varying curvature. Then  $(\bar{R}_t, \bar{R}_b)$  represents a sort of average value of radii of curvature along the ray.

Return to the electromagnetic problem in Figure 13. We assume that  $m(\bar{s})$  is large and is slowly varying for all  $\bar{s}$  in the range  $0 \leq \bar{s} \leq s$ . Then an approximate asymptotic solution for the surface magnetic field at  $\vec{r}_2$  due to the dipole source in (7.1) is given by

$$\vec{H}(\vec{r}_2) \approx \vec{M} \cdot (\hat{b}_1 \hat{b}_2 H_b + \hat{t}_1 \hat{t}_2 H_t) (DF) \quad (7.7a)$$

where

$$H_b = G(s) \left\{ \left(1 - \frac{j}{ks}\right) \tau v(\xi) - \left(\frac{1}{ks}\right)^2 \tau^3 u(\xi) + j(\sqrt{2k\bar{R}_t})^{-2/3} \right. \\ \left. \cdot [\tau v'(\xi) + (\bar{R}_t/\bar{R}_b) \tau^3 u'(\xi)] \right\} \quad (7.7b)$$

$$H_t = G(s) \left( \frac{j}{ks} \right) [\tau v(\xi) + (1 - \frac{2j}{ks}) \tau^3 u(\xi) + j(\sqrt{2k\bar{R}_t})^{-2/3} \tau^3 u'(\xi)] \quad (7.7c)$$

$$G(s) = \frac{k^2 Y_0}{2\pi j} \frac{e^{-jks}}{ks}, \quad Y_0 = (120\pi)^{-1} \quad (7.7d)$$

The Fock functions  $u$  and  $v$  and their derivatives  $u'$  and  $v'$  are described in the Appendix. Several remarks about the solution in (7.7) are in order.

(i) It is derived in an approximate manner from the classical work of Fock [17] and the recipe of GTD, as detailed in [10]. All traditional GTD solutions depend on  $\bar{R}_c$ , not  $\bar{R}_b$ . In (7.7b), the term containing  $(\bar{R}_c/\bar{R}_b)$  was introduced through an Ansatz suggested in [9]. Because of the fact that  $u'$  decays faster than  $v'$ , this term is important only if  $\bar{R}_c$  is very large and  $\bar{R}_b$  is finite. An example occurs in the axial propagation along a cylinder, where  $\bar{R}_c \rightarrow \infty$  and  $\bar{R}_b$  is equal to the radius of the cylinder. For this particular example, it is only with this additional term that (7.7b) agrees with the rigorous asymptotic solution (derived recently by J. Boersma in an unpublished note). Thus, the Ansatz in [9] is at least partially verified.

(ii) For the special case that  $\Sigma$  is a planar surface ( $R_c = R_b \rightarrow \infty$ ), (7.7) recovers the known exact solution given in (5.8). When  $\Sigma$  is a cylinder, (7.7) is reduced to (5.6).

(iii) The solution is valid for any combination of  $\vec{r}_1$  and  $\vec{r}_2$ . In the penumbra region ( $\vec{r}_2$  is close to  $\vec{r}_1$  and  $\xi \ll 1$ ), (7.7) gives approximately the known planar solution. In the deep shadow ( $\xi \gg 1$ ), the residue series representation of the Fock functions can be used, and (7.7) is identified as the creeping-wave contribution.

(iv) Except for the very simple surfaces such as a cylinder, cone or sphere, no explicit parameter equations can be found for the geodesics [18]. Thus, for a general surface, one may have to rely on numerical techniques for determining the geodesics and the divergent factor.

## 8. GREEN'S FUNCTION OF A CONE

Let us apply the formula (7.7) to the field on an infinite cone, described by the equations (Figure 14a)

$$x = r \sin \theta_0 \cos \phi, \quad y = r \sin \theta_0 \sin \phi, \quad z = r \cos \theta_0 \quad (8.1)$$

where  $\theta_0$  is the half-cone angle ( $0 < \theta_0 < \pi/2$ ). Since the cone is a developable surface, the rays (geodesics) on a developed cone (Figure 14b) are straight lines [18]. Due to the source at  $\vec{r}_1 = (r_1, \theta_0, \phi_1)$ , the main contribution of the field at  $\vec{r}_2 = (r_2, \theta_0, \phi_2)$  comes from the shortest ray described by

$$r_1 \sin \Omega_1 = r_2 \sin \Omega_2 \quad (8.2)$$

As the ray propagates away from the source point  $\vec{r}_1$ , it reaches the highest altitude at M where  $\Omega_2 = \pi/2$ . After M, the ray travels downward away from the cone tip. The various parameters defined in Section 7 can be simply calculated from the cone geometry, and expressed in terms of coordinates  $(r_1, \phi_1)$  and  $(r_2, \phi_2)$ . The arclength is

$$s = \{r_1^2 + r_2^2 - 2r_1r_2 \cos [(\phi_2 - \phi_1) \sin \theta_0]\}^{1/2} \quad (8.3)$$

The angle  $\Omega_1$  at  $\vec{r}_1$  is

$$\Omega_1 = \sin^{-1} \left\{ \frac{r_2}{s} \sin [(\phi_2 - \phi_1) \sin \theta_0] \right\} \quad (8.4)$$

We choose  $|\Omega_1| < \pi/2$  if  $r_2^2 < s^2 + r_1^2$ , and  $|\Omega_1| > \pi/2$  if otherwise. The other parameters are

$$\Omega_2 = \Omega_1 + (\phi_2 - \phi_1) \sin \theta_0 \quad (8.5)$$

$$\bar{R}_t = \frac{\sqrt{r_1 r_2} \tan \theta_0}{\sin \Omega_1 \sin \Omega_2}, \quad \bar{R}_b = \frac{\sqrt{r_1 r_2} \tan \theta_0}{\cos \Omega_1 \cos \Omega_2} \quad (8.6)$$

$$\xi = \left(\frac{1}{2} k r_1 \sin \Omega_1 \sin \theta_0\right)^{1/3} |\phi_2 - \phi_1| \cos^{2/3} \theta_0 \quad (8.7)$$

$$\tau = (ks/\xi)^{1/2} (2k^2 r_1 r_2)^{-1/6} (\sin \Omega_1 \sin \Omega_2 \cos \Omega_0)^{1/3} \quad (8.8)$$

$$DF = 1 \quad (8.9)$$

When the above parameters in (8.3) through (8.9) are substituted into (7.7), we obtain an approximate solution for the surface field on a cone due to a direct surface ray contribution. Let us consider a special observation point  $\vec{r}_2$  such that

$$ks \gg 1, \quad \Omega_1 \text{ and } \Omega_2 \text{ are not close to zero} \quad (8.10)$$

After making use of the residue series representation for the Fock functions (Appendix) and keeping only the leading terms, then the two components of the field in (7.7) are reduced to

$$H_b \sim \frac{k^2 (\sin \Omega_1 \sin \Omega_2 \csc \theta_0)^{1/3}}{1528 (k^2 r_1 r_2)^{1/6} (ks)^{1/2}} \exp \left\{ -0.88\xi - j\left(\frac{5\pi}{12} + 0.51\xi + ks\right) \right\} \quad (8.11a)$$

$$H_t \sim 0 [(ks)^{-3/2}] \quad (8.11b)$$

which agree with the rigorous asymptotic solutions given in Equations (50) and (53) of [19]. (In making the comparison, note the corresponding notations used in [1] and here:  $-i \rightarrow j$ ,  $\theta_c \rightarrow \theta_0$ ,  $L_1 \rightarrow s$ ,  $r_> \rightarrow r_1$ ,  $r_< \rightarrow r_2$ ,  $\beta_{s>} \rightarrow \pi/2 - \Omega_1$ , and  $\bar{q}_1 \rightarrow |t_1'|$ .) We emphasize that the result in (8.11) or that in [19] is valid only under the conditions in (8.10). For an arbitrarily located observation point, (7.7) should be used.

Two final remarks about the formula in (7.7) are in order. (i) For a given source and observation point, there are infinitely many rays (geodesics) passing through them. The contribution from each ray can be

calculated from (7.7), and the final field solution is the superposition of all ray contributions. In most practical problems (all the numerical computations presented in this paper), only the ray with the shortest arclength gives the significant contribution to the field solution, whereas all other rays may be ignored. (ii) Depending on the polarization and the distances of the source and observation points from the cone tip, there may be another significant contribution to the field from the diffraction at the tip. In such a case, the total field at any point contains two dominant contributions: one from the direct ray according to formula (7.7), and one from the tip-diffracted ray. More about the latter will be given in Section 9.

## 9. MUTUAL ADMITTANCE BETWEEN SLOTS ON A CONE

On the surface of a cone, let us consider two arbitrarily oriented slots. Under the assumption that the dimensions of the slots are relatively small compared with the radii of curvature of the cone surface, the shapes of slots are taken to be rectangular on a developed cone.

Referring to Figure 15, we describe the dimensions and the positions of the two slots by  $(a_n, b_n)$  and  $[c_n, (n-1)\phi_0, \omega_n]$ ,  $n = 1, 2$ . Thus, the radial separation of the two slots is  $(c_2 - c_1)$  and the angular separation is  $\phi_0$ . The angle  $\omega_n$  measures the deviation of the longitudinal direction of slot  $n$  from the radial direction of the cone. As usual, we assume that the slots are thin, and that their lengths are roughly a half-wavelength. Then the aperture field in each slot can be adequately approximated by a simple cosine distribution, which is the "one-mode" approximation described in Section 4.  $Y_{12}$  has two dominant high-frequency contributions: one from the direct rays going from slot 1 to slot 2, and the other from the rays diffracted at the tip of the cone, viz.,

$$Y_{12} \sim Y_{12}^d + Y_{12}^t \quad (9.1)$$

The first term  $Y_{12}^d$  may be explicitly written as \*

$$Y_{12}^d = \frac{-2}{(a_1 b_1 a_2 b_2)^{1/2}} \int_{-a_1/2}^{a_1/2} dy_1 \int_{-b_1/2}^{b_1/2} dz_1 \int_{-a_2/2}^{a_2/2} dy_2 \int_{-b_2/2}^{b_2/2} dz_2 \\ \times (\cos \frac{\pi}{a_1} y_1) (\cos \frac{\pi}{a_2} y_2) g(1,2) \quad (9.2a)$$

where

$$g(1,2) = H_b \cos \omega_3 \cos \omega_4 + H_t \sin \omega_3 \sin \omega_4 \quad (9.2b)$$

\* Coordinates  $(y_2, z_2)$  here have their origin at the center of slot 2 (Figure 15), not at the center of slot 1 as in the cylinder case (Figure 7).

The Green's function components ( $H_b, H_t$ ) are given in (7.7), and angles ( $\omega_3, \omega_4$ ) are shown in Figure 15. In evaluating the integrals in (9.7a), for two given points ( $y_1, z_1$ ) and ( $y_2, z_2$ ), we must calculate some geometrical parameters appearing in  $H_b$  and  $H_t$ . Those calculations lead to the following results

$$r_n = [c_n^2 + y_n^2 + z_n^2 - 2c_n \sqrt{y_n^2 + z_n^2} \cos(\omega_n - \omega_{n+4})]^{1/2} \quad (9.3a)$$

$$\phi_n = (\sin \theta_0)^{-1} \sin^{-1} [\sqrt{y_n^2 + z_n^2} r_n^{-1} \sin(\omega_n - \omega_{n+4})] \quad (9.3b)$$

$$\omega_{n+4} = \tan^{-1}(z_n/y_n) \quad (9.3c)$$

$$\omega_{n+2} = \Omega_n + (\pi/2) - \omega_n - \phi_n \sin \theta_0 + (n-1)\phi_0 \sin \theta_0 \quad (9.3d)$$

where  $n = 1$  and  $2$ . We evaluate the integrals in (9.2a) numerically with the aid of a computer.

Next, let us consider  $Y_{12}^t$ , the part of mutual admittance due to the rays diffracted at the cone tip. We approximate it by

$$Y_{12}^t \approx T \sin \omega_1 \sin \omega_2 \quad (9.4)$$

where  $T$  is derived in [2] and is given by

$$T = \sigma_0 \frac{(a_1 b_1 a_2 b_2)^{1/2}}{30\pi^4 c_1 c_2 \sin \theta_0} \left( \frac{\tan \theta_0}{2\pi} \right)^{1/2} \frac{\sin(kb_1/2) \sin(kb_2/2)}{(kb_1/2)(kb_2/2)} \cdot \exp j\left(\frac{\pi}{4} - kc_1 - kc_2\right) \quad (9.5)$$

Here  $\sigma_0$  is the zeroth-order tip diffraction coefficient and is a function of the half-cone angle  $\theta_0$ . A numerical table of  $\sigma_0$  for several typical values of  $\theta_0$  is given in [2]. We have fitted those values by a simple expression, viz.,

$$\sigma_0 = A \exp(jB) \quad , \quad (9.6)$$

where

$$A = 1.3057\theta_0^{-1} - 1.755 + 2.772\theta_0 - 1.459\theta_0^2$$

$$B = 2.7195 + 1.4608\theta_0 - 1.1295\theta_0^2 + 0.6566\theta_0^3 \quad .$$

Both  $\theta$  and  $B$  are in radians. It has been checked that the numerical values of  $\sigma_0$  calculated from (9.6) are in excellent agreement with those tabulated in [2].

The final solutions for  $Y_{12}$  (total mutual admittance) and  $Y_{12}^d$  (partial mutual admittance) are given in (9.1), (9.2), and (9.4). For a given geometry of the slots and cone, the two surface integrals in (9.2a) are evaluated numerically by choosing an integration grid roughly equal to  $0.05\lambda \times 0.05\lambda$ . Unless specified otherwise, all numerical computations are based on two identical slots with slot length =  $0.5\lambda$  and width =  $0.2\lambda$ .

a. "Equivalent" cylinder. It has been conjectured in [2] that, in calculating  $Y_{12}^d$  (the contribution from the direct rays) approximately, the cone may be replaced by an "equivalent" cylinder with radius

$$R = \frac{1}{2}(c_1 + c_2) \sin \theta_0 \quad . \quad (9.7)$$

This conjecture has been quantitatively checked out in [8]. The conclusion is that the "equivalent" cylinder gives a good approximation for a small-angled cone, e.g.,  $\theta_0 = 15^\circ$ . However, the error in  $Y_{12}^d$  calculated from the "equivalent" cylinder can be as large as 2.5 db for a large-angled cone ( $\theta_0 = 30^\circ$ , for example).

b. Comparison with experiments. A set of experimental data on the mutual coupling between two X-band open-ended waveguides ( $0.9'' \times 0.4''$ )

on a cone was reported in [2]. As a function of frequency, measurements were done on the coupling coefficient  $S_{12}$ , which is related to  $Y_{12}$  through the formula in (3.3). In Figures 16 and 17, three sets of data are presented: (i) the experimental data; (ii) the theoretical results from the present analysis in which the calculation of  $Y_{12}^d$  is based on a cone, e.g., Equation (9.2); (iii) the theoretical results from [2] in which  $Y_{12}^d$  is calculated from the exact modal solution of an "equivalent" cylinder. Several observations can be made. (a) Both theoretical results are in good agreement with the experimental data (with the present result being slightly better). As explained in (9a), the "equivalent" cylinder method works because the cone angles ( $\theta_0 \sim 10^\circ$ ) are small. (b) The peaks and valleys are caused by the interference between  $Y_{12}^d$  and  $Y_{12}^t$ , which are of comparable magnitudes due to the large angular separations ( $60.8^\circ$  and  $80^\circ$ ). (c) There exists a slight shift in frequency ( $\Delta f/f \sim 3$  percent) between the theoretical and experimental valleys in Figure 16. We speculate that this may be due to a slight phase inaccuracy in  $Y_{12}^t$ .

c. Mutual admittances of circumferential slots. In Figures 18 to 20,  $Y_{12}^d$  and  $Y_{12}^t$  for two circumferential slots are displayed as functions of angular separation  $\phi_0$  and the radial separation ( $c_1 - c_2$ ). We note that the effect of  $Y_{12}^t$  can modify the curves of  $Y_{12}^d$  in several different ways. When the slots are at the same latitude (Figure 18), the direct coupling is weak. Thus, tip contribution is noticeable even at a small angular separation. As the radial separation is increased (Figure 19), the tip contribution is almost negligible for  $\phi_0 < 65^\circ$ . When the two slots are widely separated in the radial direction with one slot near the tip (Figure 20), the tip contribution gets stronger, the direct contribution

gets stronger, and the direct contribution becomes insensitive to  $\phi_0$ . Hence, the oscillation on the  $Y_{12}$  curve has a much larger period. In fact, there is only a half-"cycle" in the range  $0 < \phi_0 < 90^\circ$ , and  $Y_{12}$  appears to be shifted from  $Y_{12}^d$  by a fixed amount.

d. Effect of slot orientation on mutual admittance. Consider two slots separated by  $1 \lambda$  along the radial direction. The magnitude of  $Y_{12}$  as functions of the slot orientation angles  $\omega_1$  and  $\omega_2$  is plotted in Figure 21. As expected, the maximum value (-73 db) occurs when both slots are circumferential ( $\omega_1 = \omega_2 = 90^\circ$ ). This value is above 14 db, higher than that when both slots are radial ( $\omega_1 = \omega_2 = 0$ ). The minimum value (-113 db) of  $Y_{12}$  occurs when the top slot is radial and the bottom one is circumferential. This result confirms a common belief that the mutual coupling between two orthogonal slots is generally negligible.

## 10. SELF-ADMITTANCE OF A SLOT ON A CYLINDER OR A CONE

The formula for calculating mutual admittance  $Y_{12}$  in (4.2) can be used to calculate the self-admittance  $Y$  (or the alternative notation  $Y_{11}$ ), provided that slot 1 coincides with slot 2. However, in the actual numerical evaluation of GTD expressions such as (6.3), (6.6), and (9.2), a mathematical difficulty arises as explained below.

Let us concentrate on (9.2) with  $a_1 = b_1$ ,  $a_2 = b_2$ ,  $c_1 = c_2$ , and  $\phi_0 = 0$ , which is the direct ray contribution  $Y^d$  to the self-admittance of a slot on a cone. This integral is divergent, due to the fact that, as point  $Q_1$  approaches point  $Q_2$  (Figure 15), the Green's function in (9.2b) becomes infinite as

$$g(1,2) \sim Cs^{-3}, \quad s \rightarrow 0, \quad (10.1a)$$

where  $s$ , defined in (8.3), is the distance between the two points, and the parameter  $C$  is

$$C = \frac{1}{j240\pi^2 k} (2 - 3 \cos^2 \Omega_1). \quad (10.1b)$$

It is well-known that the singularity of cubic power is non-integrable with respect to a surface integral. This difficulty can be traced back to the derivation of the Green's function  $g$ . Strictly speaking,  $g$  is a distribution and can be written as

$$g = D\bar{g}, \quad (10.2)$$

where  $D$  is a second-order differential operator with respect to coordinates of point  $Q_2$ , and  $\bar{g}$  is the Green's function of a vector potential component. A "legitimate" expression corresponding to (9.2a) should read

$$Y^d = -\frac{2}{ab} \iint dy_2 dz_2 \left( \cos \frac{\pi y_2}{a} \right) \{ D [ \iint dy_1 dz_1 \left( \cos \frac{\pi y_1}{a} \right) \bar{g} ] \} , \quad (10.3)$$

which is convergent, and  $Y^d$  has a well-defined finite value. However, in writing (9.2a), we have interchanged the differential operator  $D$  and the second surface integration operator in (10.3). This interchanging is not permissible and, therefore, leads to the divergent integral in (9.2a).

Since (10.3) contains a differential operator and is not suitable for numerical evaluation, we prefer to work with (9.2a), provided of course that we can extract the correct finite part from the divergent integral. To this end, we rewrite the Green's function in (9.2a) as

$$g = g_0 + g_1 . \quad (10.4)$$

The first term  $g_0$  in (10.4) is the Green's function of an infinite ground plane, and is given by the well-known expression, c.f. (5.8),

$$g_0 = G(s) \left[ \cos^2 \Omega_1 + \frac{j}{ks} (1 - \frac{j}{ks}) (2 - 3 \cos^2 \Omega_1) \right] . \quad (10.5)$$

Note that, as  $s \rightarrow 0$ ,  $g_0$  has exactly the same singular behavior in (10.1) as  $g$ . This is expected, because in the sufficiently small neighborhood of a point source, the cone can be approximated by its tangent plane.

The second term  $g_1$  ( $g_1 = g - g_0$ ) in (10.4) is the difference between the Green's function of a cone and that of a plane. Near the source, it can be shown from (9.2a) and (10.5) that

$$g_1 \sim C_1 s^{-3/2} , \quad s \rightarrow 0 , \quad (10.6a)$$

where

$$C_1 = (1920\bar{R}_t)^{-1} k^{-1/2} \pi^{-3/2} (1 - j)(2 - 3 \sin^2 \Omega_1) . \quad (10.6b)$$

When (10.4) is substituted into (9.2a), the self-admittance  $Y^d$  on a cone is decomposed into two components, namely,

$$Y^d = Y_0^d + Y_1^d \quad (10.7)$$

The singularity of  $g_1$  at the source point specified in (10.6) is integrable. Thus, there is no difficulty in evaluating  $Y_1^d$  numerically.

The first term  $Y_0^d$  is the admittance of a slot on a plane. It is defined by (9.2a) after replacing  $g$  by  $g_0$  in (10.5). From (5.6d) and (10.5), we recognize the following identity:

$$g_0 = \left(1 + \frac{1}{k^2} \frac{\partial^2}{\partial y_2^2}\right) G(s) \quad (10.8)$$

Note that (10.8) is in the form of (10.2). Substituting (10.8) into (9.2a) and interchanging integration and differentiation operators, we obtain

$$Y_0^d = -\frac{2}{ab} \iint dy_2 dz_2 \cos\left(\frac{\pi y_2}{a}\right) \left\{ \left(1 + \frac{1}{k^2} \frac{\partial^2}{\partial y_2^2}\right) \left[ \iint dy_1 dz_1 \cos\left(\frac{\pi y_1}{a}\right) G(s) \right] \right\} \quad (10.9)$$

The integral in (10.9) is now convergent, and can be considered as the "finite part" of the divergent integral in (9.2a). For numerical evaluation, (10.9) in the space domain is converted to that in the Fourier transform domain. Following Rhodes [20], it is simplified and the final result reads

$$\text{Re}Y_0^d = \frac{a}{15\pi^4 k} \int_0^k d\alpha C(\alpha) \beta \left\{ \int_0^{\beta b} J_0(t) dt - J_1(\beta b) \right\} \quad (10.10a)$$

$$\begin{aligned} \text{Im}Y_0^d = \frac{-a}{15\pi^4 k} & \left\{ \int_0^k d\alpha C(\alpha) \beta \left[ \int_0^{\beta b} Y_0(t) dt - Y_1(\beta b) - \frac{2}{\pi \beta b} \right] \right. \\ & \left. + \frac{2}{\pi} \int_k^\infty d\alpha C(\alpha) \gamma \left[ \int_0^{\gamma b} K_0(t) dt + K_1(\gamma b) - \frac{1}{\gamma b} \right] \right\} \quad (10.10b) \end{aligned}$$

where  $\beta = (k^2 - \alpha^2)^{1/2}$  ,  $\gamma = (\alpha^2 - k^2)^{1/2}$  , and

$$C(\alpha) = \frac{\cos^2(\alpha a/2)}{1 - (\alpha a/\pi)^2} . \quad (10.11)$$

This is no difficulty in evaluating (10.10) numerically.

In summary, the direct ray contribution of  $Y^d$  for self-admittance of a slot on a cone as given in (9.2a) is divergent, due to an "illegal" interchange of integration and differentiation operators in the derivation process. The (correct) finite part of the divergent integral is given in (10.7), where  $Y_0^d$  is given in (10.10), and  $Y_1^d$  in (9.2a) after replacing  $g$  by  $g_1$ . The same difficulty arises in the case of a cylinder, and it is treated by the same procedure as in the case of a cone.

We have derived the self-admittance  $Y$  of a slot on three types of surfaces: (i) For an infinite plane, the final solution  $Y = Y^d$  is given in (10.10). (ii) For an infinite cylinder,  $Y = Y^d$  is given in (10.7). For a circumferential slot,  $Y_1^d$  is given by the integral in (6.3) after replacing  $g_\phi$  by  $(g_\phi - g_0)$ , and recognizing that  $\Omega_1 = (\pi/2) - \theta$  and  $A_1 = A_2$ . For an axial slot,  $Y_1^d$  is given by the integral in (6.6) after replacing  $g_z$  by  $(g_z - g_0)$ , and  $\Omega_1 = \theta$  and  $A_1 = A_2$ . (iii) For an infinite cone,  $Y$  has two contributions as described in (9.1). If one realized that the two slots in Figure 15 are identical, and occupy the same position on the cone,  $Y^E$  is given in (9.4) and  $Y^d$  in (10.7). To calculate  $Y_1^d$ , we use (9.2a) after replacing  $g$  by  $g_1$ , where  $g_1$  can be gathered from (10.4), (9.2b), and (10.5). Numerical results of  $Y$  on the above three surfaces are presented below.

Slot on a plane. As a function of slot length  $a$ , we plot  $(a/2b)Y$  in Figure 22 for three different values of slot width  $b$ . Those curves

are practically linear, and can be described for  $0.4 \leq (a/\lambda) \leq 0.6$  to a good accuracy by

$$Y \approx \frac{2b}{a} \{ [1.029 + j0.596] + (3.75 + jB) \left( \frac{a}{\lambda} - 0.5 \right) \} \text{ millimho} \quad (10.12)$$

where  $B = 44, 33,$  and  $21$  for  $b = 0.0001\lambda, 0.001\lambda,$  and  $0.01\lambda,$  respectively.

Relation to dipole impedance. As discussed in Section 4, there is an alternative definition for the (self- or mutual) admittance of a slot.

This alternative self-admittance  $\bar{Y}$  is related to the present  $Y$  by (4.4) or

$$\bar{Y} = (a/2b)Y \quad . \quad (10.13)$$

From the duality relation in Maxwell's equations, it can be shown (p. 519 of [11]) that for the special case  $a = \lambda/2,$

$$\bar{Z} = \frac{1}{4} (120\pi)^2 (2\bar{Y}) \quad , \quad (10.14)$$

when  $\bar{Z}$  is the input impedance of a centrally fed, half-wavelength dipole radiating in the free space (not in a half-space as in the case of a waveguide-fed slot). From (10.12) through (10.14), we find that for a half-wavelength dipole,

$$\bar{Z} = 73.12 + j 42.36 \text{ ohm} \quad , \quad (10.15)$$

which agrees with the results in [11], [20].

a. Slot on a cylinder. Consider a circumferential slot of dimension  $0.9'' \times 0.4''$  on an infinitely long cylinder whose radius is  $3.8''$ .

Figure 23 shows  $Y$  calculated by the present GTD solution and that by the exact modal series solution in [2]. These two solutions are in agreement within 0.5% in magnitude and one degree in phase. Note that, under the "one-mode approximation," the modal series solution [2] is exact. It is amazing that the present GTD solution gives such an accurate result for  $kR \sim 18$ .

b. Slot on a cone: variation with radial distance. In all of the following cone calculations, the slot has the dimensions of  $0.5\lambda \times 0.05\lambda$ , except when stated otherwise. In Figures 24 and 25, the slot is circumferentially oriented on a cone with  $\theta_0 = 30^\circ$ , and the variation of  $Y$  with the radial distance  $c$  is presented. We observe two effects: (i) As  $c$  is increased, the radius  $R = c \sin \theta_0$  of the "equivalent" cylinder becomes larger and larger. The magnitude of  $Y$  decreases and approaches the asymptotic value of the slot on a plane. (ii) At  $c = 2\lambda$ , the tip contribution  $|Y^t|$  is less than 1% of the  $|Y|$ , and this contribution diminishes as  $c$  increases.

c. Slot on a cone: variations with cone angle. As  $\theta_0$  is increased, the cone surface becomes flatter. Therefore,  $Y$  in Figure 26 approaches its value on a plane.

d. Slot on a cone: variations with slot length. It is interesting to observe from Figure 27 that the minimum values of  $|Y|$  for both the cone and plane cases occur roughly at  $a = 0.45\lambda$ , not at the resonant length  $a = 0.5\lambda$ .

e. Slot on a cone: variation with slot orientation angle. Figure 28 shows that there is about a 10% increase in  $|Y|$  as  $\omega$  varies from 0 (radial slot) to  $\pi/2$  (circumferential slot).

## 11. ACTIVE ELEMENT PATTERN

As explained in Sections 2 and 3, there are two types of active element patterns:  $P_1(\theta, \phi)$  under the short-circuited condition in Figure 3, and  $Q_1(\theta, \phi)$  under the match-loaded condition in Figure 4. Within the one-mode approximation (Section 4), we may set  $\lambda = 0$  in Figure 3. Then  $P_1$  becomes simply the radiation pattern of a single slot on a completely filled conducting surface (as if all other slots were absent). Its calculation is thus greatly simplified. Once  $P_1, P_2, \dots, P_N$  in an array are known, the other active element pattern  $Q_1$  can be determined from the matrix relation in (2.10).

Within the one-mode approximation,  $P_1(\theta, \phi)$  can be calculated by ray techniques as follows: The aperture distribution  $\vec{E}_1$  of slot 1 in Figure 29a is first replaced by an equivalent magnetic surface current  $\vec{K}_1 = \vec{E}_1 \times \hat{z}$  in Figure 29b, which radiates over a completely filled conducting surface  $\Sigma$ . By using the superposition principle, the problem of calculating pattern  $P_1(\theta, \phi)$  due to  $\vec{K}_1$  becomes the determination of the Green's function due to a magnetic dipole  $M$  on  $\Sigma$  (Figure 29c). Depending on the location of the observation point, the GTD calculation of the Green's function is carried out as follows:

(i) Observation point A is in the lit region. The field at A is that on the direct ray MA from the point source. The only effect of the conducting surface  $\Sigma$  is to image the source, thus doubling its strength.

(ii) Observation point B is in the shadow region. The ray path from the source to B follows a geodesic MD of the surface until a point of detachment D. From there on, the ray continues to B along a straight line DB tangent to  $\Sigma$  without abruptly changing direction.

(iii) The lit and shadow regions are separated by the tangent plane MT of surface  $\Sigma$ . A small neighborhood of MT is called the transition regions, through which the fields calculated from (i) and (ii) should bend smoothly into each other.

Various formulas, which exist for calculating fields on the rays described above [14], [21], [22], have been applied to calculate  $P_1(\theta, \phi)$  of a slot on a cylinder [6], or a cone [4], [22]. Because of the facts that (a) calculation steps are already available in book form [14], and (b) there are still several unsettled (unanswered) questions concerning the transition functions, torsion effect, numerical accuracy, etc., we refer interested readers to the literature for further details concerning the calculation of active element patterns by GTD.

APPENDIX

FOCK FUNCTIONS

In this appendix we define and list some useful formulas of the functions  $w_1(t)$ ,  $w_2(t)$ ,  $v(\xi)$ ,  $u(\xi)$ , and  $v_1(\xi)$ . These functions are commonly known as Fock functions.

(i) Definition: For a complex  $t$  and a real  $\xi$ ,

$$w_1(t) = \frac{1}{\sqrt{\pi}} \int_{\Gamma_1} dz \exp \left( tz - \frac{1}{3} z^3 \right) \quad (\text{A-1})$$

$$w_2(t) = \frac{1}{\sqrt{\pi}} \int_{\Gamma_2} dz \exp \left( tz - \frac{1}{3} z^3 \right) = w_1^*(t) \quad (\text{A-2})$$

$$v(\xi) = \frac{1}{2} e^{j\pi/4} \xi^{1/2} \frac{1}{\sqrt{\pi}} \int_{\Gamma_1} \frac{w_2(t)}{w_2'(t)} e^{-j\xi t} dt \quad (\text{A-3})$$

$$u(\xi) = e^{j3\pi/4} \xi^{3/2} \frac{1}{\sqrt{\pi}} \int_{\Gamma_1} \frac{w_2'(t)}{w_2(t)} e^{-j\xi t} dt \quad (\text{A-4})$$

$$v_1(\xi) = e^{j3\pi/4} \xi^{3/2} \frac{1}{\sqrt{\pi}} \int_{\Gamma_1} t \frac{w_2(t)}{w_2'(t)} e^{-j\xi t} dt \quad (\text{A-5})$$

where integration contour  $\Gamma_1(\Gamma_2)$  goes from  $\infty$  to 0 along the line  $\text{Arg } z = -2\pi/3 (+2\pi/3)$  and from 0 to  $\infty$  along the real axis. Because of different time conventions,  $w_1(w_2)$  above is equal to  $w_2(w_1)$  defined in [17].

(ii) Residue series representation: For real positive  $\xi$ ,

$$v(\xi) = e^{-j\pi/4} \sqrt{\pi} \xi^{1/2} \sum_{n=1}^{\infty} (\tau'_n)^{-1} e^{-j\xi\tau'_n} \quad (\text{A-6})$$

$$u(\xi) = e^{j\pi/4} 2\sqrt{\pi} \xi^{3/2} \sum_{n=1}^{\infty} e^{-j\xi\tau_n} \quad (\text{A-7})$$

$$v_1(\xi) = e^{j\pi/4} 2\sqrt{\pi} \xi^{3/2} \sum_{n=1}^{\infty} e^{-j\xi\tau'_n} \quad (\text{A-8})$$

$$v'(\xi) = \frac{1}{2} e^{-j\pi/4} \sqrt{\pi} \xi^{-1/2} \sum_{n=1}^{\infty} (1 - j2\xi\tau'_n)(\tau'_n)^{-1} e^{-j\xi\tau'_n} \quad (\text{A-9})$$

$$u'(\xi) = e^{j\pi/4} 3\sqrt{\pi} \xi^{1/2} \sum_{n=1}^{\infty} \left(1 - j\frac{2}{3}\xi\tau_n\right) e^{-j\xi\tau_n} \quad (\text{A-10})$$

where  $\tau_n = |\tau_n| \exp(-j\pi/3)$ ,  $\tau'_n = |\tau'_n| \exp(-j\pi/3)$ , and

n	$ \tau_n $	$ \tau'_n $
1	2.33811	1.01879
2	4.08795	3.24820
3	5.52056	4.82010
4	6.78671	6.16331
5	7.99413	7.37218

n	$ \tau_n $	$ \tau'_n $
6	9.02265	8.48849
7	10.04017	9.53545
8	11.00852	10.52766
9	11.93602	11.47506
10	12.82878	12.38479

(iii) Small argument asymptotic expansion: For real positive  $\xi$  and  $\xi \rightarrow 0$ ,

$$v(\xi) \sim 1 - \frac{\sqrt{\pi}}{4} e^{j\pi/4} \xi^{3/2} + \frac{7j}{60} \xi^3 + \frac{7\sqrt{\pi}}{512} e^{-j\pi/4} \xi^{9/2} - 4.141 \times 10^{-3} \xi^6 + \dots \quad (\text{A-11})$$

$$u(\xi) \sim 1 - \frac{\sqrt{\pi}}{2} e^{j\pi/4} \xi^{3/2} + \frac{5j}{12} \xi^3 + \frac{5\sqrt{\pi}}{64} e^{-j\pi/4} \xi^{9/2} - 3.701 \times 10^{-2} \xi^6 + \dots \quad (\text{A-12})$$

$$v_1(\xi) \sim 1 + \frac{\sqrt{\pi}}{2} e^{j\pi/4} \xi^{3/2} - \frac{7j}{12} \xi^3 - \frac{7\sqrt{\pi}}{64} e^{-j\pi/4} \xi^{9/2} + 4.555 \times 10^{-2} \xi^6 + \dots \quad (\text{A-13})$$

$$v'(\xi) \sim \frac{3\sqrt{\pi}}{8} e^{-j3\pi/4} \xi^{1/2} + \frac{7j}{20} \xi^2 + \frac{63\sqrt{\pi}}{1024} e^{-j\pi/4} \xi^{7/2} - 2.485 \times 10^{-2} \xi^5 + \dots \quad (\text{A-14})$$

$$u'(\xi) \sim \frac{3}{4} \sqrt{\pi} e^{-j3\pi/4} \xi^{1/2} + \frac{5j}{4} \xi^2 + \frac{45\sqrt{\pi}}{128} e^{-j\pi/4} \xi^{7/2} - 2.221 \times 10^{-1} \xi^5 + \dots \quad (\text{A-15})$$

(iv) Numerical evaluation: For  $\xi \geq \xi_0$ , the residue series representation with the first ten terms in the summation can be used. For  $\xi \leq \xi_0$ , the small argument asymptotic expansion with the first five terms can be used. It has been indicated in [7] that the smoothest crossover is obtained if  $\xi_0 = 0.6$ . In the present study, we set  $\xi_0 = 0.7$ , where the difference in the two representations is less than 0.1% in magnitude and  $0.9^\circ$  in phase.

#### REFERENCES

- [1] G. E. Stewart and K. E. Golden, "Mutual admittance for axial rectangular slots in a large conducting cylinder," IEEE Trans. Antennas Propagat., vol. AP-19, pp. 120-122, 1971.
- [2] K. E. Golden, G. E. Stewart, and D. C. Pridmore-Brown, "Approximation techniques for the mutual admittance of slot antennas on metallic cones," IEEE Trans. Antennas Propagat., vol. AP-22, pp. 43-48, 1974.
- [3] P. C. Bargeliotas, A. T. Villeneuve, and W. H. Kummer, "Phased array antennas scanned near endfire," Final Report (January 1975-March 1976), Contract N00019-75-0160, Hughes Aircraft Company, Culver City, California, 1976.
- [4] L. B. Felsen, A. Hessel, J. Shapira, and J. Schmoys, "Ray analysis of mutual coupling in conformal array," Polytechnic Institute of New York, Final report for Contract N00123-73-C-1481, 1974.
- [5] Y. Hwang and R. G. Kouyoumjian, "The mutual coupling between slots on an arbitrary convex cylinder," ElectroScience Laboratory, Department of Electrical Engineering, The Ohio State University, Semi-Annual Report 2902-21, prepared under Grant NGL 36-003-138, 1975.
- [6] P. H. Pathak, "Analysis of a conformal receiving array of slots in a perfectly-conducting circular cylinder by the geometrical theory of diffraction," ElectroScience Laboratory, Department of Electrical Engineering, The Ohio State University, Technical Report ESL 3735-2, prepared under Contract N00140-74-C-6017, 1975.
- [7] Z. W. Chang, L. B. Felsen, and A. Hessel, "Surface ray methods for mutual coupling in conformal arrays on cylinder and conical surface," Polytechnic Institute of New York, Final Report (September 1975-February 1976), prepared under Contract N00123-76-C-0236, 1976.
- [8] S. W. Lee and R. Mittra, "Mutual admittance between slots on a cylinder or cone," University of Illinois at Urbana-Champaign, Electromagnetics Laboratory Report No. 77-24, 1977.
- [9] S. W. Lee and S. Safavi-Naini, "Approximate asymptotic solution of surface field due to a magnetic dipole on a cylinder," IEEE Trans. Antenna Propagat., vol. AP-26, pp. 593-598, 1978.
- [10] S. W. Lee, "Mutual admittance of slots on a cone: Solution by ray technique," IEEE Trans. Antennas Propagat., vol. AP-26, 1978.
- [11] E. C. Jordan and K. Balmain, Electromagnetic Waves and Radiating Systems, 2nd Ed., Englewood Cliffs, New Jersey: Prentice-Hall, 1968, Chapter 14.

- [12] R. C. Hansen, "Formulation of echelon dipole mutual impedance for computer," IEEE Trans. Antennas Propagat., vol. AP-20, pp. 780-781, 1972.
- [13] J. B. Keller, "Geometrical theory of diffraction," J. Opt. Soc. Amer., vol. 52, pp. 116-130, 1962.
- [14] R. G. Kouyoumjian, "The geometrical theory of diffraction and its application," in Topics in Applied Physics, R. Mittra, Ed. New York: Springer-Verlag, 1975.
- [15] L. B. Felsen and N. Marcuvits, Radiation and Scattering of Waves. Englewood Cliffs, New Jersey: Prentice-Hall, 1973, pp. 477 and 483.
- [16] R. F. Harrington, Time Harmonic Electromagnetic Fields. p. 110. New York: McGraw-Hill, 1961.
- [17] V. A. Fock, Electromagnetic Diffraction and Propagation Problems. New York: Pergamon Press, 1965.
- [18] S. W. Lee, "Differential geometry for GTD applications," University of Illinois at Urbana-Champaign, Electromagnetics Laboratory Report No. 77-21, 1977.
- [19] K. K. Chan, L. B. Felsen, A. Hessel, and J. Shmoys, "Creeping waves on a perfectly conducting cone," IEEE Trans. Antennas Propagat., vol. AP-25, pp. 661-670, 1977.
- [20] D. R. Rhodes, "On a fundamental principle in the theory of planar antennas," Proc. IEEE., vol. 52, pp. 1013-1021, 1964.
- [21] P. H. Pathak and R. G. Kouyoumjian, "An analysis of the radiation from apertures in curved surfaces by the geometric theory of diffraction," Proc. IEEE, vol. 62, pp. 1438-1461, November 1974.
- [22] S. Safavi-Naini and R. Mittra, "Source radiation in the presence of smooth convex bodies," University of Illinois at Urbana-Champaign, Electromagnetics Laboratory Report No. 78-3, 1978; also to appear in Radio Science.

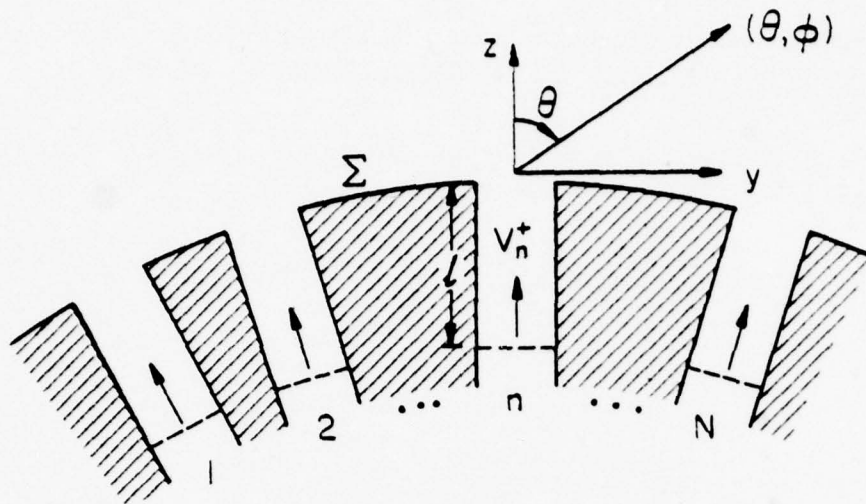


Figure 1. Array of  $N$  identical slots which are fed by waveguides.

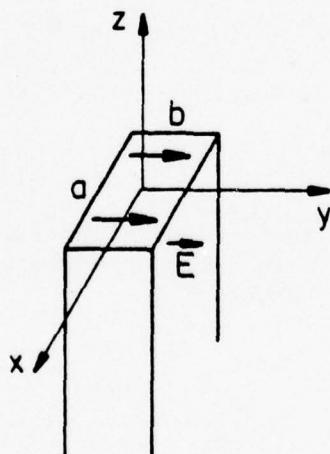


Figure 2. A slot fed by a rectangular waveguide of the same cross-section ( $a \times b$ ).

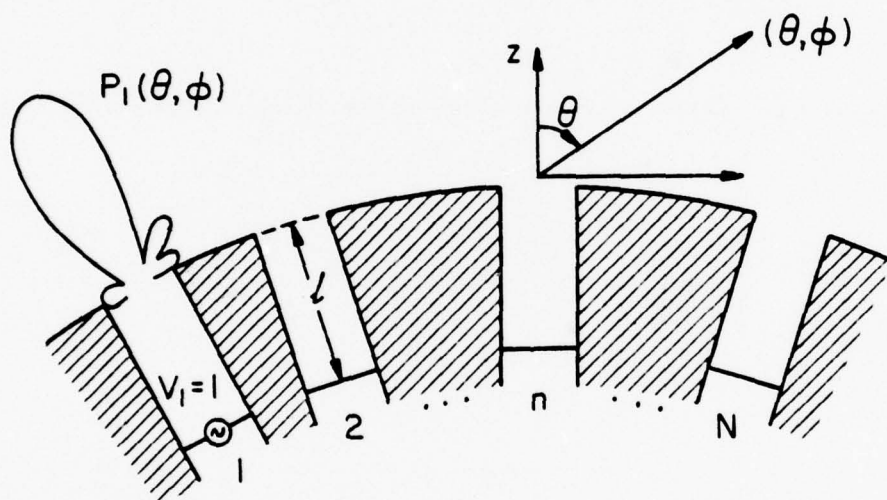


Figure 3. The radiation pattern obtained by  $V_1 = 1$ ,  $V_n = 0$  for  $n \neq 1$  is called the short-circuited active element pattern  $P_1$ .

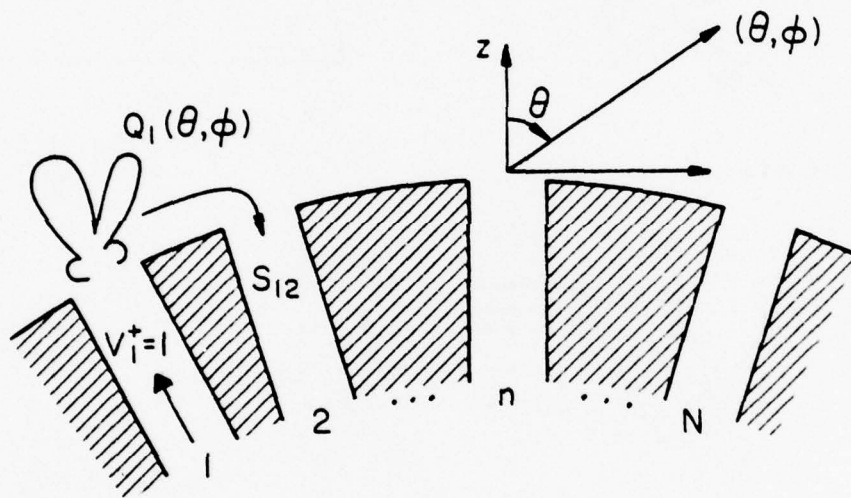
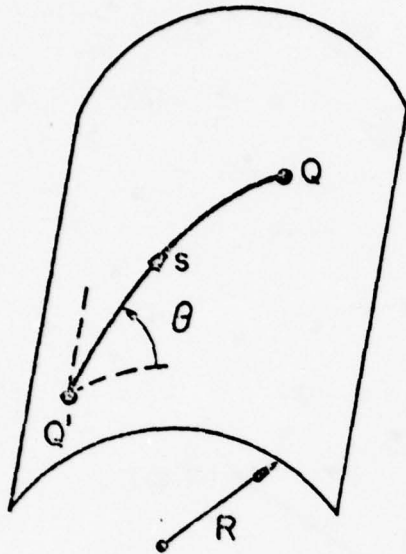
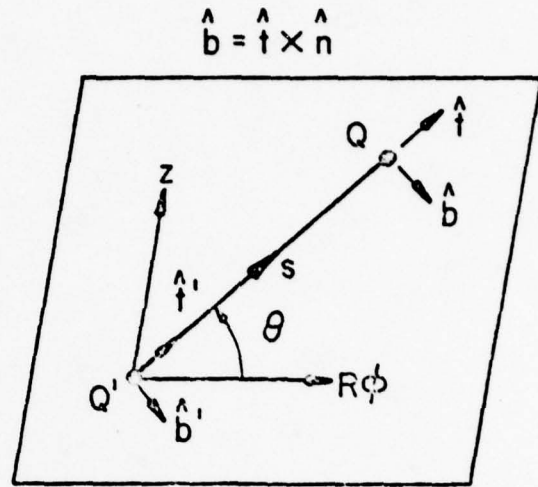


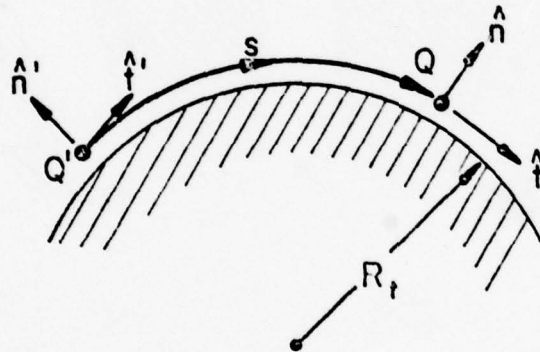
Figure 4. With  $V_1^+ = 1$  and all other elements match-loaded, the radiation pattern is called match-loaded active element pattern  $Q_1$ .



(a) 3-D view



(b) Developed cylinder



(c) Cut along  $\theta$ -direction

Figure 5. A surface ray from source point  $Q'$  to observation point  $Q$  on a cylinder of radius  $R$ .

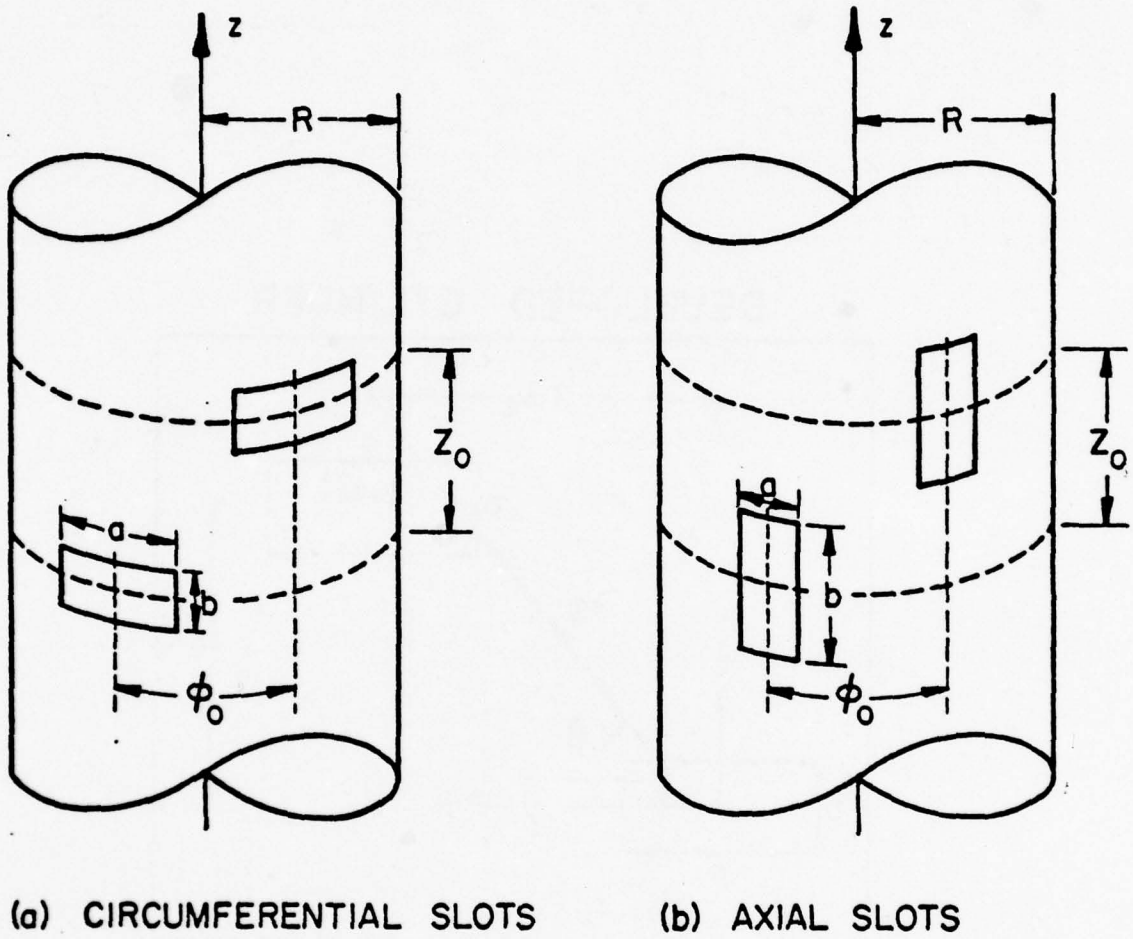


Figure 6. Two identical slots on the surface of a cylinder.

### DEVELOPED CYLINDER

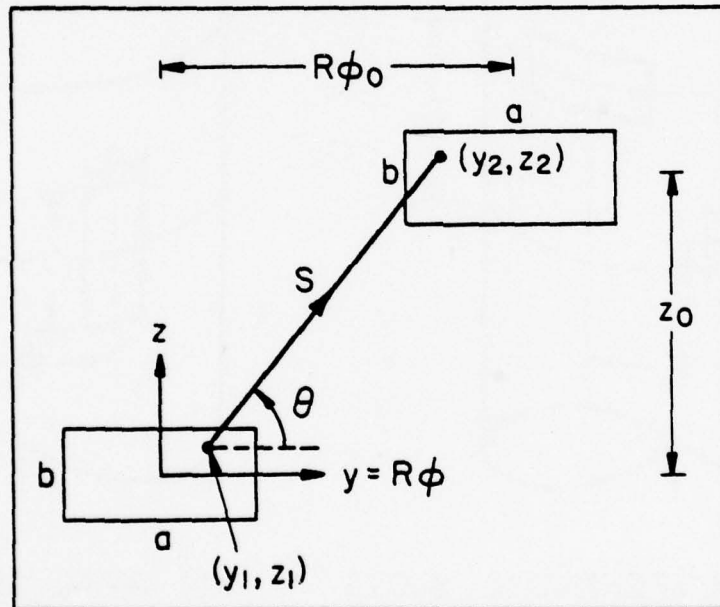


Figure 7. Two identical circumferential slots on the surface of a cylinder. The figure shows the developed cylinder.

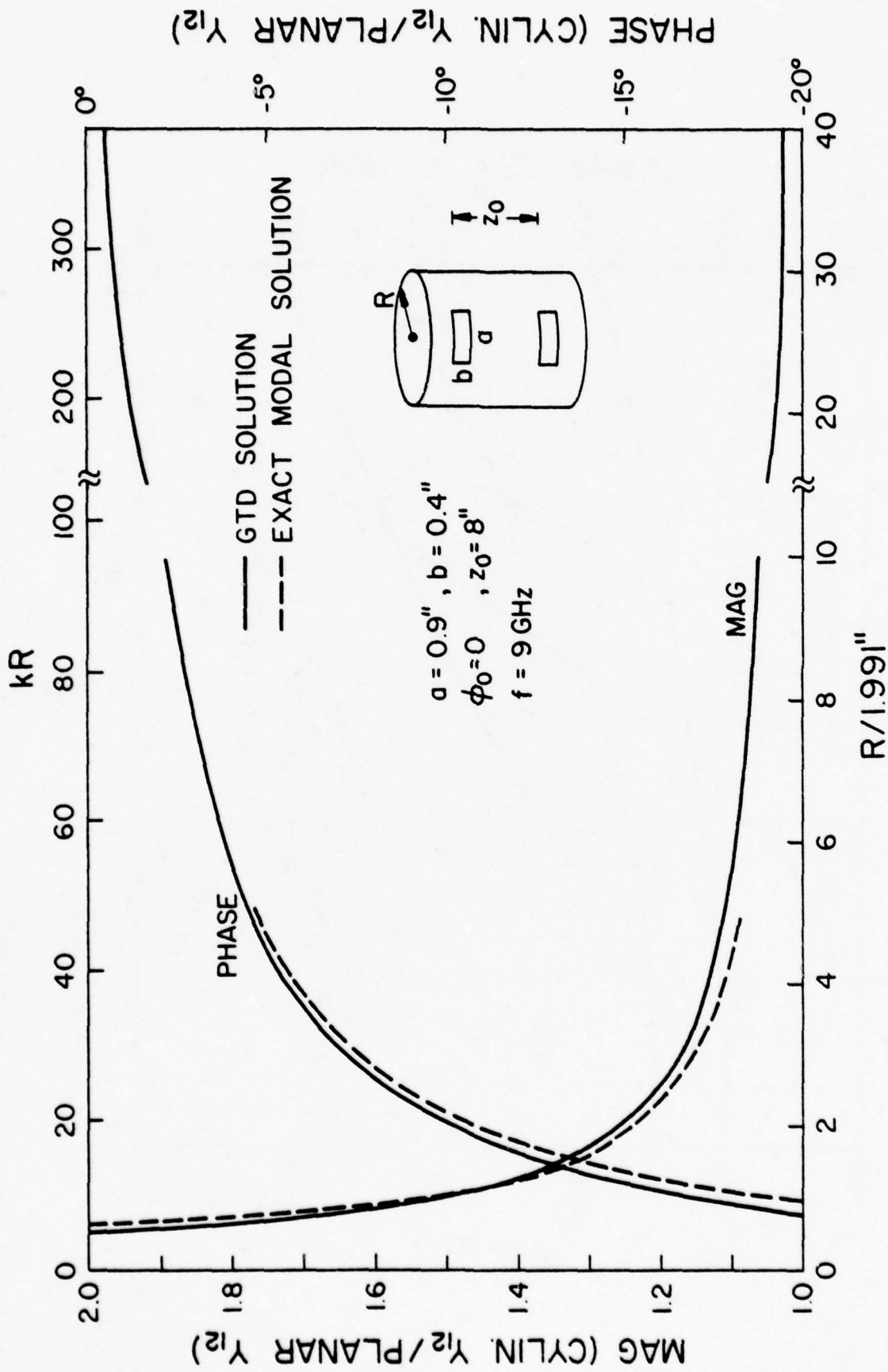


Figure 8. Mutual admittance  $Y_{12}$  of two identical circumferential slots on a cylinder as a function of the radius  $R$  of the cylinder.  $Y_{12}$  is normalized by  $Y_{12}$  on a plane which is  $5.37 \times 10^{-5} \exp(j53.55^\circ)$  mho.

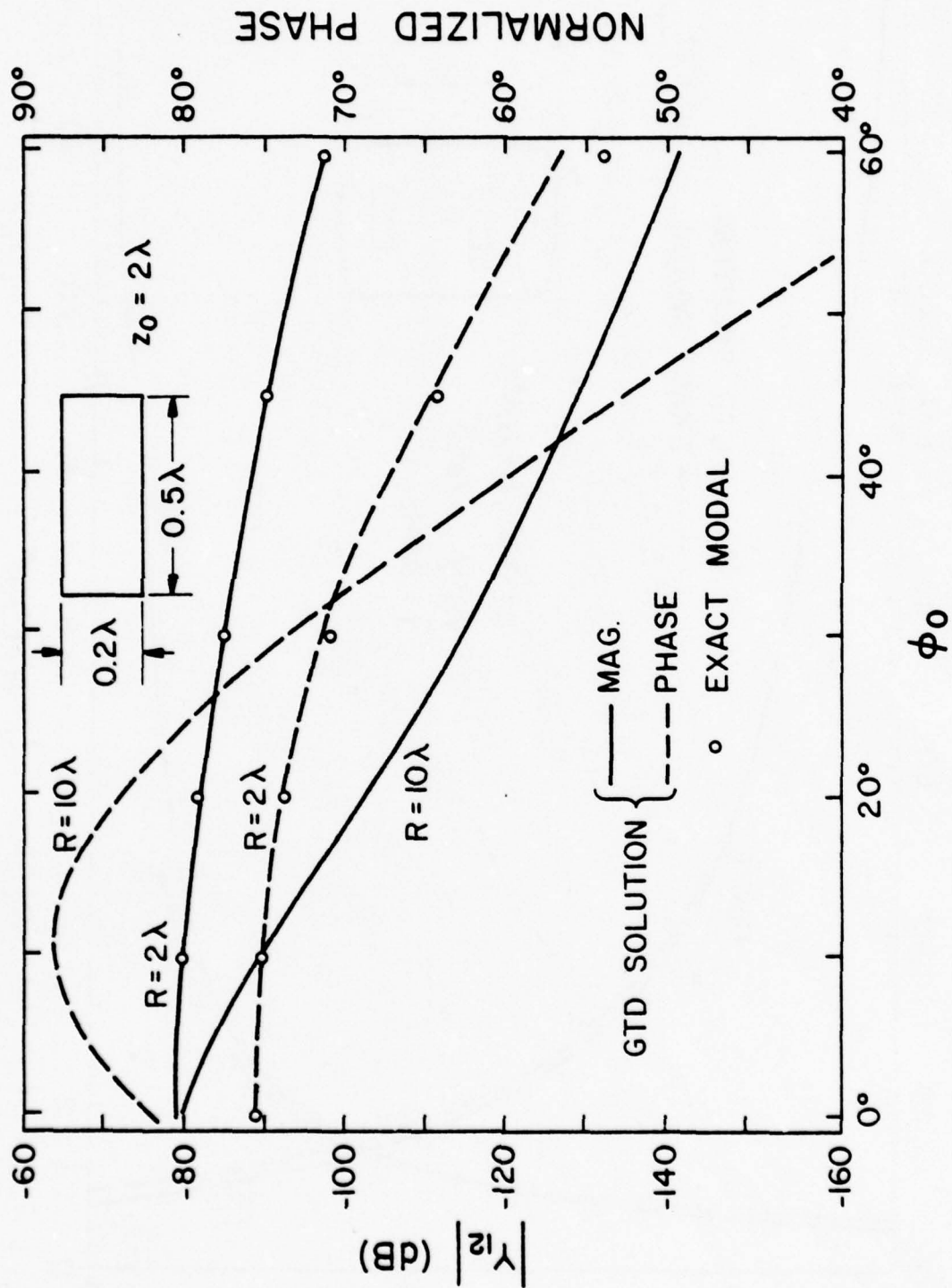


Figure 9. Mutual admittance  $Y_{12}$  between two circumferential slots as a function of  $\phi_0$ .

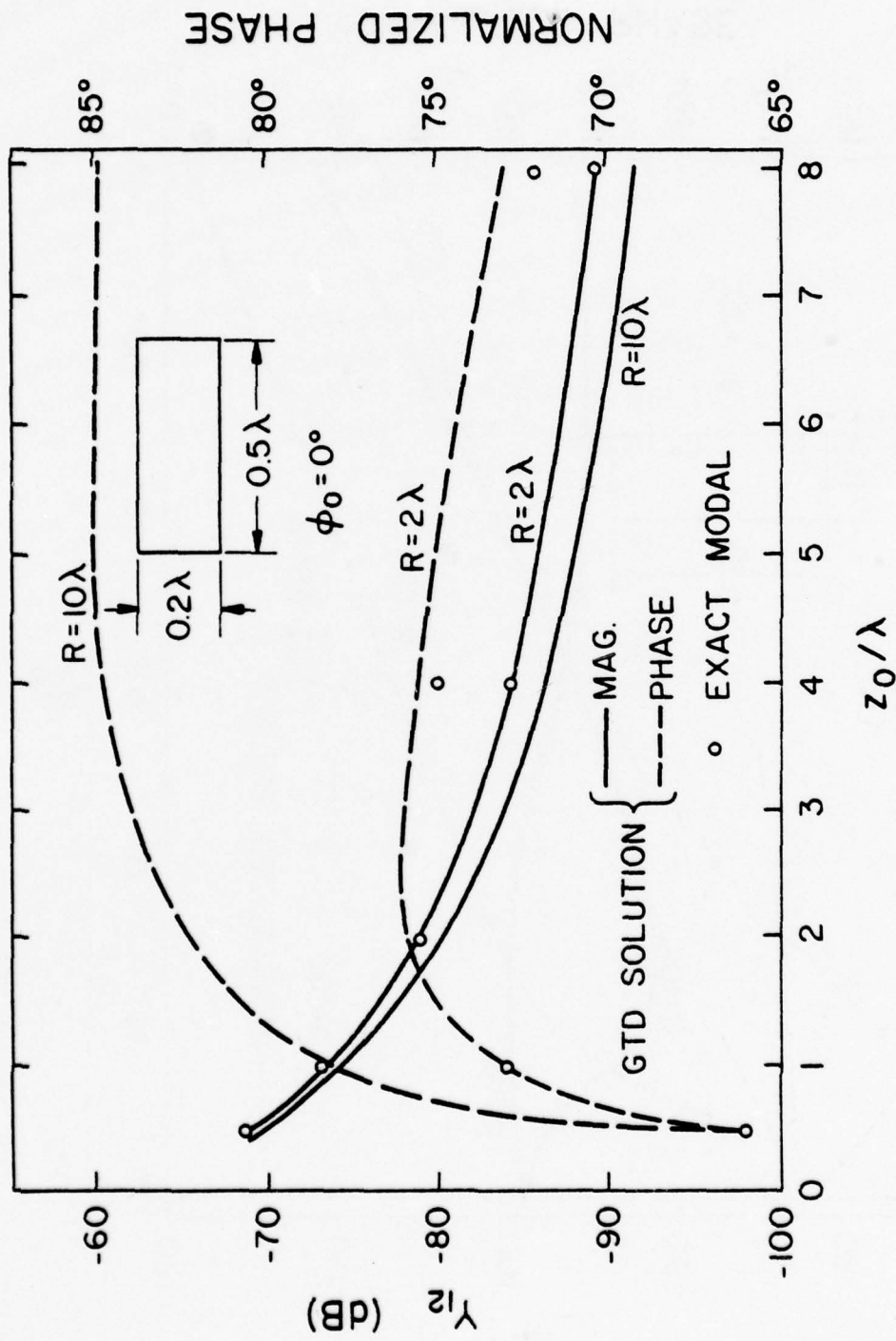


Figure 10. Mutual admittance  $Y_{12}$  between two circumferential slots as a function of  $z_0$ .

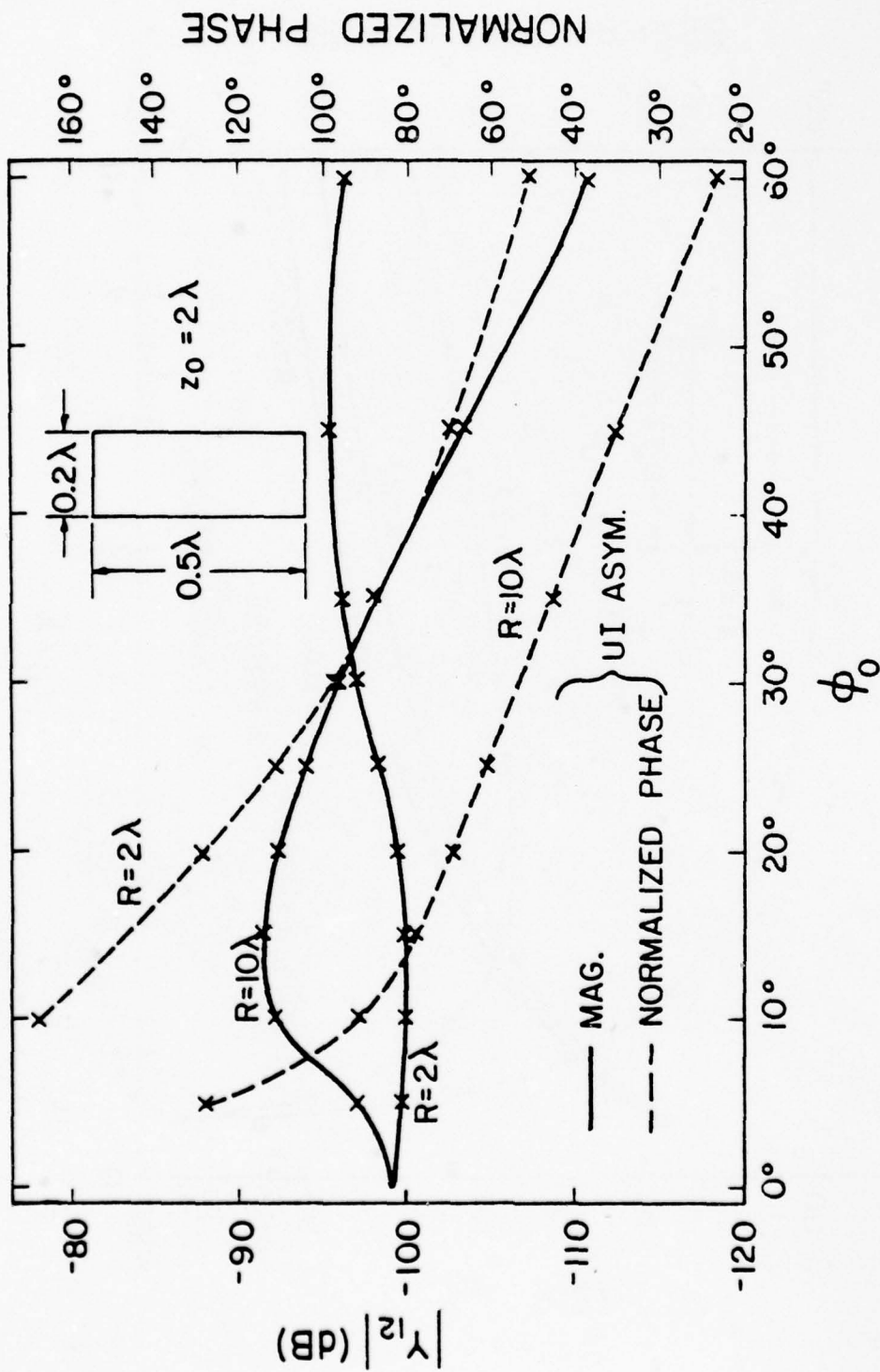


Figure 11. Mutual admittance  $Y_{12}$  between two axial slots as a function of  $\phi_0$ .

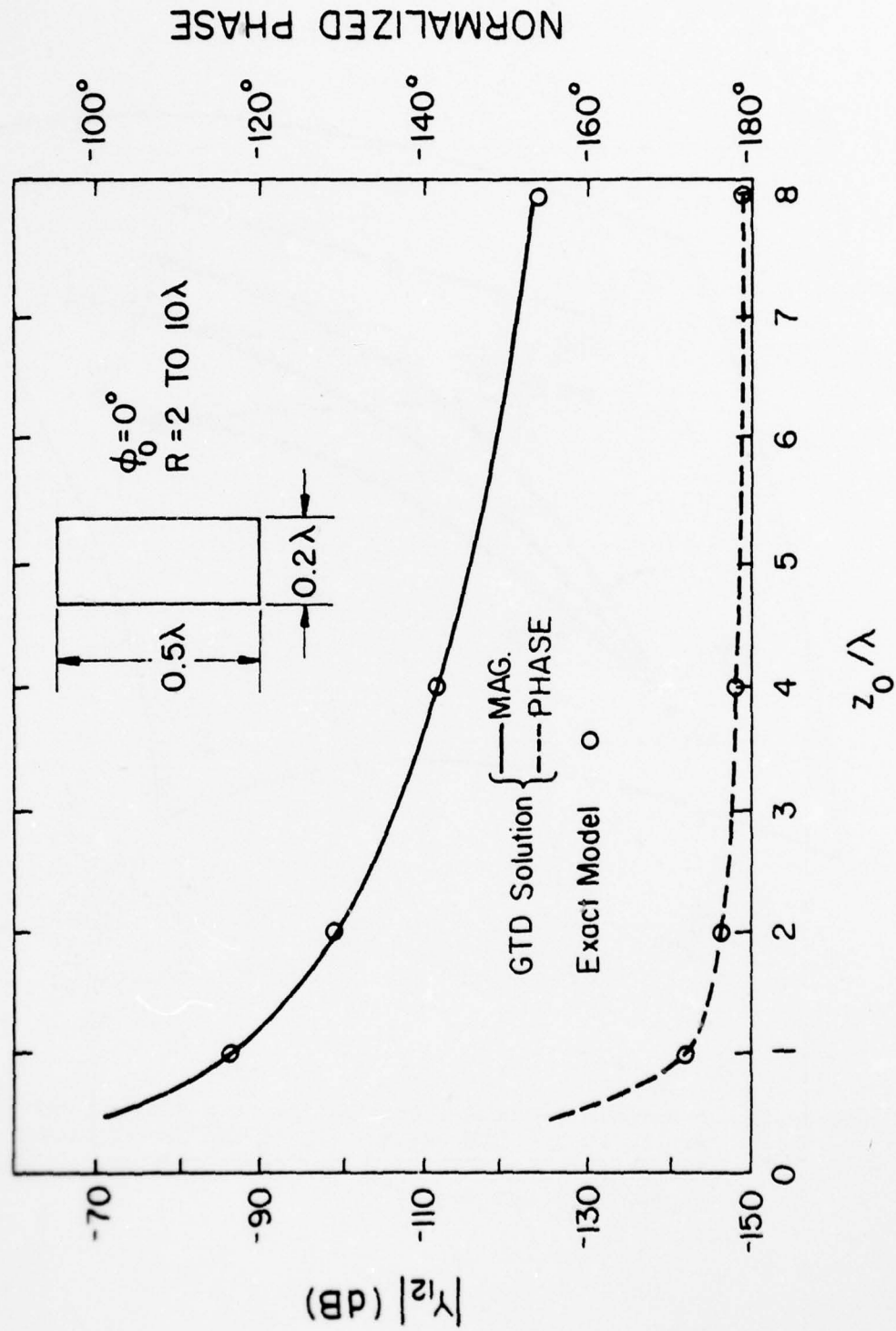


Figure 12. Mutual admittance  $Y_{12}$  between two axial slots as a function of  $z_0$ .

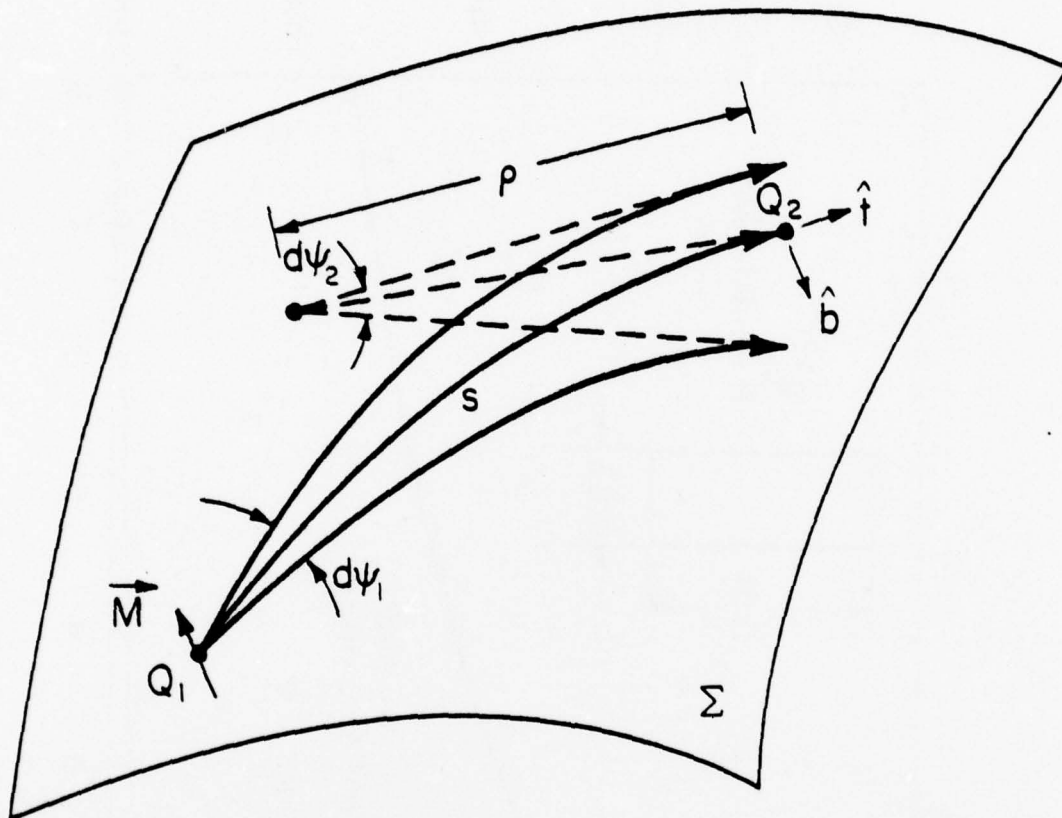
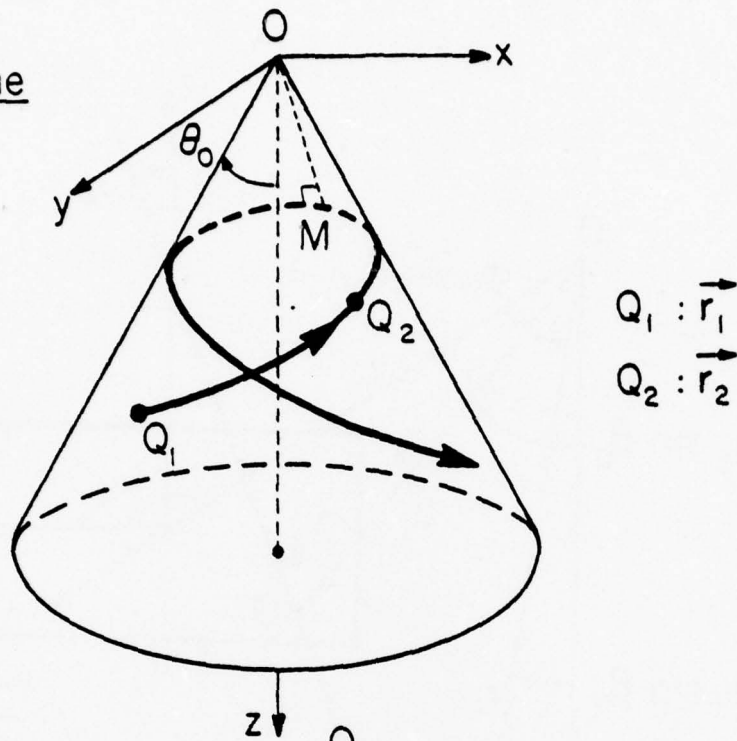


Figure 13. A surface ray pencil originating from the magnetic dipole source at  $Q_1$ . The central ray of the pencil passes through the observation point  $Q_2$ . The angle extended by the pencil is  $d\psi_1$  at  $Q_1$  and  $d\psi_2$  at  $Q_2$ .

(a) 3-D Cone



(b) Developed Cone

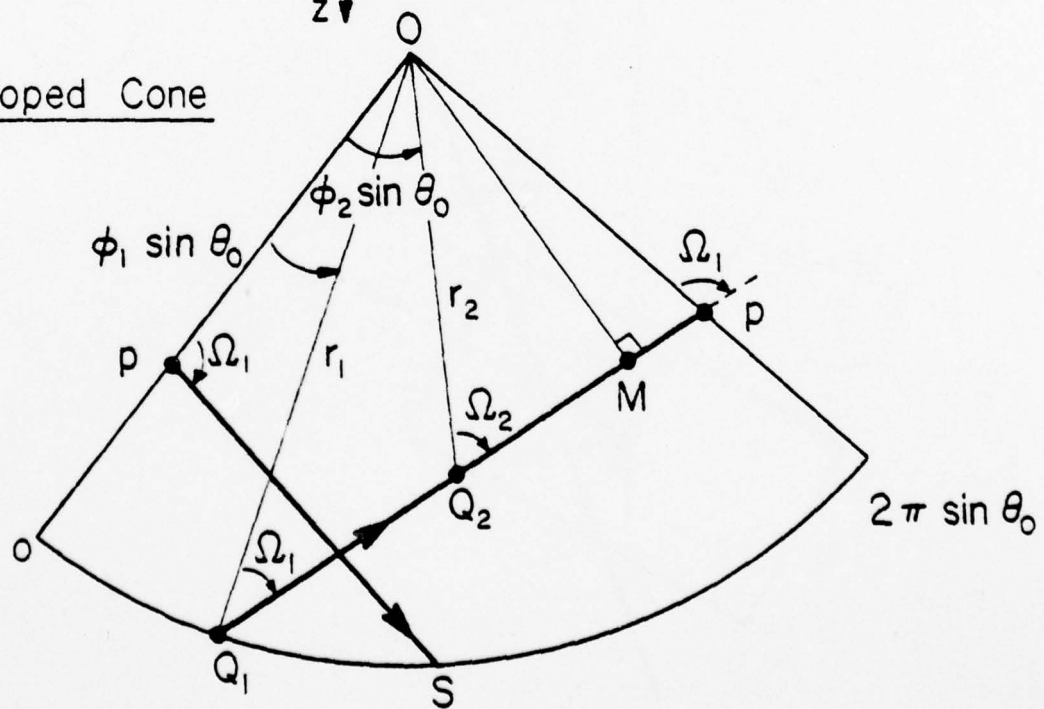


Figure 14. A surface ray from source point  $Q_1$  to observation point  $Q_2$  on a cone with half cone angle  $\theta_0$ .



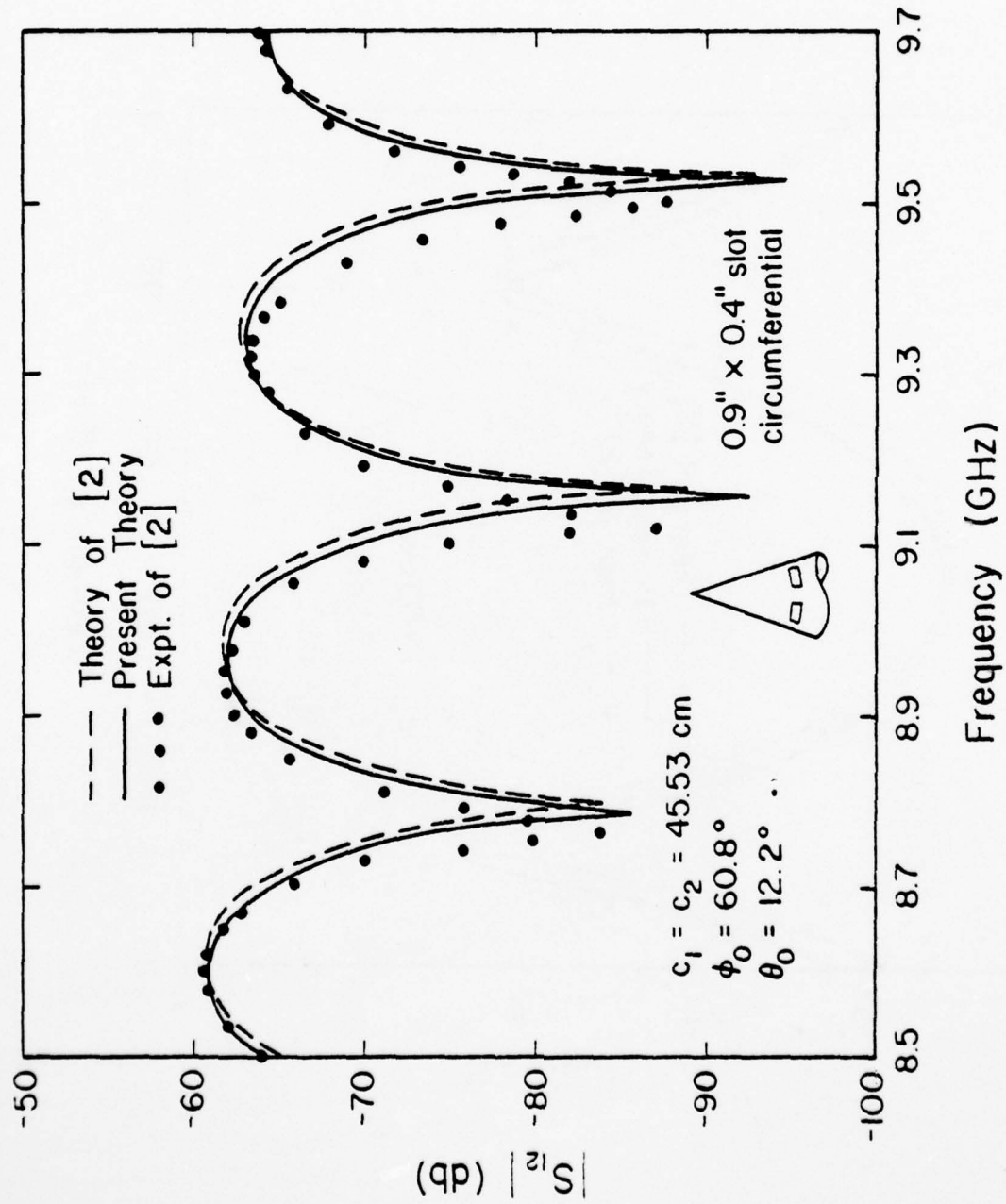


Figure 16. Coupling coefficient  $S_{12}$  between two circumferential slots on a cone as a function of frequency.

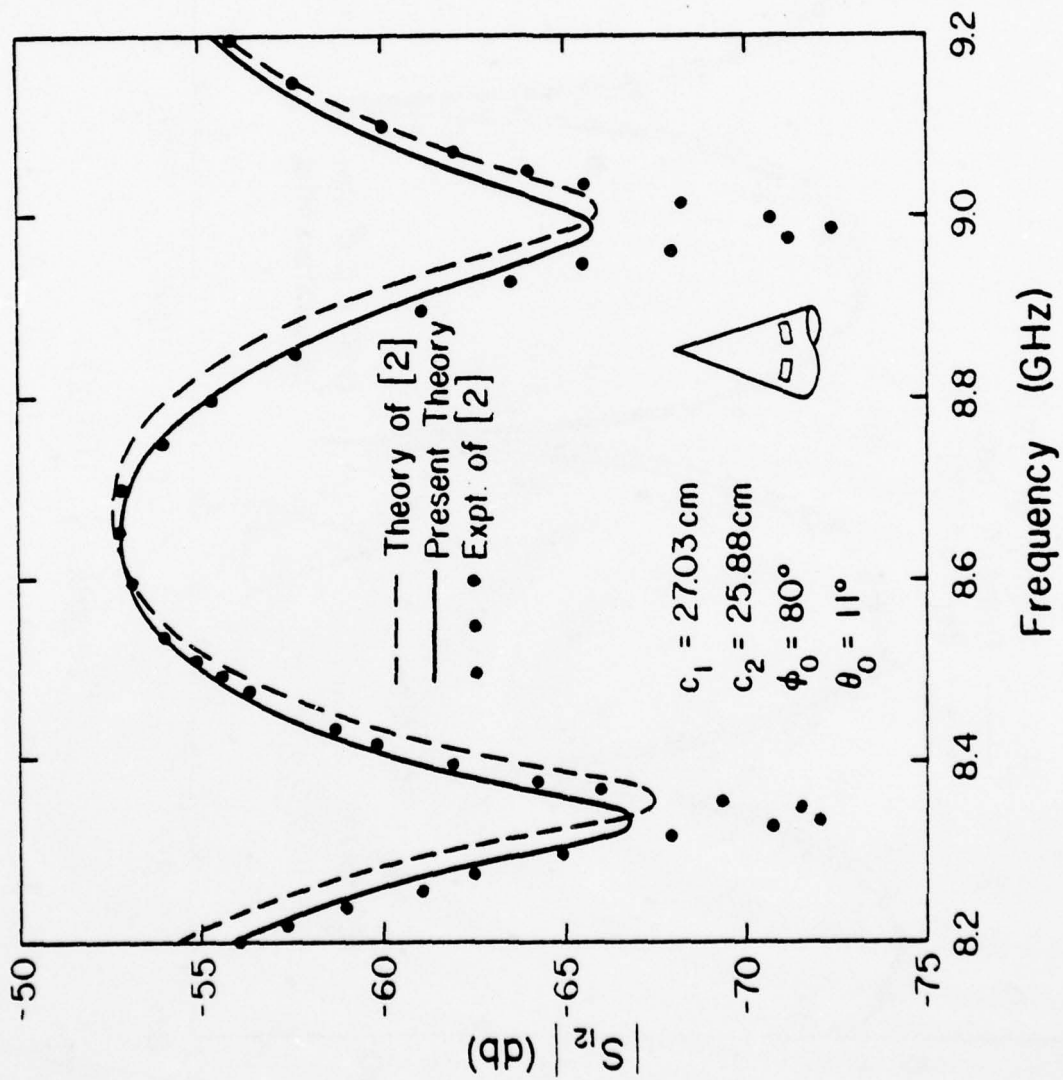


Figure 17. Coupling coefficient  $S_{12}$  between two circumferential slots on a cone as function of frequency.

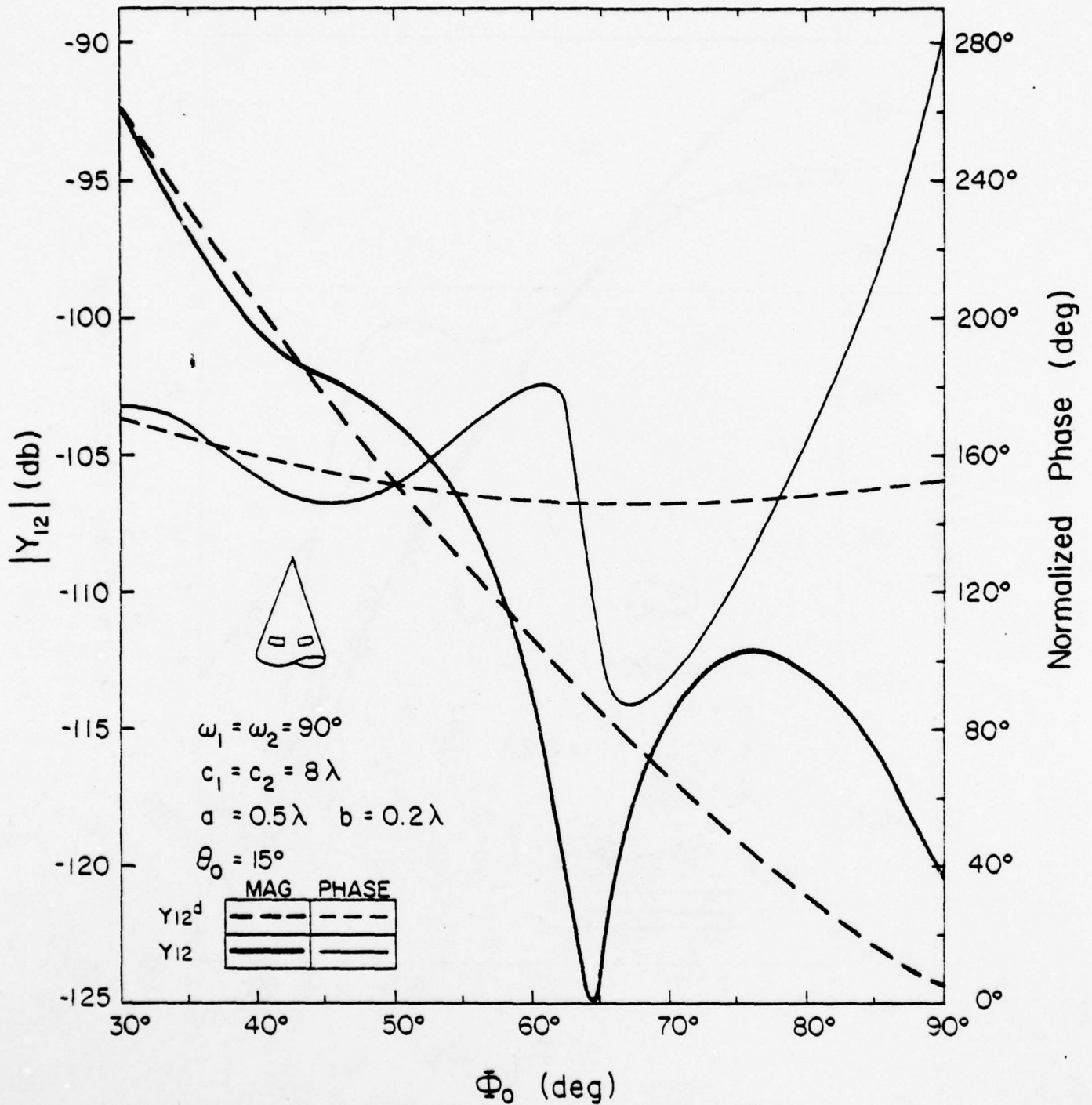


Figure 18. Mutual admittances  $Y_{12}$  between two circumferential slots on a cone calculated from GTD solution.

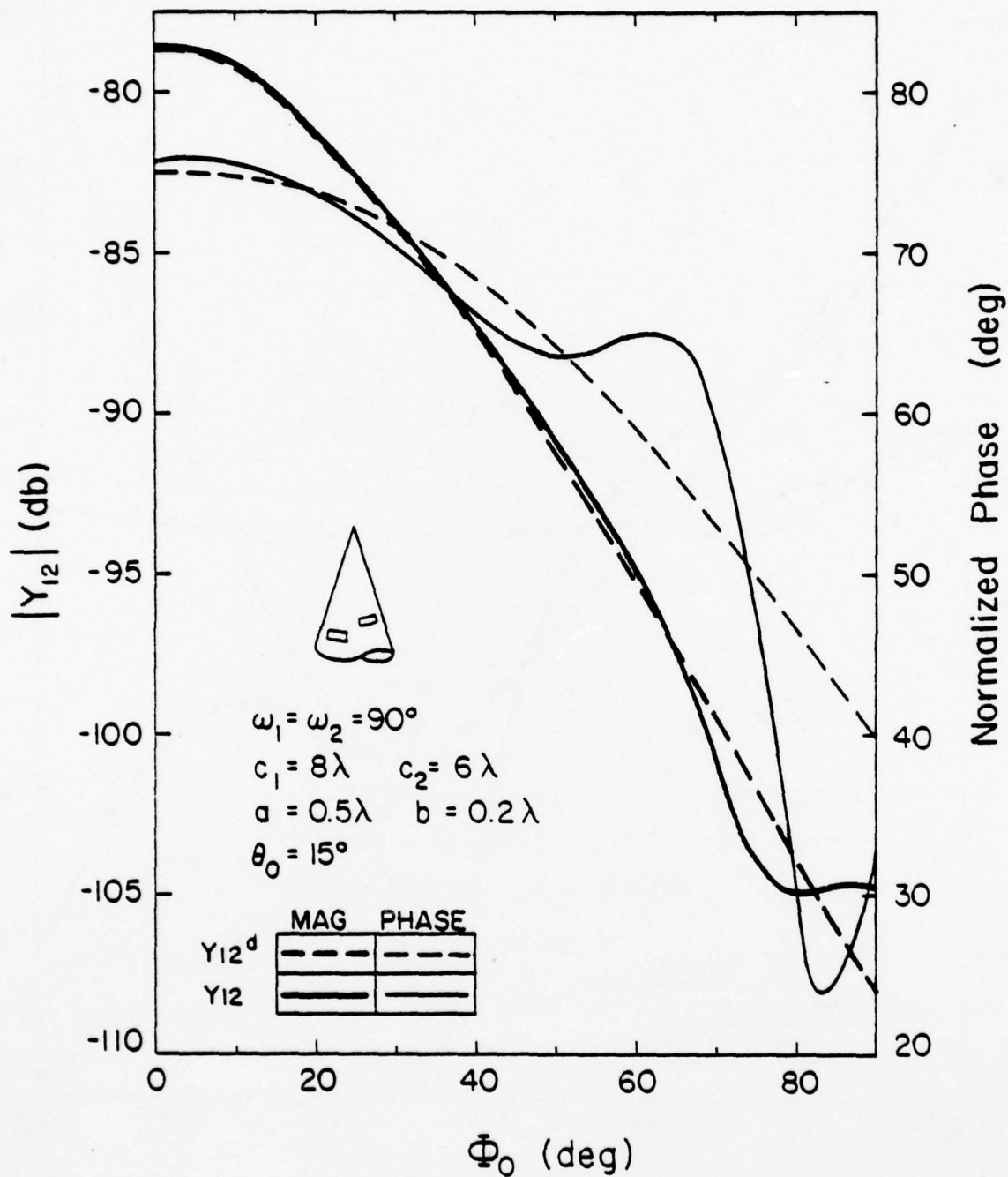


Figure 19. Mutual admittances  $Y_{12}$  between two circumferential slots on a cone calculated from GTD solution.

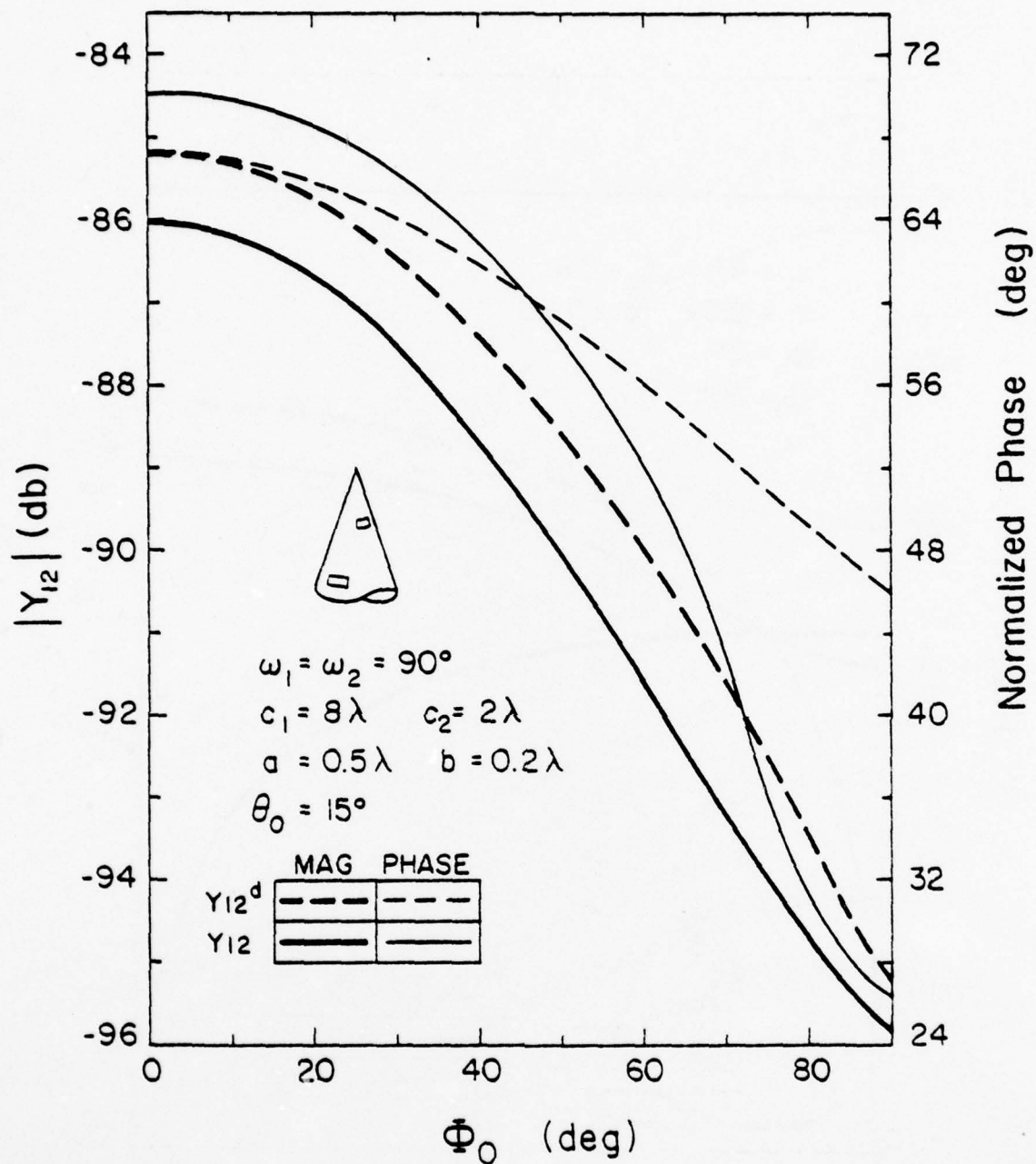


Figure 20. Mutual admittance  $Y_{12}$  between two circumferential slots on a cone calculated from GTD solution.

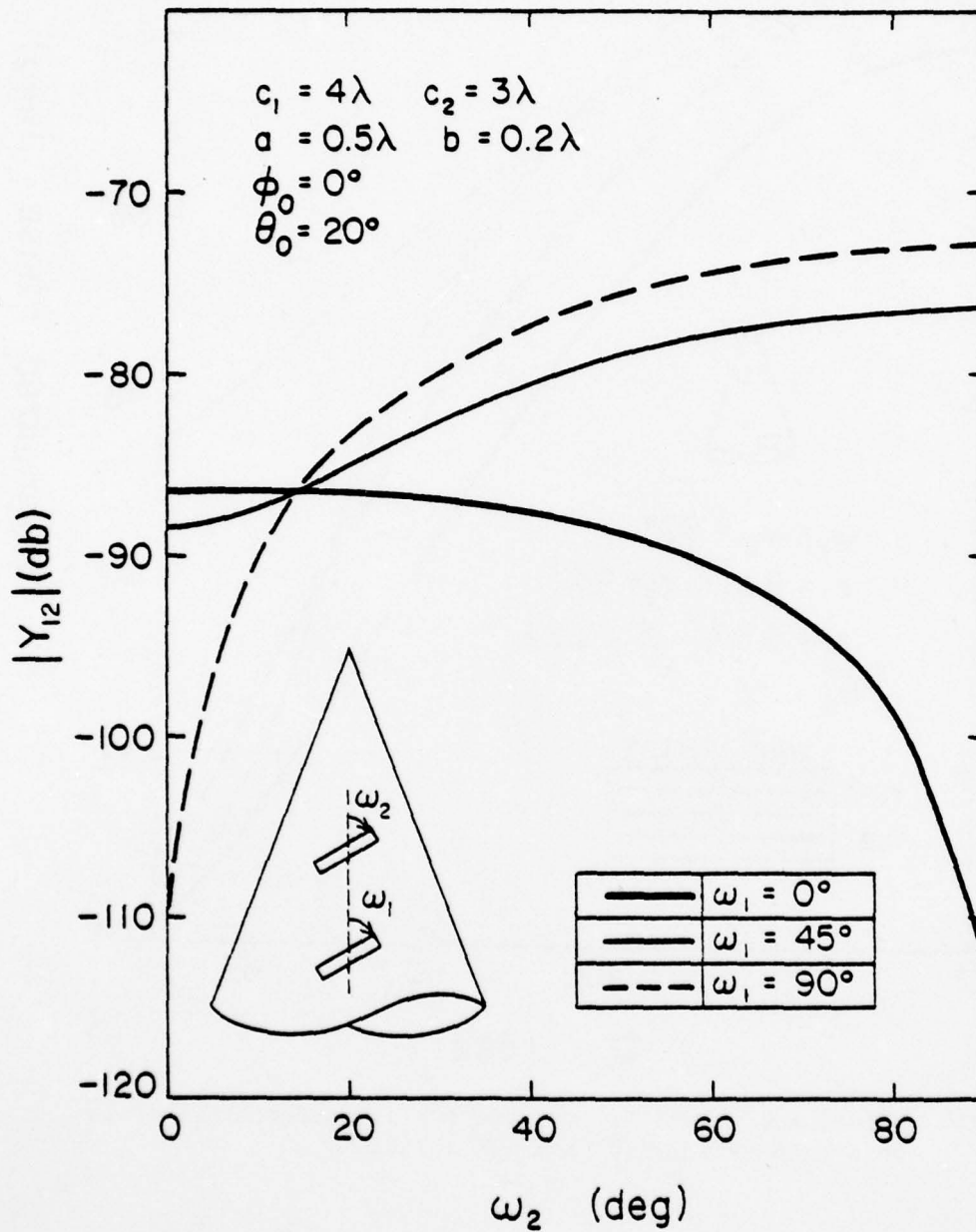


Figure 21. Mutual admittance  $Y_{12}$  between two arbitrarily oriented slots on a cone calculated from GTD solution.

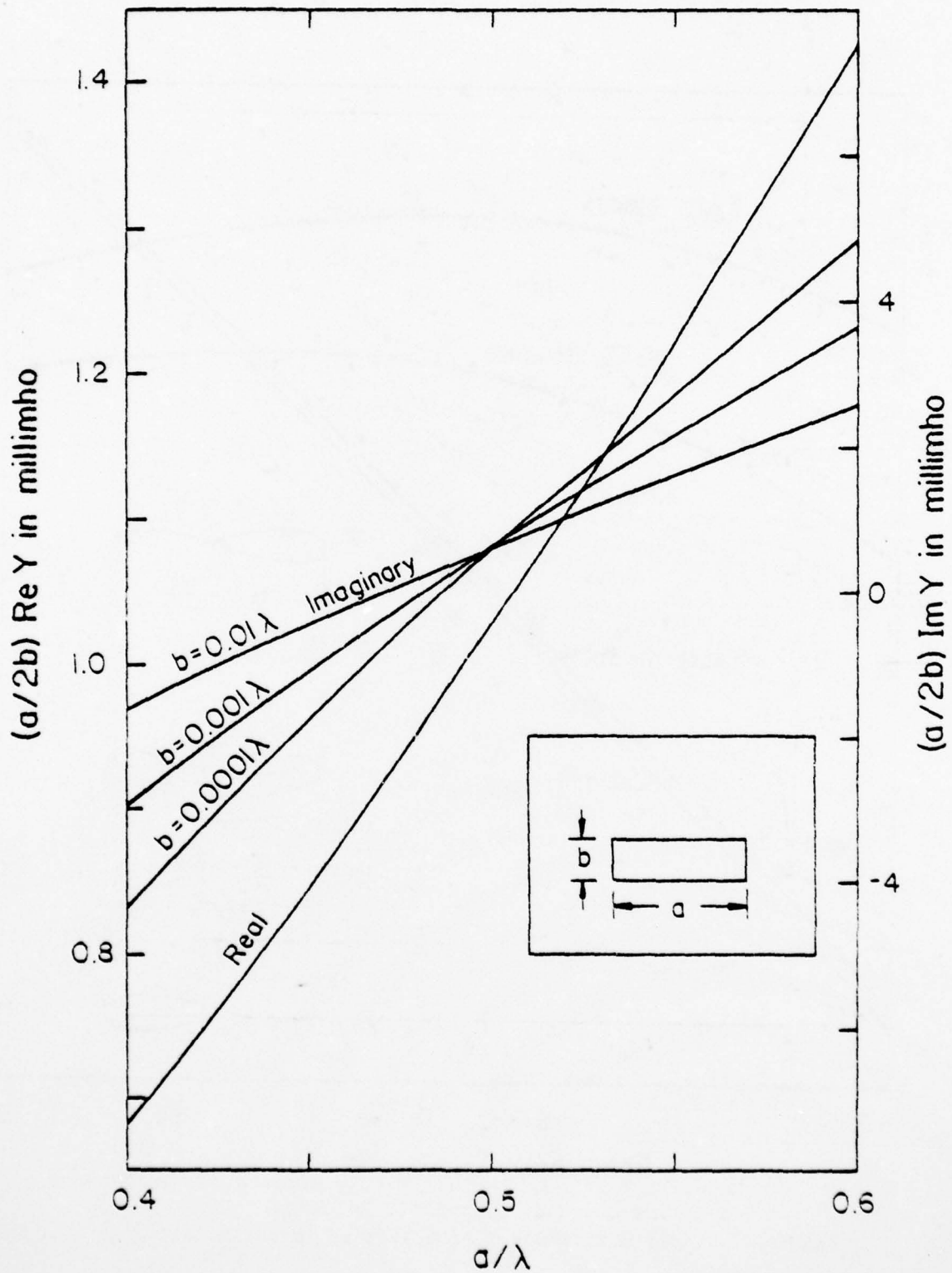


Figure 22. Self-admittance  $Y$  of a slot on an infinite plane.

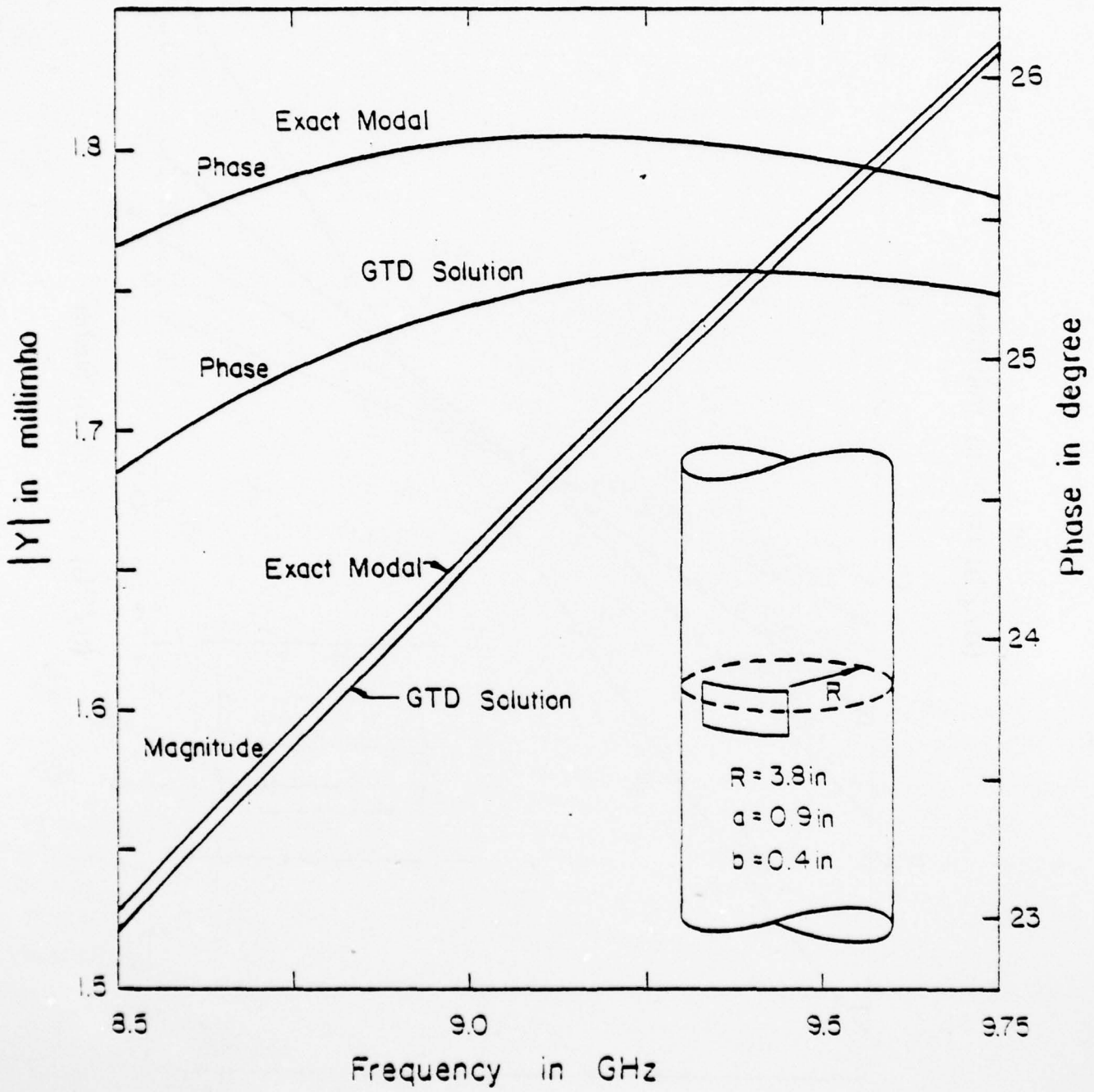


Figure 23. Self-admittance  $Y$  of a slot on an infinitely long cylinder.

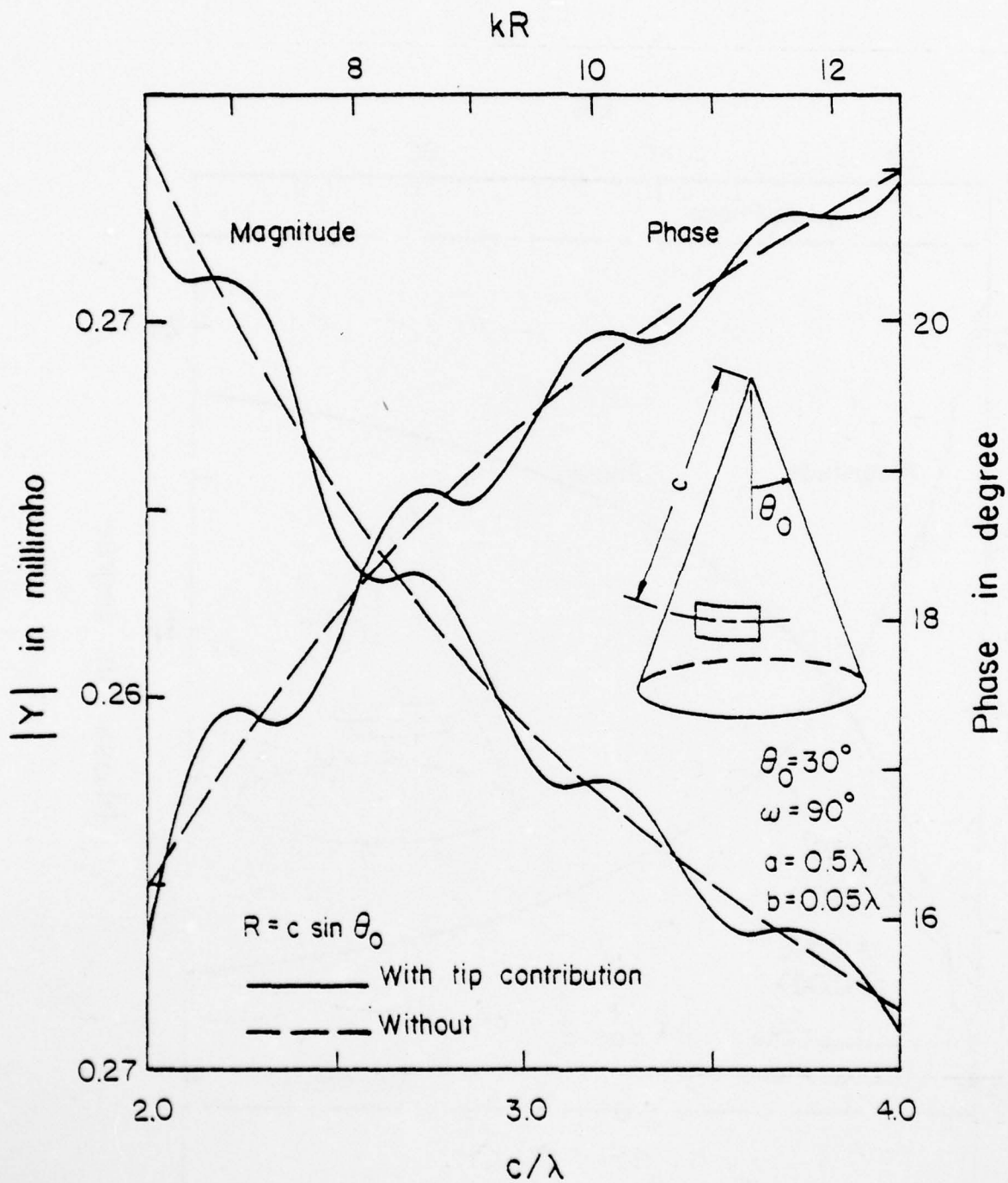


Figure 24. Self-admittance  $Y$  of a slot on a cone as a function of radial distance  $c$ .

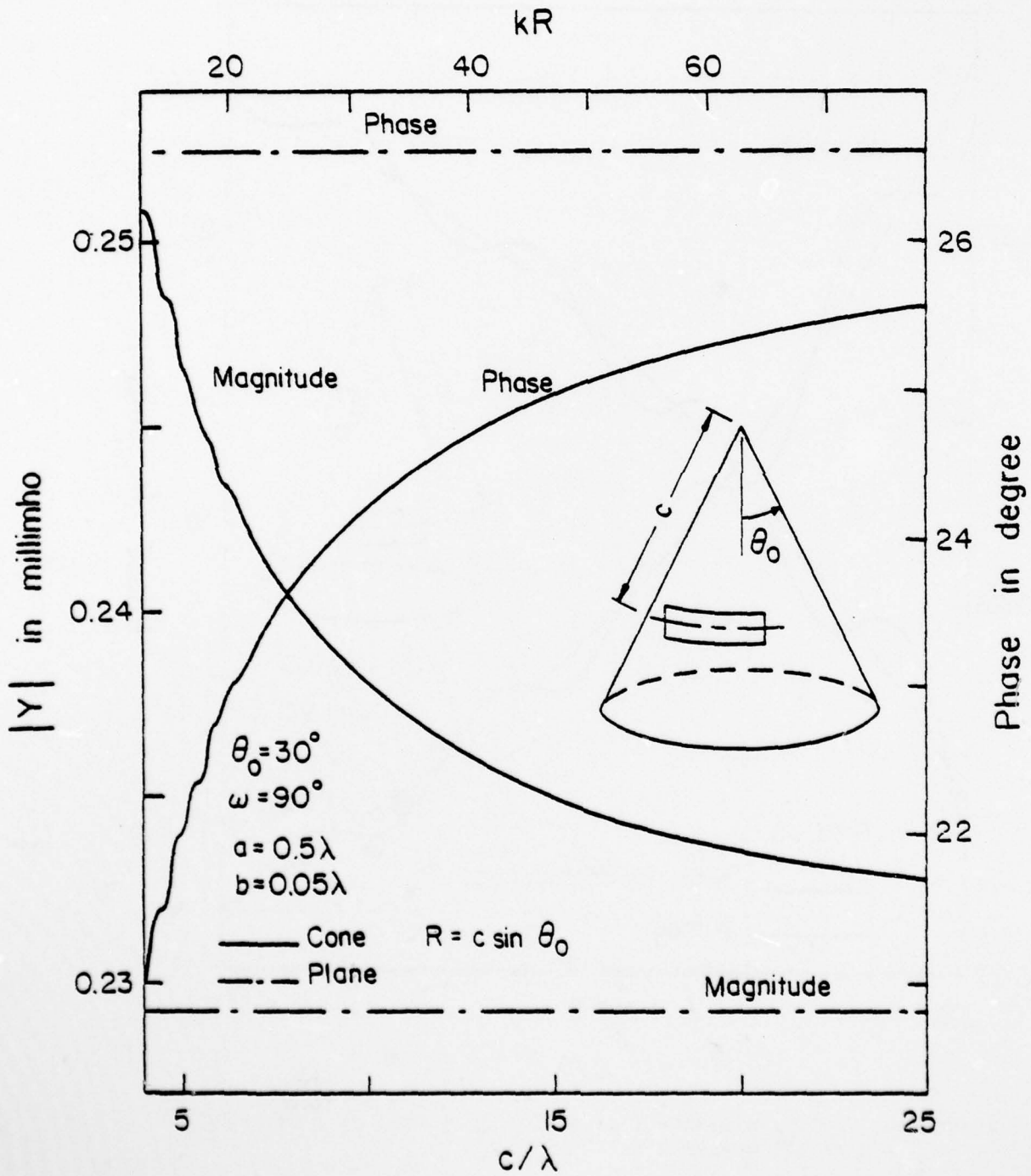


Figure 25. Same as Figure 24, except with larger radial distance  $c$ .

AD-A066 330

ILLINOIS UNIV AT URBANA-CHAMPAIGN ELECTROMAGNETICS LAB F/G 9/5  
AN INVESTIGATION ON CHARACTERIZING MUTUAL COUPLING BETWEEN TWO --ETC(U)  
JAN 79 S W LEE, R MITTRA, J BOERSMA, E YUNG N00019-78-C-0064  
UNCLASSIFIED UIEM-79-2 NL

3 of 3  
AD  
A066330



END  
DATE  
FILMED  
5-79  
DDC

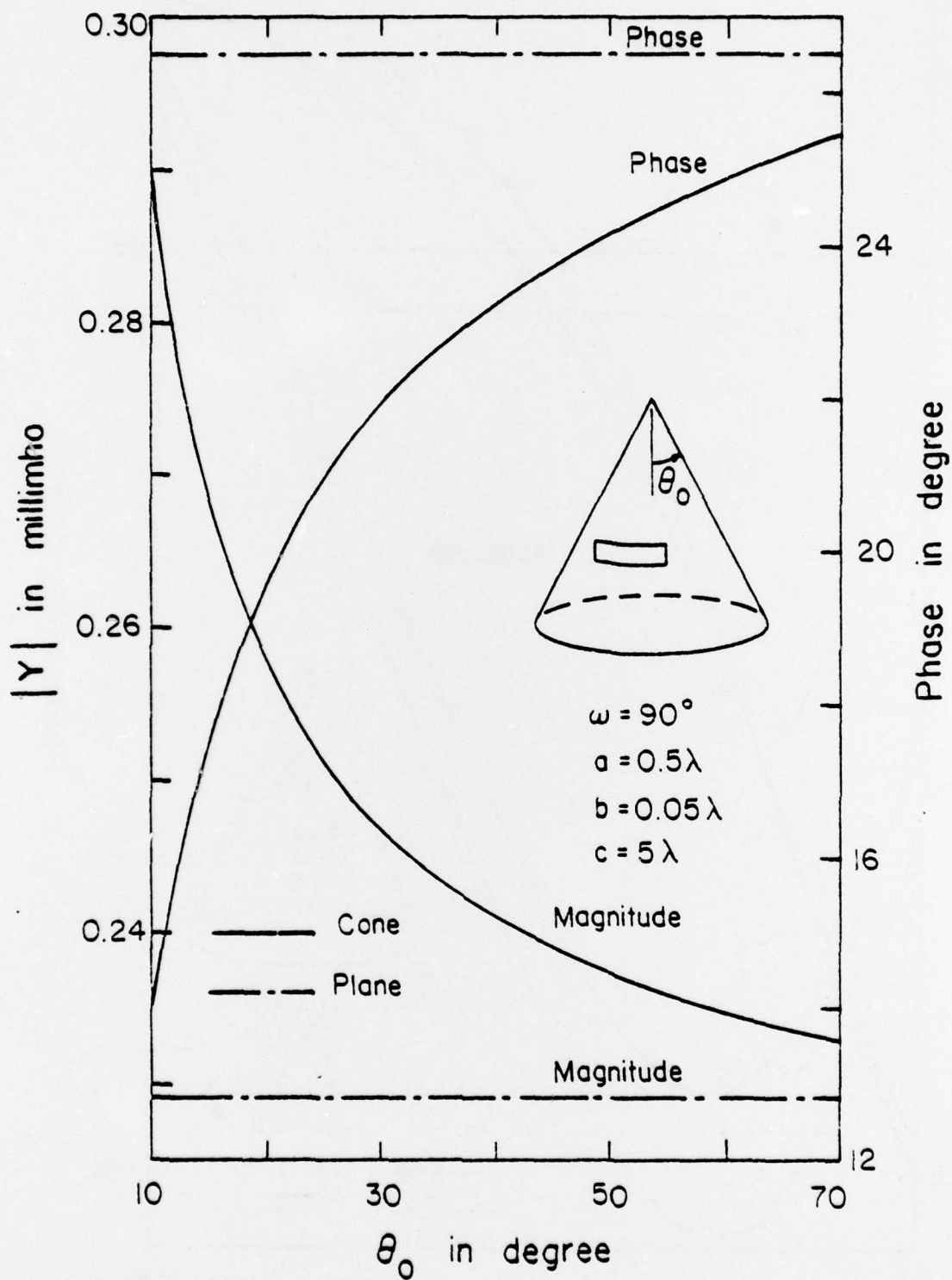


Figure 26. Self-admittance of a slot on a cone as a function of half-cone angle  $\theta_0$ .

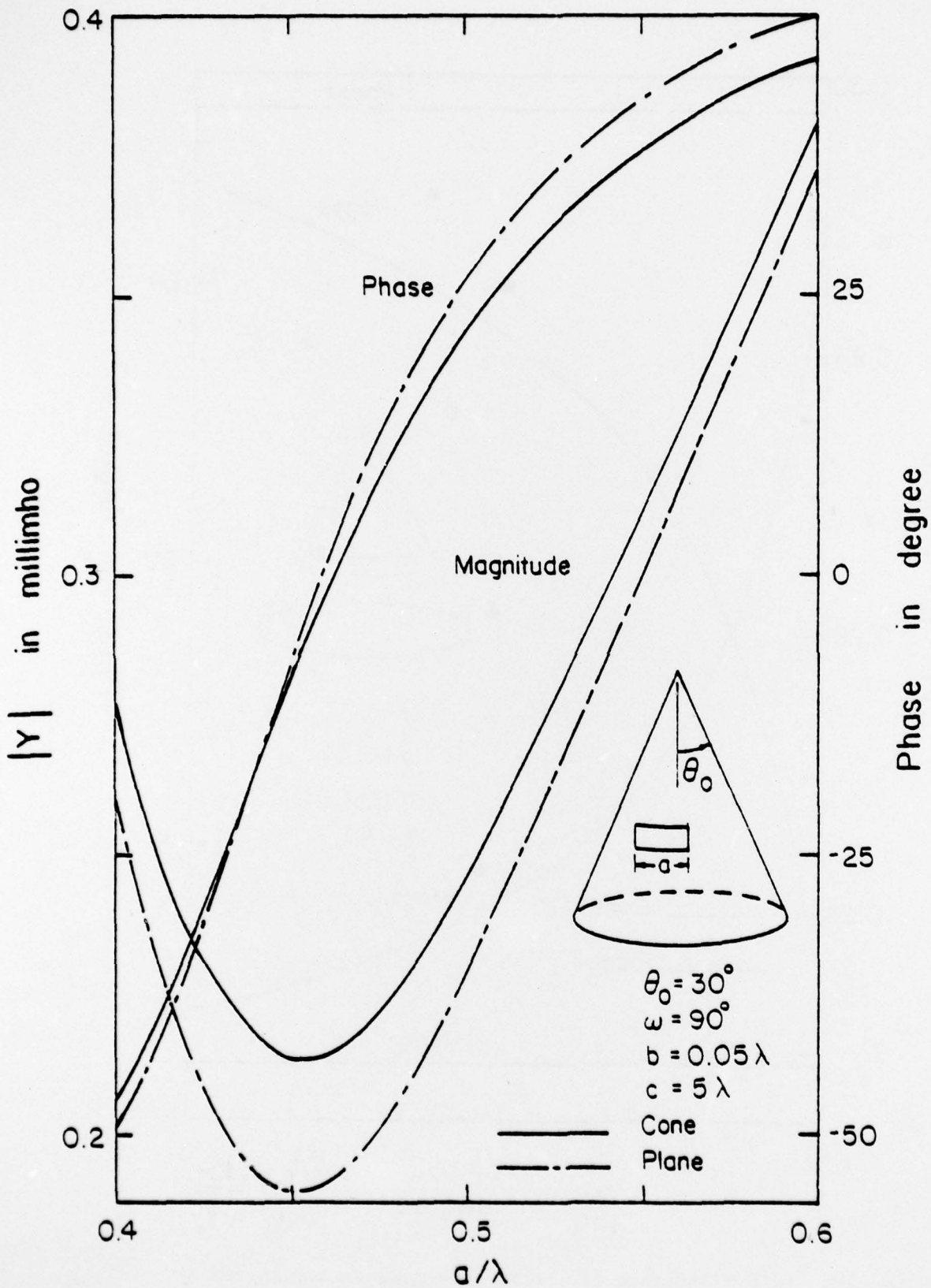


Figure 27. Self-admittance  $Y$  of a slot on a cone as a function of slot length  $a$ .

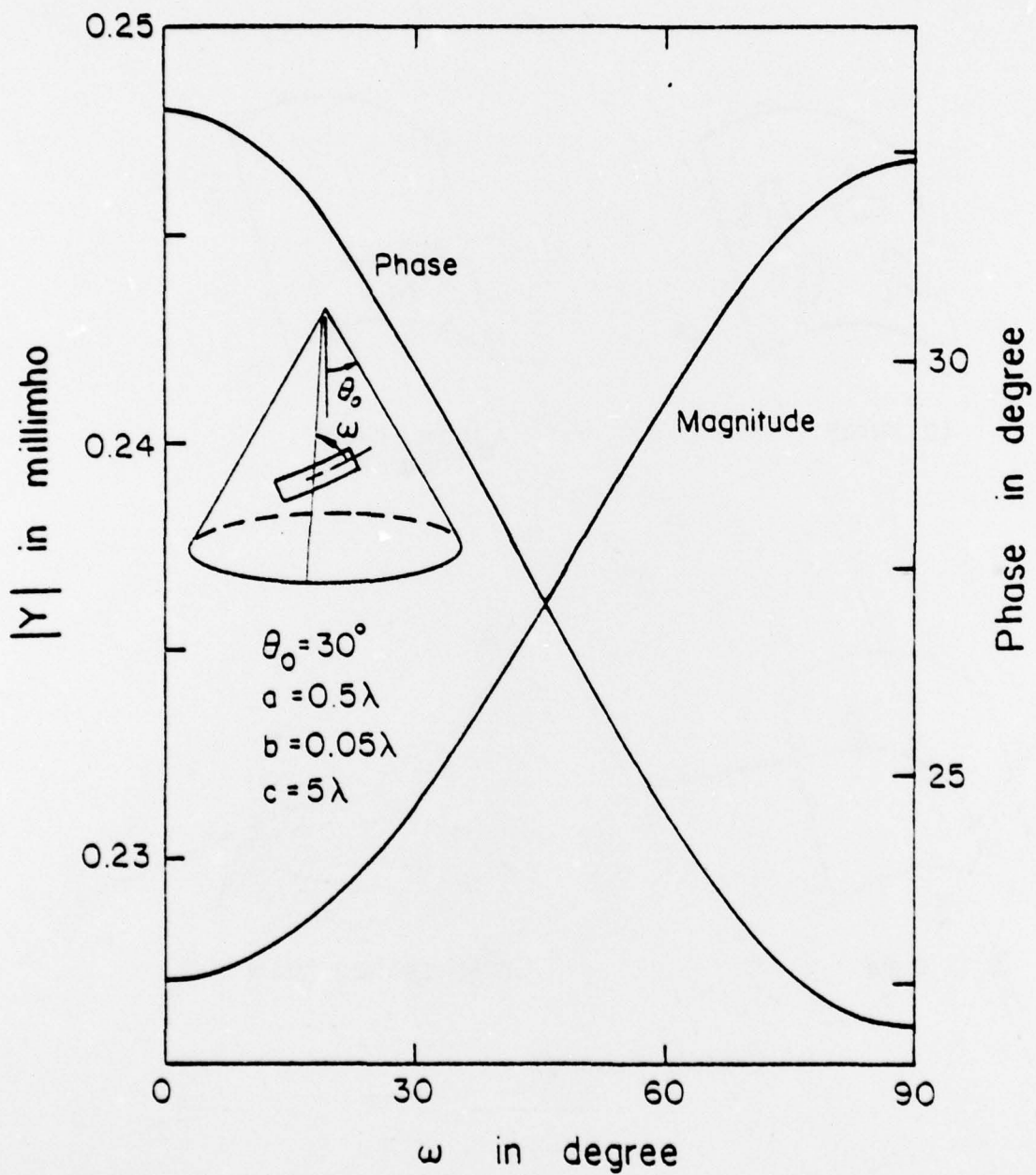
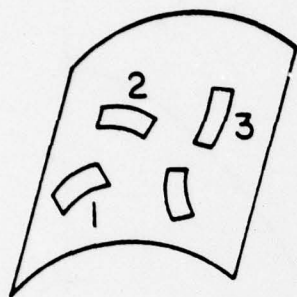
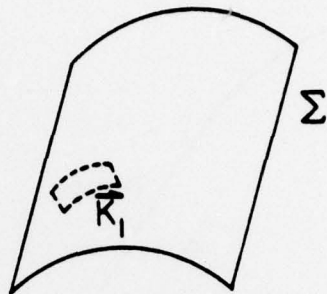


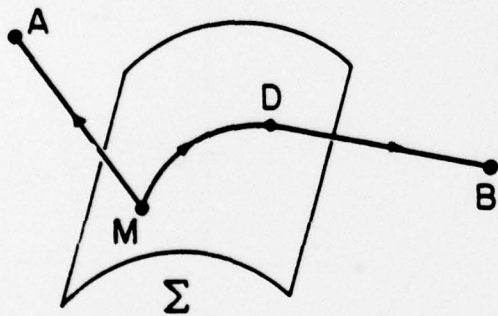
Figure 28. Admittance  $Y$  of a slot on a cone as a function of orientation angle  $\omega$ .



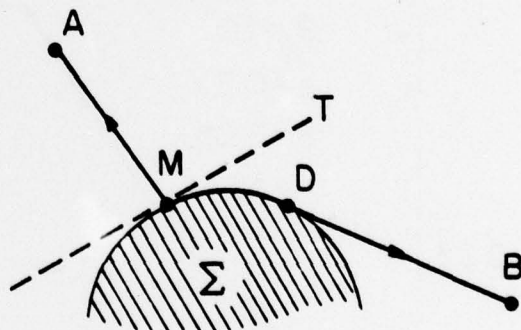
(a) Array



(b) Equivalent Source



3-D View



Cross-section View

(c) Green's Function

Figure 29. Calculation of short-circuited active element pattern  $P_1(\theta, \phi)$  from slot 1 by GTD.